Copyright

by

Christine Theresa Weber

2008

The Dissertation Committee for Christine Theresa Weber Certifies that this is the approved version of the following dissertation:

Leakage through Defects in Geomembrane Liners under High Hydraulic Heads

Committee:

Jorge G. Zornberg, Supervisor

Stephen G. Wright

Robert B. Gilbert

Howard M. Liljestrand

Graham F. Carey

Leakage through Defects in Geomembrane Liners under High Hydraulic Heads

by

Christine Theresa Weber, B.S., M.Eng.

Dissertation

Presented to the Faculty of the Graduate School of

The University of Texas at Austin

in Partial Fulfillment

of the Requirements

for the Degree of

Doctor of Philosophy

The University of Texas at Austin

August 2008

Dedication

To My Parents

All the love and thanks in world

And

To my Grandma, Margie Cooper

I miss you

Acknowledgements

I would like to acknowledge my supervisor, Dr. Jorge Zornberg, for his encouragement, guidance and wisdom throughout my years as a PhD student. He provided me with a wonderful opportunity to learn about the use of geosynthetics in dams, for which I am very grateful. I have thoroughly enjoyed my time and my work here at UT. I would also like to thank Dr. Bob Gilbert and Dr. Steve Wright for sharing with me their wealth of knowledge, particularly with respect to certain aspects of my research. Their insight was invaluable. I would also like to express my sincerest gratitude to Dr. Graham Carey and Dr. Howard Liljestrand for serving on my doctoral committee. I appreciate all their advice and support along the way.

This research was partially funded by the Geosynthetic Institute and was conducted as part of the Center of Polymers in Hydraulic Structures. In particular, I would like to acknowledge Dr. Bob Koerner for his support. I greatly appreciated the opportunity to work on such an amazing project.

I would like to thank the University of Texas at Austin College of Engineering (specifically Mr. Louis T. Pirkey) and the Society of Women Engineers for providing financial support and giving me a wonderful opportunity to achieve my goals.

I would like to thank the many friends and colleagues that I had the most delightful opportunity to get to know during my stint at UT. To my research group (Jeff, John, Ranjiv, Brian, and Julio), you are like my second family and I truly consider you brothers. I have enjoyed our time together and I truly thank you from the bottom of my

heart for putting up with me. I wish you all the best in your future endeavors. I will truly miss you all. I would also like to thank John and Becky for always being there for me, particularly when I just needed a place to stay during my transition into the real world.

To Mary, Jessy, Sophie and Mindy, I cannot express my thanks enough for being so supportive and for listening to my sometimes frequent venting episodes. I would have to say that without you, I might not be sane at this point in time.

Most importantly, my eternal gratitude goes to my family, every single one of you. I am not sure there are words for how much I love you and how much your love and support have meant to me while I have been traveling down this hard, toilsome but incredibly rewarding road. But I have only been successful at achieving my goals because of you.

"O Lord, my God, I will give you thanks forever." – Psalm 30:12b (NASB)

Leakage through Defects in Geomembrane Liners under High Hydraulic Heads

Publication No._____

Christine Theresa Weber, PhD

The University of Texas at Austin, 2008

Supervisor: Jorge G. Zornberg

Dams are among the most critical of civil engineering structures and are susceptible to damage due to seepage. Geomembranes have been used to minimize seepage problems in dams since 1959. However, geomembranes are vulnerable to damage, in the form of tears and punctures, during installation and throughout the service life. These defects impact the effectiveness of a geomembrane as an infiltration barrier resulting in leakage through the geomembrane liner and into the body of the dam. The majority of previous studies conducted to investigate leakage through defects in geomembranes considered heads below 0.3 m, which corresponds to flow for conditions experienced by landfill liners.

The main objectives of this study were to quantify the leakage rate through defects in geomembrane lining systems for dam and to evaluate the implications of the leakage on the performance of dams. Experimental, analytical and numerical studies were conducted as part of this investigation. The experimental testing program included permeameter cell tests for the following lining systems: i) geomembranes over clay

layers, ii) geomembranes over sand layers and iii) geomembranes over geosynthetic clay liners. The permeameter tests were conducted to investigate the effects of soil type, initial water content, dry unit weight and hydraulic head on leakage through a defect in a geomembrane liner. The analytical component was conducted to evaluate the transmissivity at the interface and radius of wetted area for the tests conducted as part of the experimental component. The numerical component of this study was performed using the finite element method to simulate the experimental tests and the performance of actual dams. Ultimately, the laboratory tests and subsequent analyses were used to develop a set of tools (e.g., empirical models, design recommendations) that are expected to assist engineers in the design of geomembrane lining systems for dams. Also, the study was used to identify and address potential concerns (e.g., global stability) that may result in failure of systems in which geomembrane liners are used. This study is expected to contribute to a better understanding of the performance of geomembranes as dam liners.

The presence of a geomembrane, even with a defect, was found to reduce the amount of leakage that occurs through a soil layer. New predictive equations were developed to estimate leakage through defects in composite lining systems. The finite element analyses indicated that a dam with a geomembrane with very large defects would not develop pore pressures that were similar to those observed for an unlined dam. The factor of safety for the unlined dam was improved by the placement of a geomembrane on the upstream face. Consequently, a geomembrane may also eliminate the need for a blanket drain at the downstream toe, which could decrease the cost of construction.

Table of Contents

List of Tables

List of Figures

Chapter 1: Introduction

1.1 MOTIVATION

Dams and levees are among the most critical of civil engineering structures. They provide an important source of water for agricultural, municipal and industrial use and are often an integral part of emergency flood management systems. Around 60% of the dams in U.S. are earthfill and/or rockfill dams over 7 m in height (National Inventory of Dams [NID] 2005). The majority of dams in the United States have been in service for at least 40 years (World Commission on Dams 2000). As dams age, deterioration and structural damage are of major concern as they can lead to water loss and even failure. Currently, over $4 billion is being spent in California alone to retrofit dams and levees in order to maintain the integrity of an important part of the state's flood management infrastructure (California Secretary of State 2006; Schwarzeneggar 2006).

Earthen dams and levees can be susceptible to desiccation, which results in cracks on the upstream face, and piping of fines from the dam core. Piping and internal erosion within the dam itself due to seepage forces can lead to instability. A feasible solution to prevent the degradation and erosion of an earthen dam involves the use of geosynthetics to line the upstream face of the dam or its core. Geomembranes have been used to minimize dam seepage problems since 1959, beginning in Europe (Sembenelli and Rodriguez 1996; Lacroix 1984). The benefits of using a geomembrane liner in a dam include the minimizing seepage through the dam, improving its stability and long-term performance, and minimizing the costs of construction. Because transportation costs are high, the cost of material for dam construction increases significantly if the appropriate soil is not readily available. A geomembrane liner can be a cost-effective alternative, allowing readily available material to be used.

An important issue to consider in regards to using geomembranes is the vulnerability of the thin polymeric material to damage both during installation and throughout the service life. This damage, typically involving tears and punctures, impacts the effectiveness of a geomembrane as an infiltration barrier and results in leakage through the geomembrane liner and into the body of the dam.

Defects are expected to occur even if good construction quality control and assurance procedures are used during installation. Giroud and Bonaparte (1989) conducted a study, based on data obtained from quality assurance and forensic analyses, to determine the frequency of defects expected in landfill liners. The authors found that an average of one defect occurred per 10 m of field seam (where two geomembrane sheets are attached together in the field) without quality assurance or quality control. Also, an average of one defect per 300 m of field seam was found to occur when quality assurance and control measures are used. In a more recent study, Nosko and Touze-Foltz (2000) used an electrical damage detection system to evaluate the size, location and cause of damage during construction for over 300 landfill sites. The majority of the damage occurred on the flat portion of the landfill floor with punctures and tears created by the installation equipment and stones in the protection layer. Based on these data, it is expected that defects will also be present in the geomembrane lining system for dams. The number of the defects in the geomembrane liner can be minimized, but not completely eliminated, by implementing construction quality assurance (CQA) programs.

Leakage through defects can be minimized by installing additional liner components (i.e., geosynthetic clay liners [GCLs], compacted clay liners [CCLs]). Federal and state agencies that oversee the dams in the United States have been resistant to the use of geomembranes in dams because these are relatively new materials and concerns have been raised regarding their long-term performance in the field. Some

states require that a secondary compacted clay liner be installed beneath the geomembrane to ensure a watertight barrier when a geomembrane is being used to line a dam. However, the use of additional liners is not expected to eliminate leakage through the lining system. For GCLs, the presence of a defect may result in the loss of bentonite, which could make the liner less effective. For CCLs, the leakage through a defect could result in piping and loss of fines.

Previous studies have been conducted to determine the leakage rate through the liner and the factors affecting that flow rate. The majority of these studies have only considered leakage through defects in geomembrane landfill liners (i.e., systems with low heads). However, these studies have included assessments of the different variables that affect the leakage rate and the characteristics of flow through a geomembrane liner. Such variables include size and shape of defect, type and thickness of geomembrane, hydraulic conductivity of the underlying soil layer, thickness of the underlying soil layer, applied effective stress (overburden), and hydraulic head, albeit low heads have only been considered.

Characteristics that need to be established in order to predict the flow through a defect in a geomembrane include transmissivity of the interface and radius of wetted area. A schematic of the fluid flow through a defect for two particular cases is shown in Figure 1.1. As shown in the figure, water flows through the defect with negligible head loss, as long as the defect has a larger diameter than the thickness of the geomembrane (Giroud and Bonaparte 1989). Flow then occurs across the interface and infiltrates into the underlying soil layer (Figure 1b) (Brown et al. 1987). If the contact between the geomembrane and soil layer is perfect (no gaps), then flow occurs only into the soil layer (Figure 1a). However, a perfect contact should not be expected in field projects. For example, wrinkles may form in the geomembrane due to heat and equipment leaves

tracks and indentations in the soil. The magnitude of the interface gap was found to be correlated with the size of the soil particles (Brown et al. 1987), and therefore, gap thickness depends on the hydraulic conductivity of the underlying soil. These factors influence the quality of the contact between the soil and the geomembrane.

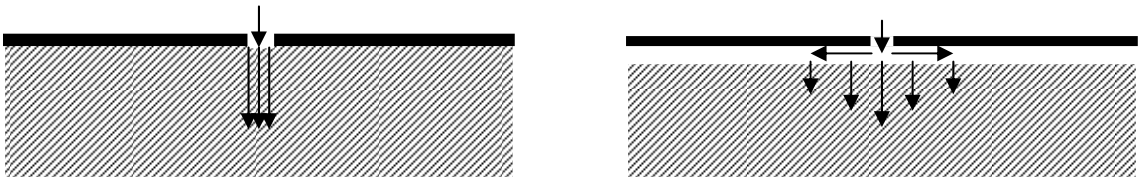

a) b)

Figure 1.1: Fluid flow through a geomembrane defect: (a) with perfect interface contact and (b) with imperfect interface contact (gap)

Transmissivity of the interface between the geomembrane liner and underlying material (e.g., soil, GCL) is the product of the interface gap thickness and the hydraulic conductivity of the interface, with units of $[L^2/T]$. The application of effective stresses on the geomembrane has been shown to decrease the gap thickness (Brown et al. 1987; Barroso et al. 2006). A reduction in the interface gap thickness would also reduce the transmissivity, which ultimately leads to a decrease in the leakage rate through the lining system (Brown et al. 1987). According to previous studies (Rowe 1998; Touze-Foltz et al. 1999), the radius of wetted area is defined as the radius within which the flow occurs. The definition of the radius of wetted area is based on the assumption that the flow is axisymmetric, radiating out from the defect, and the transmissivity is uniform across the interface. The radius of wetted area is a function of the transmissivity of the interface, the hydraulic head, the hydraulic conductivity of the underlying material, and the area of the defect (Rowe 1998; Touze-Foltz et al. 1999).

1.2 OBJECTIVES OF THIS STUDY

The overall objective of this study is to quantify the leakage through defects in geomembrane lining systems and to evaluate the implications of that leakage on the performance of dams. Experimental, analytical and numerical analyses were conducted as part of this investigation. The experimental component was conducted to quantify the leakage rate through a defect in a geomembrane over a soil layer for two different soils and a range of hydraulic heads, initial moisture conditions, and initial dry unit weights. The analytical component was conducted to evaluate the transmissivity at the interface and radius of wetted area for the tests conducted as part of the experimental component. Finally, the numerical component was carried out to investigate the characteristics of flow through defects in a geomembrane liner for conditions beyond those evaluated in the experimental component of this study. Also, the numerical component includes an evaluation of leakage through defects in a geomembrane liner placed on the upstream face of a dam. The laboratory tests and subsequent analyses were used to develop a set of tools (i.e., empirical models, design recommendations, etc.) that will assist engineers in the design of geomembrane lining systems for dams. Also, potential benefits from the use of geomembrane liners (e.g., improvement in global stability) were identified and evaluated. This study is expected to lead to a better understanding of the performance of geomembranes as dam liners.

The specific objectives for the research program were to:

- Provide a database of experimental results that quantify the leakage rates through geomembrane defects for the case of hydraulic heads that are representative of dams.
- Evaluate the interface transmissivity between the geomembrane and underlying material and investigate the concept of radius of wetted area.

- Determine the validity of current equations used to predict leakage through defect in a geomembrane under high heads and develop predictive tools to estimate leakage through defects in a geomembrane liner under high hydraulic heads.
- Assess the effect of defect size, frequency and location on the pore pressures within a dam with a geomembrane liner on the upstream face and evaluate the implications of leakage through defects on the stability of an embankment dam.

1.3 DISSERTATION OUTLINE

This dissertation is organized into seven chapters. After this introductory chapter, the background information regarding geosynthetics and geosynthetic lining systems is detailed in Chapter 2. Also included in Chapter 2 is a literature review of previous studies conducted to investigate leakage through defects in geomembrane liners.

The materials used for the experimental program are presented in Chapter 3. This includes two types of soil and a variety of geosynthetics. Also discussed in Chapter 3 is a description of the testing equipment used for the experimental program and the specimen preparation procedures.

The results of the experimental program and interpretation of the results are presented in Chapters 4 through 6. Specifically, the results and analysis for tests involving a geomembrane liner over a layer of sand are presented in Chapter 4. The results and analysis for tests involving a geomembrane liner over a compacted clay liner are presented in Chapter 5. Chapter 6 includes the results and analysis for tests involving a geomembrane liner over GCLs. Also included in Chapters 5 and 6 are proposed equations that may be used to estimate leakage through defects in a geomembrane lining system for a dam.

Numerical simulation of leakage through defects in geomembrane lining systems was performed using finite elements. The results of these analyses are presented in

Chapter 7. Numerical simulations were conducted to simulate the experimental setup and subsequently compare numerical results with the experimental data. Two-dimensional and three-dimensional simulations of dams designed with a geomembrane liner were performed to determine the implications on their performance of leakage through defects in geomembrane liners.

A summary of the conclusions drawn from the work presented in this dissertation is presented in Chapter 8. A list of recommendations for future work in this area is also included in Chapter 8.

Chapter 2: Geosynthetic Lining Systems

2.1 INTRODUCTION

Geomembranes have been used for the lining of dams since 1959, beginning in Europe (Sembenelli and Rodriguez 1996) and Canada (Lacroix 1984). Specifically, these polymeric sheets have been used as a hydraulic barrier on the upstream face in roller-compacted concrete dams, to retrofit masonry and concrete dams, and as the main impervious layer in fill dams. A major concern regarding the use of geomembranes in dams is their vulnerability to damage during installation and throughout the service life of the dam. Damage to the geomembrane impacts the effectiveness of the liner as an infiltration barrier, resulting in leakage through the geomembrane liner and into the body of the dam.

Studies have been conducted in the past to quantify leakage through defects in geomembrane liners. These studies are the basis for the research presented herein. However, previous studies were conducted to better understand leakage through defects in structures other than dams, namely landfill liners. For example, current formulations assist engineers in the sizing of the leak detection systems as part of the design of landfill liner systems. Unlike dams, landfill liners are exposed to leachate rather than just water and the height of fluid is required by federal law not to exceed 0.3 m. Several of the studies that were conducted on leakage through landfill liners evaluated worst-case scenarios for up to 3 m of leachate, which are still considerably below the water heads of most dams.

2.2 GEOSYNTHETIC DAM LINING SYSTEMS

Geomembranes have been used as dam liners since 1959. Two dams were constructed virtually simultaneously with geomembrane liners: Terzaghi Dam in Canada and Contrada Sabetta Dam in Italy (Lacroix 1984; Sembenelli and Rodriguez 1996). Both dams are still in operation and the geomembrane liners are performing well. Since 1959, there have been an increasing number of projects in which geomembranes were selected for use in dams. This includes the use of geomembranes either as part of a rehabilitation program for an old, deteriorating dam or as part of the primary hydraulic barrier in newly constructed dams.

2.2.1 Geosynthetics

Geosynthetics are defined as planar, polymeric materials that are used in combination with geotechnical materials (e.g., soil, rock, etc.) in civil engineering applications (IGS 2000). Specific types of geosynthetics include geomembranes, geotextiles, geonets, and geogrids. These materials have been used to perform a variety of functions in transportation, water resources, environmental and geotechnical engineering projects.

Functions that geosynthetics can perform include hydraulic barriers, filtration/separation, reinforcement, or in-plane drainage. For some projects, geosynthetics can be cost-effective alternatives to the use of soil, due to savings in both material costs and construction time,.

In dams, geogrids have been used as reinforcement for the foundation and as reinforcement for the fill of the dam. Also, geotextiles have been used as the filter component of the blanket and chimney drains. Geomembranes have been used as hydraulic barriers installed on the upstream face of a dam or inside the dam at the core. When using geomembranes, nonwoven geotextiles have often been used as protection

layers, by providing a cushion that prevents the puncturing of a liner by sharp or protruding objects. Geotextiles have also been used as the drainage components behind the geomembrane. In certain designs involving geomembranes, a drainage layer has been placed under the geomembrane to maintain equilibrium in the lining system in case of a rapid drawdown and prevents a build-up of pressure.

2.2.1.1 Geomembranes

A geomembrane is defined as a very low-permeability synthetic membrane liner or barrier used with any geotechnical engineering-related material so as to control fluid migration in a human-made project, structure or system (ASTM D 4439). Geomembranes are rather thin and can be either polymeric or bituminous in nature. Intact geomembranes (i.e., without defects) are practically impervious to liquid flow. The permeability of geomembranes is measured using water-vapor transmission tests and ranges from 10^{-12} to 10^{-15} m/s, which is significantly smaller than the hydraulic conductivity of most soils (Koerner 1998). Because of the low hydraulic conductivity of intact geomembranes, the main mechanism of water infiltration involves flow through defects.

Each polymer resin can provide different benefits for the performance of a geomembrane liner. For example, polyvinyl chloride (PVC) geomembranes are more flexible than high density polyethylene (HDPE) geomembranes. However, HDPE geomembranes are more resistant to degradation, such as that caused by ultraviolet (UV) radiation. There are two types of polymers: thermosets and thermoplastics. Additives, such as carbon black, improve UV resistance of the material, which can increase the service lifetime of exposed geomembranes.

Exposed geomembranes are easier to repair or replace, but exposure leaves the material vulnerable to damage from debris in the reservoir and UV degradation. Yet

additives have greatly improved resistance to this type of degradation. Covered geomembranes are less vulnerable to damage and degradation from the elements; however, repairs on the liner are difficult, and more expensive, to make since the cover material must be removed to access the geomembrane. Also, cover materials can puncture the geomembrane during installation.

2.2.2 Inventory of Dams

2.2.2.1 National Inventory of Dams

According to the National Inventory of Dams [NID {2005)], there are over 79,000 dams in the United States. The NID is a database of dams in U.S. maintained by the United States Army Corps of Engineers (USACE) with the help of state and federal agencies such as Association of State Dam Safety Officials (ASDSO) and the Federal Emergency Management Agency (FEMA). In 1999, the NID was posted on the internet for the first time (http://crunch.tec.army.mil/nidpublic/webpages/nid.cfm), and the most recent update to the database conducted by the USACE was published on the internet in 2005.

The database contains large amounts of information for each dam, including name, location, owner, year built, type of dam (e.g., rockfill, arch), purpose (e.g., irrigation, water supply), dam height, reservoir information (e.g., storage capacity), and the downstream hazard potential. Of particular interest for this study are earthfill and/or rockfill dams that have a height greater than 7 m. Also contained in the NID is information regarding the core of the dam, specifically identification of the waterproofing material and its position in the dam. This includes information regarding the presence of a geomembrane as the watertight element.

According to NID (2005), over 85% of the dams in the U.S. are earthfill and/or rockfill dams. 60% of those are taller than 7 m. Only 16 of the over 38,000 earthfill and rockfill dams over 7 m in height are reported to have a plastic "watertight member." All of these reported dams have the geomembrane installed on the upstream face of the dam. There are a large number of dams in the NID for which the makeup of the core of the dam is not reported, possibly because it is unknown. As a result, it is possible that the number of dams in the US with "plastic" waterproofing exceeds 16, but the exact number is not known at this time.

2.2.2.2 ICOLD Bulletin

Koerner and Wilkes (2007) summarized an updated version of the International Commission on Large Dams (ICOLD) Bulletin 78, which was originally released in 1991, on the use of geomembranes in dams worldwide. The revised Bulletin is a state-of-the-practice report and contains information on 250 dams from all around the world that are lined with geomembranes. The information in the ICOLD Bulletin includes the location of each dam. The number of dams, in percentages, located in various regions around the world is shown in Figure 2.1. Almost half of the 250 dams included in the survey for the ICOLD Bulletin are located in Europe, whereas only 38 geomembrane-lined dams are located in the United States. According to Koerner and Wilkes (2007), almost 65% (or 162) of these 250 lined dams are either earthfill or rockfill dams that have heights up to 110 m. Only 21 of the geomembrane-lined earthfill or rockfill dams over 7 m in height reported in the ICOLD Bulletin are located in the U.S. Surprisingly, the 16 geomembrane-lined dams reported in the NID (2005) are not among the dams cited in the ICOLD Bulletin. However, there were a large number of dams in the NID that did not have the watertight member reported and the dams reported in the ICOLD Bulletin were

among those. This brings to 37 the total of earthfill and rockfill dams that exceed 7 m in height with geomembrane liners in the United States.

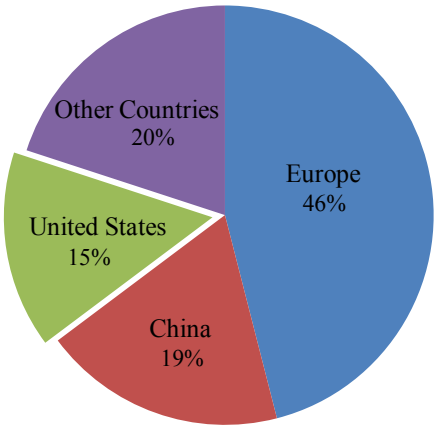

Figure 2.1: Locations for geomembrane-lined dams (after Koerner and Wilkes 2007)

Geomembrane liners have been installed during construction or as part of a rehabilitation project, and have been placed on the upstream face or inside the dam as part of the core. Schematics of dams that have geomembrane liners installed on the upstream face and inside the dam itself are shown in Figure 2.2. As shown in Figures 2.2a and 2.2b, a geomembrane installed on the upstream face can either be covered or left exposed. Figures 2.2c and 2.2d illustrate two different configurations that have been used for the installation of a geomembrane in the core of a dam. The schematic views shown in Figure 2.2 are just a few of the many configurations that have been used in the past for the installation of a geomembrane lining system for a fill dam.

Details specifying the positioning of the geomembrane and when it was installed for the 162 earthfill and rockfill dams included in the ICOLD Bulletin are listed in Table 2.1. The majority of the fill dams that have an internal geomembrane are located in China (Koerner and Wilkes 2007). Most of the dams in the U.S. reported in the ICOLD

Bulletin and the NID (2005) have geomembranes located on the upstream face of the dam.

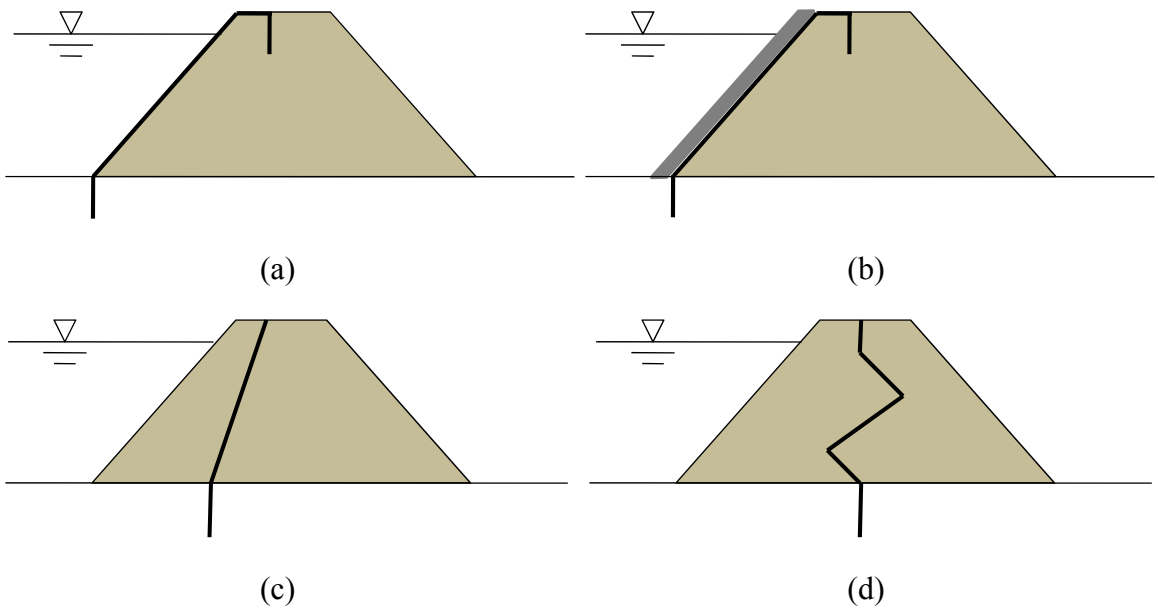

Figure 2.2: Schematic views of typical configurations for the geomembrane liners: a) exposed on upstream face, b) covered on upstream face, c) internal inclined and d) internal zig-zag

Table 2.1: Positioning of geomembrane liners used in fill dams worldwide (Koerner and Wilkes 2007)

Construction Timing	Upstream Exposed	Upstream Covered	Internal	Total
New Construction	14	49	14	77
Rehabilitation	20	31	4	55
Unknown	10	20	0	30
Total	44	100	18	162

The most common type of polymeric geomembrane used to line dams (over 60%) is PVC, as shown in Table 2.2. As discussed in Section 2.2, PVC geomembranes are more flexible than other available geomembranes, which allows the liner to deform with

the dam minimizing the risk of tearing or puncturing. Polyethylene resins, such as linear low-density polyethylene (LLDPE) and HDPE, are also popular choices for lining dams. All 250 dams reported in the ICOLD Bulletin are included in Table 2.2.

Table 2.2: Types of geomembranes used in dams (After Koerner and Wilkes 2007)

GM type	Basic Material	Abbreviation	Total Dams			Percentage (%)
			Exposed	Covered	Total	
Polymeric	Polyvinyl Chloride	PVC	73	70	143	60.3
Polymeric	Linear Low Density Polyethylene	LLDPE	0	28	28	11.8
Polymeric	High Density Polyethylene	HDPE	2	11	13	5.5
Polymeric	Chlorosulphonated polyethylene	CSPE	3	5	8	3.4
Polymeric	Other		8	16	24	10.1
Bituminous	Various		10	11	21	8.9
Total known*					237	100

*The remaining 13 dams in the total survey are of mixed types.

For fill dams, ICOLD (2007) recommends placing a geotextile or other drainage layer behind the liner to collect any leakage that permeates through the geomembrane and prevents a build-up of pressure behind the liner, regardless whether the liner is exposed or covered. The drainage layer also acts as a filter zone for the dam, necessary for fill dams where the supporting layer has a lower hydraulic conductivity than the fill material.

2.2.3 Case Histories

Four case histories involving dam construction projects in which geomembrane lining systems were installed, either on the upstream face or in the core, were selected for discussion in this section. Two cases, Zhushou Dam and Jibiya Dam, involve the use of a geomembrane liner in a dam constructed using less than ideal soil materials. The other

two cases, Mission Dam and Idaho Springs Dam, involve the use of a composite liner system consisting of a geomembrane and a secondary liner (e.g., GCL). These cases provide good examples of projects that would require quantification of leakage as part of their design.

2.2.3.1 Zhushou Dam (China)

As shown in Table 2.1, the majority of geomembrane liners have been installed on the upstream face of the dam, minimizing water infiltration into the dam. However, geomembranes have also been used in place of, or in addition to, clay or other soil of low hydraulic conductivity that is often used in the core of a dam.

Tao et al. (2002) presented a case involving the use of a geosynthetic composite layer in the interior of a dam. The Zhushou Reservoir is located in SiChuan Province, China. The reservoir is confined by a 60.5 m high rockfill dam with a clay core and a grout curtain. The cross-section of the dam, along with results of the study conducted by the authors, is shown in Figure 2.3. The results of the study are not the purpose of including the figure. Of particular interest in Figure 2.3 is the location of the geosynthetic lining system. During construction, there was a shortage of the gravelly clay that had been selected as the core wall material. As shown in Figure 2.3, a geotextile-geomembrane composite was then installed on the upstream side of the core wall as an impervious layer. Also, a geotextile was placed as a filter on the downstream side of the core because it was more cost-effective than using soil in terms of material and installation costs.

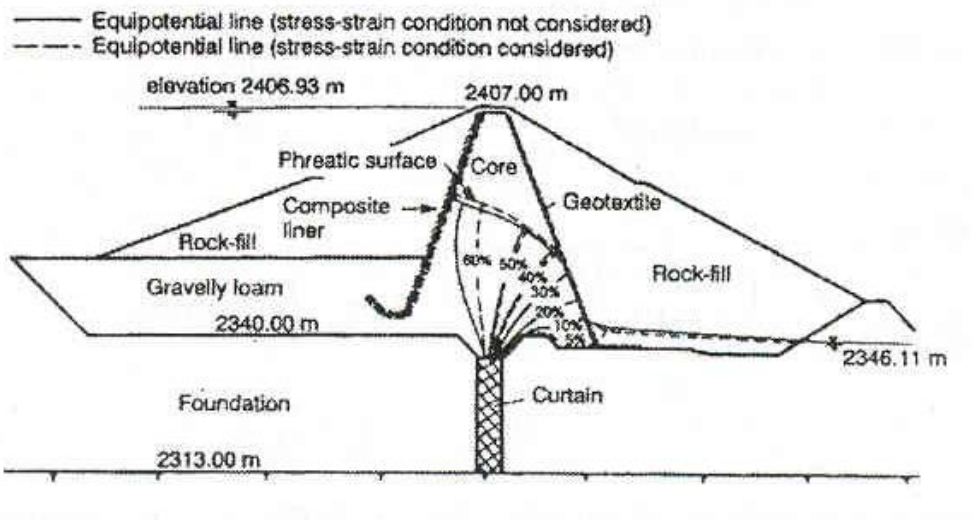

Figure 2.3: Cross-section of Zhushou Dam (Tau et al. 2002)

2.2.3.2 Jibiya Dam (Nigeria)

Sembenelli (1990) reports the case of a dam in which the soils that were available at the site had a high hydraulic conductivity and were inappropriate for use as the core material for the dam. Consequently, a geomembrane liner was used as the waterproofing element. Jibiya Dam is a 23.5 m high embankment dam that was constructed in 1989 in Nigeria, Africa. A cross-section of the upstream face of the dam is shown in Figure 2.4. The foundation soils included sands with a high hydraulic conductivity. Also, the soil at the abutments had the potential for collapsing when wet. The embankment dam was constructed entirely using the local sands. A continuous, flexible impervious liner placed on the upstream face of the dam was selected because of the possibility of uncontrolled, differential settlements, the susceptibility of erosion of the embankment, and the high hydraulic conductivity of the fill. The lining system selected after a thorough investigation of the available materials was a 2.1 mm thick PVC geomembrane with a nonwoven polyester geotextile. As shown in Figure 2.4, the geocomposite liner was covered with concrete slabs as protection against damage during operation.

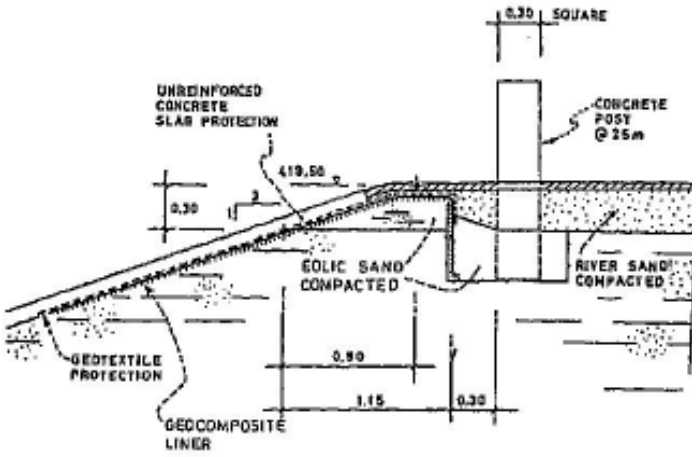

Figure 2.4: Cross-section of the upstream face of Jibiya Dam (Sembenelli 1990)

2.2.3.3 Terzaghi Dam (Canada)

Terzaghi Dam, originally known as Mission Dam, is located in British Columbia, Canada. This 52 m high earth and rockfill dam was constructed in 1960 and included a geomembrane installed on the upstream face of the dam (Lacroix 1984). A cross-section of the dam is shown in Figure 2.5.

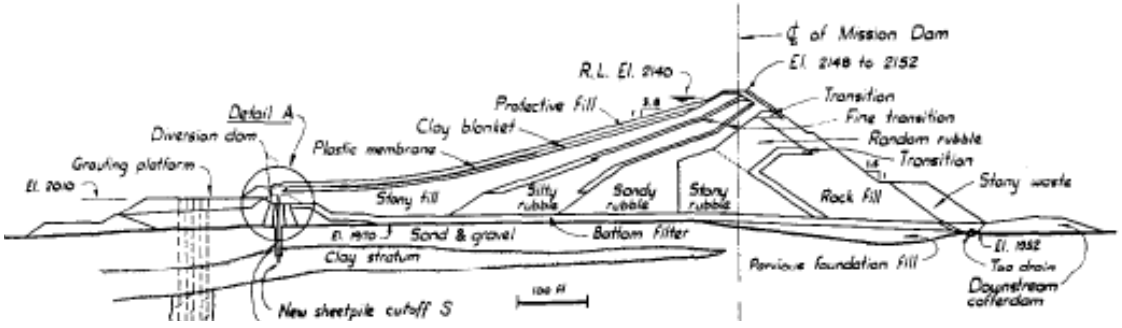

Figure 2.5: Cross-section of Mission Dam (Terzaghi and Lacroix 1964)

A polyvinyl chloride (PVC) geomembrane was placed over a 1.5 m-thick clay layer that covered a stony till and was covered with a protective layer of rubble (Terzaghi and Lacroix 1964). The purpose of the geomembrane liner was to apply an even pressure

over the entire surface of the clay layer and to prevent cracking in the clay layer. Cracking of the clay could decrease the effectiveness of the clay layer at minimizing the seepage through the dam. The polymeric material was selected because it was flexible enough to move with deformations of the dam, strong enough to resist tearing due to the deformations, and the impermeability of the material. Defects were found in the geomembrane during construction, despite precautions taken to prevent damage to the liner during installation. The damages were repaired using patches. Inspections of the geomembrane were conducted at various times during the operation of the dam. Sinkholes formed in the clay layer and, while the geomembrane deformed with the upstream facing of the dam, sometimes the strains became too large and the geomembrane ruptured (Lacroix 1984). An example of one of the sinkholes is shown in Figure 2.6. Strains of 160% were observed in the geomembrane at the location of that sinkhole. Nonetheless, the geomembrane liner performed as expected by minimizing the cracking of the clay layer, maintaining integrity of the clay layer, and minimizing seepage through the dam.

Figure 2.6: Sinkhole on upstream face of Terzaghi Dam (Lacroix 1984)

2.2.3.4 Idaho Springs Dam (Colorado)

Idaho Springs Dam, located in central Colorado, is an earth dam constructed in 1978 (NID 2005). The dam was built to control flooding and provide local water supply. In the year 2000, significant seepage was observed from the downstream face of the dam embankments in five different locations (Figure 2.7). The seepage problems were attributed to deterioration of the dam. Consequently, a rehabilitation project was undertaken to improve the long-term dam performance (Olsta and Carine 2005).

According to Olsta and Carine (2005), the plan originally selected to fix the seepage problem in the dam included sealing the leaks using concrete, installing drains at the downstream toe and applying asphalt grouting to the dam face. However, once the dam facing had been exposed, evidence of piping was observed and the voids were larger than expected. Accordingly, an alternative design was adopted to repair the dam. This involved the installation of a geosynthetic lining system that included a geosynthetic clay

liner (GCL). The GCL selected for the rehabilitation project consisted of a powdered bentonite core sandwiched between two carrier geotextiles. A 0.5 mm geomembrane was laminated to the outer surface of the GCL. The lining system was installed on the upstream face of the dam along with a soil and rip-rap cover placed over the liner. The project was completed in 2001, and currently, no evidence of seepage on the downstream face has been observed since its completion.

Figure 2.7: Evidence of seepage at the downstream toe of Idaho Springs Dam prior to rehabilitation (Olsta and Carine 2005)

2.2.4 Reasons for Use of Geosynthetic Lining Systems in Dams

Some earth dams are constructed as part of flood management systems and only retain water during heavy rainfall events. The effectiveness of the dam to retain the water

in the reservoir is hindered if the clay barrier is exposed. Specifically, the embankments are susceptible to desiccation cracking that, once the reservoir fills up with water, would lead to an increase in the hydraulic conductivity of the soil. A geomembrane liner placed on the upstream face of an embankment dam would minimize desiccation as well as maintain the hydraulic barrier throughout the various seasons.

A common problem during construction of a dam is the shortage of specified low-hydraulic conductivity material available at or near the construction site. Hauling of the appropriate material often leads to a significant increase in the project costs (Tau et al. 2002; Sembenelli 1990). Geomembranes have been used in these situations as the hydraulic barrier either installed on the upstream face or inside the dam as part of the core. The geosynthetic liners provided a cost-effective alternative and allowed the readily-available material to be used.

Deterioration of an embankment over time can occur and factors into the life of a dam. Geomembrane liners are a cost-effective solution that can be used to inhibit deterioration processes in existing dams as well as to prevent the onset of seepage-induced degradation in new dams. By installing a geosynthetic lining system on the upstream face, degradation of the soil on the downstream side can be minimized and stability is maintained.

Under the federal guidelines for landfill design, geomembranes are required components of the liner system. Since defects are practically unavoidable in the field, synthetic liners are paired with a compacted clay liner (CCL) or geosynthetic clay liner (GCL) to minimize the amount of liquid that permeates through the bottom of a landfill, thus minimizing the potential for environmental contamination. A composite lining system installed on a dam could reduce the leakage through a defect in the geomembrane component in much the same way as a composite liner in a landfill, except the heads are

higher for dams. This concept was demonstrated in the Idaho Springs Dam project presented in Section 2.2.3.4.

2.3 LEAKAGE THROUGH GEOSYNTHETIC LINING SYSTEMS

Many studies, experimental and analytical, have been conducted to estimate the leakage rate through defects in geomembrane liners. All but one of these studies, a study conducted by Fukuoka (1986), considered hydraulic heads well below those imposed on typical dams during their operation. Consequently, available analytical and empirical models that can be used to estimate leakage through defects were developed for conditions representative of landfill liners. The existing models may not be appropriate for use with lining systems under high hydraulic heads.

2.3.1 Defects in Geomembrane Liners

As stated previously, intact geomembranes are relatively impermeable; however, because geomembranes are so thin, damage to the liner can occur during installation and throughout the design life of a dam. Thorough construction quality assurance (CQA) can reduce the size and frequency of defects, but the geomembrane is still expected to have holes that will allow water to infiltrate into the body of the dam. For design purposes, it is important to assume conservative yet realistic values for the size and frequency of defects that will occur in the field. The expected size and frequency of defects will determine how much leakage will occur through a geomembrane liner. Studies have been conducted using various leak detection methods to determine the average size and frequency of defects in landfill liners and holding ponds (Giroud and Bonaparte 1989; Nosko and Touze-Foltz 2000). However, studies on the frequency and defects in geomembrane liners for dams are not currently available. Nonetheless, landfills and ponds have slopes that are analogous to the embankments of earth dams. Nosko and

Touze-Foltz (2000) conducted a study that identified the location and the size of defects and investigated the mechanisms responsible for the damages.

Nosko and Touze-Foltz (2000) used an electrical damage detection system to evaluate the size, location and cause of damage during installation of geomembrane liners for over 300 landfill sites (more than 3,250,000 m^2). On the side slopes, the most common form of damage was reported to be punctures caused by underlying stones, although imperfect welds and construction equipment also created numerous defects in the geomembrane. The majority of the defects ranged in size from 0.5 to 10 cm^2 (equivalent to defect diameters of 0.8 to 3.6 cm). Overall, there were 4,194 defects detected, which translates to approximately one defect per 800 m^2. Of course, this approximation of defect frequency is before CQA is performed and repairs made to the geomembrane, which would reduce the number and size of defects. However, there is a limit to the size of defect that can be detected, thus CQA may not eliminate the presence of defects. Defects can also develop after completion of construction. Nonetheless, using a frequency of one defect per 800 m^2 would yield conservative predictions of the leakage rate through a geomembrane liner.

Giroud and Bonaparte (1989) presented field data regarding defect size and frequency that were obtained from construction quality assurance and control (CQA and CQC) programs and forensic analysis for landfills and surface impoundments. Typical causes of defects in geomembranes include, but are not limited to, discontinuous seams, seam failures, damage inflicted by construction equipment, and puncturing by stones that compose the lining system. The frequency of seam defects in a geomembrane liner without CQA was reported to be about one defect for every 10 m of field seam. This is reduced to an average of one defect every 300 m of field seam with good CQA. The authors recommend using a frequency of one defect for every 4000 m^2 of geomembrane

for design. At the time of this study, there was not enough documentation regarding defect size, but Giroud and Bonaparte (1989) recommend using a defect area of 1 cm^2 for calculations used to size components of the lining system, such as the leakage collection system, and using a defect area of 3.1 mm^2 for predictions aimed at defining the performance of the liner under typical operating conditions.

2.3.2 Experimental Programs

Experimental testing programs to evaluate leakage through defects in geomembranes were initially conducted by Fukuoka (1986) and Brown et al. (1987). Fukuoka (1986) conducted large-scale permeameter tests to investigate leakage through defects in a reservoir liner for heads up to 40 m. Brown et al. (1987) conducted smaller permeameter tests to measure leakage rates through defects for landfill liners for heads up to 1 m. The authors of both studies recognized the presence of a gap between the geomembrane and the soil layer beneath and that flow occurred laterally along that interface as well as into the soil layer. Subsequent experimental studies have been conducted to measure leakage rates through defects in geomembranes placed over a variety of materials: gravel (Benson et al. 1995), fine sand (Walton et al. 1997), clay with field-quality soil surface (Cartaud et al. 2005), and GCL over a clay layer (Barroso et al. 2006). Each of these studies made an important contribution to the understanding of the flow through defects in geomembrane liners. However, the applicability of these studies cannot be extrapolated to the case of dams, as these studies were all conducted for conditions typical of landfill liners.

2.3.2.1 Fukuoka (1986)

Most relevant to the research presented herein is the experimental study conducted by Fukuoka (1986) because the study included heads higher than 10 m. The

author conducted tests for the design of a lining system for a reservoir with continuously fluctuating water levels, ranging from 13 m to 40 m. A 1.5 m diameter permeameter, shown in Figure 2.8, was used for the experimental study. The large permeameter consisted of two portions: the upper part of the permeameter contained the water under pressure applied to the geomembrane while the lower portion of the tank contained a soil layer. The soil layer was 0.5 m thick. The upper tank was partially filled with water and then pressurized to simulate up to 40 m of water head.

A 1-mm thick PVC geomembrane was selected for use in this study and was placed over a soil layer with a hydraulic conductivity of approximately 10^{-7} m/s. Two types of defects in the PVC geomembrane were evaluated in this study: round holes (simulating punctures) and cuts (simulating long seam defects). Defect diameters that were tested ranged from 2 mm to 100 mm, and cut lengths from 20 mm to 100 mm long were tested. The soil used in this study was a cohesive soil with gravel. An underlying 5-cm thick sand layer was used to collect the effluent from the system. The effluent was measured over time to determine the leakage rate. Piezometers were placed in the soil layer to measure the pore pressures in the soil layer during the tests. Tests were conducted with and without a non-woven geotextile between the geomembrane and soil layer. The use of a geotextile was proposed in order to protect the geomembrane from puncture by the gravelly subgrade.

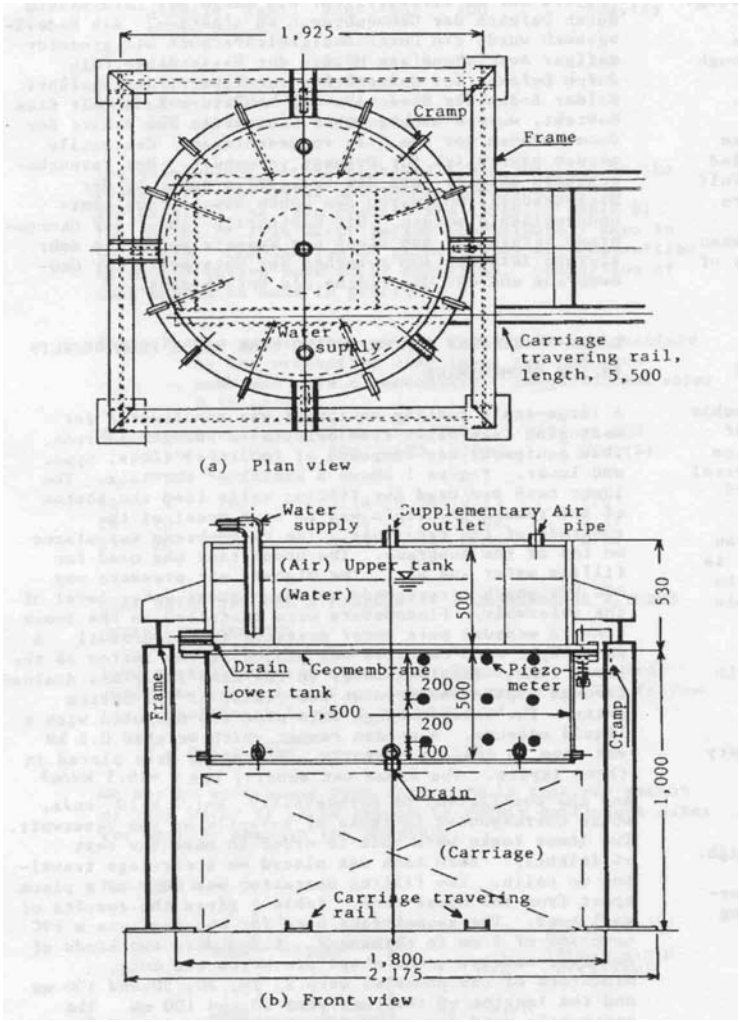

Figure 2.8: Schematic view of the tank used in the experimental tests conducted by Fukuoka (1986)

Fukuoka (1986) observed that leakage rates through the lining system without the geotextile were larger than the leakage rates through the lining system with the geotextile. This outcome was contrary to the expected trend from these tests. The author's explanation of the smaller leakage rates from lining systems with a geotextile beneath the geomembrane was that the geotextile compressed when using high hydraulic heads, effectively reducing its in-plane flow capacity. This led to a reduction in the leakage through the defect in the geomembrane. Fukuoka (1986) also found that leakage rates

increased by two orders of magnitude when the surface of the underlying soil layer contained gravel. The presence of gravel at the interface between the geomembrane and the soil layer increased the gap thickness, which increased the transmissivity of the interface.

The experimental study conducted by Fukuoka (1986) only considered two water heights (13 and 40 m) and only one type of soil (gravelly clay). However, these tests were conducted for a specific site with a gravelly clay soil and for a specific project of a reservoir with a fluctuating water level. Since the soil at the site contained gravel, the tests included a geotextile as a cushion layer for the protection of the geomembrane. Fukuoka (1986) focused on the transmissivity of the geotextile at the interface rather than the transmissivity of the interface between the geomembrane and the underlying soil layer (i.e., without a geotextile). Studies have not been conducted to evaluate the transmissivity between a geomembrane liner and a soil layer under high hydraulic heads.

2.3.2.2 Brown et al. (1987)

Brown et al. (1987) conducted permeameter tests to measure the leakage rate through the defect in geomembranes over soil for conditions representative of landfill liners (heads less than 0.3 m). The objective of this study was to understand the mechanisms of leakage through a defect and to determine what parameters most affected the leakage rate. The parameters that were varied during the experimentation were the head of liquid above the liner, the hydraulic conductivity of the subgrade, the size and shape of the defect, and the type and thickness of the geomembrane. The flow rate out of the cell was monitored throughout the duration of the tests.

Brown et al. (1987) tested a wide range of polymer types and thicknesses to determine if the geomembrane characteristics affected the leakage rate. The tested geomembranes included round holes drilled into the material, slits cut into the material,

and gaps in a seam. These variations in defects were used to determine how the defect shape and size affected the leakage rate. A range of hydraulic heads was applied to the lining systems to determine how the water level affects the leakage rate through a defect. The highest pressure that was applied to the permeameter cell (through the use of a pressure vessel) was equivalent to 1 m of water. The effect of soil hydraulic conductivity was investigated by varying the mix ratio of two different soils: a kaolin clay mixed with washed sand (hydraulic conductivity of approximately $5x10^{-9}$ m/s) and a sandy loam (hydraulic conductivity of approximately $2x10^{-6}$ m/s). Results from the experimental study indicated that geomembrane type and thickness did not have a significant effect on the leakage rate. The hydraulic head, hydraulic conductivity of the soil layer beneath the geomembrane and the size and shape of the defects all had significant effects on the leakage rates through the system. However, the interface transmissivity was not affected by the size or shape of the defect.

Brown et al. (1987) also evaluated the presence of a gap at the interface between the geomembrane and compacted soil layer. The authors concluded that water seeping through the defect flowed laterally across the interface while, at the same time, infiltrated into the underlying soil layer. An equivalent gap size was back-calculated, using an analytical model that was developed during the study, by assuming gap widths until the calculated flow rates matched the flow rates measured during the experimental tests. Specific gap thicknesses were correlated to the hydraulic conductivity of the underlying soil (Table 2.3). Brown et al. (1987) used these gap thicknesses to calculate the leakage rates and radii of interface flow using the analytical model developed in their study for a range of heads and defect diameters. An example of the curves resulting from these calculations by Brown et al. (1987) is shown in Figure 2.9. Leakage rates and wetted radius increase linearly with increasing head for larger defect diameters. Leakage rates

and wetted radius increase nonlinearly with increasing head for comparatively small defect diameters.

Table 2.3: Suggested gap widths for field conditions (Brown et al. 1987)

Soil Hydraulic Conductivity (cm/s)	Gap Thickness (mm)
$1x10^{-4}$	0.15
$1x10^{-5}$	0.08
$1x10^{-6}$	0.04
$1x10^{-7}$	0.02

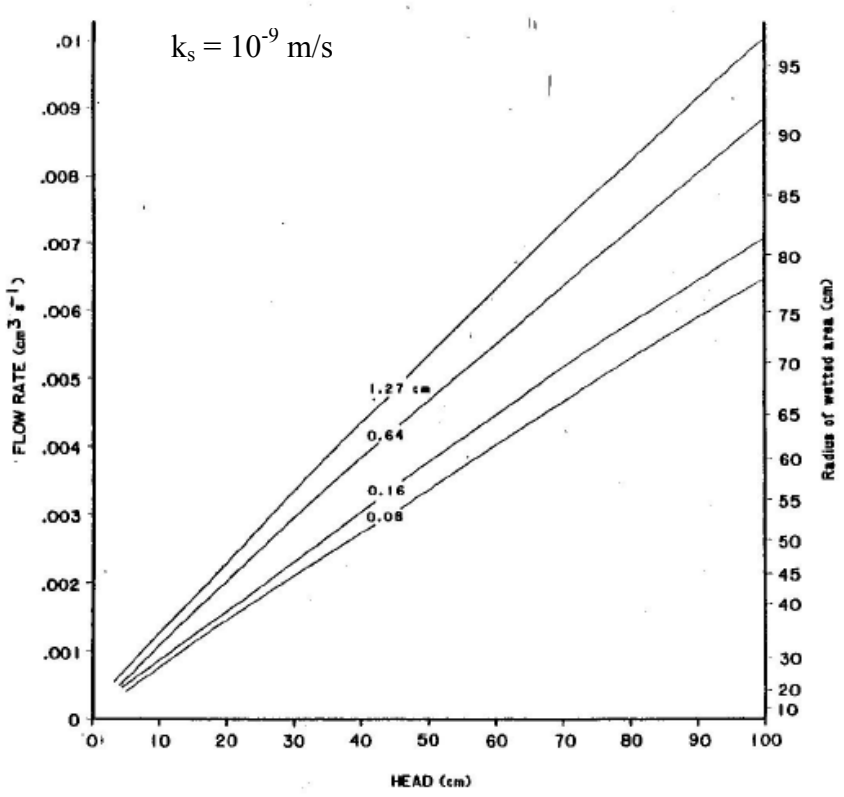

Figure 2.9: Calculated leakage rates and radius of wetted area for a range of defect diameters as a function of hydraulic heads (Brown et al. 1987)

Brown et al. (1987) also conducted several tests under heads of 10 m to evaluate the effect of the higher head on flow through a defect in the geomembrane component of a composite liner. The authors observed evidence of erosion in the form of "parabolic holes" in the surface of the soil layer and a "general compression of the soil." The authors determined that the likelihood for erosion to occur increased for smaller defects and higher heads. However, the density of the compacted clay layer was not reported by Brown et al. (1987). Also, the leakage rates for the tests under higher heads were not reported.

Brown et al. (1987) provided the basis for the research presented herein, both the experimental program and the analysis of the experimental data. However, Brown et al. (1987) did not develop a relationship between head and leakage rate. Also, the head used in the majority of the tests conducted by the authors was significantly below that representative of most earth dams. The research presented in the following chapters will involve heads up to forty times larger than those evaluated by Brown et al. (1987) for landfill conditions.

2.3.2.3 Geomembrane-GCL Tests

Barroso et al. (2006) conducted a series of tests on composite liners consisting of a geomembrane, a GCL and a compacted clay liner (CCL) for landfill conditions (heads less than 3 m). In particular, the authors investigated the effect of GCL prehydration, confining stress and hydraulic head on leakage rates through composite liners that included defects in the geomembrane. The defect used in the tests was a 3-mm circular hole in a 2-mm thick HDPE geomembrane. Small (0.2 m diameter), intermediate (1 m diameter) and large cells (2.2 m square) were used during this study. The small-scale tests were used to evaluate the influence of the aforementioned parameters, as well as the influence of the type of geotextile at the interface between the geomembrane and the

GCL. Also, the impact of the type of bentonite in the GCL on the flow rate through composite liners was evaluated. The larger scale tests were used to validate the small-scale test results and to determine the feasibility of extrapolating laboratory data to field conditions. Hydraulic heads up to 1.2 m of water were applied to the specimens and confining stresses up to 200 kPa were imposed on the lining systems. The flow into the permeameter for each test was monitored over the duration of the test. An example of the flow rates as a function of time for several tests conducted in this study are shown in Figure 2.10. In the early stages of the tests, the flow rates are high but as time passes, the flow rates decrease until a steady rate is achieved.

In France, it is recommended that a GCL be hydrated prior to placing it in service and that the hydration process occurs after overburden stress has been applied. However, Barroso et al. (2006) determined that the effect of GCL prehydration on the leakage rate through composite liners was inconclusive. An increase in effective stress was found to lead to a decrease in the flow rate, whereas an increase in hydraulic head led to an increase in the final flow rates. The leakage rates from the small-scale tests were on the same order of magnitude but slightly higher than those in the large-scale and intermediate-scale tests. Barroso et al. (2006) considered that the results from small-scale tests represent an upper bound of flow rates that would occur in the field, based on the results from the larger scale tests.

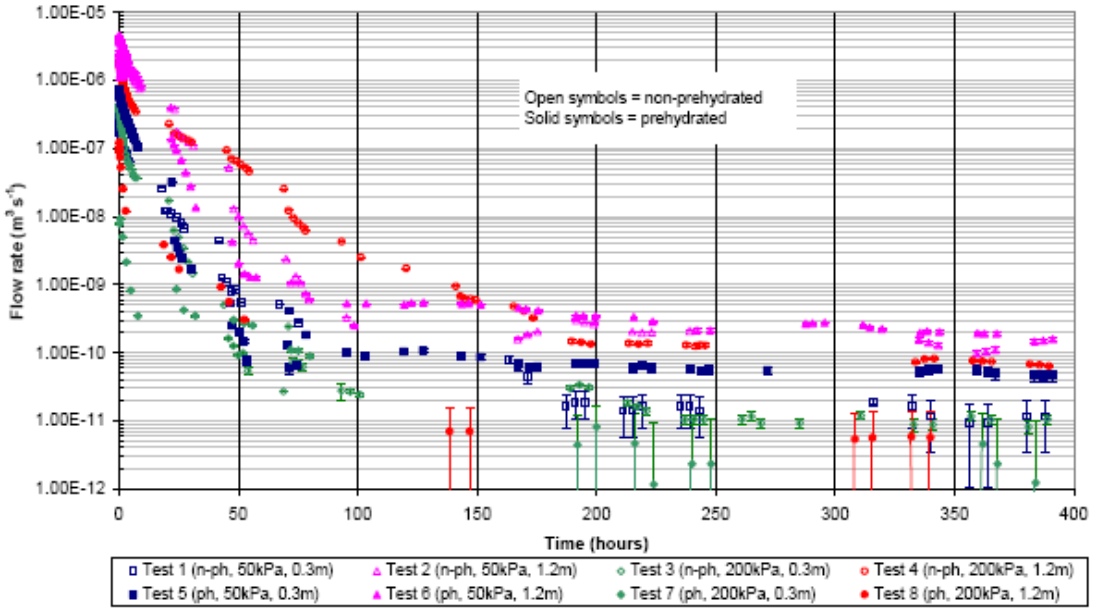

Figure 2.10: Leakage rates for geomembrane-GCL-clay tests (Barroso 2005)

Barroso (2005) used dye to measure the radius of wetted area for tests involving geomembranes, GCLs and CCLs. The dye was added to the system once steady-state flow had been achieved. The dye was used to visualize the flow pathways, or flow patterns, at the interface and the dyed area was measured to obtain the radius of wetted area. Examples of the dyed area observed in this study are shown in Figure 2.11. As shown in the figure, the GCL was marked to designate nine equally-sized areas, which were used to determine the symmetry of the flow at the interface. From the results, the flow at the interface appears to be nonuniform. Also, a nonwoven geotextile at the interface results in a larger wetted area due to the in-plane flow capacity when compared with a woven geotextile.

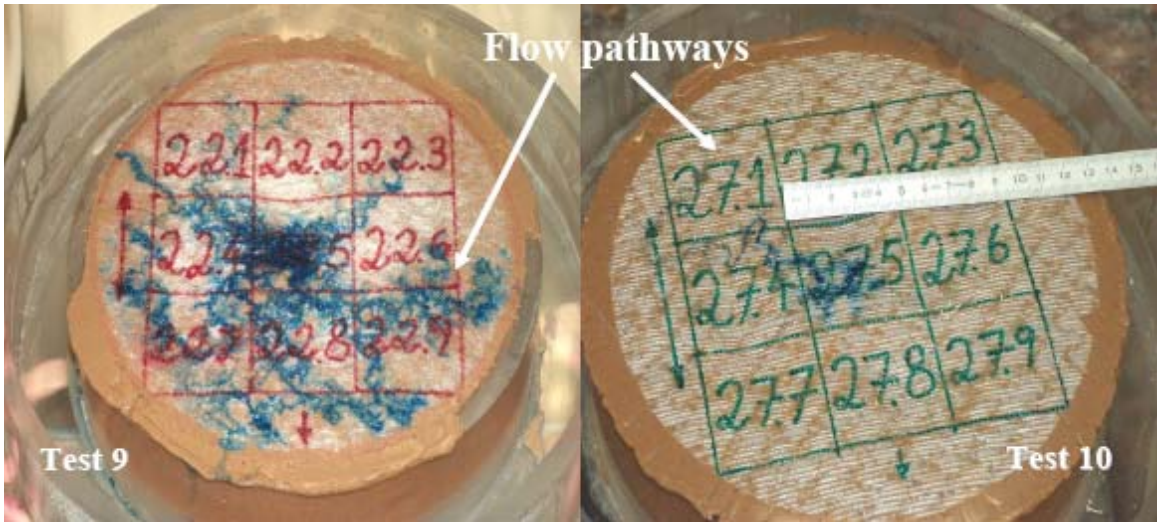

(a) (b)

Figure 2.11: Wetted areas for: a) nonwoven geotextile at interface with the geomembrane and b) woven geotextile at the interface with the geomembrane (Barroso 2005)

Barroso et al. (2006) conducted a thorough investigation of leakage through defects in a composite liner system, but only for heads below 1.2 m. The use of a GCL in a composite liner under high heads has yet to be investigated. While Barroso (2005) used dye to quantify the radius of wetted area and to evaluate the non-uniformity of the interface, the radius of wetted area has not been visualized for composite lining systems under high heads. Dye will be used in the experimental program discussed in later chapters to evaluate the wetted radius for high heads.

2.3.3 Analytical Studies

As mentioned in Section 2.3.2.2, Brown et al. (1987) developed an analytical solution for flow through a flawed geomembrane liner. Giroud and Bonaparte (1989) adapted the equations from Brown et al. (1987) to include the transmissivity of the interface as an additional parameter. Flow across the interface between the

geomembrane and the underlying soil was characterized using Newton's viscosity law and applying it to flow between two smooth, parallel plates. The interface transmissivity can be expressed as:

$$\theta = \frac{\rho g s^3}{12\eta} \tag{2.1}$$

where θ is the transmissivity of the interface [L^2/T], ρ is the density of the liquid, g is the acceleration due to gravity, s is the spacing between the geomembrane and the soil (or gap thickness), and η is the viscosity of the liquid. In cases where a geotextile is placed between the soil and the geomembrane, θ represents the transmissivity of the geotextile:

$$\theta = k_p t_{gt} \tag{2.2}$$

where k_p is the hydraulic conductivity of the geotextile in the planar direction and t_{gt} is the thickness of the geotextile. A common assumption is that the interface spacing is uniform. However, this assumption is invalid if wrinkles are present. Consideration of a non-uniform transmissivity results in complex formulations with many uncertainties, including the variations in gap thickness (Touze-Foltz et al. 2001).

For a given radius r, the total flow through a defect in a geomembrane, Q, equals the radial flow through the interface, Q_r, plus the flow into the soil, Q_s: $Q = Q_r + Q_s$. The radial flow at the interface and in the soil can be expressed using Darcy's Law as follows (Giroud and Bonaparte 1989):

$$Q_r = -kiA = -2\pi r\theta \frac{dh}{dr} \tag{2.3}$$

$$Q_s = kiA = 2k\pi r^2 \frac{h + H_s}{H_s} \tag{2.4}$$

where h is the hydraulic head acting on top of the low-permeability soil, k is the hydraulic conductivity of the soil, and H_s is the thickness of the soil layer. Equations (2.3) and (2.4) can be differentiated to obtain (Giroud and Bonaparte 1989):

$$dQ_r = -2\pi r\theta \left(\frac{1}{r}\frac{dh}{dr} + \frac{d^2h}{dr^2} \right) dr \tag{2.5}$$

$$dQ_s = 2k\pi r \frac{h + H_s}{H_s} dr \tag{2.6}$$

$$dQ_r + dQ_s = 0 \tag{2.7}$$

The flow through the defect, Q, is independent of the radius. Substituting Equations (2.5) and (2.6) into Equation (2.7) leads to (Giroud and Bonaparte 1989):

$$\frac{1}{r}\frac{dh}{dr} + \frac{d^2h}{dr^2} = \frac{k_s}{\theta}\left(1 + \frac{h}{H_s} \right) \tag{2.8}$$

This differential equation can be solved using Modified Bessel functions.

Rowe (1998) presented a general analytical solution for leakage through a composite liner, which was later adapted by Touze-Foltz et al. (1999). The solution can be used to determine leakage through a defect in a geomembrane placed over a low-permeability layer of thickness of H_L, such as a compacted clay liner (CCL) or a geosynthetic clay liner (GCL). The composite liner in turn rests on a more permeable foundation layer of thickness H_f, which is also included in the calculations. The contact quality between the geomembrane and the low-permeability layer is assumed to be

imperfect; thus, the equation includes the transmissivity, θ, of a gap or a geotextile (as is the case with a GCL). Equation (2.8) can be rearranged to get the following form (Rowe 1998):

$$\frac{d^2h}{dr^2}+\frac{1}{r}\frac{dh}{dr}-\alpha^2 h=\alpha^2 C \tag{2.9}$$

where α and C are defined by:

$$\alpha=\sqrt{\frac{k_s}{\left(H_L+H_f\right)\theta}} \tag{2.10}$$

$$C=H_L+H_f \tag{2.11}$$

Here k_s is the harmonic mean of saturated hydraulic conductivity of the underlying materials (low permeability layer and foundation layer). The transmissivity θ in Equation (2.10) is the same transmissivity that can be calculated using Equation (2.1). The general solution to Equation (2.9) involves the use of modified Bessel functions of the zero-order, K_0 and I_0, and requires two boundary conditions to solve for the constants A and B (Touze-Foltz et al. 1999).

$$h(r)=AI_o(\alpha r)+BK_o(\alpha r)-C \tag{2.12}$$

The head distribution along the interface, as defined by Equation (2.12), is shown in Figure 2.12. The radius of the defect, r_0, and the radius of wetted area, R, define the range of r over which the flow through the interface is of interest. The radius of the

wetted area is defined by Rowe (1998) as the radius at which the slope of the pressure head at the interface between the geomembrane and the underlying soil layer equals zero.

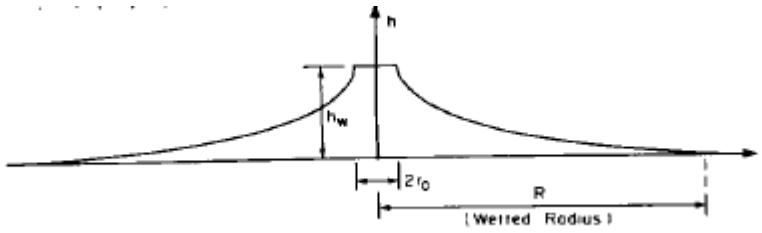

Figure 2.12: Schematic view of the head distribution at the interface between the geomembrane and the underlying soil layer (Rowe 1998)

Rowe (1998) solved the governing equation for the special case where the radial flow and head at *R* are zero. This case is consistent with field conditions. The boundary conditions to determine the constants of the general solution are (Rowe 1998):

$$h(r_0) = h_w \tag{2.13}$$

$$h(R) = 0 \tag{2.14}$$

$$Q_r(R) = 0 \tag{2.15}$$

However, to calculate the hydraulic head using Equation (2.12) with these boundary conditions, the radius of wetted area must be known. The radius of wetted area can be estimated by finding when the change in pressure head is zero at *R*, or, in other words, solving the following equation for *R* (Touze-Foltz et al. 1999):

$$\frac{dh}{dr}(R) = AI_0(\alpha R) + BK_0(\alpha R) - C = 0 \tag{2.16}$$

The constants *A* and *B* were defined by Touze-Foltz et al. (1999) as follows:

$$A = \frac{(h_w + C) K_1(\alpha R)}{K_1(\alpha R) I_0(\alpha r_0) + K_0(\alpha r_0) I_1(\alpha R)} \tag{2.17}$$

$$B = \frac{(h_w + C) I_1(\alpha R)}{K_1(\alpha R) I_0(\alpha r_0) + K_0(\alpha r_0) I_1(\alpha R)} \tag{2.18}$$

where K_1 and I_1 are modified Bessel function of the first order. Equation (2.16) is easily solved using an iterative solver such as Newton-Raphson. The total flow rate through a defect in a geomembrane liner for *field conditions* is calculated by (Touze-Foltz et al. 1998):

$$Q = \pi r_0^2 k_s \frac{h_w + C}{C} - 2\pi r_0 \theta \alpha \left[A I_1(\alpha r_0) - B K_1(\alpha r_0) \right] \tag{2.19}$$

The flow rate calculated using Equation (2.19) is not correct unless Equation (2.16) is satisfied. To solve for the leakage rate, there are two equations [Equations (2.16) and (2.19)] and two unknowns (wetted radius, R and leakage rate, Q). The transmissivity is considered to be a known value, but since it is difficult to quantify, the transmissivity is often estimated or assumed.

Touze-Foltz et al. (1999) also developed a model using the same governing differential equation and general solution, but considered a different set of boundary conditions than those used by Rowe (1998). In particular, Touze-Foltz et al. (1999) evaluated the problem using a set of boundary conditions consistent with the laboratory permeameter tests used in this study, as follows:

$$h(r_0) = h_w \tag{2.20}$$

$$h(R_c) = h_s \tag{2.21}$$

where h_s is a specified head at the radius of the cell, R_c. The constants of the general solution, A_p and B_p, are (Touze-Foltz et al. 1999):

$$A_p = \frac{(h_w + C)K_0(\alpha R_c) - (h_s + C)K_0(\alpha r_0)}{K_0(\alpha r_0)I_0(\alpha R_c) - K_0(\alpha R_c)I_0(\alpha r_0)} \tag{2.22}$$

$$B_p = \frac{(h_w + C)I_0(\alpha R_c) - (h_s + C)I_0(\alpha r_0)}{K_0(\alpha r_0)I_0(\alpha R_c) - K_0(\alpha R_c)I_0(\alpha r_0)} \tag{2.23}$$

The total flow rate through a defect in a geomembrane liner for *laboratory conditions* can be calculated using the following equation (Touze-Foltz et al. 1999):

$$Q = \pi r_0^2 k_s \left(\frac{h_w + C}{C}\right) - 2\pi r_0 \theta \alpha \left[A_p I_1(\alpha r_0) - B_p K_1(\alpha r_0)\right] \tag{2.24}$$

Equation (2.24) takes into account that the hydraulic head at the permeameter wall will be greater than zero if the radius of the cell is smaller than the radius of the wetted area. The radial flow rate will be equal to zero at the permeameter wall. Note that the flow rates calculated using Equations (2.19) and (2.24) do not consider flow due to matric suction in the soil layer. Also, only one-dimensional flow through the soil layer is considered. A simple spreadsheet can be used to perform the calculations needed to solve for the leakage rate and radius of wetted area for a given transmissivity. An example of the spreadsheet used to perform the calculations of the analytical models is included in Appendix C.

Barroso (2005) used the model developed by Touze-Foltz et al. (1999) to back-calculate the interface transmissivity from the experimental data for enhanced composite liner systems involving a geomembrane, GCL and CCL together. To back-calculate the

transmissivity using the analytical models, the transmissivity is varied until the calculated leakage rate matches the measured leakage rate. Brown et al. (1987) back-calculated gap thicknesses in the same way using the data obtained from their experimental program. The radius of wetted area is obtained during the calculation of the leakage rate using the analytical model developed by Touze-Foltz et al. (1999), as the solution is not valid unless the condition posed by Equation (2.16) is true.

The term "radius of wetted area" is somewhat of a misnomer in that flow actually occurs outside of the radius of wetted area. The analytical model is based on an assumption that the flow through the defect only occurs within the radius of wetted area. However, lateral flow occurs outside the radius of wetted area. This aspect of the analytical model was investigated as part of the numerical study discussed later in Section 7.3. A possible alternative, and perhaps more accurate, title for the radius of wetted area is the "radius of interface flow." Flow is still occurring in the underlying soil layer, but the flow across the interface becomes negligible outside the radius of interface flow. From the point forward, the "radius of wetted area" will be referred to the "radius of interface flow," unless when referring to a previous study or otherwise noted. Note that the notation R will not be changed.

2.3.4 Numerical Studies

Foose et al. (2001) conducted 2D and 3D numerical simulations, using the finite difference code MODFLOW, to study the leakage through composite liners (geomembrane over a compacted clay liner (CCL) or geomembrane over a GCL). The leakage through a circular defect was modeled as an axisymmetric system with area around the defect modeled as a block of soil, one quadrant of the entire area. A no-flow boundary condition was used to simulate a geomembrane and a constant head boundary condition was used for the cells that represented the defect. The bottom boundary

condition was free-draining with a constant head of zero. The interface between the geomembrane and the soil layer was also included in the model as a thin layer with a transmissivity and thickness ranging from perfect contact to poor contact. Non-uniform grid spacing was used for the model, with the grid spacing increasing the distance from the defect increases. Very small grid spacing is required in the vicinity of the defect because of the significant gradients at that location.

The results from the numerical study conducted by Foose et al. (2001) were compared against predictions obtained using existing empirical equations (Giroud 1997) and analytical models (Rowe 1998). For composite liners including GCLs with an imperfect contact, the results of the 3D finite difference model agree well with Rowe's (1998) model (when transmissivities are larger than $2x10^{-12}$ m^2/s). The wetted radius calculated using Rowe's (1998) model also compares well with the radius of wetted area obtained by 3D simulations. Giroud's (1997) equation significantly overestimates the flow through the liner, although these results may be attributed to the use of transmissivity values from the experiments conducted by Harpur et al. (1993), which may not correspond to field conditions. For composite liners involving CCLs, both Rowe's (1998) model and Giroud's (1997) equation yield leakage rates that agree with results of the finite difference model. The hydraulic head imposed on the composite liner system for the numerical simulations was limited to values corresponding to landfill conditions (0.3 m). Numerical simulations such as those conducted by Foose et al. (2001) have yet to be conducted for lining systems for dams and for the hydraulic heads representative of dams.

2.3.5 Equations for Prediction of Leakage Rates through Defects in Geomembranes

The use of analytical and numerical simulations requires some effort to solve for leakage rates through defects in geomembrane liners. Equations were developed in order

to simplify the process of estimating leakage through a defect in a geomembrane. All equations currently available in the literature were formulated to approximate leakage for conditions representative of landfill liners (i.e., heads less than 0.3 m).

2.3.5.1 Giroud and Bonaparte (1989)

Giroud and Bonaparte (1989) conducted a review of leakage through geomembrane liners by compiling published and unpublished test data and analytical studies that investigated leakage mechanisms. The authors' goal was to provide landfill designers with design recommendations to use in practice.

Permeation through a geomembrane liner without a defect was discussed in detail by Giroud and Bonaparte (1989), although the majority of flow through a liner occurs through holes and tears in the geomembrane. Giroud and Bonaparte (1989) presented data for tests that only involved the use of water, but acknowledged that some chemicals would permeate faster through the polymeric material. Based on the compiled data, the permeability of an undamaged geomembrane was estimated to be approximately 10^{-14} m/s.

The authors defined two types of defects: pinholes and holes. Pinholes have openings that are smaller than the geomembrane thickness. Holes have openings larger than the geomembrane thickness. Pinholes, a product of the manufacturing process that has vastly improved over the years, are uncommon. Nevertheless, the flow through pinholes can be calculated using Poiseuille's equation for flow through pipes:

$$Q = \frac{\pi \rho g h_w d^4}{128 \eta T_g} \tag{2.25}$$

where Q is the flow rate, ρ is the fluid density, g is the acceleration due to gravity, h_w is the hydraulic head on the geomembrane, d is the diameter of the pinhole, η is the dynamic viscosity of the liquid, and T_g is the thickness of the geomembrane.

Leakage through holes that are larger than pinholes is greatly affected by the material beneath the geomembrane. If the soil underlying the geomembrane has a hydraulic conductivity greater than 10^{-3} m/s, Giroud and Bonaparte (1989) recommended using Bernoulli's equation for free flow through an orifice to estimate leakage, as follows:

$$Q = Ca\sqrt{2gh_w} \tag{2.26}$$

where C is a coefficient related to the sharpness of the edges of the orifice (C = 0.6 for sharp edges was recommended by the authors), and a is the area of the defect. Benson et al. (1995) showed that Equation (2.26) is appropriate for estimating leakage through defects under low heads, when the geomembrane is placed over gravels. The coefficient C was varied until the calculated flow rates more closely matched the experimental results.

If the geomembrane liner is placed over a soil with a hydraulic conductivity below than 10^{-3} m/s, leakage rates cannot be estimated using Bernoulli's orifice equation since the soil layer would impede flow through the defect. Giroud and Bonaparte (1989) developed a model to estimate leakage when the geomembrane is placed over a soil with low hydraulic conductivity. Brown et al. (1987) developed charts that can be used for predicting leakage rates and radii of interface flow (Figure 2.9) for systems involving geomembranes over compacted clay liners under low hydraulic heads. These charts were generated using the analytical model and the suggested gap thicknesses developed by

Brown et al. (1987). As discussed in Section 2.3.2.2, the gap thicknesses were back-calculated using the Brown et al. (1987) analytical model and the experimental data. Giroud and Bonaparte (1989) developed "empirical" equations specifically for the study conducted by Brown et al. (1987) as a way to interpolate and extrapolate values from the charts, such as that shown in Figure 2.9. The equations developed by Giroud and Bonaparte (1989) to calculate the leakage rate and the radius of wetted area are as follows:

$$Q = 0.7a^{0.1}k_s^{0.88}h_w \tag{2.27}$$

$$R = 0.5a^{0.05}k_s^{-0.06}h_w^{0.5} \tag{2.28}$$

where Q is the leakage rate (m^3/s), a is the area of the defect (m^2), k_s is the hydraulic conductivity of the underlying soil (m/s) and h_w is the head of water on top of the geomembrane (m). These equations, especially Equation (2.27), would later be generalized by Giroud et al. (1989) for use in landfill lining systems.

A general note should be made regarding the use of the term "empirical" used to qualify the equations presented in this section. Beginning with Giroud and Bonaparte (1989) and continuing through Touze-Foltz and Giroud (2003), the authors have used the term "empirical" to describe the equations that were developed in their studies. According to the Merriam-Webster dictionary, empirical is defined as "originating in or based on observation or experience." In research contexts, empirical relationships have often been developed based on results obtained from laboratory testing. However, the equations that were developed first by Giroud and Bonaparte (1989) and later by Touze-Foltz and Giroud (2003) are not based on laboratory data but rather numerical experimentation using analytical models such as the one developed by Touze-Foltz et al.

(1999). Consequently, the so-called "empirical" equations are actually approximations obtained from parametric studies conducted using the analytical models. While less rigorous, these approximations are easier to use than the analytical models.

2.3.5.2 Giroud et al. (1989) & Giroud (1997)

Giroud et al. (1989) developed a more general equation for estimating the leakage rate through a defect in a geomembrane liner over a low-permeability soil. The authors also considered the quality of the contact between the geomembrane and the underlying soil layer. Giroud et al. (1989) considered poor contact quality as a geomembrane liner with large wrinkles and good contact as a geomembrane liner with minimal wrinkles. Using the analytical model developed by Brown et al. (1987), the equations developed by Giroud et al. (1989) are as follows:

Good Contact: $$Q = 0.21 a^{0.1} k_s^{0.74} h_w^{0.9} \quad (2.29)$$

Poor Contact: $$Q = 1.15 a^{0.1} k_s^{0.74} h_w^{0.9} \quad (2.30)$$

Equations (2.29) and (2.30) are for circular defects and must be used with SI units.

A major assumption for Equations (2.29) and (2.30) was that the hydraulic gradient through the underlying soil layer was unity (i = 1), although this is not technically accurate. According to Giroud et al. (1989), the depth of water on top of the geomembrane should be less than the thickness of the underlying soil layer for Equations (2.29) and (2.30) to be valid. Giroud et al. (1989) stated that, under these conditions, the leakage rate can be assumed to be independent of the thickness of the underlying soil layer. However, in order to take into account higher gradients, Giroud (1997) developed the following:

Good Contact: $$Q = 0.21 i_{avgo} a^{0.1} k_s^{0.74} h_w^{0.9} \quad (2.31)$$

Poor Contact: $$Q = 1.15 i_{avgo} a^{0.1} k_s^{0.74} h_w^{0.9} \quad (2.32)$$

where i_{avgo} is the average hydraulic gradient in a low-permeability soil as defined by (Giroud 1997):

$$i_{avgo} = 1 + 0.1\left(h_w / H_s\right)^{0.95} \quad (2.33)$$

where H_s is the thickness of the low-permeability soil layer. Equations (2.31) and (2.32) require the use of SI units and should only be used to estimate leakage rates through defects in systems where hydraulic heads are below 3 m.

2.3.5.3 Touze-Foltz and Giroud (2003)

Touze-Foltz and Giroud (2003) presented the methodology for developing an "empirical" equation for predicting leakage through defects in geomembrane liners. The general form of the equation for circular defects was:

$$Q = C_q h_w^x a^y k_s^z \left[1 + \lambda\left(\frac{h_w}{H_s}\right)^{\mu}\right] \quad (2.34)$$

where Q is the leakage rate, C_q is a coefficient that describes the contact quality, h_w is the head applied to the geomembrane, a is the area of the defect, and k_s is the saturated hydraulic conductivity of the soil, i_s is the average hydraulic gradient, and H_s is the thickness of the soil layer. The exponents x, y, z, and μ and the factors λ and C_q are the

unknowns in this equation and were solved for by the authors using the methodology laid out by Touze-Foltz and Giroud (2003).

Touze-Foltz and Giroud (2003) selected a range of values for each variable in the equation (h_w, a, k_s, H_s) was selected in order to define the boundaries of the solution. For example, the range of hydraulic heads used in the study conducted by Touze-Foltz and Giroud (2003) was 0.3 to 3 m. The equation is developed for a specific range of head (i.e., a head of 5 m would be outside the range of validity).

Once the range of each variable is defined, a sensitivity analysis is performed for each variable (i.e., value of one variable is changed while the remaining variables are held constant). The analysis was conducted using the analytical model developed by Touze-Foltz et al. (1999) [Equation (2.19)] for field conditions to calculate the leakage rate for each combination of variables. The transmissivity was needed to solve for the leakage rate using Equation (2.19). The transmissivity is related to the contact condition being considered in the sensitivity analysis. Estimated values for the transmissivity for different contact qualities were obtained (for SI units only) using (Touze-Foltz and Giroud 2003):

Excellent Contact: $$\log \theta = -1.7476 + 0.7155 \log k_s \quad (2.35)$$

Good Contact: $$\log \theta = -1.3564 + 0.7155 \log k_s \quad (2.36)$$

Poor Contact: $$\log \theta = -0.5618 + 0.7155 \log k_s \quad (2.37)$$

These relationships are based on the values for gap thickness (and hydraulic conductivity) suggested by Brown et al. (1987) and listed in Table 2.3. For each contact condition, calculations were performed systematically for the full range of variables using the analytical model developed by Touze-Foltz et al. (1999) for field conditions. Linear

regression was used to approximate the value of each exponent based on the results of the rigorous calculations using the analytical solution.

Three contact conditions were considered for the study conducted by Touze-Foltz and Giroud (2003), which corresponded with the three transmissivity equations [Equations (2.35) to (2.37)]. The sensitivity analysis resulted in the following equations for predicting leakage through defects for each contact quality (Touze-Foltz and Giroud 2003):

Excellent: $$Q = 0.096 a^{0.1} h_w^{0.9} k_s^{0.74} \left[1 + 0.1 \left(h_w / H_s \right)^{0.95} \right] \quad (2.38)$$

Good: $$Q = 0.21 a^{0.1} h_w^{0.9} k_s^{0.74} \left[1 + 0.1 \left(h_w / H_s \right)^{0.95} \right] \quad (2.39)$$

Poor: $$Q = 1.15 a^{0.1} h_w^{0.9} k_s^{0.74} \left[1 + 0.1 \left(h_w / H_s \right)^{0.95} \right] \quad (2.40)$$

Equations (2.38) to (2.40) must be used with SI units and should only be used to estimate leakage through a circular defect and for a hydraulic head below 3 m.

Equations (2.39) and (2.40) are the same as Equations (2.31) and (2.32). However, Touze-Foltz and Giroud (2003) used the analytical model developed by Touze-Foltz et al. (1999) to perform the sensitivity analysis while Giroud (1997) used the model developed by Brown et al. (1987). The calculations were performed using the more recent analytical model (i.e., Touze-Foltz et al. 1999) to verify the accuracy and ensure the consistency of Equations (2.38) to (2.40).

2.3.5.4 Touze-Foltz and Barroso (2006)

Touze-Foltz and Barroso (2006) developed an "empirical" equation for systems involving a geomembrane-GCL interface, using the same form of equation as the previous "empirical" equations [Equation (2.34)] and the same methodology. In order to

perform the sensitivity analysis using the analytical solution developed by Touze-Foltz et al. (1999) [Equation (2.19)] for field conditions to develop the new equation, Touze-Foltz and Barroso (2006) estimated the transmissivity using the following equation (for SI units only):

$$\log\theta = -2.2322 + 0.7155\log k_{GCL} \tag{2.41}$$

where k_{GCL} is the hydraulic conductivity of the GCL. Using Equation (2.41), Touze-Foltz and Barroso (2006) developed the following equation to approximate flow through a defect in a geomembrane over a GCL:

$$Q = 2\times10^{-4} h_w^{0.87} a^{0.07} k_s^{0.64}\left[1 + 0.31\left(h_w/H_s\right)^{0.79}\right] \tag{2.42}$$

The "empirical" equation for a geomembrane-GCL contact was developed for use with SI units and for systems subjected to low hydraulic heads. Equation (2.42) has not been validated for high heads and should only be used for systems with small circular defects that have diameters ranging from 2 to 20 mm. Equations for larger circular defects are presented in Touze-Foltz and Barroso (2006) for systems with GCLs and Touze-Foltz and Giroud (2005) for systems without GCLs.

2.3.6 Remarks

Most of the studies conducted so far have focused on leakage under low hydraulic heads. The outcomes of these studies, whether it is an empirical equation or a recommendation for interface gap spacing, may not be applicable for evaluating leakage through geomembranes used in dam applications. Consequently, there is a need for investigating the leakage through defects in geomembranes subjected to high hydraulic

heads (e.g.., heads over 7 m). Contact conditions are likely affected by the increase in hydraulic head but the extent of the effect is unknown. Also, the radius of interface flow is a function of the head but this radius has not been quantified for high heads. The analytical models developed by Touze-Foltz et al. (1999) for field and laboratory conditions should, in principle, be valid for high heads, but such predictions have not been validated with experimental results.

Chapter 3: Equipment and Methods for the Experimental Program

3.1 INTRODUCTION

This study includes an experimental testing component carried out to quantify leakage and other characteristics of flow through defects in a geomembrane liner system under high hydraulic heads. The specific details for these materials are discussed in the following sections.

Two permeameter cells were constructed for use in the experimental program: a small permeameter (6-inch diameter) and a larger permeameter cell (13-inch diameter). The test cells are rigid wall permeameters constructed of clear acrylic tubing that allows for visual observation of the wetting front during testing.

3.2 CHARACTERISTICS OF THE SMALL PERMEAMETER TESTS

Two small permeameter cells were constructed for use in the experimental program. The schematic view for the small permeameter cell is shown in Figure 3.1a. Each cell included two parts: the bottom part contained the soil layers and the upper portion functioned as a water reservoir above the geomembrane. Soil layers were prepared inside the lower portion of the cell and the geomembrane was placed on top of the soil layer. An O-ring and a cork gasket were used to maintain a pressure-tight seal between the geomembrane and the permeameter cell. The upper portion of the cell was connected to a pressurized water supply tank. The water supply tank and the small permeameter cell are shown in Figure 3.1b. The laboratory house pressure supplied up to 100 psi, which is equivalent to a hydraulic head of 70 m. The pressures used in the experimental program ranged from 5 to 60 psi, which corresponds to 3.5 to 42 m of head.

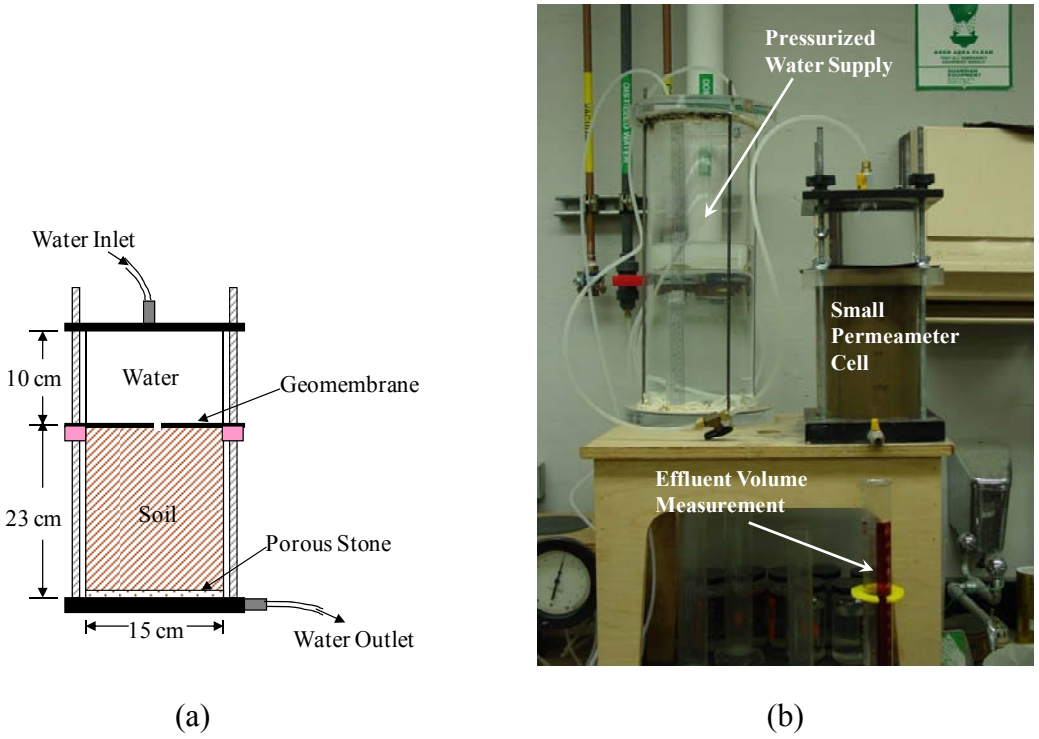

Figure 3.1: a) Schematic view of small permeameter cell and b) picture of small permeameter cell

A schematic view of the small permeameter for a test setup involving a GCL is shown in Figure 3.2. For tests involving GCLs, the GCL is placed between the geomembrane and the soil layer. As shown in Figure 3.1a, the geomembrane is placed directly over the soil layer for tests without GCLs. A porous stone was placed at the base of the small permeameter cell for tests involving a silty clay. A piece of filter paper was placed at the bottom of the cell to minimize clogging of the porous stone by fine clay particles. For tests that included a GCL, the porous stone at the bottom of the cell was replaced by a geocomposite (geotextile/geonet). The use of a geocomposite in lieu of a porous stone was necessary to prevent clogging of the porous stone by bentonite migrating from the GCL.

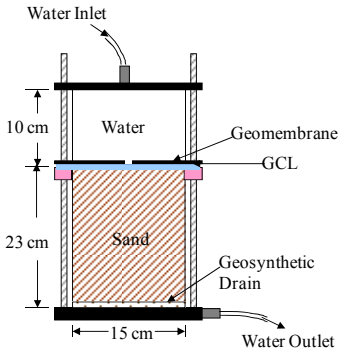

Figure 3.2: Schematic view of small permeameter for the test series involving GCLs

The water inlet and outlet were located at the top and bottom of the cell, respectively. A pressure regulator with an attached pressure gauge was used to control the hydraulic heads applied to the system. Flow into the system was monitored by recording the volume of water in the supply tank (see Figure 3.1b) over time. The accuracy of the measurements for the flow into the cell was ±10 mL. The volume of effluent was measured over the duration of each test using a graduated cylinder or a scale. The graduated cylinders used to measure the outflow, shown in Figure 3.1b, were accurate to the ±5 mL. The advancement of the wetting front within the soil layer was monitored during initial infiltration of the test and before outflow began. The results of this monitoring will allow for a comparison with predictions made using infiltration models.

Some tests were conducted for several weeks with long time periods between readings. Evaporation of the effluent water from the graduated cylinder occurred during this time. The evaporation rate in the laboratory was measured using the same graduated cylinder and was found to be approximately 1 mL/day. Consequently, a correction for evaporation was applied to the effluent volumes measured during the tests.

The permeameter tests were not constant head tests since the water level in the pressurized supply tank decreased during testing. However, the decrease in head was only a small fraction of the pressure applied to the system. The permeameter cell setup in relation to the water supply tank is shown in Figure 3.3. The tank was approximately 0.6 m in height while the hydraulic heads used in the study ranged from 7 m to 42 m. As shown in Figure 3.3, the geomembrane was located at approximately mid-height of the tank, or at approximately 0.3 m from the base of the cell. When the water in the supply tank was above the elevation of the geomembrane (see Figure 3.3), the height of water in the tank increased the head being applied to the geomembrane (i.e., the specified range of head from 7 to 42 m). Once the water level in the tank fell below the surface of the geomembrane (Figure 3.3), the total hydraulic head was less than the applied pressure by no more than 0.3 m. This variation in head applied to the geomembrane equated to a maximum change of 4.5% for an applied head of 7m and a maximum change of 0.5% for an applied head of 42 m. Therefore, the change in head induced by changes in the water level in the supply tank during testing was assumed to be negligible.

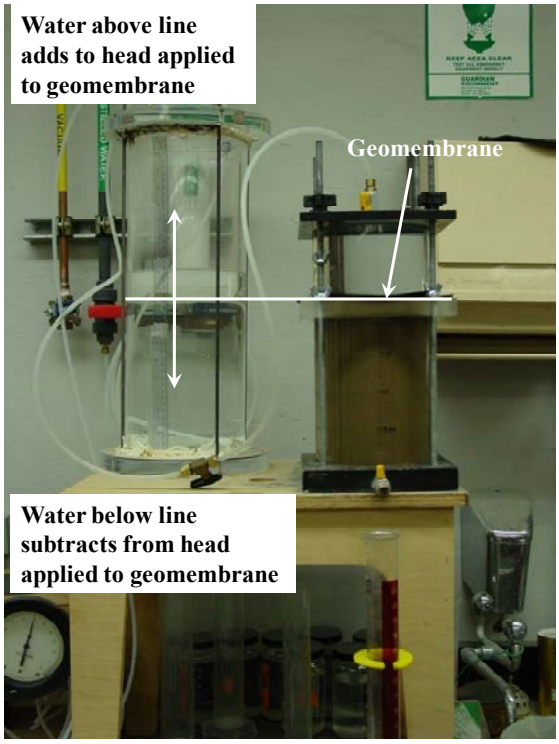

Figure 3.3: Visual description of water supply system and the variation in head applied to geomembrane during a test in the small permeameter

3.2.1 Time Domain Reflectometry

Time domain reflectometry (TDR) has been used in the field and in the laboratory to measure the volumetric moisture content of soils. A TDR probe is shown in Figure 3.4. The probe is used to measure the dielectric constant of the soil into which it is inserted and the dielectric constant is used to determine the volumetric water content. A TDR system was used in this study to investigate the changes of moisture content in the soil underlying a geomembrane during infiltration through a defect and into an unsaturated soil layer.

Figure 3.4: TDR probes used in experimental program

The TDR system used in this study included a cable tester, a 16-channel multiplexer, and 8-cm long TDR probes. The cable tester sends an electromagnetic pulse along the coaxial cable to the TDR probe and then measures the time it takes for the pulse to travel along the probe. The velocity of the pulse is a function of the amount of water in the pores of the soil. The velocity of the electromagnetic pulse is related to the dielectric constant of the soil. The cable tester processes the waveform of the pulse, which allows determination of the dielectric constant for the soil. The volumetric water content is subsequently determined using pre-established correlations.

The TDR probes were small enough to fit inside the small permeameter test cell. The locations of the TDR probes in relation to the permeameter cell are shown in Figure 3.5. Three probes were placed at elevations of 5, 10 and 15 cm from the bottom of the 23-cm tall cell. Each probe had a 3-m long coaxial cable, shown in Figure 3.4, which was connected to the multiplexer. The cable tester was set to take readings from each probe every two minutes. The readings were then downloaded from the cable tester and processed.

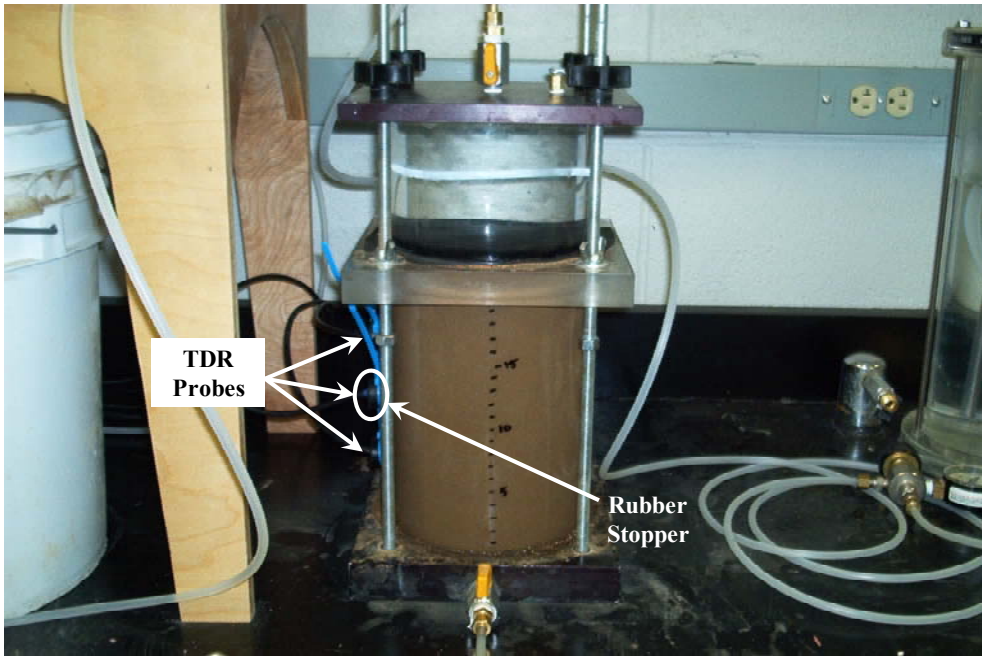

Figure 3.5: Cell with TDR probes placed at 5, 10 and 15 cm from the base of the cell

The infiltration of water into the unsaturated soil layer allowed evaluation of the early stages of permeameter tests, during which the moisture content increases from the initial value to a final steady-state value. Specifically, changes in volumetric moisture content allowed determination of the time when the wetting front arrived at the location of the TDR probes in the permeameter cell. An example of TDR data obtained during a permeameter test is shown in Figure 3.6. Advancement of the moisture front induced by leakage through a geomembrane defect will be compared with results from infiltration models and visual observations taken during each test.

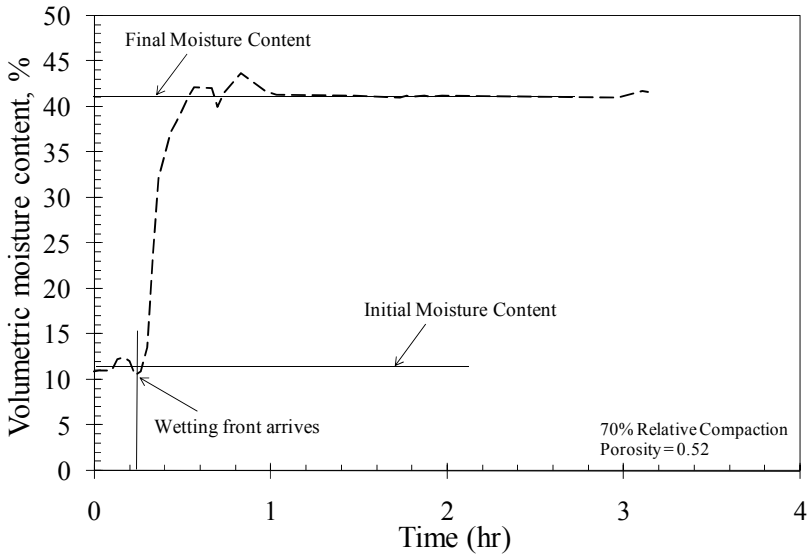

Figure 3.6: Example of volumetric moisture content data obtained using TDR system

3.2.2 Materials

3.2.2.1 Soil Description

Two types of soil were used for the experimental testing program: a silty clay and a medium-fine sand. The characteristics of these soils are provided in this section.

RMA Soil Type II

One of the soils being used in the experimental portion of this study was obtained from the Rocky Mountain Arsenal (RMA) near Denver, Colorado. The soil has a liquid limit of 29 and a plasticity index of 17. Using the Unified Soil Classification System (USCS), the RMA Soil Type II is classified as a CL soil. The grain size distribution curve and the compaction curve for this soil were obtained from McCartney (2007) and are shown in Figures 3.7 and 3.8. The optimum moisture content for this soil is 11.9% and the maximum dry unit weight is 18.6 kN/m^3 (McCartney 2007).

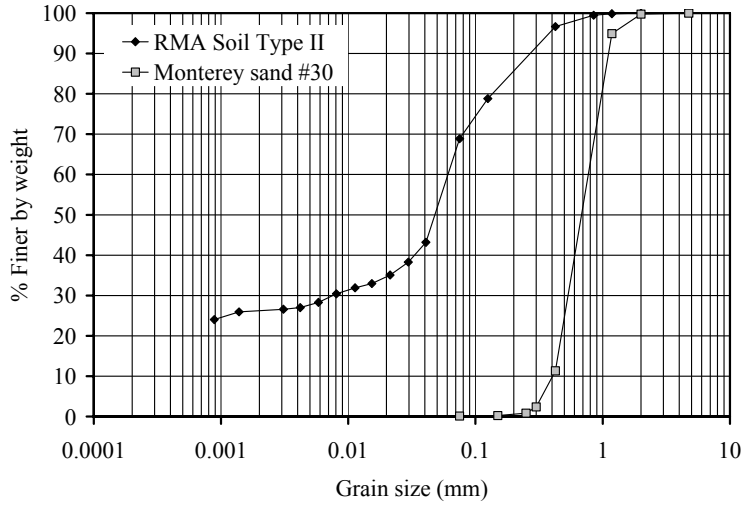

Figure 3.7: Grain size distribution curves for RMA Soil Type II and Monterey #30 sand (McCartney 2007)

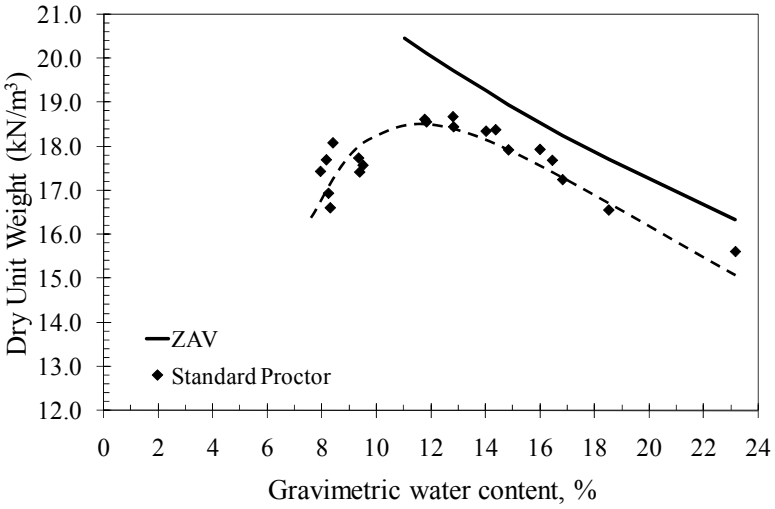

Figure 3.8: Compaction curve for RMA Soil Type II (After McCartney 2007)

McCartney (2007) measured the saturated hydraulic conductivity of RMA Soil Type II for a range of compaction water contents and dry unit weights. Falling head and constant head tests were conducted using flexible wall permeameters and rigid wall

permeameters, respectively. The saturated hydraulic conductivity for the RMA Soil Type II ranges from $2x10^{-7}$ m/s to $4x10^{-10}$ m/s, depending on compaction moisture content and compaction effort (McCartney 2007). Since the range in hydraulic conductivity is so large, hydraulic conductivity tests were conducted for the target water contents and dry unit weight that was used in the permeameter tests conducted as part of this study.

The hydraulic conductivity for the soil used in the testing program was measured using the same permeameter cell as the tests in this study (Figure 3.1). The soil was prepared using the same procedures as for a test with a geomembrane but the geomembrane was not placed over the soil. The hydraulic conductivity tests were conducted for three different heads: 7, 14 and 21 m. The results of the hydraulic conductivity tests are shown in Figure 3.9. As expected, the effect of head on the hydraulic conductivity was minor. For the target water content of 12% and a relative compaction of 90% of the maximum dry unit weight, the measured hydraulic conductivity is $8x10^{-9}$ m/s.

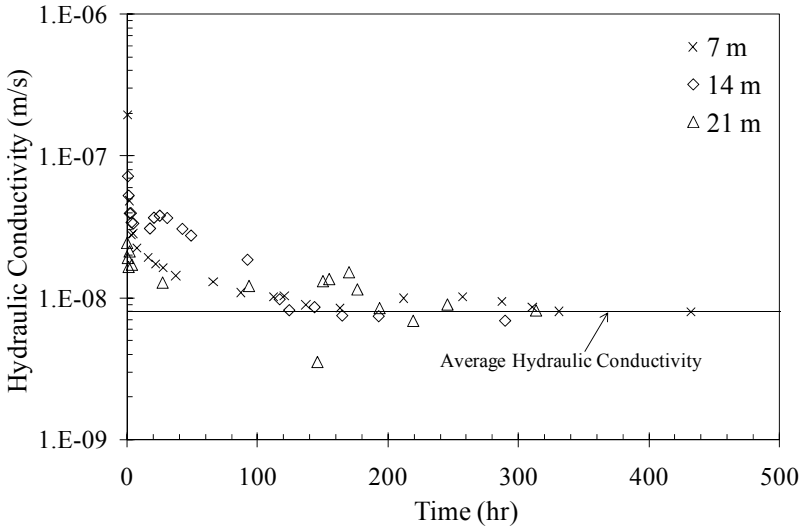

Figure 3.9: Hydraulic conductivity measurements for RMA Soil Type II

McCartney (2007) measured the hydraulic conductivity for RMA Soil Type II for a relative compaction of 70% with initial water contents similar to those used in this experimental study. The hydraulic conductivity for a relative compaction of 70% is $2x10^{-7}$ m/s. This value was used to simulate unfavorable soil conditions at a construction site.

For each test involving RMA Soil Type II, the soil layer used was not initially saturated and did not reach saturation over the duration of the test. Since the hydraulic conductivity of unsaturated soil is lower than the saturated hydraulic conductivity, the saturated value can be considered an upper bound.

Monterey #30 Sand

The other soil used in the experimental testing program was Monterey #30 sand. Properties for the sand were obtained from Li (2005). Monterey #30 is a clean, uniformly-graded sand that classifies as SP according to the USCS. The granulametric curve for the sand is also shown in Figure 3.7. The average diameter of the soil particles (d_{50}) is 0.7 mm and the sand has a uniformity coefficient of 1.8 and a coefficient of curvature of 1.0. Minimum and maximum void ratios are 0.56 and 0.76, respectively. These void ratios allowed the relative density to be determined for the soil layers used for testing.

The saturated hydraulic conductivity of Monterey #30 sand was determined for three relative densities under an effective stress of 10 psi. These tests were conducted using a conventional flexible wall permeameter. For a relative density of 75%, which was the density selected for several tests in this experimental study, the saturated hydraulic conductivity for the sand is $2.7x10^{-6}$ m/s. However, hydraulic conductivity tests were also conducted using the permeameter cell shown in Figure 3.1. As shown in Figure 3.10, the hydraulic conductivity for the sand was found to be $3.5x10^{-5}$ m/s, which

was different from the previously measured value by an order of magnitude. The difference between the two values can be attributed to the permeameter in which the soil was tested. The first set of hydraulic conductivity tests were conducted using flexible wall permeameters, while the second set of tests was conducted using the rigid-wall permeameter cells. An effective stress was applied to the soil layer in the flexible permeameter, which likely changed the density of the sand, leading a lower hydraulic conductivity. Since the second set of hydraulic conductivity tests were conducted using the same cell in which the leakage tests were conducted, these results were adopted to characterize the hydraulic properties of the Monterey #30 Sand.

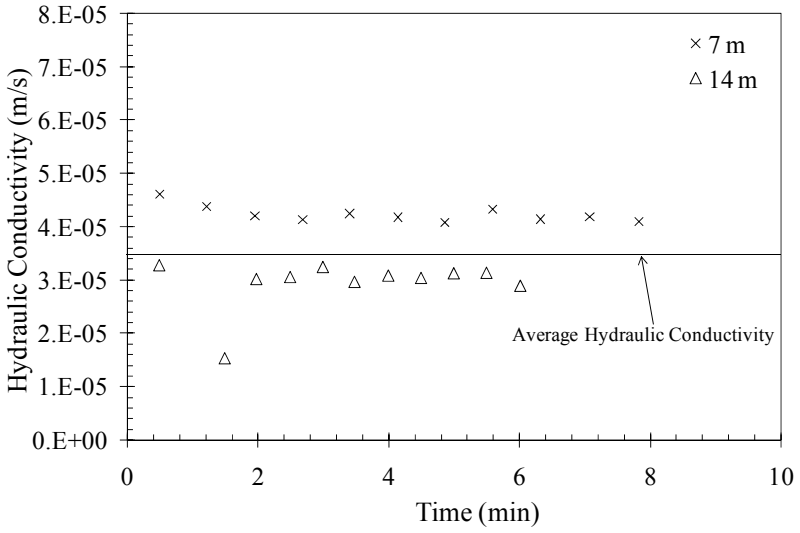

Figure 3.10: Hydraulic conductivity measurements for Monterey #30 sand

Water Retention Curves

The water retention curve (WRC) defines the relationship between the volumetric moisture content of the soil and the matric potential, or suction. As the volume of water in the soil decreases, the suction increases. There are several models that can be used to represent a WRC for a given soil, including Brooks and Corey (1964) and van Genuchten

(1980). The WRC will be used for approximating the unsaturated hydraulic properties of the soil in the numerical simulations conducted as part of this study.

The van Genuchten (1980) model was used in this study to approximate the WRC for a soil, as follows (after van Genuchten 1980):

$$\theta = \theta_r + (\theta_s - \theta_r)\left[\frac{1}{1+(\alpha h_\psi)^n}\right]^m \quad (3.1)$$

where θ is the volumetric moisture content, θ_r is the residual volumetric moisture content, θ_s is the saturated volumetric moisture content, h_ψ is the suction head, α, m and n are curve-fitting parameters. The curve-fitting parameter m is related to the parameter n as follows:

$$m = 1 - \frac{1}{n} \quad (3.2)$$

Values for the van Genuchten parameters for the two soils used in this study, as well as for the GCL, are listed in Table 3.1. The van Genuchten parameters for the RMA Soil Type II were obtained from McCartney (2007). The van Genuchten parameters for the Monterey #30 sand were obtained from Kuhn (2007). The parameters for the GCL used in this study were obtained from Barroso (2005). The three WRCs approximated by the van Genuchten parameters in Table 3.1 are shown in Figure 3.11. The WRC for the Monterey #30 sand had the steepest slope of the three soils, as shown by the van Genuchten model.

Table 3.1: van Genuchten parameters

van Genuchten Parameters	RMA Type II (CL)	Monterey #30 (SP)	Bentofix GCL
k_s (m/s)	$7x10^{-9}$	$3.5x10^{-5}$	$5x10^{-11}$
α (kPa^{-1})	0.08	0.55	0.15
n	1.23	1.4	1.67
m	0.19	0.29	0.40
θ_r	0.0032	0.03	0.05
θ_s	0.38	0.46	0.69

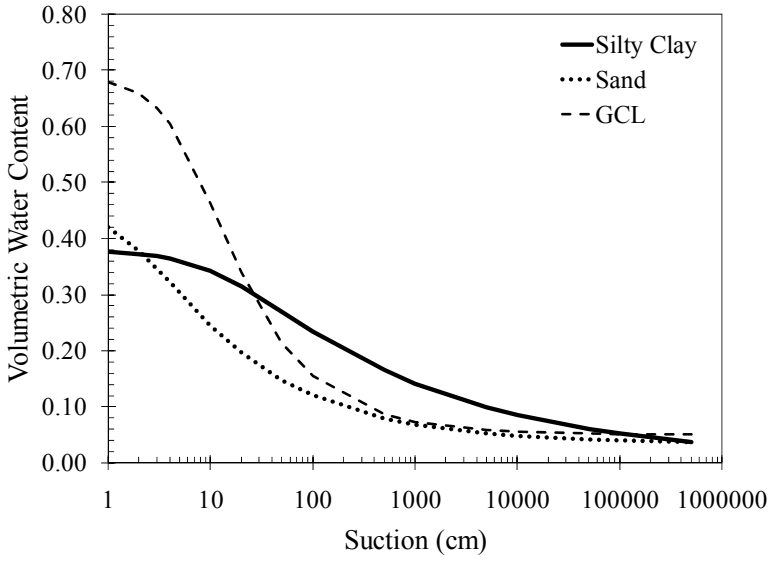

Figure 3.11: Water retention curves for the soils used in the experimental study

3.2.2.2 Geosynthetics

The two main types of geosynthetics used in this experimental study are the geomembranes and the geosynthetic clay liners (GCLs). These materials are discussed in this section.

Geomembranes

The primary component of the permeameter tests conducted as part of the experimental program was the geomembrane. The geomembrane selected as the liner in the permeameter tests was a linear low-density polyethylene (LLDPE) polymer with a thickness of 40 mils (1 mm). The manufacturer's specifications, including elongation and puncture resistance, for the geomembranes used in the permeameter tests are listed in Table 3.2. Previous studies had indicated that the leakage through defects is insensitive to the type and thickness of geomembranes. Therefore, the flexible nature of LLDPE was adopted as it is flexible, allowing better accommodation to deformations of the system. A circular defect with a diameter of 1.6 mm was drilled at the center of the geomembrane specimen. A small defect diameter was selected in an effort to keep the radius of interface flow within the boundaries of the cell and to minimize the boundary effects of the walls of permeameter cell.

Table 3.2: Specifications for geomembranes used in the permeameter tests (After GSE 2004)

GSE UltraFlex (40-mil LLDPE Geomembrane)		
Tested Property	**ASTM Test Method**	**Minimum Value**
Thickness (mm)	D 5199	0.91
Density (g/cm^3)	D 1505	0.92
Tensile Properties		
Strength at Break (N/mm)	D 6693 Type IV	27
Elongation at Break (%)	D 6693 Type IV	850
Tear Resistance (N)	D 1004	98
Puncture Resistance (N)	D 4833	276
Carbon Black Content (%)	D 1603	2
Reference Property		**Nominal Value**
Oxidative Induction Time (min)	D 3895	>100
Roll Length (m)		171
Roll Width (m)		6.9
Roll Area (m^2)		1171

Geosynthetic Clay Liners

A GCL consists of a layer of bentonite clay (granular or powdered) sandwiched between carrier geosynthetics. The carrier geosynthetics are typically geotextiles (nonwoven and/or woven) but some GCL products have geomembranes bonded directly to the bentonite layer instead of a geotextile. Bentonite is a highly expansive clay formed from volcanic ash and has a very low hydraulic conductivity when saturated, often less than 10^{-11} m/s. Several studies have shown that GCLs have self-healing capabilities due to the highly expansive nature of the bentonite in the presence of water. If the damage were to occur to a GCL (e.g., puncture, tear), researchers demonstrated that a hole over 30 mm in diameter can seal itself, maintaining the integrity of the GCL as a hydraulic barrier (Shan and Daniel 1991; Bouazza 2002). The self-healing behavior could prove useful for systems involving a geomembrane-GCL composite liner under high heads. The severity of a tear and resulting leakage in the composite liner could be reduced by the presence of the GCL.

The GCL was used in the experimental study to evaluate leakage through a composite liner system, in which a geomembrane is placed over a GCL. The GCL used in this study was Bentofix NWL. The GCL consisted of granular bentonite confined by two non-woven geotextiles (the bottom geotextile is scrim-reinforced). The specifications for the GCL, including carrier geotextile properties and peel strength, are listed in Table 3.3. The hydraulic conductivity of this GCL is quality controlled by the manufacturer to be less than 5×10^{-11} m/s (GSE 2003). An example of a GCL specimen used in the experimental study is shown in Figure 3.12. In the tests involving GCLs, the Bentofix NWL was placed between the LLDPE geomembrane and a sand layer.

Table 3.3: Specifications for GCLs used in permeameter tests (After GSE 2003)

Bentofix Thermal Lock NWL GCL		
Tested Property	**ASTM Test Methods**	**Value**
Geotextile Properties		
Cap Nonwoven (g/m^2)	D 5261	200
Bottom Scrim Nonwoven (g/m^2)	D 5261	200
Bentonite Properties		
Min Swell Index	D 5890	24 mL/2 g
Max Moisture Content (%)	D 4643	12
Max Fluid Loss (mL)	D 5891	18
Finished GCL Properties		
Bentonite (kg/m^2)	D 5993	3.66
Tensile Properties		
Tensile Strength (kN/m)	D 6768	8
Grab Strength (N)	D 4632	667
Grab Elongation (%)	D 4632	100
Min Peel Strength (N), (N/m)	D 4632, D 6496	66, 438
Max Hydraulic Conductivity (m/s)	D 5084	$5x10^{-11}$
Max Index Flux ($m^3/m^2/s$)	D 5887	$1x10^{-8}$
Internal Shear Strength (kPa)	D 6243	24
Roll Dimensions		
Width x Length (m x m)	-	4.7 x 45.7
Area per Roll (m^2)	-	216
Packaged Weight (kg)	-	1179

Figure 3.12: GCL sample used in permeameter tests

3.2.3 Preparation of the Soil Layer

3.2.3.1 Tests Involving Silty Clay

Pre-processing of the RMA Soil Type II included drying, crushing, grinding and sieving using a #10 sieve. The processed soil was then moisture-conditioned to obtain the target water content to be used in each test. Target water contents for the tests conducted using RMA Soil Type II ranged from 7% to 13%.

The procedure for molding a soil layer for the permeameter tests involving RMA Soil Type II is shown in Figure 3.13. Once the desired moisture content for the soil was achieved, soil layers were compacted in 5-cm layers directly into the permeameter cell. An example of a compacted lift is shown in Figure 3.13a. For each layer, the mass of soil added was compacted to a specific thickness that yielded the desired relative compaction (e.g., 90% of the maximum standard Proctor dry unit weight of 18.6 kN/m^3). The surface of each compacted layer was scarified in an effort to eliminate the transition between layers. An extension ring, shown in Figure 3.13b, was used to assist with the

compaction, containing the soil during compaction of the uppermost layers. As shown in Figure 3.13c, the soil was compacted to an elevation slightly above the lip of the permeameter.

The soil layer was then trimmed either flush with the lip of the permeameter or with the soil surface slightly above the lip of the permeameter, depending on the contact quality adopted for the test. An example of the soil layer after trimming and preparation was completed is shown in Figure 3.13d. A cork gasket was used to maintain a watertight seal between the geomembrane and the permeameter. The presence of the cork gasket formed a slight gap between the geomembrane and the surface of the soil. By trimming the soil layer so that it is flush with the lip of the permeameter, the contact between the geomembrane and the soil was not intimate due to the gap created by the cork gasket. To obtain an intimate contact between the geomembrane and the soil, the soil layer was trimmed so that the soil surface was slightly above the cork gasket. The soil layers were not saturated before the beginning of testing and had an initial degree of saturation between 20 and 50%, depending on the water content and dry unit weight of the soil.

(a)

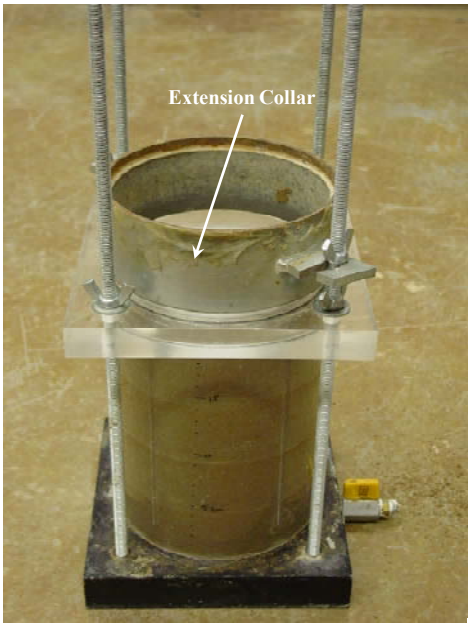

(b)

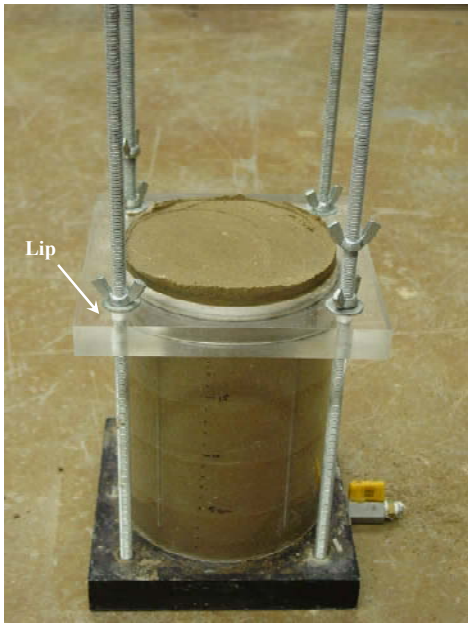

(c)

(d)

Figure 3.13: Soil layer preparation for tests on RMA Soil Type II: a) soil was compacted in layers, b) an extension ring was used to assist in compaction of upper layers, c) soil was compacted to slightly above lip of permeameter cell, and d) the soil layer was trimmed to form desired contact quality

The TDR system was only used for the tests involving RMA Soil Type II and, as mentioned previously, the TDR probes were located at permeameter elevations of 5, 10 and 15 cm. Compaction of the soil layer was challenging since each TDR probe needed to be horizontally level. The first layer of soil was compacted in place. The TDR cable was threaded through the hole in the side of the permeameter and sealed with a rubber stopper (see Figure 3.5). The TDR probe was slanted upward and rested on some loose soil for the next layer. The remainder of the soil for that layer was added and compacted. The final positioning of the probe was horizontal within the layer. This procedure was repeated for the remaining TDR probes. After completion of the tests, the soil around each TDR probe was collected in order to measure the water content directly and validate the measurements obtained using the TDR system.

3.2.3.2 Tests Involving Sand

The procedure for preparing a soil layer for the permeameter tests involving Monterey #30 sand is shown in Figure 3.14. The soil was placed in 5-cm thick layers directly into the cell. An example of a single lift is shown in Figure 3.14a. The mass of soil needed to obtain a relative density of 75% was determined using the minimum and maximum void ratio. A shaking table, shown in Figure 3.14b, was used to achieve the target relative density by vibrating the permeameter cell after each layer was placed. As shown in Figure 3.14c, the final lift of the sand was smoothed flush with the lip of the permeameter. Before testing began, the soil layers were saturated from the bottom of the cell to minimize the amount of air entrapped within the sand. A sand layer in the process of being saturated from the bottom is shown in Figure 3.14d. During saturation, a geotextile was placed over the soil to minimize disturbance to the surface of the soil layer.

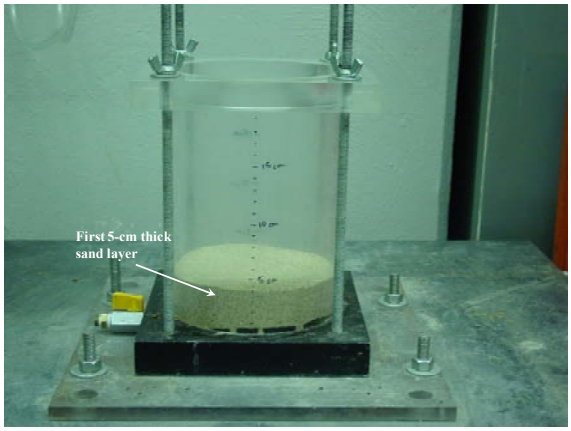

(a)

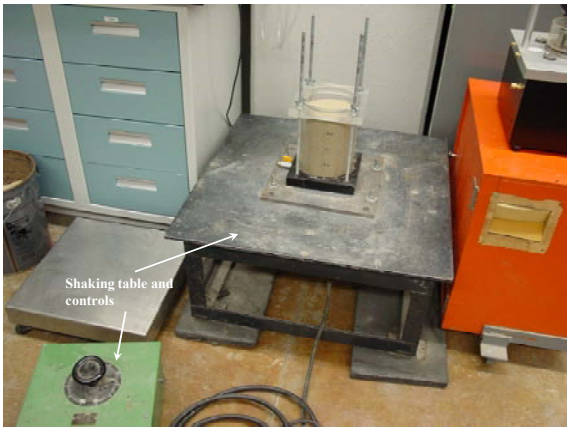

(b)

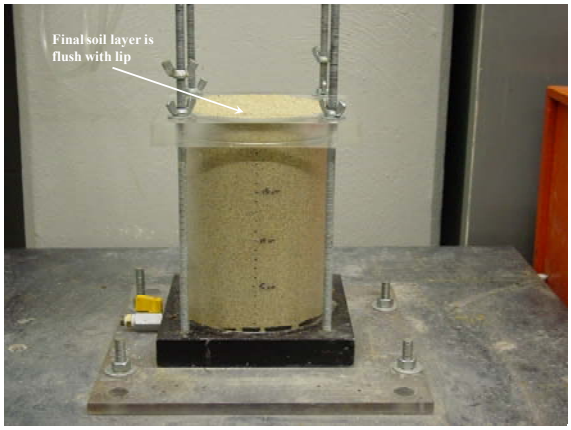

(c)

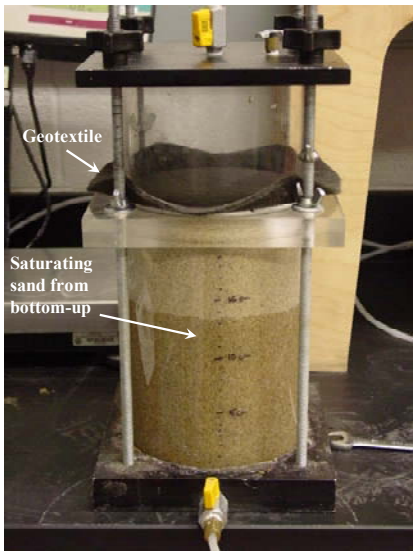

(d)

Figure 3.14: Soil layer preparation for tests on Monterey #30 sand: a) soil was placed in layers, b) a shaking table was used to vibrate the soil layer to obtain the target relative density, c) soil layer was flush with the lip of the permeameter cell, and d) saturation of the sand layer from the bottom

3.3 CHARACTERISTICS OF THE LARGE PERMEAMETER TESTS

A permeameter cell with a diameter of 13 inches was also used to conduct tests in the experimental component of this study. A schematic view of the larger permeameter is shown in Figure 3.15. The large permeameter was similar in design to the smaller cell, having an upper and lower half, but the geomembrane was held in place between the two halves without the support of a lip. Only O-rings were used to seal the cell. As shown in Figure 3.16, the upper portion of the permeameter cell was connected to a pressurized water supply tank. The water inlet and outlet were located at the top and bottom of the cell, respectively. A pressure regulator with an attached pressure gauge was used to control the hydraulic heads applied to the system. Flow into the system was monitored by recording the volume of water in the supply tank over time. The accuracy of the measurements for the flow into the cell was ±10 mL. The volume of effluent was measured over the duration of each test using a graduated cylinder or a scale. The graduated cylinders used to measure the outflow were accurate to the ±5 mL.

Tests were conducted using the large permeameter cell to verify the results from the small permeameter by evaluating the effect of the cell boundaries. The radius of interface flow for tests being conducted using the small permeameter was expected to be greater than the diameter of the small cell. Use of the large cell allowed the measurement of the radius of interface flow. A tracer dye called Rhodamine WT was used to visualize the flow patterns in the soil layer beneath the geomembrane allowing experimental determination of the radius of interface flow. A concentration of 0.1% by volume of Rhodamine WT was added to the water used for the large-permeameter test involving dye, which resulted in the dark purple color seen in Figure 3.17.

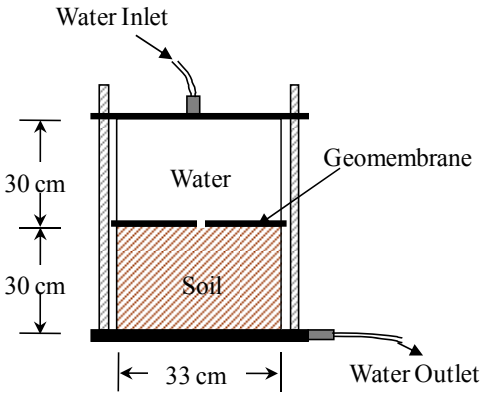

Figure 3.15: Schematic view of large permeameter cell

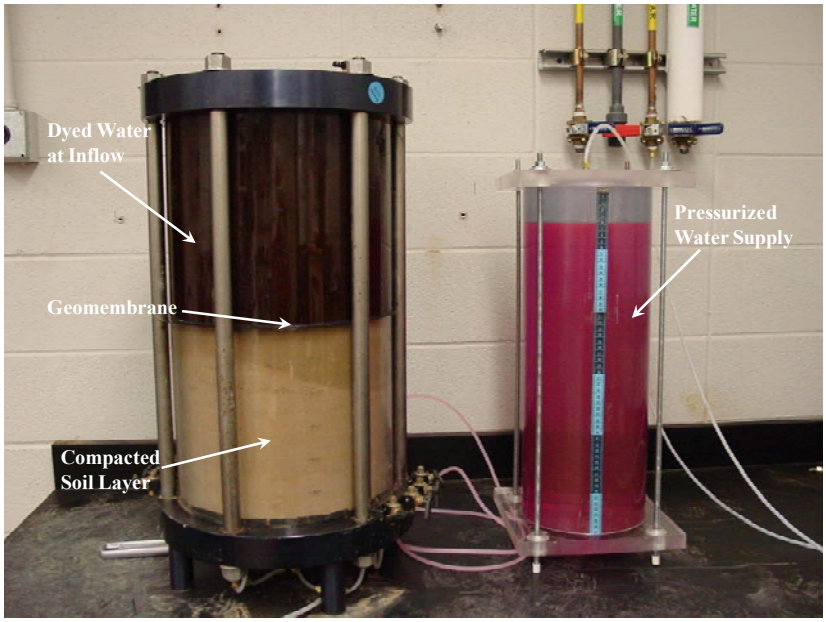

Figure 3.16: Large permeameter with geomembrane liner over the as-compacted soil layer with dye

3.4 SCOPE OF EXPERIMENTAL PROGRAM

The experimental component of this study was conducted to evaluate the leakage through defects in geomembrane liners under high hydraulic heads. An important objective of the testing program was to generate a database of leakage rate values

considering a range of variables, including hydraulic head, interface quality, soil unit weight and soil type. Three main test series conducted as part of the experimental study include:

i) Geomembrane-only (GM-Only) tests involving a geomembrane in direct contact with a sand layer (no secondary liner);

ii) Geomembrane-compacted clay liner (GM-CCL) tests on a composite liner system that included a geomembrane in direct contact with a clay layer;

iii) Geomembrane-geosynthetic clay liner (GM-GCL) tests on a composite liner system comprised of a geomembrane over a GCL placed on a sand layer.

For tests involving GCLs, both unhydrated GCLs (UGCLs) and GCLs hydrated prior to testing (HGCLs) were used to determine the effect of prehydration on the leakage through a defect in a composite lining system. Tests were also conducted for systems without geomembranes to establish an upper bound for flow through the soil layers. These test series included Sand-Only, CCL-Only, and GCL-Only. It should be noted that the GCL-Only tests included a sand layer beneath the GCL as a foundation layer. All experimental tests presented in the following chapters are listed in Table 3.4. The test designation (e.g., GM-CCL-1), applied head and objectives for each test series are listed in Table 3.4.

Table 3.4: Scope of experimental testing program

Series	Tests	Hydraulic Head (m)	Soil Type	Objectives
GM-Only	GM-1	3.5	Monterey #30 Sand	To quanitfy leakage through defects in a geomembrane liner placed over a soil with high hydraulic conductivity
	GM-2	7		
	GM-3	14		
	GM-4	17.5		
	GM-5	21		
	GM-6	28		
	GM-7	35		
GM-CCL	GM-CCL-L1	0.53	RMA Soil Type II Silty Clay	To quantify the leakage through defects in composite lining systems consisting of a geomembrane and a compacted clay liner (CCL) of low density
	GM-CCL-L2	0.53		
	GM-CCL-L3	35		
	GM-CCL-1	7	RMA Soil Type II Silty Clay	To quantify the leakage through defects in composite lining systems consisting of a geomembrane and a compacted clay liner (CCL)
	GM-CCL-2	14		
	GM-CCL-3	21		
	GM-CCL-4	28		
	GM-CCL-5	35		
	GM-CCL-6	42		
	GM-CCL-5P	35	RMA Soil Type II Silty Clay	To determine effect of contact quality on the leakage rate through GM-CCL composite liner system
	GM-CCL-LC1	0.3	RMA Soil Type II Silty Clay	To determine effect of permeameter size on the leakage through GM-CCL composite liner system (these two tests were conducted using the large permeameter cell)
	GM-CCL-LC2	7		
GM-GCL	GM-UGCL-1	7	Monterey #30 Sand	To quantify the leakage through defects in composite lining systems consisting of a geomembrane and an unhydrated geosynthetic clay liner
	GM-UGCL-2	14		
	GM-UGCL-3	21		
	GM-HGCL-1	14	Monterey #30 Sand	To quantify the leakage through defects in composite lining systems consisting of a geomembrane and a hydrated geosynthetic clay liner To determine effect of prehydration of GCL on leakage through defects in a GM-GCL composite liner
	GM-HGCL-2	21		
	GM-HGCL-3	28		
	GM-HGCL-4	28		
	GM-HGCL-5	35		
	GM-HGCL-6	42		
	GM-HGCL-P	7	Monterey #30 Sand	To determine effect of contact quality on the leakage rate through GM-GCL composite liner system
Sand-Only	SP-1	7	Monterey #30 Sand	To quantify upper bound and hydraulic conductivity through a sand layer without a geomembrane
	SP-2	14		
CCL-Only	CCL-1	7	RMA Soil Type II Silty Clay	To quantify upper bound and hydraulic conductivity through a compacted clay liner without a geomembrane
	CCL-2	14		
	CCL-3	21		
GCL-Only	UGCL-Only	14	Monterey #30 Sand	To quantify upper bound and hydraulic conductivity through a GCL over sand without a geomembrane
	HGCL-Only	14	Monterey #30 Sand	

3.5 APPROACH TO INTERPRETATION OF EXPERIMENTAL DATA

Before covering specific details of the laboratory tests and the results of those tests in the following chapters, the rationale behind how the experimental data was interpreted is discussed in this section. This is a general discussion and will not include specifics regarding data that are shown herein. These specifics will be presented in the following sections.

The volume of water flowing into and out of the permeameter was monitored over time. An example of the cumulative volume data for one of the tests is shown in Figure 3.17a. Driven by the hydraulic head imposed on the system, water flowed through the defect and infiltrated the soil layer. As the wetting front progressed through the soil layer, the pore spaces of the unsaturated soil were filled with water and the volumetric water content, as well as the degree of saturation, increased. The wetting front advanced through the soil layer until it reached the bottom of the cell, at which point outflow began.

The collected volume of water was used to calculate the flow rates. The slopes of the inflow and outflow volume curves, shown in Figure 3.17a, correspond to the inflow and outflow rates, shown in Figure 3.17b, for the system being tested. The difference between the inflow and outflow cumulative volumes corresponds to the volume of water in being stored in the pores of the initially unsaturated soil layer and in the components of the cell (e.g., the porous stone). The slopes of the volume curves become constant after approximately 150 hours, which means that the flow rates are approaching a constant value after 150 hours.

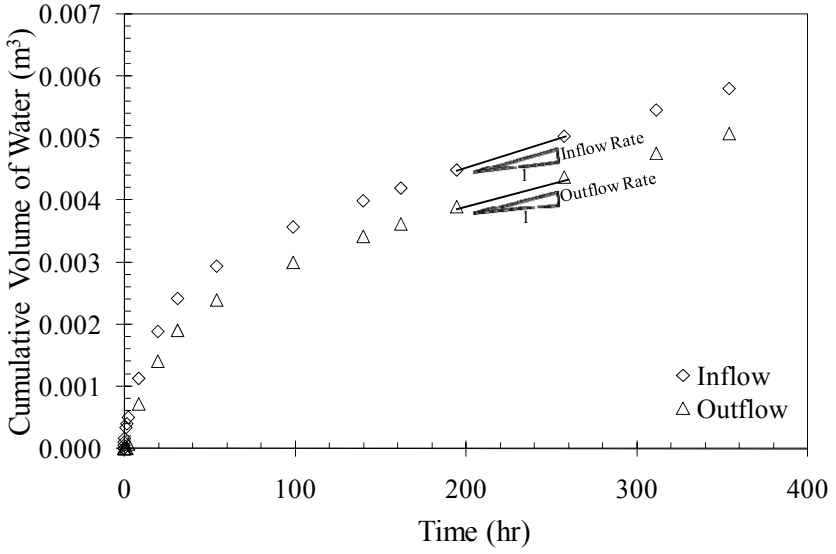

(a)

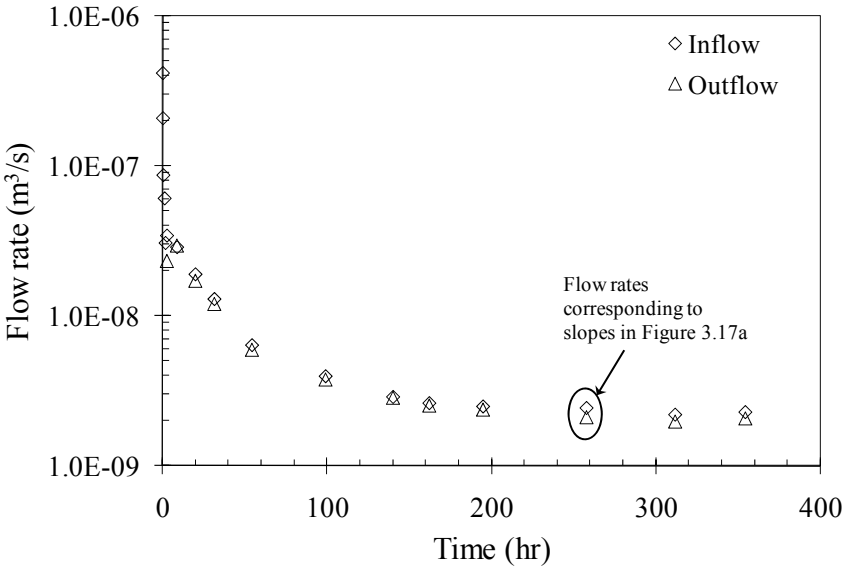

(b)

Figure 3.17: Examples of (a) cumulative volume and (b) flow rates into and out of the permeameter cell for a geomembrane-compacted clay liner test

A close-up of the cumulative water volume curve for the early stages of the permeameter test is shown in Figure 3.18. As shown in the figure, the time at which outflow began, or breakthrough time, is between two and three hours. Outflow is equal to zero until breakthrough occurs because the soil is initially unsaturated. For saturated soil layers, outflow would begin immediately and the gap between the inflow and outflow curves would not be present.

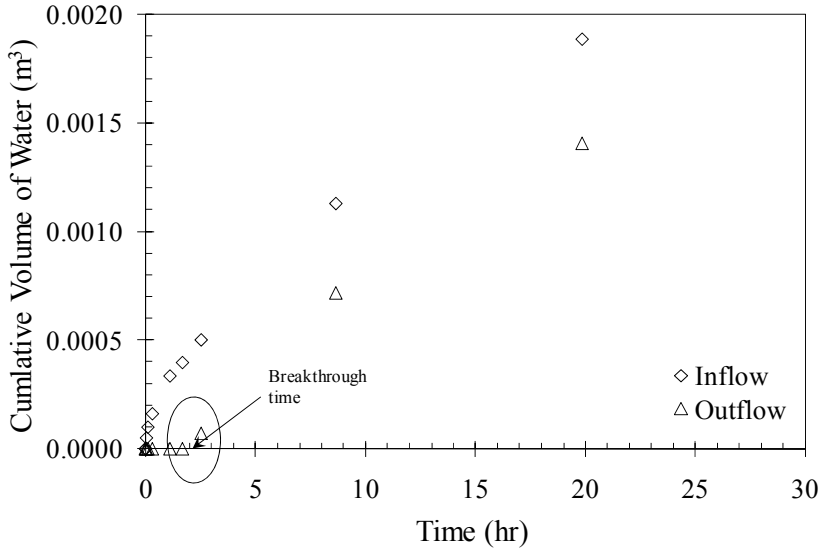

Figure 3.18: Close up of the cumulative volume curve for the early stages

The tests shown in Figure 3.17 were continued until the flow in the system stabilized to a steady rate. The ratio between outflow and inflow was also calculated to determine if a steady-state flux had been achieved. The outflow/inflow ratio, shown in Figure 3.19, was calculated by dividing the outflow rate by the inflow rate. The outflow/inflow ratio was highly variable during the early stages of the test, as shown in Figure 3.19a. Fluctuations in the outflow/inflow ratio indicate that flow through the system has not stabilized to a steady-state and that the inflow and outflow rates are not equal. However, as time progressed during a test, the inflow and outflow ratio

approached one as the flow in the system stabilized, at which point the fluctuations in the flow ratio were minimal. For the case shown in Figure 3.19b, there was higher variability in the outflow/inflow ratio than the case shown in Figure 3.19a, even as the measured flow rates became constant. Although the variability in Figure 3.19b can be considered acceptable, the primary criterion selected to determine when a steady rate had been achieved during a test was the actual measured flow rates (i.e., flow rates shown in Figure 3.17).

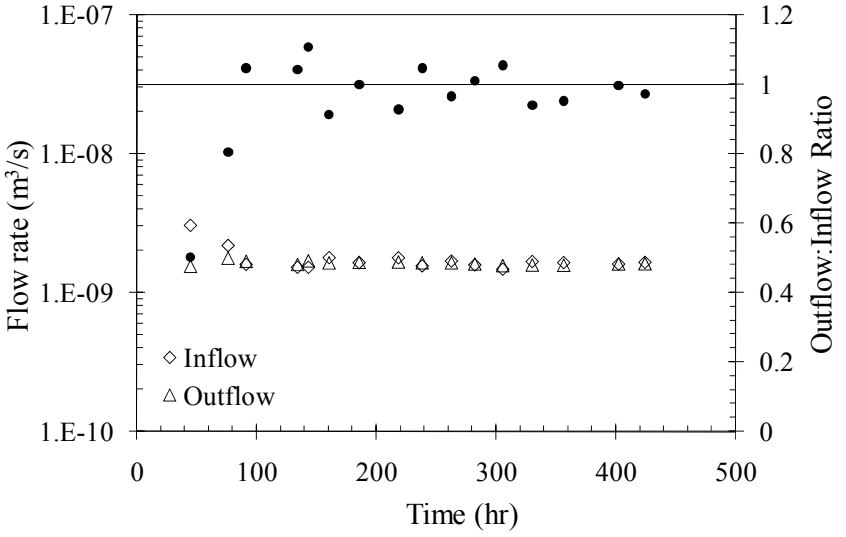

(a)

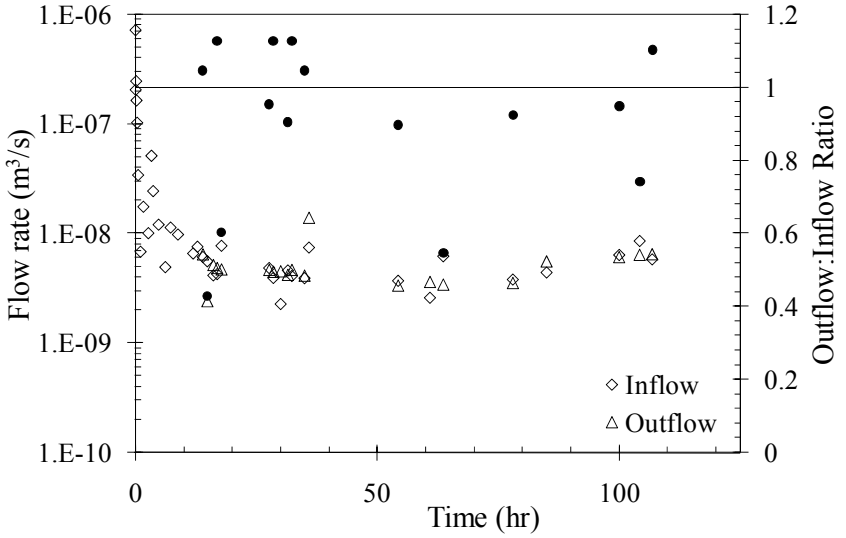

(b)

Figure 3.19: Examples of outflow-inflow ratio for tests in small permeameter cell: a) good outflow-inflow ratio and b) poor outflow-inflow ratio

Two methods were used to report the final leakage rates for tests involving the permeameter cells. The first method consists of taking an average slope of the

cumulative volume curve (inflow) once the slope has become constant as shown in Figure 3.20a. The leakage rates determined using this method are referred to as the "average values." The second method is simply reporting the value of the leakage rate at the end of the test, or the "end values" as shown in Figure 3.20a. As shown in Figure 3.20b, the difference between the two methods is not significant. The first method (i.e., "average values") was adopted to report the leakage rates in this study. Specifically, the leakage rates reported in the next three chapters are the "average values" of the inflow rates obtained once flow in the system has stabilized (i.e., a steady rate has been reached).

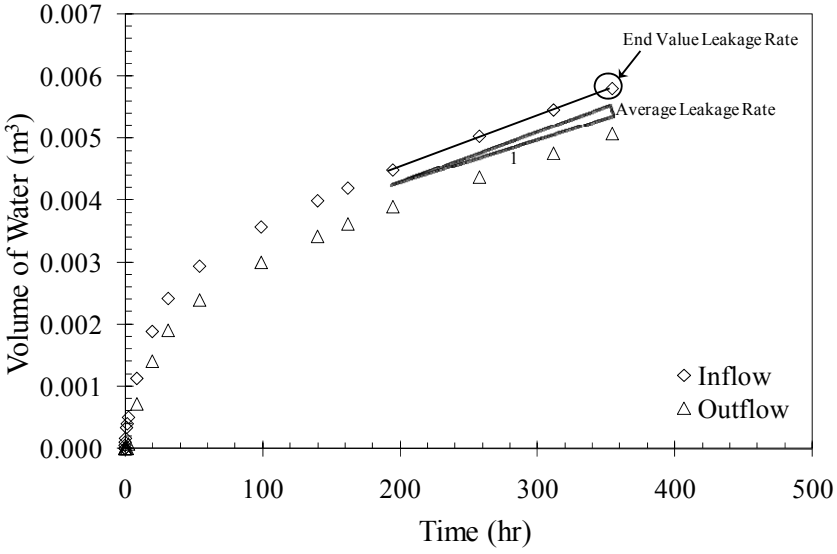

(a)

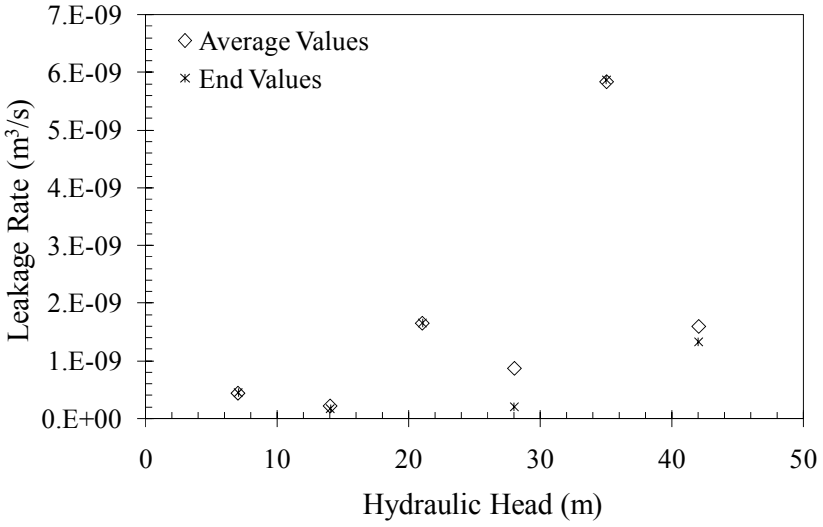

(b)

Figure 3.20: Comparison between “average values” and “end values” for leakage rates

Chapter 4: Geomembrane-Only Tests

4.1 INTRODUCTION

The experimental results and analysis presented in this chapter involve a geomembrane placed in direct contact with a layer of soil with a high hydraulic conductivity. The primary objective of this test series was to quantify the leakage rate through a defect in a geomembrane liner over a soil layer with a high hydraulic conductivity. Also, the permeameter tests were used to investigate the effectiveness of a geomembrane in minimizing flow through such a system. The effect of head above the geomembrane liner was evaluated using data obtained from the geomembrane-only (GM-only) test series. Another objective of this component of the study presented herein was to verify the suitability of existing predictive tools for estimating the leakage through defects in a geomembrane liner over soil with relatively high hydraulic conductivity.

4.2 EXPERIMENTAL RESULTS FOR GEOMEMBRANE-ONLY TESTS

Experimental tests were conducted using the small permeameter cell as part of the GM-Only test series with the objective of creating a database of leakage rates. Tests were conducted using the equipment, methods and materials for the small permeameter cell discussed in Chapter 3. The cumulative volume of water and flow rate recorded during each test, as well as the specific soil properties for each test discussed in this section, are included in Appendix A.

A layer of Monterey #30 sand was prepared to a relative density of 75%, resulting in a soil layer with a total unit weight of 15.8 kN/m^3 and a porosity of 0.39. The procedure involved saturating the soil layer prior to initiation of testing. The same sand layer was utilized for all tests in this test series, which involved tests conducted at

increasing values of hydraulic head. The seven tests in the GM-Only series were conducted using heads ranging from 3.5 to 35 m, as summarized in Table 4.1. A circular defect with a diameter of 1.6 mm was made at the center of the 1 mm-thick LLDPE geomembrane.

Table 4.1: Details of the GM-Only test series

Test #	Head Above Liner (m)	Leakage Rate (m^3/s)
GM-1	3.5	4.0×10^{-6}
GM-2	7	7.1×10^{-6}
GM-3	14	1.2×10^{-5}
GM-4	17.5	1.5×10^{-5}
GM-5	21	1.7×10^{-5}
GM-6	28	2.0×10^{-5}
GM-7	35	2.3×10^{-5}

For each test in the GM-Only test series, the volume of water that flowed into and out of the cell was recorded with time. Cumulative water volume and leakage rates, shown in Figure 4.1, were obtained from the measurements made during each test. Since the soil layer was saturated prior to testing, outflow began immediately after initiation of the test. Also because of the initial saturated condition of the sand, the volume of water flowing into the permeameter cell was essentially the same as the volume of water flowing out of the system throughout the test, confirming that water was not being stored in the sand (Figure 4.1a). The average run time for each test was 10 minutes.

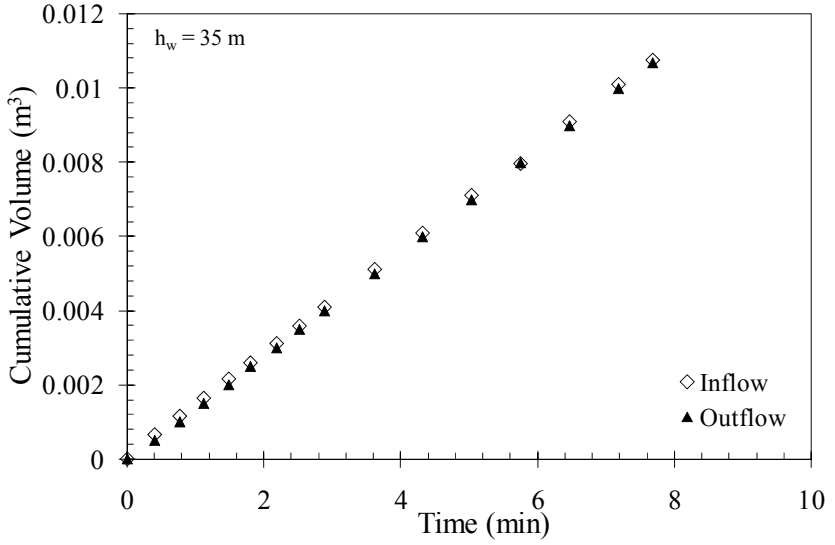

(a)

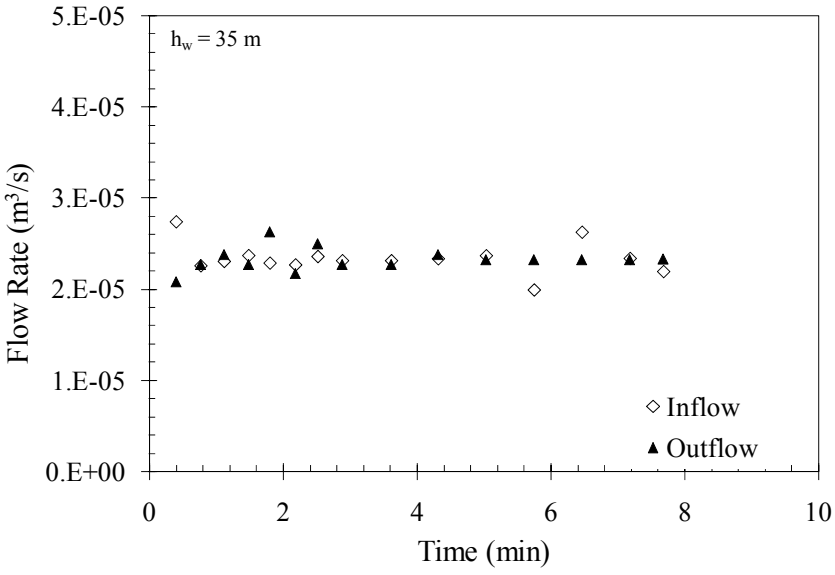

(b)

Figure 4.1: Example of results from geomembrane-sand tests: (a) cumulative volume and (b) flow rates for Test GM-7

The leakage rate values shown in Figure 4.2 were obtained for each one of the seven tests conducted in the GM-Only test series. As shown by these results, the leakage rate increased with increasing hydraulic head, but the relationship is non-linear.

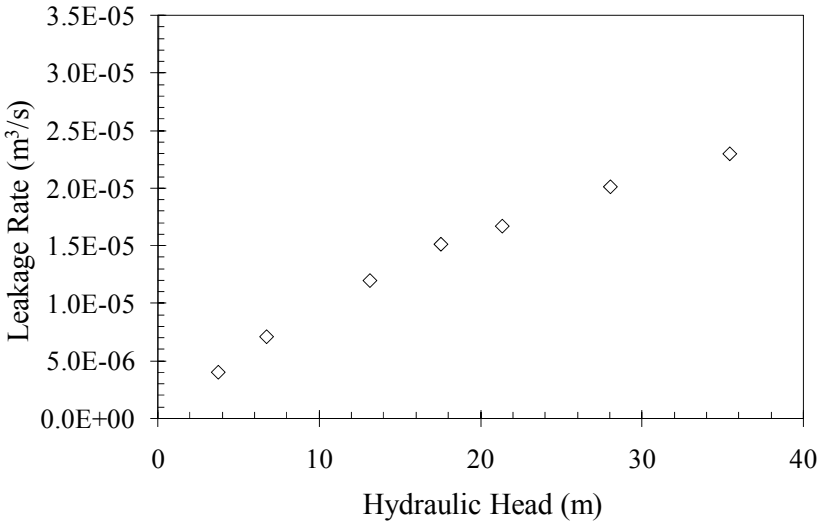

Figure 4.2: Leakage rates for a range of heads for the GM-Only test series

Tests were also conducted on layers of Monterey #30 (without a geomembrane) in order to measure the hydraulic conductivity of the soil using the same permeameter cell as used for measuring leakage rates in this study. The leakage rates obtained from the tests without geomembranes are included in Table 4.2. These leakage rates are an order of magnitude higher than the leakage rates measured in the GM-Only test series (Table 4.1). The hydraulic conductivity for the Monterey #30 sand was calculated using the leakage rates obtained from the permeameter tests without a geomembrane. The average hydraulic conductivity was 3.7×10^{-5} m/s.

Preliminary tests were conducted in this study involving a geomembrane placed over an unsaturated sand layer. In these tests, it was observed that flow only occurred through the center of the cell. Wetting of the sand at the cell boundaries was not

observed. Since the soil was a sand, capillary action and horizontal gradients were not significant enough to visibly draw water away from the central portion of the soil layer. Consequently, it was decided to conduct all tests in this series using sand under saturated conditions.

Table 4.2: Leakage rates for Monterey #30 sand without a geomembrane

Test #	Head Above Liner (m)	Leakage Rate (m^3/s)	Hydrualic Conductivity (m/s)
SP-1	7	2.2×10^{-5}	4.2×10^{-5}
SP-2	14	3.2×10^{-5}	3.1×10^{-5}

4.3 ANALYSIS OF GEOMEMBRANE-ONLY TESTS

The leakage rates obtained from the GM-Only test series presented in the previous section were used to validate existing equations used to predict flow through defects in the a geomembrane liner over a soil with relatively high hydraulic conductivity. The experimental data was compared with flow rates calculated using Darcy's law and Bernoulli's orifice equation.

4.3.1 Leakage Rates: Upper and Lower Bounds

Darcy's law may be used to provide upper and lower bounds of the flow through a clay layer due to a defect in a geomembrane. The lower bound of the flow can be predicted as:

$$Q = kia \tag{4.1}$$

where Q is the leakage rate, k is the hydraulic conductivity of the soil, i is the hydraulic gradient, and a is the area of the defect. The hydraulic gradient is the change in total head loss across the soil layer divided by the length of the soil layer. The upper bound of the flow can be estimated as:

$$Q = kiA \tag{4.2}$$

where A is the cross-sectional area of the permeameter cell. Flow rates that were calculated using the total cross-sectional area of the permeameter are representative of the flow rate through an unlined soil layer. The upper and lower bound of the flow are shown in Figure 4.3, along with the data from the GM-Only test series.

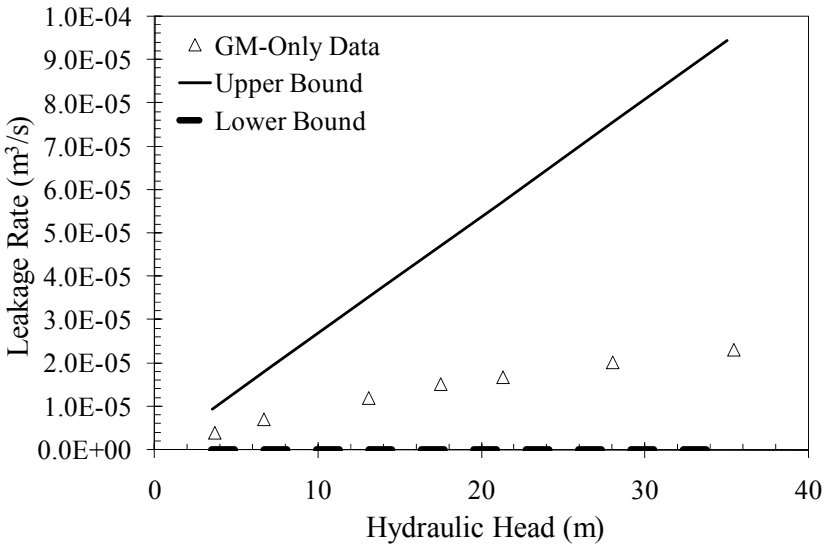

Figure 4.3: Comparison of flow rates calculated using Darcy's law and leakage rates from GM-Only test series

The measured leakage rates from the experimental testing program are below the flow rates over the total cross-sectional area (no geomembrane liner). The difference in the leakage rates between the measured and calculated values increases as the hydraulic head increases. Darcy's law is based on the premise that flow through the soil is directly proportional to the hydraulic gradient. However, the trend in the data from the GM-Only test series was non-linear. Since the sand layer under the geomembrane does not significantly impede the flow through the defect, the system may be approximated as free flow through an orifice, as shown in the next section.

4.3.2 Bernoulli's Equation for Flow through an Orifice

Giroud and Bonaparte (1989) recommended using Bernoulli's equation for flow through an orifice for systems with a geomembrane liner overlying highly permeable soils. Bernoulli's orifice equation takes into account head losses due to contraction of the flow area. In this case, the water infiltrating through a defect in a geomembrane liner flows from a larger area (area of the permeameter cell) to a smaller area (area of the defect). The measured leakage rates from the GM-Only test series were compared with the leakage rates predicted using Bernoulli's orifice equation (Equation 2.26).

As shown in Figure 4.4, different values for the empirical coefficient, C were used to find the best fit for the data. Giroud and Bonaparte (1989) suggested a value of C = 0.6 for use with flow through defects in geomembranes. However, a coefficient of C = 0.6 yields leakage rates that are larger than the measured values. Instead, a lower value for the coefficient C was found to provide a better fit to the experimental data. The difference between the coefficient value suggested by Giroud and Bonaparte (1989) and the value providing a better fit to the experimental data may be attributed to the high hydraulic heads that were used in this study. The orifice coefficient is also affected by the sharpness of the orifice edges, roughness of the defect interior and diameter of the defects.

The results of the laboratory tests shown in Figure 4.4 suggest that Bernoulli's equation for flow through an orifice can be used to estimate leakage for flow through a small defect in a geomembrane over a sand layer. Although the good match depended on the selection of the proper flow coefficient, C, the trend of leakage rates predicted using the orifice equation was consistent with the experimental measurements. In summary, use of Equation (2.26) with properly calibrated C-coefficients for high heads is

considered to be suitable for prediction of the leakage through systems in which a geomembrane liner is placed over a highly permeable soil under high heads.

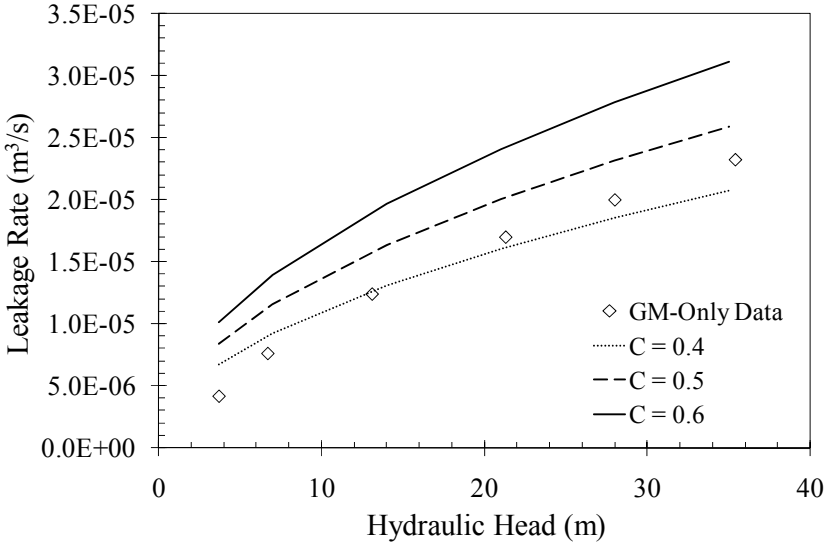

Figure 4.4: Comparison of leakage rates from GM-Only tests with Bernoulli's orifice equation

Chapter 5: Geomembrane-Compacted Clay Liner Tests

5.1 INTRODUCTION

The experimental results and analysis presented in this chapter include a composite liner system that consists of a geomembrane placed in direct contact with a compacted clay liner (CCL). The test series presented in this chapter was conducted as part of the experimental program to quantify the leakage rate through a defect in a geomembrane-compacted clay liner (GM-CCL) system under high hydraulic heads. Placing a geomembrane in direct contact with a clay layer is representative of conditions where a geomembrane is installed on the clay core of dam (see Figure 2.2) or where a compacted clay liner is placed beneath the geomembrane to minimize the leakage through the lining system. The effect of head above the geomembrane liner and contact quality of the interface between the geomembrane and clay layer were evaluated using data obtained from the GM-CCL test series. Other aspects of flow through a defect in a geomembrane liner, such as the transmissivity of the interface between the geomembrane and the soil layer and the radius of interface flow, were also evaluated.

Another objective of these analyses was to develop predictive tools suitable for estimating the leakage through defects in geomembrane liners placed on the upstream face or in the core of a dam. The laboratory data from the GM-CCL tests were compared against existing analytical and "empirical" models to determine their validity for predicting flow through a defect in a geomembrane-CCL composite liner under high heads. A new simplified equation was developed and compared with the experimental data.

5.2 SMALL PERMEAMETER EXPERIMENTAL RESULTS & ANALYSIS

Experimental tests were conducted using the small permeameter cell as part of the GM-CCL test series for the objective of creating a database aimed at quantifying leakage rates for variables such as hydraulic head, interface quality, and soil unit weight. Tests were conducted using the equipment, methods and materials for the small permeameter cell discussed in Chapter 3. The cumulative water volume and flow data recorded during each test and specific soil properties for each test discussed in this section are included in Appendix A.

Changes in volumetric water content were monitored during some tests using the TDR system discussed in Section 3.2.1. These data were compared with infiltration models as well as visual observation of the wetting front during the early stages of the test.

5.2.1 Leakage Rates

The degree of saturation in the clay layer at the beginning of the tests ranged from 43% to 64%. At the end of each test, the soil remained unsaturated, with degrees of saturation higher than the initial values but remaining below 90%. Specific test details, such as soil dry unit weight, porosity, initial and final water contents and degrees of saturation, are included in Tables 5.1 and 5.2. Also included in Tables 5.1 and 5.2 is the hydraulic head applied to the geomembrane and final leakage rates for each test.

5.2.1.1 Tests under Low Heads

Tests GM-CCL-L1 and GM-CCL-L2 were conducted to quantify the leakage through a geomembrane defect under a comparatively low hydraulic head (i.e., height of water applied to geomembrane) of 0.53 m. The soil layers in both tests were prepared using RMA Soil Type II, which had been moisture conditioned to a target gravimetric

water content of 7.0%. The soil layers were compacted in the permeameter cell to the target relative compaction of 70%. The dry unit weight, porosity, initial and final water contents and degrees of saturation of the soil layers for the two tests conducted under 0.53 m of water are listed in Table 5.1.

During preparation of the soil layer for Test GM-CCL-L1, the soil was trimmed flush with the lip of the permeameter cell. As discussed in Section 3.2, a cork gasket was used to maintain a pressure-tight seal between the geomembrane and the cell. The gasket created a slight gap (i.e., thickness of the cork gasket was 0.16 cm) between the geomembrane and the surface of the soil. A slight deflection was observed on the geomembrane when the head of 0.53 m was applied to the system. The contact between the geomembrane and the soil was not intimate, or "poor," due to the gap created by the trimming of the soil layer and the presence of the cork gasket. Instead, soil in Test GM-CCL-L2 was trimmed so that its surface was slightly above the cork gasket. Deflection of the geomembrane were not observed under the applied water pressure, suggesting that the geomembrane and the underlying soil layer were in intimate, or "good," contact.

Cumulative water volume and leakage rate data were obtained from the inflow and outflow measurements made during each test. Using the procedure discussed in Section 3.5, the final leakage rates for each test were determined and are listed in Table 5.1. The leakage rate for the test with "poor" contact (GM-CCL-L1) is two orders of magnitude larger than the leakage rate for the system in which the geomembrane had a more intimate contact with the soil layer (GM-CCL-L2). However, there are some differences in the initial properties of the soil layers that may also account for the difference in the leakage rates. For the test GM-CCL-L2, the porosity is lower and the initial water content is higher than for the test GM-CCL-L1, although the difference in water content could be considered negligible. The soil with a lower porosity has a lower

hydraulic conductivity than a soil with a higher porosity, which would result in a lower leakage rate.

Table 5.1: Test detail and results for low-head tests

Test #	Head Above Liner (m)	Dry Unit Weight (kN/m^3)	Relative Compaction (%)	Porosity, n	Initial		Final		Contact Quality	Leakage Rate (m^3/s)
					Water Content, w (%)	Degree of Saturation (%)	Water Content, w (%)	Degree of Saturation (%)		
GM-CCL-L1	0.53	12.9	66.0	0.52	7.3	18.6	29.4	74.7	Poor	1.2×10^{-7}
GM-CCL-L2	0.53	13.7	70.3	0.48	7.6	21.9	29.2	84.4	Good	1.2×10^{-9}

5.2.1.2 Tests under High Heads

Preliminary Testing

A preliminary test for high heads, designated GM-CCL-0, was prepared at the same target relative compaction (RC = 70%) as the two tests discussed in Section 5.2.1.1. In this case, the head applied to the system was 35 m, which was significantly higher than the previously applied head of 0.53 m. The soil layer was trimmed flush with the lip of the permeameter cell, creating a small gap and a "poor" contact between the geomembrane and soil surface. Once the high hydraulic head was applied to the system, a significant deflection of the geomembrane was observed. The cell began to leak as the geomembrane was pulled down, breaking the seal between the geomembrane, o-ring and cork gasket. The test was halted and the geomembrane was removed. While the test could not be conducted, several observations could still be made: i) the surface of the soil, which had originally been flush with the lip of the permeameter, was 3-4 cm below the original height of the soil layer, as shown in Figure 5.1a; and ii) there was a pitted area in surface of the soil layer at the location of the hole in the geomembrane, where it seems that soil particles were displaced to the sides of the cell (Figure 5.1b). The jagged edges of the pitted area suggest that erosion occurred beneath the geomembrane at the location of the defect. However, as shown in Figure 5.1a, the soil particles were not

washed out of the cell, but rather settled around the edges of the cells on the surface of the soil and/or were compressed into the soil layer. Erosion such as that shown in Figure 5.1 did not occur for the denser soil layers of the GM-CCL test series. While Brown et al. (1987) did not report the density of the compacted clay layers used their study, the erosion observed and reported by the authors was similar to that observed in Test GM-CCL-0.

GM-CCL Test Series

Six tests were conducted to quantify leakage through a geomembrane defect under high hydraulic head. The soil layers for these tests were prepared using RMA Soil Type II which had been moisture conditioned to a target water content of 11.9%, which corresponds to the optimum water content. The soil layers were compacted in the permeameter cell for a target relative compaction of 90%, which corresponds to a higher unit weight (lower porosity) that the two tests discussed in Section 5.2.1.1.

A list of the various tests conducted to evaluate the effect of head above the geomembrane liner on the leakage through a defect is presented in Table 5.2. The characteristics of the soil layer for Tests GM-CCL-1 through GM-CCL-6 and the final leakage rates are also listed in Table 5.2. In order to determine the effect of the head above the liner, the head was increased while the target water content, target relative compaction and contact quality remained unchanged. The initial water content for each test was measured from samples of the uncompacted, moisture-conditioned soil. While the target water content was the same for all tests, the moisture conditioning process led to variations in the initial water contents for each test. The final water content for each test was the average water content measured from several samples taken from the soil layer at different elevations. The water content near the surface of the soil (i.e., near the defect) was typically higher than the water content at lower elevations in the soil layer.

Variations in the relative compaction in relation to the target value can be attributed to the difficulty in exactly reproducing soil placement conditions. All six test soil layers were trimmed to obtain a good contact between the geomembrane and the surface of the soil. The quality of the contact for the GM-CCL tests was considered to be "excellent."

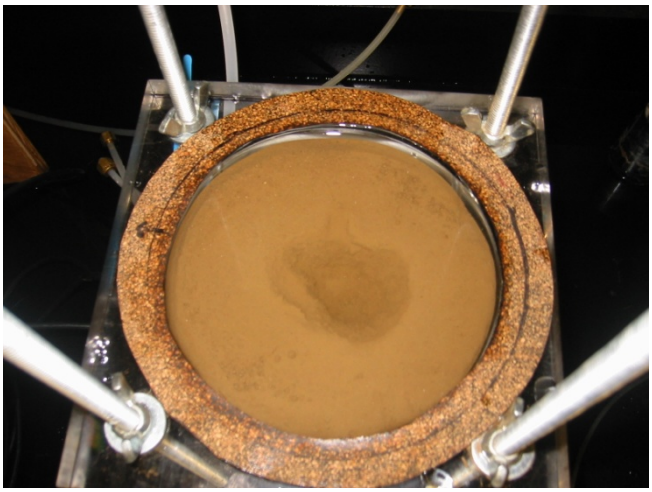

(a)

(b)

Figure 5.1: (a) View of the surface of test GM-CCL-0 showing visual observations after test with loose soil under a high head and b) close-up of eroded area beneath the geomembrane defect

Table 5.2: Test details and leakage rates for high head tests

Test #	Head Above Liner (m)	Dry Unit Weight (kN/m^3)	Relative Compaction (%)	Porosity, n	Initial		Final		Leakage Rate (m^3/s)
					Water Content, w (%)	Degree of Saturation (%)	Water Content, w (%)	Degree of Saturation (%)	
GM-CCL-1	7	16.8	86.0	0.37	11.5	53.3	17.0	78.8	4.3×10^{-10}
GM-CCL-2	14	17.0	87.2	0.36	12.1	58.2	16.5	79.2	2.1×10^{-10}
GM-CCL-3	21	17.1	87.8	0.36	11.1	54.6	17.0	83.8	1.7×10^{-9}
GM-CCL-4	28	17.3	88.6	0.35	12.8	64.6	-	-	8.7×10^{-9}
GM-CCL-5	35	17.5	89.6	0.34	9.8	51.0	15.7	81.5	5.8×10^{-9}
GM-CCL-6	42	17.1	87.5	0.36	13.7	66.6	-	-	1.6×10^{-9}

An example of the cumulative water volume data for these tests is shown in Figure 5.2a. Note that there is a gap between the cumulative volume curves for flow into and out of the system. The difference between the two curves (732 cm^3) is approximately equal to the change in the volume of water being stored in the pores of the initially unsaturated soil and in the porous stone at the bottom of the cell (approximately 700 cm^3). A close-up of the early stages of Test GM-CCL-5 is shown in Figure 5.2b. As shown in the figure, flow into the cell begins immediately while the outflow at the beginning of the test is zero because breakthrough only occurred after a period of times. The outflow remains at zero until about 2 hours into the test.

The leakage rates measured over time during the six permeameter tests in the GM-CCL test series for high heads are shown in Figure 5.3. The leakage rates were high in the early stages of the test and decreased as the time progressed, as shown in Figure 5.3. This observed decrease in leakage rate over time is consistent with reported infiltration pattern into a dry soil profile under ponded conditions (Tindall and Kunkel 1999). As discussed by Tindall and Kunkel (1999), the infiltration rate is initially high because of the high initial gradients within the soil layer. As the wetting front advances through the soil layer, the hydraulic gradient decreases.

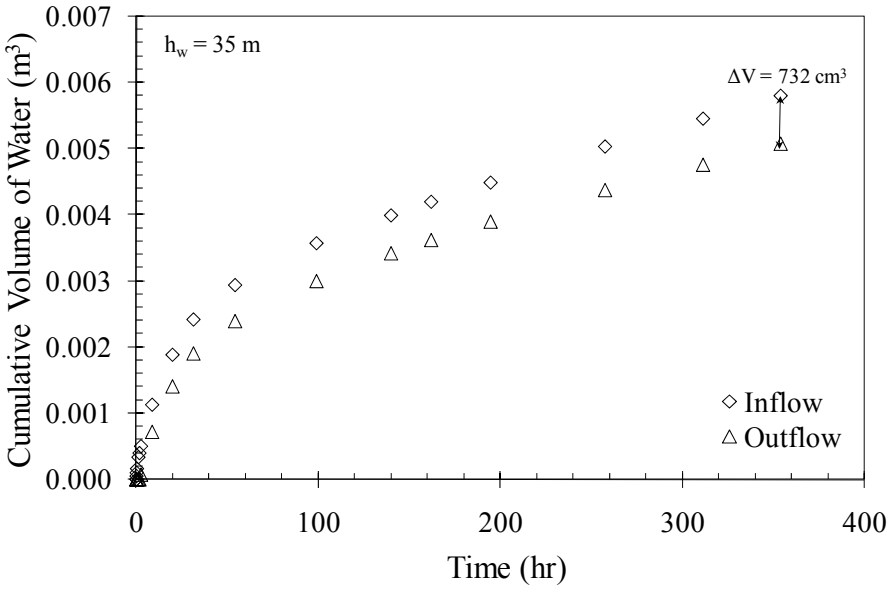

(a)

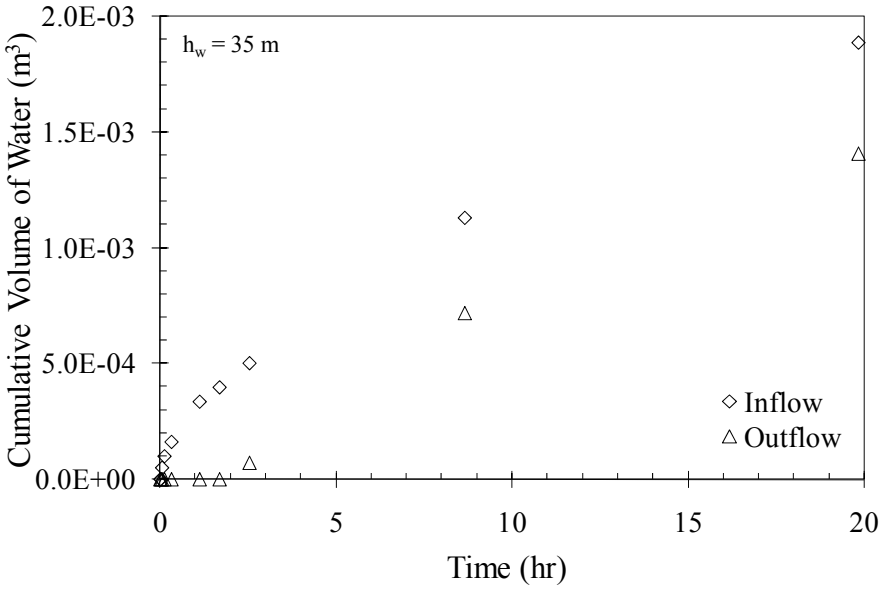

(b)

Figure 5.2: Test results from test GM-CCL-5: a) cumulative volume data and b) a close-up of the early stages of the test showing when outflow began

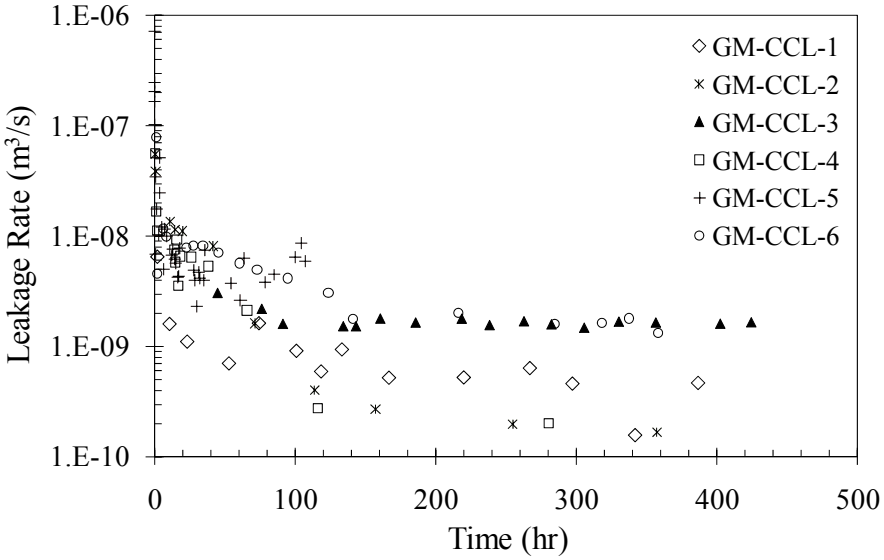

Figure 5.3: Leakage rates over time for the geomembrane-clay tests conducted under high heads

The final leakage (inflow) rates obtained for tests GM-CCL-1 through GM-CCL-6 are shown in Figure 5.4. Leakage rates through the defect in the geomembrane liner over the CL soil show increasing values with increasing hydraulic head. While there is some scatter in the data, a linear trend could be assumed. Also, Test GM-CCL-5 (data point at a head of 35 m in Figure 5.4) had a leakage rate of 5.8×10^{-9} m^3/s, which was above the expected range of flow rates for the GM-CCL test series. The results from test GM-CCL-5 can be considered to be an outlier because the initial water content of the soil layer was lower than rest of the tests in the GM-CCL series. All things being equal, a soil layer with a low initial water content would have a higher hydraulic conductivity (and thus a higher leakage rate) than a soil layer with an initially high water content.

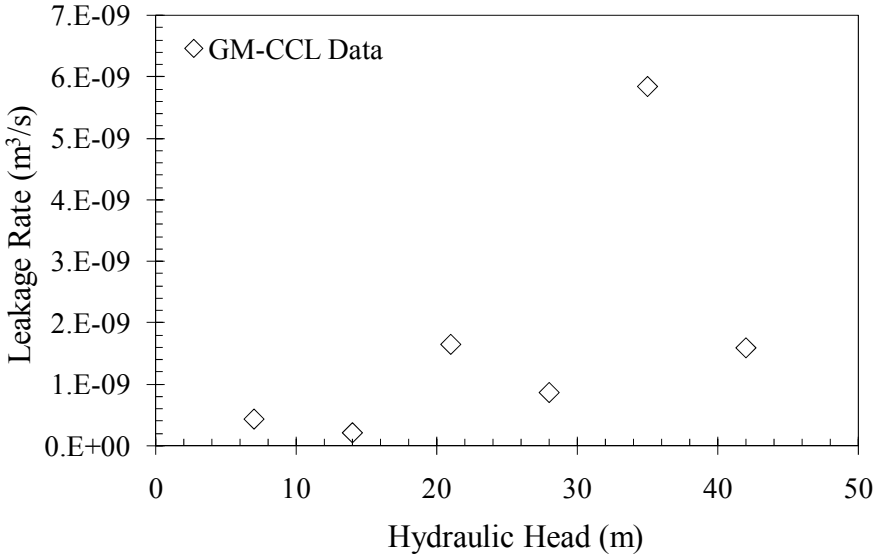

Figure 5.4: Leakage rates over a range of hydraulic heads for geomembrane-clay systems under high heads

Tests CCL-1 through CCL-6 were conducted using RMA Soil Type II for the same target water content and relative compaction without a geomembrane in order to measure the hydraulic conductivity of the soil using the same permeameter cell as used for measuring leakage rates in this study. The leakage rates obtained from the tests without geomembranes are listed in Table 5.3. The leakage rates from tests without geomembranes are an order of magnitude higher than the leakage rates measured in the GM-CCL test series, which are included in Table 5.2. Leakage rates through a soil layer can be reduced by placing a geomembrane over the soil even if there is a defect in the liner. The hydraulic conductivity for the RMA Soil Type II (relative compaction of 90%) was calculated using the leakage rates obtained from the permeameter tests without a geomembrane. The average hydraulic conductivity was 8.3×10^{-9} m/s.

Table 5.3: Leakage rates for RMA Soil Type II without a geomembrane

Test #	Head Above Liner (m)	Leakage Rate (m^3/s)	Hydraulic Conductivity (m/s)
CCL-1	7	4.6×10^{-9}	8.18×10^{-9}
CCL-2	14	8.6×10^{-9}	8.59×10^{-9}
CCL-3	21	1.4×10^{-8}	8.11×10^{-9}

5.2.1.3 Upper and Lower Bounds

Darcy's law may be used to estimate upper and lower bounds of the flow through a clay layer due to a defect in a geomembrane. The lower bound of the flow can be predicted by considering one-dimensional flow over the area of the defect only, as follows:

$$Q = kia \tag{5.1}$$

where Q is the leakage rate, k is the hydraulic conductivity of the soil, i is the hydraulic gradient, and a is the area of the defect. The hydraulic gradient is the change in total head loss across the soil layer divided by the length of the soil layer. The upper bound of the flow can be estimated as:

$$Q = kiA \tag{5.2}$$

where A is the cross-sectional area of the permeameter cell. Flow rates that were calculated using the total cross-sectional area of the permeameter are representative of the flow rate through an unlined soil layer. The upper and lower bound of the flow are shown in Figure 5.5, along with the data from the GM-CCL test series.

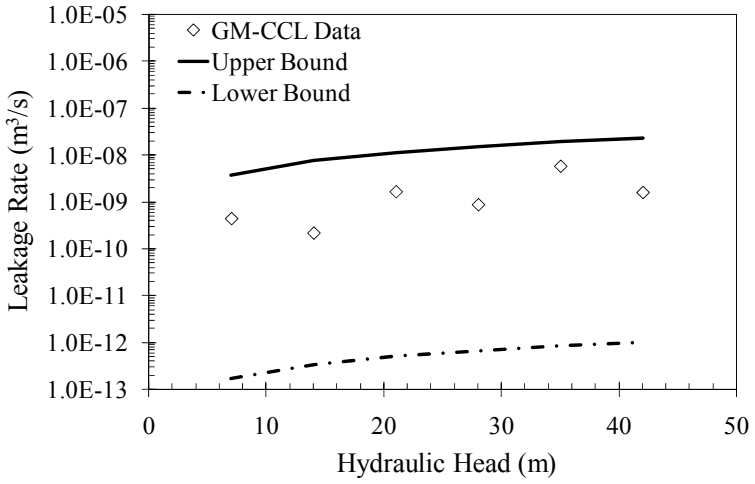

Figure 5.5: Comparison of flow rates calculated using Darcy's law and leakage rates from GM-CCL test series

The leakage rates in Figure 5.5 are shown on a semi-logarithmic scale since the predicted and measured flow rates range over several orders of magnitude. As expected, the leakage rates measured in the experimental testing program, shown in Figure 5.5, are less than those predicted for the case without a geomembrane liner and greater than those predicted for the case of perfect contact. This indicates that, for the GM-CCL test series, water flows over an average area larger than just the defect area but less than the entire cross-sectional area of the permeameter cell.

5.2.2 Evaluation of the Quality of Contact between a Geomembrane and Soil Layer

Two sets of tests were conducted to investigate the effect of the quality of the contact between the geomembrane and the underlying soil layer. High heads are expected to push the geomembrane against the clay surface leading to an improved contact condition between the geomembrane and the soil layer.

RMA Soil Type II was used in this phase of the study. The first set of tests was presented in Section 5.2.1.1 and involved low heads (0.5 m). The soil properties and

leakage rates of these tests conducted under low heads are listed in Table 5.1. As previously discussed, the leakage rate for the test with "poor" contact quality between the geomembrane and the soil layer (GM-CCL-L1) is two orders of magnitude larger than leakage rate for the test with "good" contact quality (GM-CCL-L2).

A set of tests was also performed under high hydraulic heads to determine the effect of hydraulic head on the interface contact quality. The properties of the soil layers and the leakage rates for the tests under high heads are listed in Table 5.4. The difference in leakage rates for "poor" and "good" contact conditions under high heads is less than an order of magnitude. The leakage rate for test GM-CCL-5P ("poor" contact) is lower than the leakage rate for test GM-CCL-5 ("good" contact); however, the difference is not significant and can been attributed to differences in the initial water content and dry unit weight of the two samples. Overall, the results indicate that the quality of the contact of the interface between the geomembrane and the soil layer is not as significant for high heads as it is for low heads.

Table 5.4: Test details and leakage rates for tests with different interface contact quality

Test #	Head Above Liner (m)	Dry Unit Weight (kN/m^3)	Relative Compaction (%)	Porosity, n	Initial		Final		Contact Quality	Leakage Rate (m^3/s)
					Water Content, w (%)	Degree of Saturation (%)	Water Content, w (%)	Degree of Saturation (%)		
GM-CCL-5	35	17.5	89.6	0.34	9.8	51.0	15.7	81.5	Good	5.4×10^{-9}
GM-CCL-5P	35	16.0	82.2	0.40	10.7	44.1	16.2	66.8	Poor	2.5×10^{-9}

5.2.3 TDR Results

5.2.3.1 Volumetric Water Contents

The initial and final volumetric water contents measured using the TDR probes were compared with the volumetric water contents measured directly from soil layers. The directly-measured and TDR-measured volumetric water contents for four tests are

listed in Table 5.5. The directly-measured initial moisture contents (i.e., not measured using the TDR system) included in Table 5.5 are the average values of soil samples collected prior to compaction. The directly-measured final volumetric moisture contents were obtained from soil samples taken at and around the location of each TDR probe (elevations of 5, 10 and 15 cm). Accordingly, the final volumetric water contents obtained directly and final volumetric water contents obtained using the TDR system were from the same location in the permeameter. Overall, independent of the method of measurement, the volumetric content at the end of each test appeared to be uniform with depth across the entire soil layer.

The volumetric water contents for the soil layers compacted at a relative compaction of 70%, GM-CCL-L1 and GM-CCL-L2, are similar (Table 5.5). Also, the measurements taken directly and measurements obtained using the TDR probes for both tests are similar. There was an average difference of about 5% between directly-measured and TDR-measured volumetric water contents for the tests involving soil layers with a low relative compaction. However, for denser soils (GM-CCL-5 and GM-CCL-5P), there is about a 30% discrepancy between the volumetric moisture contents taken using the two different methods. The larger difference (i.e., 30% compared to 5% difference) between the two methods of measuring volumetric moisture content for soil layers with a higher relative compaction (i.e., GM-CCL-5 and GM-CCL-5P) may be attributed to the difference in the density of the soil. This is because TDR calibration curves are sensitive to the density of the soil in which they are embedded (McCartney 2007).

Table 5.5: Volumetric water contents (θ) for specific geomembrane-clay tests

Test #	Head Above Liner (m)	Dry Unit Weight (kN/m^3)	Elevation from Bottom of Cell (cm)	Initial		Final	
				Average Conventionally Measured θ (%)	TDR Measured θ (%)	Conventionally Measured θ (%)	TDR Measured θ (%)
GM-CCL-L1	0.53	12.9	5	9.6	9.9	40.5	40.2
			10		8.6	38.3	39.8
			15		10.9	36.8	42.0
GM-CCL-L2	0.53	13.7	5	10.6	11.7	40.5	44.0
			15		11.5	41.2	42.0
GM-CCL-5	35	17.5	5	17.8	20.9	30.0	35.0
			10		19.9	25.5	32.6
			15		21.2	28.5	33.0
GM-CCL-5P	35	16.0	5	17.7	23.5	25.0	35.5
			10		23.1	27.5	27.5
			15		24.4	27.0	31.6

5.2.3.2 Wetting Front

The movement of the wetting front through the unsaturated soil layer was monitored for several tests in the GM-CCL test series. Two sets of measurements were recorded during the tests: 1) visual observations of the wetting front, and 2) measurements from TDR probes located at elevations of 5, 10 and 15 cm from the bottom of the cell. The soil layer height is 23 cm, which means that the first TDR probe is located 8 cm below the geomembrane and soil interface.

Since the TDR probes are used to record changes in the dielectric constant, which corresponds to the changes in water content in the soil, the advancement of the wetting front through the soil layer can be obtained. The data obtained using the TDR system for Test GM-CCL-L1 is shown in Figure 5.6. For Test GM-CCL-L1, the volumetric water content was constant at an average initial value of 9.5% until the wetting front arrived at the location of a TDR probe. The time of arrival is indicated by an increase in the volumetric water content, as shown in Figure 5.6. As infiltration of water into the soil layer continued, the volumetric water content increased to an average final value of 40%.

The final volumetric moisture content for Test GM-CCL-L1 was less than the maximum saturated value of 51.5%. The TDR probe at an elevation of 15 cm would register the increase in moisture content first, followed by the TDR probes at 10 cm and 5 cm, respectively.

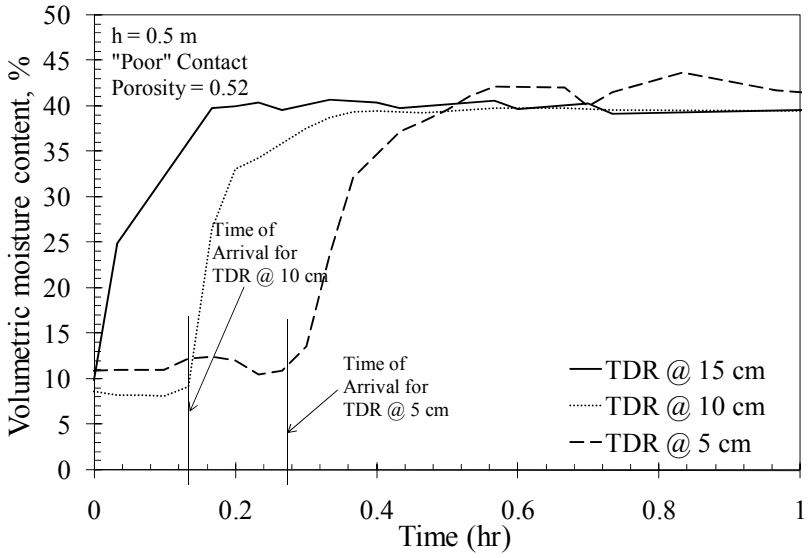

Figure 5.6: Example TDR data: measurements from GM-CCL-L1

The time at which the wetting front arrived at each location was noted and compared with the visual observations made during the same test. The TDR results involve three data points since there were only three TDR probes in the cell. The visual observations and the TDR results for Tests GM-CCL-L1 and GM-CCL-L2 are shown in Figure 5.7. In some tests, like that shown in Figure 5.7a, the time at which outflow began did not necessarily correspond with the time at which the wetting front was recorded (i.e., visually observed) to have reached the bottom of the cell. For tests conducted under low hydraulic heads, the times of arrival for tests at each probe location measured using TDR matched well with the times of arrival obtained by visual observations made during the initial stages of the tests. Note that the scales on the plots in Figure 5.7a and Figure 5.7b

are the same, illustrating that the velocity of the moisture front is higher in tests with "poor" contact quality than tests with "good" contact quality.

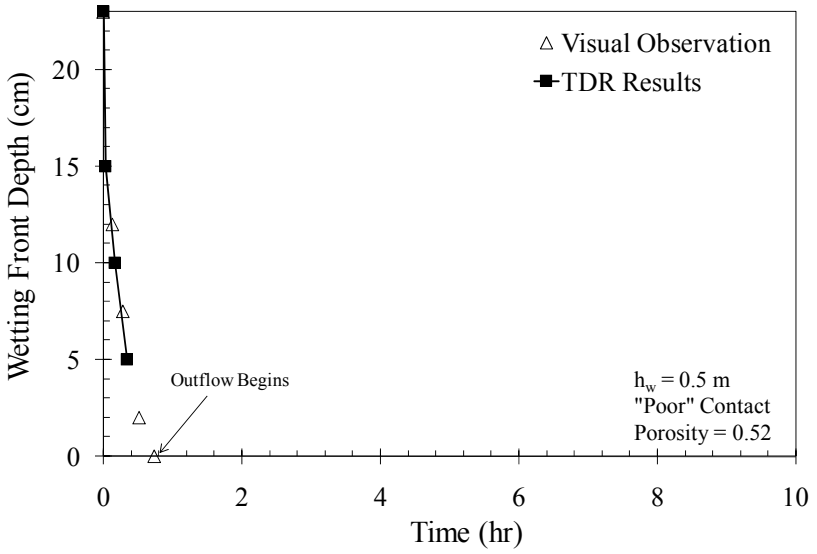

(a)

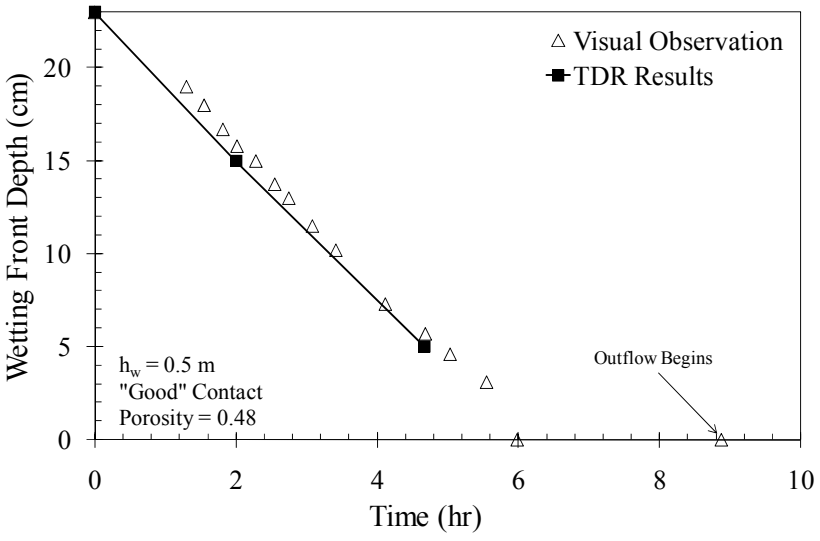

(b)

Figure 5.7: Comparison of TDR wetting front measurements with visual observations from tests with low heads: a) GM-CCL-L1 and b) GM-CCL-L2

The TDR measurements and the visual observations obtained for tests GM-CCL-5 and GM-CCL-5P are shown in Figure 5.8. The same scale is used for Figure 5.8a and Figure 5.8b. The measurements made using TDR corresponded with the visual observations in these tests, conducted using higher heads, as well.

The times at which outflow began for the tests conducted under low heads were compared with the breakthrough times for the tests conducted under high heads. For the tests involving low head shown in Figure 5.7, outflow began within one hour for the system with "poor" interface contact quality while the system with "good" contact quality did not begin to leak until almost nine hours had passed. For tests involving high heads shown in Figure 5.8, the same trend was observed with the test with "poor" contact exhibiting outflow at about 2.5 hours compared to the test with "good" contact, which had outflow beginning at 14 hours. The time to outflow for soil layers with a higher dry unit weight (soil with lower porosity) were larger than the soil layers with a lower dry unit weight (soil with higher porosity), even though the denser soil layers were subjected to significantly higher heads.

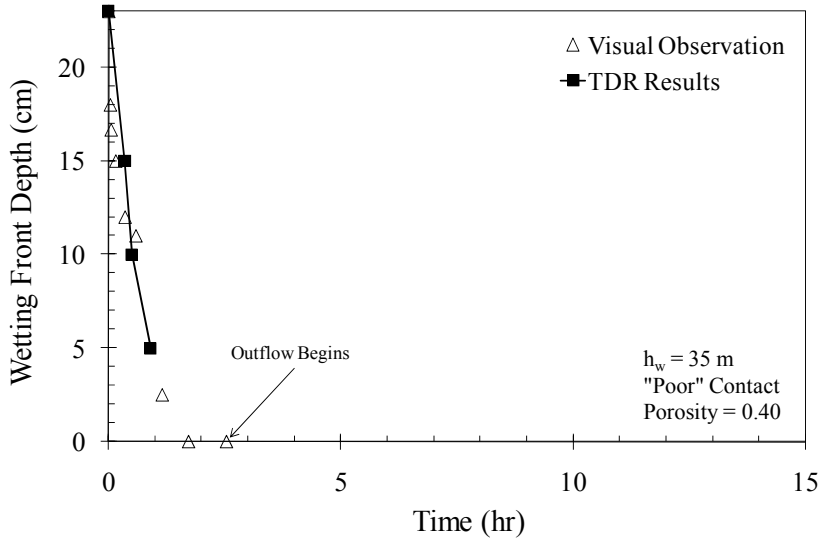

(a)

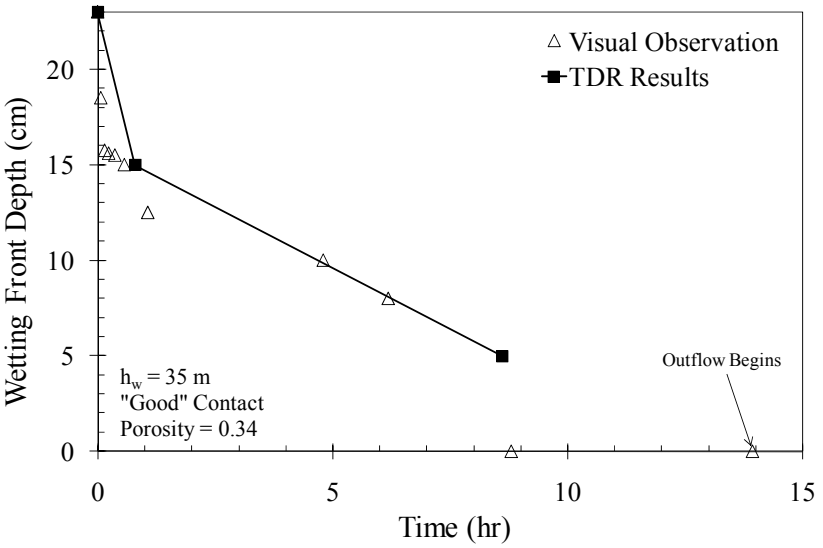

(b)

Figure 5.8: Comparison of TDR wetting front measurements with visual observations from tests with high heads: a) GM-CCL-5P and b) GM-CCL-5

5.2.3.3 Green-Ampt 1-D Model

Green and Ampt (1911) developed a one-dimensional model to approximate vertical infiltration into a homogeneous soil layer due to ponding. The Green-Ampt model is a simple one-dimensional model that is based on Darcy's law. Model assumptions include: i) the soil profile has a uniform initial water content, and ii) the wetting front has a sharp boundary between the wetted and unwetted portions of the soil profile. Movement of water in directions other than vertical are neglected and flow ahead of the wetting front is also considered negligible (Chen and Young 2006).

A general form of the Green-Ampt model, obtained using Darcy's Law, is:

$$i = K_{wet} + \frac{K_{wet}\Delta h \Delta\theta}{I} \tag{5.3}$$

$$\Delta h = h_0 - h_f \tag{5.4}$$

$$\Delta\theta = \theta_{wet} - \theta_{dry} \tag{5.5}$$

where i is the infiltration rate, I is the cumulative infiltration, K_{wet} is assumed to be the saturated hydraulic conductivity of the soil under ponded conditions, h_o is the head at the soil surface (under the ponded water), h_f the head at the wetting front ("unsaturated" head), θ_{wet} is the volumetric water content behind the wetting front, and θ_{dry} is the initial volumetric water content of the soil. Because the infiltration rate is the derivative of the cumulative infiltration over time, the general form can be rewritten in implicit form and can be solved using iterative methods:

$$I = K_{wet}t + \Delta h \Delta\theta \ln\left(1 + \frac{I}{\Delta h \Delta\theta}\right) \tag{5.6}$$

where t is time.

As shown in Figure 5.9, the curve for infiltration rate versus time for a test from the experimental program has the same shape as infiltration rate-time curve from an infiltration model. The curve shown in Figure 5.9a was generated using the Green-Ampt model for the same soil properties and head as the test to which the model is compared. The infiltration rate from Test GM-CCL-5P, shown in Figure 5.9b, is lower than that of the Green-Ampt model. The Green-Ampt model is used to calculate infiltration into a soil profile under ponded conditions, meaning that the infiltration simulated using the Green-Ampt model is for a system without a geomembrane. Due to this, the infiltration rates estimated using Green-Ampt were significantly higher than those measured during the laboratory tests.

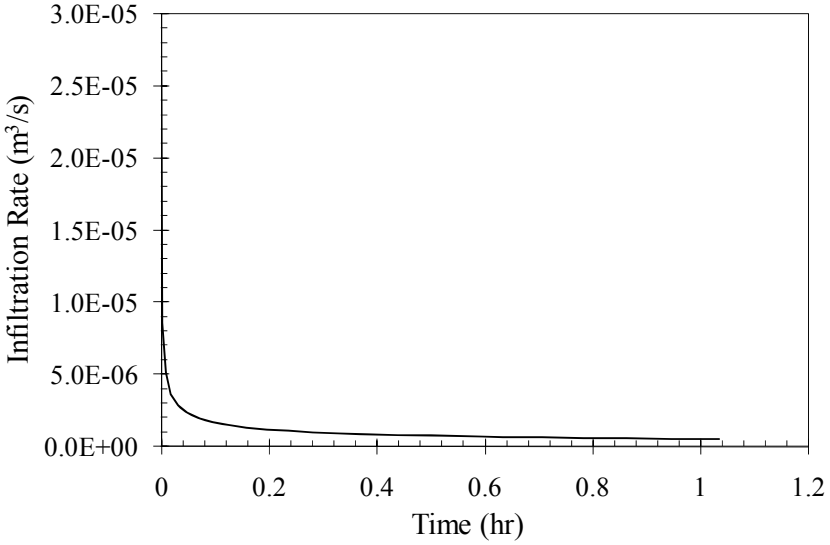

(a)

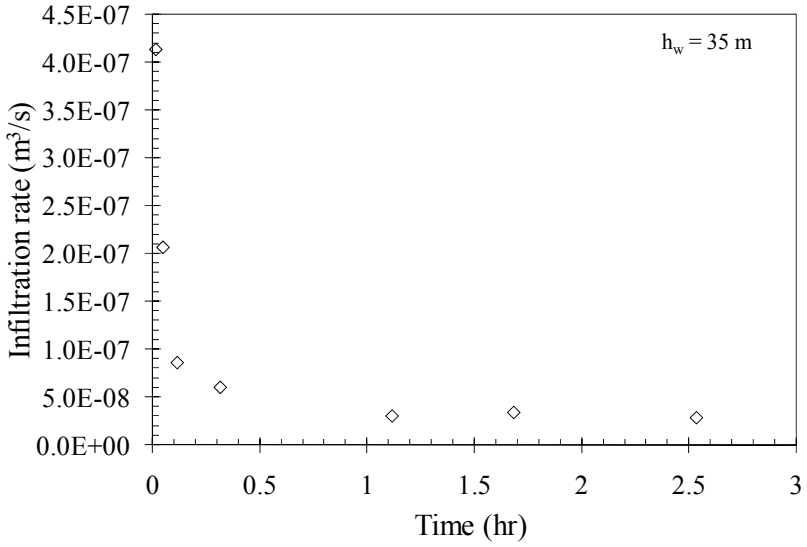

(b)

Figure 5.9: Infiltration rates over time for: a) Green-Ampt model and b) Test GM-CCL-5P

By solving Equation (5.6) using iterative methods, the depth of the wetting front, z_f, can be calculated by:

$$z_f = \frac{I}{\Delta\theta} \tag{5.7}$$

Equation (5.7) is an implicit solution for the Green-Ampt model. An explicit form of the Green-Ampt model can also be used to approximate the depth of the wetting front with time. The following explicit equation is for small times, and thus, small depths (McCray 2004):

$$t = \frac{\Delta\theta}{2\Delta h K_s} z_f^2 \tag{5.8}$$

The depth of the wetting front due to infiltration from water ponded on top of the soil profile was compared with the TDR measurements from the experimental program. The TDR measurements and the wetting front depths calculated using Green-Ampt for the tests conducted using a low hydraulic head (GM-CCL-L1 and GM-CCL-L2) are shown in Figure 5.10. The wetting front for the test with "poor" interface contact between the geomembrane and the soil layer (GM-CCL-L1), as shown in Figure 5.10a, is very similar to the wetting front estimated by the Green-Ampt model. The time at which outflow began for Test GM-CCL-L1 agreed with the time to breakthrough predicted by the Green-Ampt model. However, as shown in Figure 5.10b, the velocity of the wetting front for the test with "good" interface contact was lower than that estimated by the Green-Ampt model. The time at which outflow began, which was obtained from the leakage data, for Test GM-CCL-L2 was more than eight times larger than that predicted by the Green-Ampt model. The Green-Ampt model is a one-dimensional model while

the flow through a system with a "good" interface contact acts as a three-dimensional model with a point source for flow.

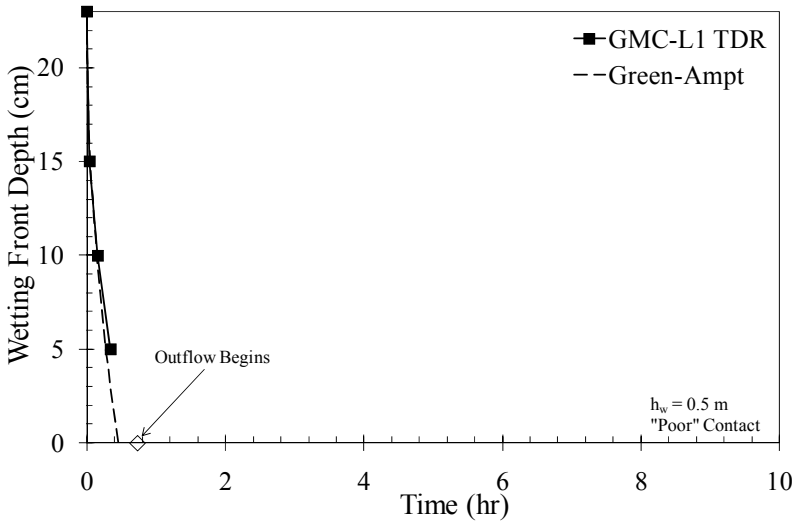

(a)

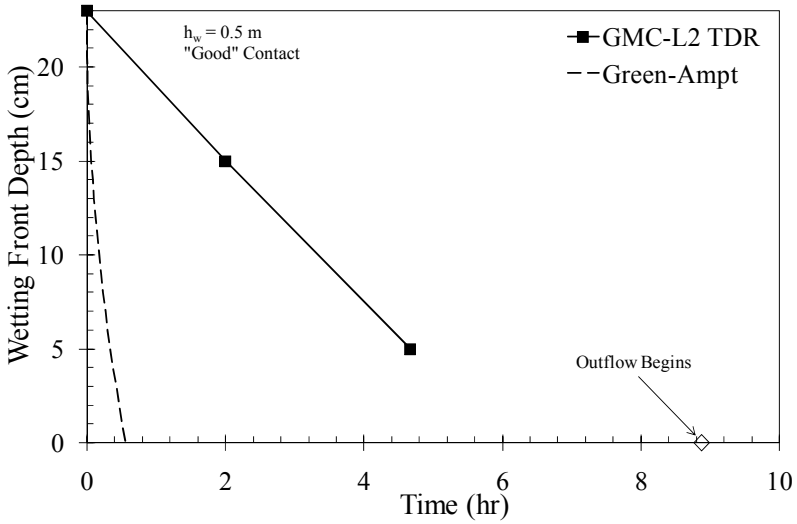

(b)

Figure 5.10: Comparison of TDR wetting front data and Green-Ampt infiltration model for low heads for: a) poor interface contact quality and b) good interface contact quality

For the wetting front in Test GM-CCL-L1 to advance through a profile at the same rate as calculated using the Green-Ampt model means that the geomembrane was not having an effect on the flow rate and that flow is occurring evenly over the surface of the soil as if the geomembrane was not there. For Test GM-CCL-L2, the wetting front advanced more slowly through the soil layer than estimated using the Green-Ampt model indicating that the infiltration into the soil layer was minimized by the presence of a geomembrane liner.

The TDR measurements from the tests conducted using a low hydraulic head, GM-CCL-5 and GM-CCL-5P, are plotted on the same scale in Figure 5.11 with the wetting front depths that were calculated using Green-Ampt. The movement of the wetting front for the test with "poor" interface contact between the geomembrane and the soil layer, GM-CCL-5P, is very similar to the movement of the wetting front estimated by the Green-Ampt model. Flow is occurring evenly over the surface of the soil as if there was no geomembrane. The time at which outflow began for Test GM-CCL-5P (obtained from the leakage data) was about twice as much as the time to breakthrough predicted by the Green-Ampt model. However, as shown in Figure 5.11b, the time at which outflow began for Test GM-CCL-5 was more than ten times that estimated by the Green-Ampt model. Also, the velocity of the wetting front for the test with "good" interface contact was lower than that predicted by the Green-Ampt model.

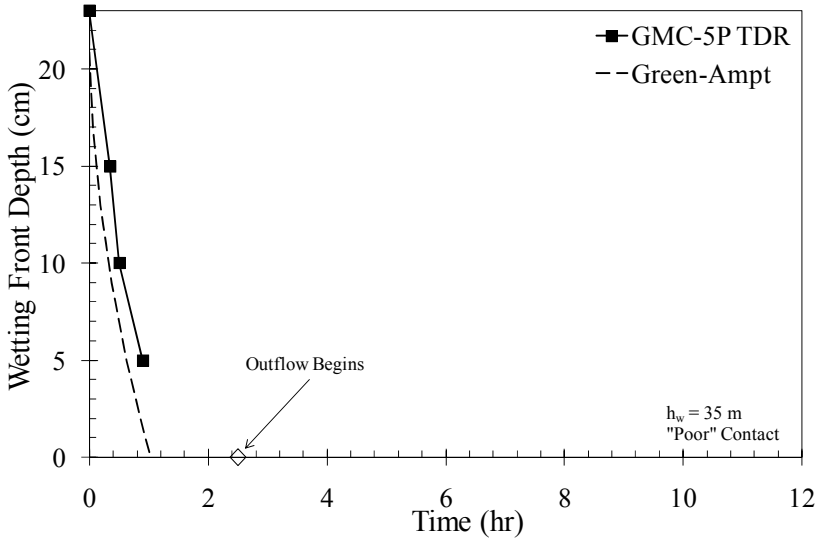

(a)

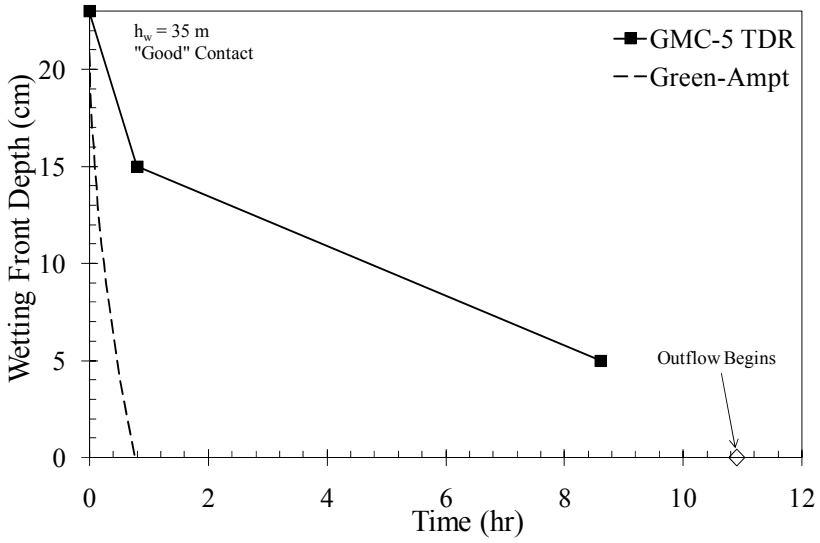

(b)

Figure 5.11: Comparison of TDR wetting front data and Green-Ampt infiltration model for high heads for a) good interface contact quality and b) poor interface contact quality

5.2.4 Transmissivity of the Interface

As discussed in Section 5.2, the leakage rates for the test series involving a geomembrane with a defect placed in direct contact with a silty clay layer indicated that flow through the defect increased linearly with hydraulic head. The mechanisms of flow through a defect in a geomembrane liner placed over a soil layer with a low hydraulic conductivity include: 1) flow into the soil layer and 2) flow across the interface between the geomembrane and the soil. The results of the GM-CCL tests were used to determine the flow across the interface, which is characterized by its transmissivity, and the radius of interface flow.

The transmissivity of the interface between the geomembrane and the soil layer can be defined as:

$$\theta = k_g \, s \tag{5.9}$$

where θ is the transmissivity, k_g is the hydraulic conductivity of the interface gap, and s is the spacing of the gap at the interface. If the interface gap is small, the transmissivity of the interface is low. The transmissivity is also related to the hydraulic conductivity of the soil beneath the geomembrane. If the soil is very permeable, flow is less likely to occur across the interface as the water will flow directly into the underlying soil layer.

As discussed in Section 2.3.3, the transmissivity at the interface between the geomembrane and the underlying soil layer is needed to solve the flow problem analytically. The transmissivity of the interface is difficult to measure directly, but it can be back-calculated using measured leakage rates. For simplicity, the interface is assumed to be uniform, with a uniform gap thickness and thus a uniform transmissivity. However, the assumption of uniform interface may not be satisfied in the field or even in the laboratory.

The transmissivity for each of the six tests of the GM-CCL test series (Table 5.2) was back-calculated the analytical model developed by Touze-Foltz et al. (1999) for laboratory conditions [Equation (2.24)]. The transmissivity was varied until the calculated leakage rate was equal to the leakage rate measured in the laboratory. The back-calculated values for the transmissivity for all six tests conducted under high heads are shown in Figure 5.12. The transmissivity appears to be independent of hydraulic head applied to the geomembrane, remaining relatively constant over the range of heads used in the experimental testing program. The harmonic mean of the back-calculated transmissivity values was $3x10^{-11}$ m^2/s. The transmissivity for an "excellent" contact quality between the geomembrane and the underlying soil layer as defined by Equation (2.35) (Touze-Foltz and Giroud 2003) is three orders of magnitude larger than any of the back-calculated values. However, Equation (2.35) was developed to estimate the transmissivity for low heads and was based on experimental data collected from tests under low heads. Also, although the transmissivity appears to be independent of head, the transmissivity was not evaluated for the lower range of hydraulic heads which were used in the experimental study conducted by Brown et al. (1989). It is plausible that the transmissivity is higher under heads lower than 7 m. Further investigation is needed to determine if this hypothesis is indeed valid. Another possible explanation for the significantly lower transmissivity determined in this study could be that the defect is clogging once the high heads are applied, restricting flow through the defect. The defect is small is in size and could be easily clogged. Also, the defect is small enough that head loss due to friction through the defect could affect the leakage rates measured during the permeameter tests, and thus having an effect on the transmissivity. The size of the permeameter cell could be another contributing factor the low leakage rates observed in this study. By not allowing flow to fully develop in the soil layer, the measured leakage

rates may be smaller than would actually occur in a larger permeameter cell. Ultimately, the reason for the significantly lower transmissivities (and leakage rates) could be attributed to any or all of the above factors.

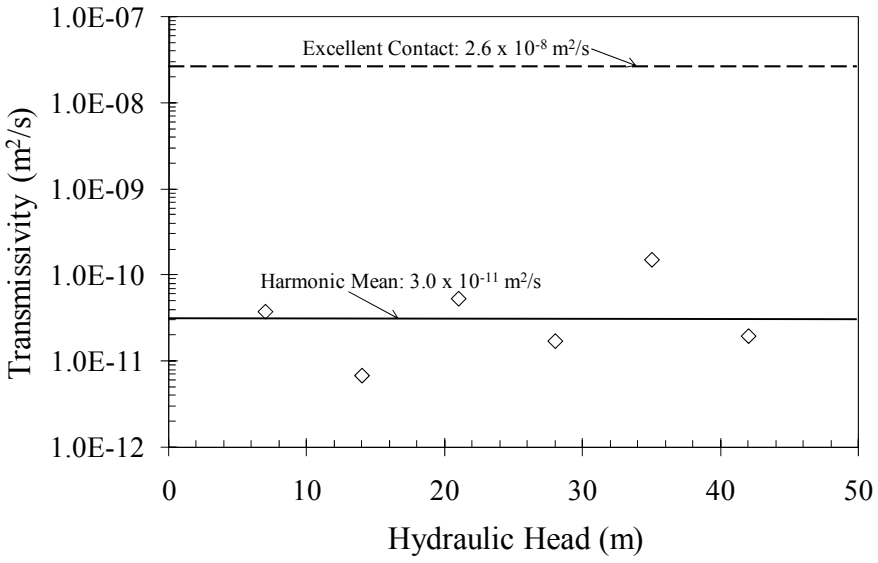

Figure 5.12: Back-calculated transmissivity for GM-CCL tests

Using the model developed by Touze-Foltz et al. (1999) [Equation (2.24)] for laboratory conditions, flow rates were estimated for the range of head used in the experimental program. The transmissivity of the interface used in Equation (2.24) was the harmonic mean of the back-calculated transmissivity from Figure 5.12. As shown in Figure 5.13, the flow rates estimated by the analytical model developed by Touze-Foltz et al. (1999) for laboratory conditions were similar to those obtained experimentally from the GM-CCL test series.

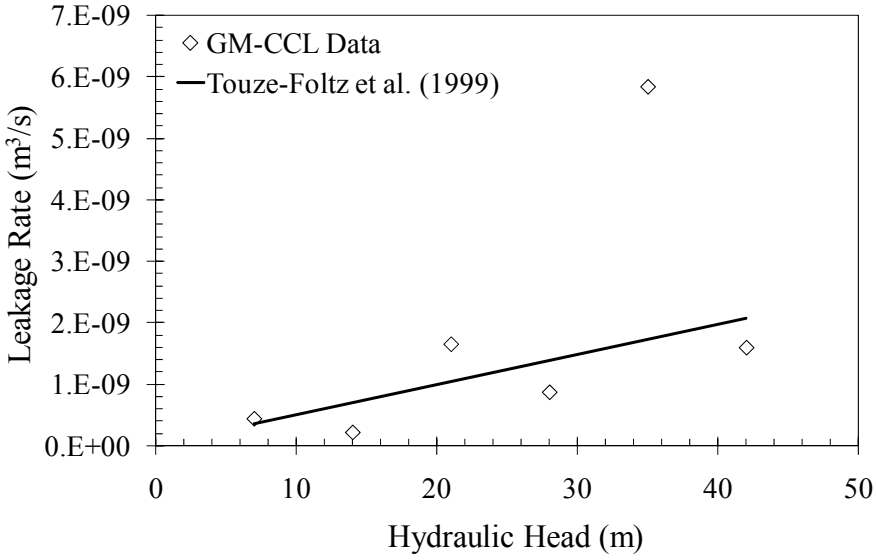

Figure 5.13: Comparison of predicted leakage rates with GM-CCL test data using average back-calculated transmissivity

5.2.5 Radius of Interface Flow

The radius of interface flow is defined by Rowe (1998) as the radius at which the change in pressure head across the interface between the geomembrane and the underlying soil layer is equal to zero. The pressure head dissipates across the interface until the change in head becomes zero at the radius of interface flow. Flow may occur outside the region defined by the radius of interface flow through mechanisms other than those contemplated in existing models (e.g., gradients of suction, diffusion).

Using Equation (2.19) developed by Touze-Foltz et al. (1999) for field conditions, the radius of interface flow was predicted by matching the measured flow rates with flow rates calculated using the radius of the defect, the hydraulic conductivity of the soil layer, and the head above the geomembrane liner. The radius of interface flow is calculated by solving the analytical solution at the point where the derivative of the pressure head distribution at the interface is equal to zero. To find the radius of interface flow, the

transmissivity of the interface is varied until the measured flow matches the calculated flow rate. The predicted radii of interface flow from the GM-CCL test series are listed in Table 5.6. The measured leakage rates are also included in Table 5.6. The tests with the lowest leakage rates also have the smallest radii of interface flow. Half of the tests had an estimated radius of interface flow of less than 15 cm, which corresponds to the diameter of the permeameter cell used to conduct the tests listed in Table 5.6. However, even though the radius of interface flow was less than radius of the cell for the Tests GM-CCL-1 to GM-CCL-3, the cell walls likely restricted flow through the system because flow was still occurring in the soil layer outside the radius of interface flow through mechanisms such as gradients due to suction. It should be noted that, although the radius of interface flow was solved for using the analytical model for field conditions, the transmissivities that correspond to the radius of interface flow values in Table 5.6 are approximately equal to the transmissivities found using the analytical model developed by Touze-Foltz et al. (1999) for laboratory conditions.

Table 5.6: Radii of wetted area for GM-CCL Test Series calculated using analytical model

Test	Predicted Wetted Radius (m)	Measured Leakage Rate (m^3/s)
GM-CCL-1	0.09	4.3×10^{-10}
GM-CCL-2	0.04	2.1×10^{-10}
GM-CCL-3	0.10	1.7×10^{-9}
GM-CCL-4	0.23	8.7×10^{-9}
GM-CCL-5	0.15	5.8×10^{-9}
GM-CCL-6	0.17	1.6×10^{-9}

5.3 LARGE PERMEAMETER EXPERIMENTAL RESULTS & ANALYSIS

The objective of tests performed using the larger permeameter was to determine what effect, if any, the size of the cell had on leakage rate through a defect in a

geomembrane liner. The results of the large-cell tests will be compared to those presented in Section 5.2.1.

Two tests were conducted using the large permeameter. The properties of the soil layer in Tests GM-CCL-LC1 and GM-CCL-LC2 and the final leakage rates are listed in Table 5.7. The soil layer for the first test conducted using the large permeameter, GM-CCL-LC1, was prepared using RMA Soil Type II which had been moisture conditioned to achieve a target water content of 11.9%, or the optimum water content. The soil layer was compacted in the permeameter cell to a target relative compaction of 70%. For the GM-CCL-LC1 test, the geomembrane was not in intimate contact with the soil surface, meaning that the contact quality was "poor."

The soil layer for the second test that was conducted using the large permeameter, GM-CCL-LC2, was prepared using RMA Soil Type II which had been moisture conditioned to achieve a target water content of 7.0%, which was dry of optimum. The soil layer was compacted in the permeameter cell to a target relative compaction of 90%. The soil layer was trimmed to obtain a good contact between the geomembrane and the surface of the soil.

Table 5.7: Test details and leakage rates for the large-scale tests

Test #	Head Above Liner (m)	Dry Unit Weight (kN/m^3)	Relative Compaction (%)	Porosity, n	Initial		Final		Contact Quality	Leakage Rate (m^3/s)
					Water Content, w (%)	Degree of Saturation (%)	Water Content, w (%)	Degree of Saturation (%)		
GM-CCL-LC1	0.3	15.7	71.9	0.47	11.9	36.0	-	-	Poor	3.6×10^{-7}
GM-CCL-LC2	7	17.7	84.6	0.38	7.0	31.1	19.2	85.1	Good	9.5×10^{-11}

5.3.1 Leakage Rates: Small Permeameter vs. Large Permeameter

The leakage rate for GM-CCL-LC1 (3.6×10^{-7} m^3/s) is on the same order of magnitude as Test GM-CCL-L1 (1.2×10^{-7} m^3/s; see Table 5.1), which was conducted with the same defect size and same soil. However, the leakage rate for GM-CCL-LC1 is

three times larger than the leakage rate for Test GM-CCL-L1. Note that Test GM-CCL-LC1 was conducted using a slightly smaller head and with a higher initial soil water content than Test GM-CCL-L1.

Comparison of the tests conducted under a hydraulic head of 7 m indicates that the leakage rate for the test conducted in the smaller permeameter, GM-CCL-1 ($4.3x10^{-10}$ m^3/s), is almost five times larger than the leakage rate for the test conducted in the larger cell, GM-CCL-LC2 ($9.5x10^{-11}$ m^3/s). Note that the soil layer for the test in the larger permeameter had a lower initial water content. This difference could have resulted in a soil layer with a higher hydraulic conductivity and, consequently, the higher leakage rate for Test GM-CCL-LC2. Comparison of the leakage rates suggests that the size of the permeameter diameter did not play a significant role in the measured leakage rates, at least for the range of variables used in these tests.

5.3.2 Interface Flow

For Test GM-CCL-LC2, a tracer dye was added to the water supply tank at the inflow of the large permeameter. The purple dye was used to visualize the area of flow within the soil layer. After the test was completed, the geomembrane was removed to evaluate the dyed area. As shown in Figure 5.14, three concentric dyed areas were observed. The area with the heaviest concentration of the dye was located at the center of the soil layer (i.e., the location of the defect). The concentration of the dye decreased outwardly from the center of the cell. The dimensions of the two main dyed areas (i.e., Regions 1 and 2 in Figure 5.14) were measured and the measurements of the regions are listed in Table 5.8. The average diameter of the darkest area of dye (Region 1), which is the average of the two measurements taken, is 0.074 m. The average diameter of Region 2 was 0.193 m. It should be noted that steady-state flow has likely not been achieved

during the tests in the large permeameter cell, which means that the dyed areas may not be indicative of the steady-state values for the radius of interface flow.

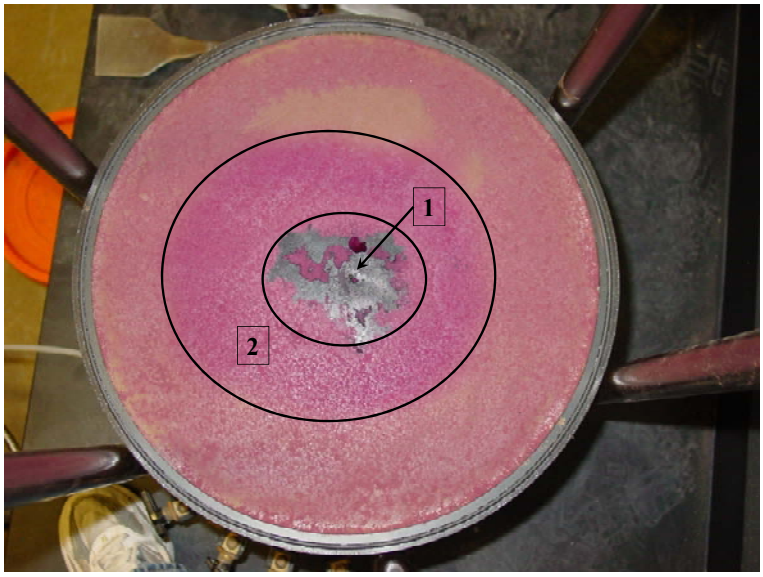

Figure 5.14: Dyed area for Test GM-CCL-LC2

Table 5.8: Measurements of the dyed areas for the Test GM-CCL-LC2

Designation	**Location**	**Diameter (m)**	
Region 1	Center (darkest)	Diameter 1	0.090
		Diameter 2	0.058
		Avg Diameter	0.074
Region 2	2nd Ring	Diameter 1	0.205
		Diameter 2	0.180
		Avg Diameter	0.193

The area of the soil surface outside of Region 2 was the area with the lightest concentration of dye. It appeared that the area beyond Region 2 was beyond the radius of interface flow. The light concentrations of dye in the region beyond Region 2 could have been caused by diffusion of the components of the dye into the soil and flow induced by

gradient in the matric potential of the unsaturated soil layer. Dye was observed in the effluent water and, upon dissection, very light traces of dye were observed in the lower portions of the soil layer.

As shown in Figure 5.14, the area with the highest concentration of dye (designated as Region 1) is highly irregular in shape with rough edges. The interface gap between the geomembrane and the soil layer is assumed to be uniform in thickness in the models used for prediction of leakage through a defect in a geomembrane over a soil layer. That is, the transmissivity is assumed to be uniform across the interface between the geomembrane and the soil layer. However, the irregularity (asymmetry) of the dyed area indicates that the interface is not uniform and that, consequently, that the transmissivity varies across the interface between the geomembrane and the soil. As shown in Figure 5.15, there were pieces of soil adhered to the underside of the geomembrane. This observation suggests that the contact between the soil and the geomembrane was excellent during the test.

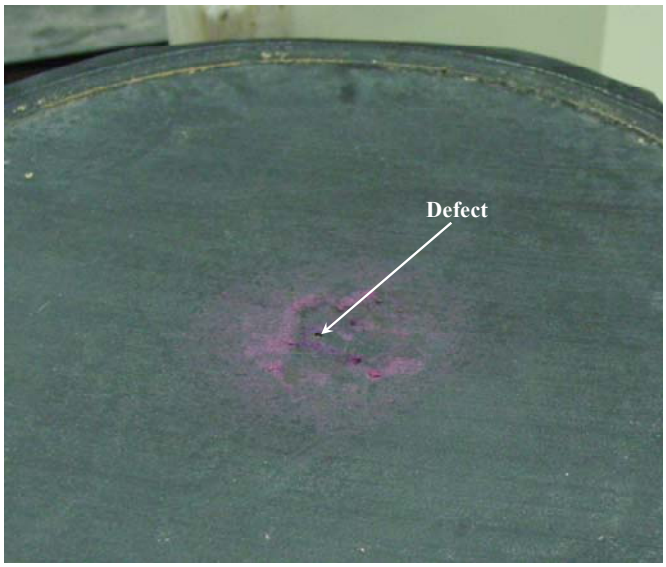

Figure 5.15: Pieces of soil on the underside of geomembrane

The soil layer in the large cell was removed and dissected in order to investigate the flow patterns within the soil beneath the geomembrane. The dissection revealed several important aspects. First, the darkest area of dye at the center of the soil layer did not penetrate past the surface of the soil. In fact, the concentration of dye just below the soil surface (less than 1 mm) had the same color as the rest of the dyed area of Region 2 (see Figure 5.16a). The soil layer was sliced in half, as shown in Figure 5.16b, to reveal a dyed area that was about 19 cm in diameter but only about 10 cm deep. The remaining portion of the soil layer was sliced in half so that only a quarter of the original soil layer was left. The dyed area shown in Figure 5.16c was 10 cm deep and about 10 cm wide (since it was only the radius of flow). Based on Figure 5.16d, it may be concluded that flow occurred almost symmetrically within the soil layer. The symmetry of the flow pattern indicates that the soil layer was homogeneous. The dyed area may give an indication of the degree of saturation, where areas over a certain degree of saturation have a higher concentration of dye than the areas with a lower degree of saturation. Further testing is required to determine the threshold degree of saturation, if any, that would lead to a higher dye concentration.

(a) (b)

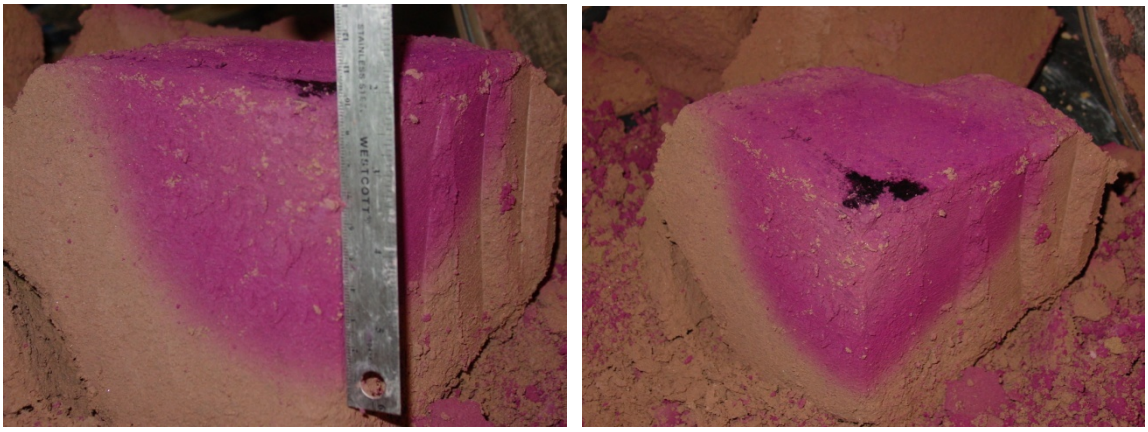

(c) (d)

Figure 5.16: Dissection of the soil layer from Test GM-CCL-LC2

For the large cell test GM-CCL-LC2, the average diameter of Region 2 was 0.193 m (or a radius of 0.0965 m). The value of the radius of interface flow predicted using the model developed by Touze-Foltz et al. (1999) for field conditions [Equation (2.19)] was 0.091 m. Therefore, based on the concentration of dye, Region 2 was considered to be area of flow defined by the radius of interface flow.

The predicted radius of interface flow and the measured value are very similar despite the fact that the analytical model for field conditions [Equation (2.19)] assumes

that flow across the interface is uniform. Yet, the shape of the central dyed area suggests that flow across the interface may not be uniform.

There was evidence of water (including both dye and non-dyed areas) across the entire surface of the soil layer in the large permeameter cell (0.33 m), which indicates that other flow mechanisms could have contributed to the leakage rates measured in the experimental testing program. Considering the derivation of Equation (2.19) shown in Section 2.3.3, the analytical model can only be used to calculate one-dimensional flow into the soil layer due to a vertical gradient. Thus, flow due to diffusion and matric potential in the unsaturated soil was not included in the calculation of the radius of interface flow.

5.4 SIMPLIFIED EQUATIONS

Several equations are currently available to estimate leakage through defects in a geomembrane liner. Touze-Foltz and Giroud (2003) developed equations for systems with a geomembrane placed over a low-permeability clay layer. Touze-Foltz and Barroso (2006) developed an equation, similar to those developed by Touze-Foltz and Giroud (2003), to estimate flow for systems involving a geomembrane over a GCL. The equation for a geomembrane-GCL contact is discussed in Chapter 6, along with the experimental data for geomembrane-GCL composite liner systems.

The existing equations for a geomembrane-CCL composite lining system are not empirical as they are not based on the experimental data. Also, all of the existing equations were developed for landfills (i.e., low heads). Despite these drawbacks, the methods that were used to develop the existing equations were used in this study as an initial basis for the development of new empirical equations based on the data obtained for high heads in the experimental testing program.

5.4.1 Existing Equations

Touze-Foltz and Giroud (2003) developed simplified equations to estimate leakage through defects in a geomembrane liner that is placed over a low-permeability soil layer (Equations 2.38 through 2.40). As discussed in Section 2.3.5, these equations are simplified versions of the analytical equation developed by Touze-Foltz et al. (1999) for field conditions. The term "low-permeability" was used to define soils with a hydraulic conductivity between 10^{-10} and 10^{-8} m/s. The hydraulic conductivity of the RMA Soil Type II under the conditions used in the experimental testing program was $7x10^{-9}$ m/s, which falls within the "low-permeability" range for these equations. The equations developed by Touze-Foltz and Giroud (2003) include a coefficient that accounts for the contact quality (i.e., poor, good and excellent). Leakage rates were predicted using Equations (2.38) through (2.40) and using the same input parameters (e.g., area of defect, hydraulic conductivity) as the tests in the GM-CCL test series. The hydraulic head used for the calculation of the flow rates ranged from 7 to 42 m.

The flow rates calculated using the equations developed by Touze-Foltz and Giroud (2003) are plotted in Figure 5.17 along with the data from the experimental testing program. As shown in the figure, the calculated flow rates are at least four orders of magnitude higher than the measured leakage rates from the GM-CCL test series. The difference between the estimated and measured values can be attributed to the fact that the heads used in the experimental study were outside the range of heads used in the development of Equations (2.38) through (2.40). The equations were developed using hydraulic heads below 3 m, while the hydraulic heads used in the experimental testing program were over 3 m.

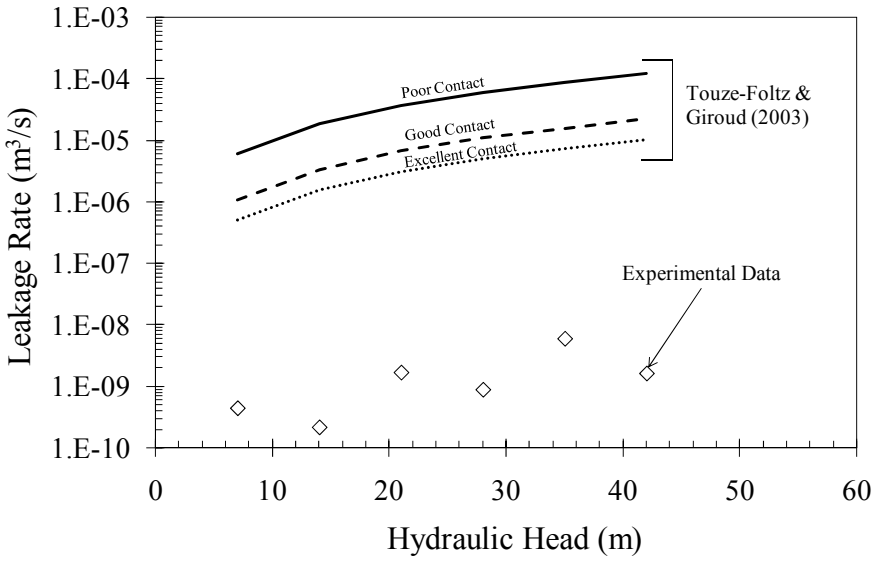

Figure 5.17: Existing simplified equations compared with GM-CCL data

5.4.2 New Equation for Estimating Leakage for GM-CCL Lining Systems

Since the existing equations were not developed for estimating flow rates under high heads, a new equation is proposed to predict flow through systems such as those investigated in the experimental testing program. A new simplified equation was developed to estimate leakage through lining systems under high hydraulic heads using the same methodology as described by Touze-Foltz and Giroud (2003). The new equation was developed using the average back-calculated transmissivity obtained from the experimental component of this study. By incorporating the experimental data in this way, the new equation is not entirely analytical in nature.

The general form of the new equation was slightly modified from the form used by Touze-Foltz and Giroud (2003) [i.e., Equation (2.34)]. Instead of considering the hydraulic gradient, i_s according to Equation (2.33), the gradient was combined into one term with its own exponent rather than using the more complex formulation implemented

by Touze-Foltz and Giroud (2003). The general form of the equation selected for this study is:

$$Q = C_q i_s^w h_w^x a^y k_s^z \tag{5.10}$$

where Q is the leakage rate, i_s is the hydraulic gradient, h_w is the height of water above the geomembrane liner, a is the area of the defect, and k_s is the saturated hydraulic conductivity of the soil layer. The empirical coefficient, C_q was used by Giroud (1997) and Touze-Foltz and Giroud (2003) to characterize the quality of the contact at the interface between the geomembrane and the soil layer (see Section 2.3.5).

As explained in Section 2.3.5.3, the exponents in Equation (5.10) were solved for using results from a sensitivity analysis for a range of values for each variable in the new equation. The ranges for each of the four parameters that were used to perform the calculations of the analytical model are listed in Table 5.9. One parameter was varied over the range of values listed in Table 5.9 while the rest of the parameters were kept constant to determine the sensitivity of the leakage rate for each variable. For each combination, the flow rates were calculated using the analytical solution presented by Touze-Foltz et al. (1999) [Equation (2.19)]. A discussion of the spreadsheet used to perform the calculations to determine the leakage rate and radius of interface flow for a given transmissivity is included in Appendix C. Linear regression was used to approximate the value of each exponent based on the results of the rigorous calculations using the analytical solution.

A value for the transmissivity of the interface is needed to solve the analytical solution, so the harmonic mean of the back-calculated transmissivity for the GM-CCL test series was utilized (see Section 5.2.4). Like the "empirical" equations developed by

Touze-Foltz and Giroud (2003), Equation (5.10) was not developed directly using the experimental data. Instead, the back-calculated transmissivity was based on the experimental results and that transmissivity was subsequently used in the development of the new simplified equation.

Table 5.9: Range of values used to develop simplified equation

Variable	Range (Units)
Area of Defect, a	0.02 - 81.0 (cm^2)
Hydraulic Head, h_w	10 - 75 (m)
Hydraulic Gradient, i_s	1.2 - 75
Hydraulic Conductivity, k_s	$1x10^{-9}$ - $1x10^{-7}$ (m/s)

The new equation for estimating leakage through geomembrane defects under high heads is:

$$Q = 1.45x10^{-7} a^{0.23} h_w^{0.78} i_s^{0.14} k_s^{0.26} \qquad (5.11)$$

Equation (5.11) must be used with only SI units. The quality of the contact for the GM-CCL tests was considered to be "excellent", and since Equation (5.11) was developed using the back-calculated transmissivity from the GM-CCL tests, the new equation can be used to predict leakage rates for excellent contact conditions.

The predicted leakage rates and the leakage rates measured in the GM-CCL test series are plotted together in Figure 5.18. Equation (5.11) provides a significantly better estimate of leakage through a defect in a geomembrane over a clay layer under high hydraulic heads than the existing simplified equations developed by Touze-Foltz and Giroud (2003).

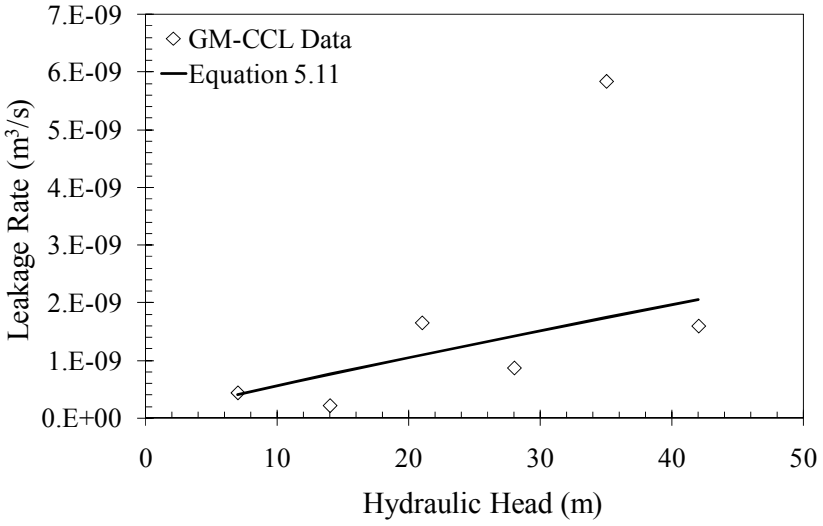

Figure 5.18: Comparison of measured and calculated leakage rates for GM-CCL test series

Equation (5.11) is a simplified version of the analytical model developed by Touze-Foltz et al. (1999) [Equation (2.19)] for the range of variables listed in Table 5.9. The results obtained using Equations (5.11) and (2.19) compared with the experimental data in Figure 5.19. The leakage rates predicted by the two models are very similar. The agreement between the analytical model and the new simplified equation was expected since both were calculated using the same parameters (i.e., defect area, hydraulic heads, hydraulic conductivity, and depth of the soil layer) and the same interface transmissivity. Consequently, Equation (5.11) provides a simple way to estimate leakage through a defect in a geomembrane liner over a clay layer.

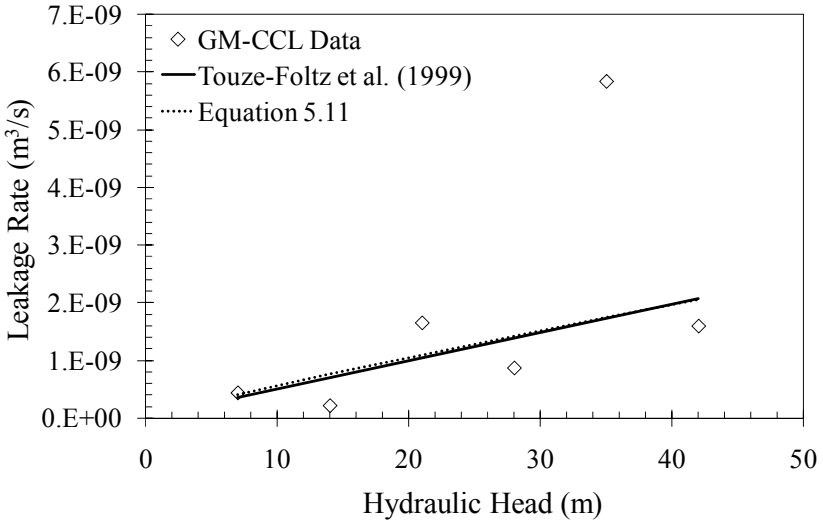

Figure 5.19: Comparing analytical and simplified models

Since excellent contact between the geomembrane and the underlying clay layer may be considered a best case scenario, the equation needed to be modified to provide a more conservative estimate of the leakage rate through a defect in a GM-CCL lining system. By adding a coefficient for the contact condition, C_q to Equation (5.11), poor contact quality can be approximated using the simplified equation.

To account for a less intimate contact at the interface between the geomembrane and soil layer, a relationship between the hydraulic head and the quality of contact was developed. The quality of contact was defined by a ratio of leakage rates for poor contact to leakage rates for excellent contact. The tests used for the development of a relationship for poor contact conditions based on leakage rates, contact quality and head above the liner were tests GM-CCL-L1 and GM-CCL-L2 and tests GM-CCL-5 and GM-CCL-5P. The leakage rate, contact quality, and head above the liner are listed in Table 5.10 for the four tests, and the ratio of poor to excellent contact is also included in the table. The difference between poor and excellent contact in terms of leakage rates for

low heads is two orders of magnitude while the leakage rates for poor and excellent contact quality for high heads are on the same order of magnitude. The relationship for head versus the contact quality ratio is shown in Figure 5.20. The relationship is linear since there are only two sets of data. More tests are needed to fully develop the relationship between hydraulic head, contact quality and leakage rate.

Table 5.10: GM-CCL tests used to determine contact condition coefficient, C_q

Test	Head Above Liner (m)	Contact Quality	Leakage Rate (m^3/s)	$Q_{poor}/Q_{excellent}$ (C_q)
GM-CCL-L1	0.53	Poor	1.2×10^{-7}	100
GM-CCL-L2	0.53	Excellent	1.2×10^{-9}	
GM-CCL-5	35	Excellent	5.4×10^{-9}	1
GM-CCL-5P	35	Poor	2.5×10^{-9}	

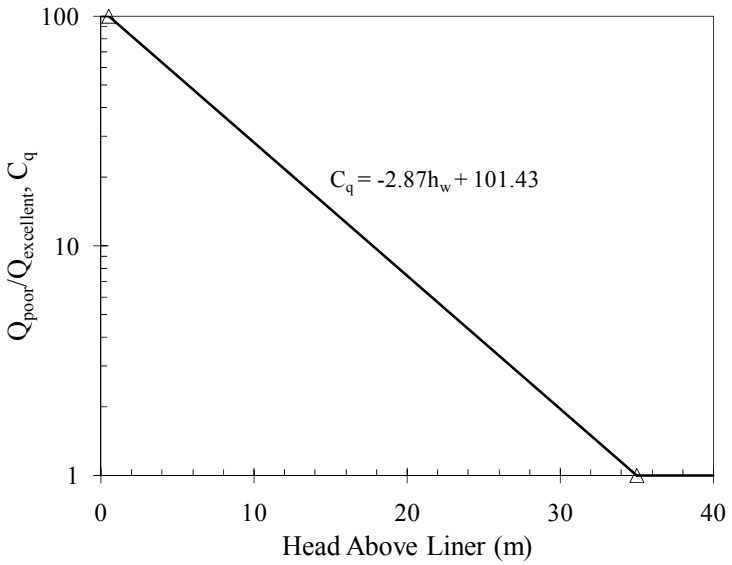

Figure 5.20: Relationship between contact quality and head above the geomembrane liner

Equation (5.11) can be rewritten to include the coefficient for contact condition as follows:

$$Q = 1.45x10^{-7}\ C_q\ a^{0.23} h_w^{0.78} i_s^{0.14} k_s^{0.26} \qquad (5.12)$$

SI units must be used to calculate the leakage rate using Equation (5.12).

Equations (5.11) and (5.12) were developed using the average back-calculated transmissivity from the laboratory tests. The analytical models developed by Touze-Foltz et al. (1999) for field and laboratory conditions are based on the assumption that flow does not occur outside the "radius of wetted area" and that flow into the soil is one-dimensional. Both of these assumptions neglect lateral flow. A coefficient that allows consideration of lateral flow, C_{lf}, is introduced in the following equation:

$$Q = 1.45x10^{-7}\ C_q\ C_{lf}\ a^{0.23} h_w^{0.78} i_s^{0.14} k_s^{0.26} \qquad (5.13)$$

where C_{lf} is a factor that takes into account the increase in flow rate due to the inclusion of lateral flow. A parametric study was conducted using finite element simulations for both the permeameter cell conditions and field conditions. The leakage rates were determined for changes in head, defect size, and hydraulic conductivity of the soil layer for the laboratory and field conditions. The average ratio of leakage rate for field conditions to leakage rate for laboratory conditions was 3. Therefore, the recommended value for the coefficient for lateral flow, C_{lf} is 3 for field conditions and C_{lf} = 1 for permeameter conditions.

It should be noted that the analytical model developed by Touze-Foltz et al. (1999) for field conditions can be solved using a spreadsheet that incorporates the use of modified Bessel functions. An example of this spreadsheet is shown in Appendix C. Equation (5.13) was developed in order to assist engineers in design by providing a quick and simple way to estimate the leakage rate through defects in geomembrane liners in the

field. However, the analytical model provides a more rigorous method to determine leakage rates.

Chapter 6: Geomembrane-Geosynthetic Clay Liner Tests

6.1 INTRODUCTION

The experimental results and analysis presented in this chapter involve a composite liner system that consists of a geomembrane placed over a geosynthetic clay liner (GCL). The test series presented in this chapter was conducted as part of the experimental program to quantify the leakage rate through a defect in a geomembrane-GCL (GM-CCL) system under high hydraulic heads. These test results allowed the evaluation of the effect of head above the geomembrane liner and contact quality of the interface between the geomembrane and the GCL. The potential loss of bentonite was also investigated as part of the experimental study. Other aspects of flow through a defect in a geomembrane liner, such as the transmissivity of the interface between the geomembrane and the soil layer and the radius of interface flow, were also evaluated.

Another objective of the analyses was to develop predictive tools suitable for estimating the leakage through defects in composite lining systems placed on the upstream face or in the core of a dam. The laboratory data from the GM-GCL tests were compared against existing analytical and "empirical" models to determine their validity at approximating flow through a defect in a geomembrane-GCL composite liner under high heads. A new simplified equation was developed and compared with the experimental data.

6.2 EXPERIMENTAL RESULTS FOR GEOMEMBRANE-GCL TESTS

Experimental tests were conducted using the small permeameter cell as part of the GM-GCL test series to quantify leakage rates for a range of variables, such as hydraulic head, interface quality and pre-hydration of the GCL. Tests were conducted using the

equipment, methods and materials for the small permeameter cell discussed in Chapter 3. The volume and flow data recorded during each test and specific soil properties for each test discussed in this section are included in Appendix A.

The contact quality between the geomembrane and the GCL, transmissivity of the interface, and the radius of interface flow were investigated to determine the effect each of these variables have on the flow of water through a defect in a composite liner that includes a GCL. The effect of pre-hydration of the GCL was investigated as part the study presented herein. Additionally, bentonite loss in the effluent of the GM-GCL tests and its effect on the leakage rates was evaluated during the experimental study.

6.2.1 Leakage Rates

The GM-GCL composite liner system was placed over a sand layer and the flow through a defect in the geomembrane liner was quantified for heads ranging from 7 to 42 m. The 1 mm-thick LLDPE geomembrane had a circular defect with a diameter of 1.6 mm located at the center of the soil layer. The soil layers were prepared using Monterey #30 sand at a relative density of 75% and the soil layer was saturated prior to testing. Two test series were conducted as part of this study: 1) tests involving unhydrated GCLs (GM-UGCL test series), and 2) tests involving GCLs hydrated under a normal stress of 20 kPa (GM-HGCL test series).

6.2.1.1 Tests Conducted using Unhydrated GCLs

GCLs are not likely to be hydrated during field installation so tests were conducted using unhydrated GCLs. The flow of water through the defect initiates the hydration process of the bentonite. The granular bentonite in the unhydrated GCL has a higher initial hydraulic conductivity, acting more like a coarse-grained material than a clay with a low hydraulic conductivity. Once the bentonite begins to hydrate, the

hydraulic conductivity begins to decrease and the leakage rate through the defect also decreases. Flow through an unhydrated GCL will be relatively high until the bentonite becomes hydrated; however, hydration occurs rather rapidly. The saturated sand layer beneath the GCL also contributes to the hydration of the GCL from below. While the presence of a saturated layer under the GCL is unrealistic, this approach was used to facilitate interpretation of the results under steady-state conditions. Nonetheless, the transient (hydration) portion of the test gives insight into the initial performance of the GM-GCL system.

As with the GM-CCL tests, the volume of water that flowed into and out of the cell was recorded over time for the GM-UGCL test series. Cumulative water volume and leakage rate curves, shown in Figure 6.1, were obtained from the volume measurements made during each test. Outflow began immediately once the test began because the sand layer was saturated prior to testing. The volume of water flowing into the permeameter cell during the early stages of the test, shown in Figure 6.1a, was approximately equal to the volume of water flowing out of the system, indicating that water was not being stored in the components of the system. Since the GCL is significantly thinner than the clay layers in the GM-CCL test series, the volume of water being stored in the bentonite was less than the volume of water being stored in the compacted clay layer. Also, the volume of water being stored in the GCL was reduced because the GCL was confined by the geomembrane under the imposed head. This confinement minimized the potential for swelling of the bentonite. As discussed in Section 3.2, the permeameter did not have a porous stone at the bottom of the cell but rather a geocomposite. The lack of a porous stone in the tests involving GCLs also contributed to minimize the volume of water stored in the system. Accordingly, the difference between the inflow and outflow volume

curves shown in Figure 6.1a was not as significant as in the tests involving a compacted clay liner (Section 5.2.1.1).

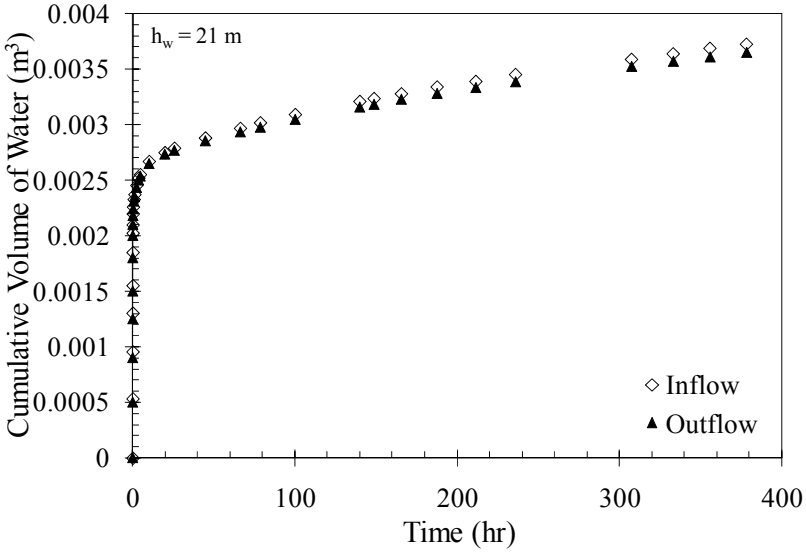

(a)

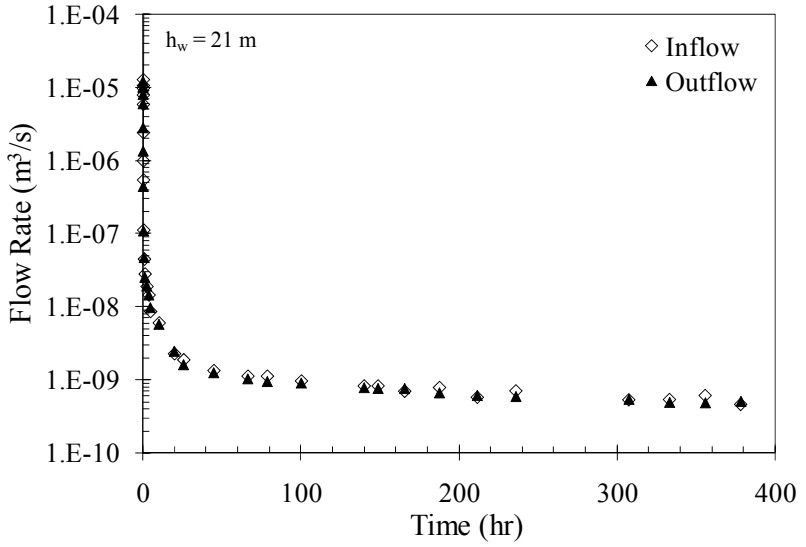

(b)

Figure 6.1: Example of: a) cumulative volume curve and b) flow rates for tests in the GM-UGCL test series

Three tests were carried out as part of this test series. The tests were terminated once a constant leakage rate was achieved. Table 6.1 lists the details of the tests, including the water head, characteristics of the sand layer and final water content of the GCL, for these three tests (GM-UGCL-1 through 3). The average initial water content of the GCLs was less than 12%, while the final water content of the GCL specimens typically exceeded 100%.

Table 6.1: Details and leakage rates for tests using unhydrated GCL

Test #	Head Above Liner (m)	Monterey #30 Sand		Bentofix GCL		Leakage Rate (m^3/s)
		Unit Weight (kN/m^3)	Porosity, n	Final Water Content, w (%)	Final Thickness (mm)	
GM-UGCL-1	7	15.9	0.39	99.5	10.1	3.3×10^{-10}
GM-UGCL-2	14	15.8	0.39	104.3	-	1.0×10^{-9}
GM-UGCL-3	21	15.7	0.40	104.6	-	5.3×10^{-10}

The leakage rates are shown in Figure 6.2 as a function of time for the various tests in the GM-UGCL series. As with the tests involving clay layers, the initial flow rates are comparatively high and decrease over time until the flow rate became constant. The explanation for the decrease in flow rate over time in the GM-UGCL tests is different that that for the GM-CCL test series. Infiltration into the GCL occurs rather rapidly because the unhydrated bentonite initially acts like a coarse-grained material. As the bentonite hydrates, the hydraulic conductivity of the GCL decreases. The hydraulic gradients across the composite liner are relatively high since the GCL component is thinner than the compacted clay liner in the GM-CCL test series.

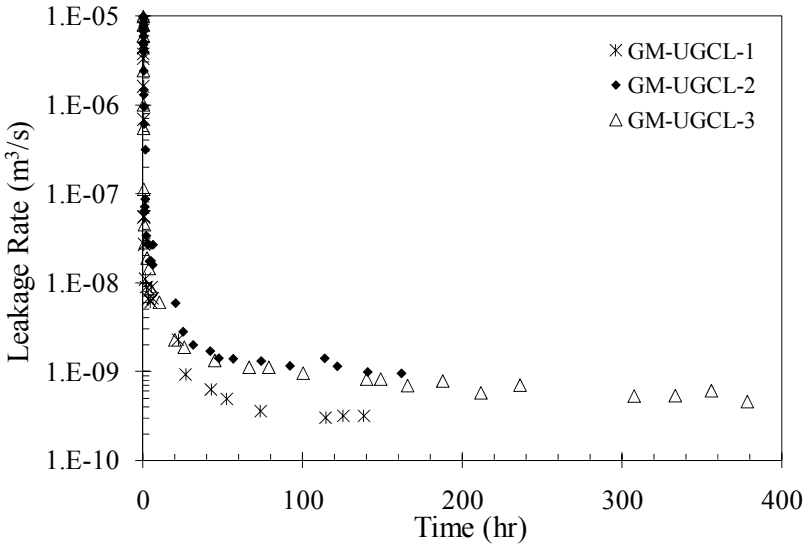

Figure 6.2: Leakage (inflow) rates as a function of time for GM-UGCL test series

The leakage rates for the tests involving unhydrated GCLs (Table 6.1) are over three orders of magnitude smaller than those measured in the GM-Only test series (Table 4.1). Consequently, the use of a GCL in the lining system significantly decreased the leakage rate through a damaged geomembrane, even under high heads. There is some scatter in the data when considering leakage rate with respect to the hydraulic head, but the discrepancies can be attributed to the variability in the GCL samples and to the preparation of the soil layers.

6.2.1.2 Tests Conducted using Hydrated GCLs

Results from tests involving unhydrated GCLs (Section 6.2.1.1) showed initially high leakage rates until the bentonite began to hydrate. Consequently, tests were also conducted using GCL specimens that were hydrated prior to testing. The tests discussed in this section were performed to determine the potential impact of pre-hydrating the GCL. In order to hydrate the GCLs, specimens were soaked in water for at least 48 hours under a normal stress of 20 kPa.

The volume of water that flowed into and out of the cell was recorded over time. The cumulative volume and leakage rate curves shown in Figure 6.3 were obtained from the volume measurements made during each test. Similar to the GM-UGCL tests, outflow began immediately once the test began since the sand layer was saturated prior to testing. Once the hydraulic head was applied, water in the sand layer flowed out of the permeameter cell. The volume of water flowing into the permeameter cell during the early stages of the test, as shown in Figure 6.3a, was approximately equal to the volume of water flowing out of the system, indicating that water was not being stored in the components of the system. However, as the test progressed, the difference between the inflow and outflow volume curves increased. This can be explained by the swelling of the GCL after the confining stress was removed. The hydrated GCL was confined during hydration, but confinement was removed when the GCL was moved to its position beneath the geomembrane, allowing the bentonite in the GCL to rebound. The application of the hydraulic head to the lining system reinstated a portion of the confining stress imposed during the pre-hydration process.

Interestingly, the difference between the cumulative volume curves is greater for the GM-HGCL test series (Figure 6.3a) than for the GM-UGCL test series (Figure 6.2a). This was unexpected, considering that the GCL was hydrated prior to testing. Also, the unhydrated GCLs would be expected to swell more than the pre-hydrated GCL.

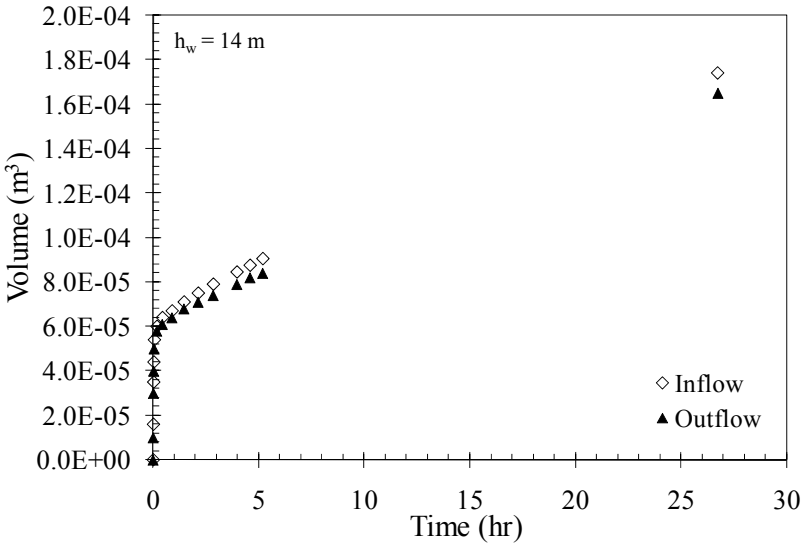

(a)

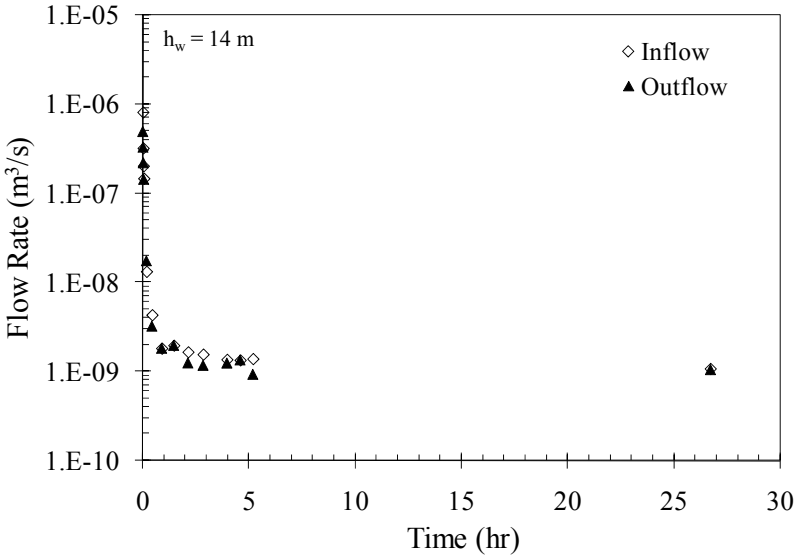

(b)

Figure 6.3: Example of a) cumulative volume curve and b) flow rates for tests in the GM-HGCL test series

Six tests were carried out until a constant leakage rate was achieved. The details, including the porosity of the sand layer and the final water content of the hydrated GCL, for these six tests (GM-HGCL-1 through 6) are listed in Table 6.2. The average initial water content of the GCLs was less than 12%, while the final water content of the GCL specimens was over 100%.

Table 6.2: Details for hydrated GCL tests

Test #	Head Above Liner (m)	Monterey #30 Sand		Bentofix GCL		Leakage Rate (m^3/s)
		Unit Weight (kN/m^3)	Porosity, n	Final Water Content (%)	Final Thickness (mm)	
GM-HGCL-1	14	15.9	0.39	103.0	8.0	1.3×10^{-9}
GM-HGCL-2	21	16.0	0.38	112.0	8.1	9.6×10^{-10}
GM-HGCL-3	28	15.9	0.39	126.2	10.0	1.4×10^{-9}
GM-HGCL-4	28	16.0	0.38	112.0	8.1	1.2×10^{-9}
GM-HGCL-5	35	15.9	0.39	126.2	10.0	1.5×10^{-9}
GM-HGCL-6	42	15.9	0.39	126.2	10.0	1.9×10^{-9}

As with the tests in the GM-CCL test series, the inflow leakage rates shown in Figure 6.4 decrease over time until reaching a constant flow rate. The hydraulic gradients across the composite liner are relatively high since the GCL component is thinner than the compacted clay liner in the GM-CCL test series. The final leakage rates shown in Figure 6.5 were observed to increase linearly with increasing hydraulic head, although there is some scatter in the data. Discrepancies can be attributed to the variability in the GCL materials and in the preparation of the soil layers. Despite the scatter, the repeatability of these tests is good, as can be observed by comparing the leakage rates between the two tests conducted under 28 m of head (less than 15% difference).

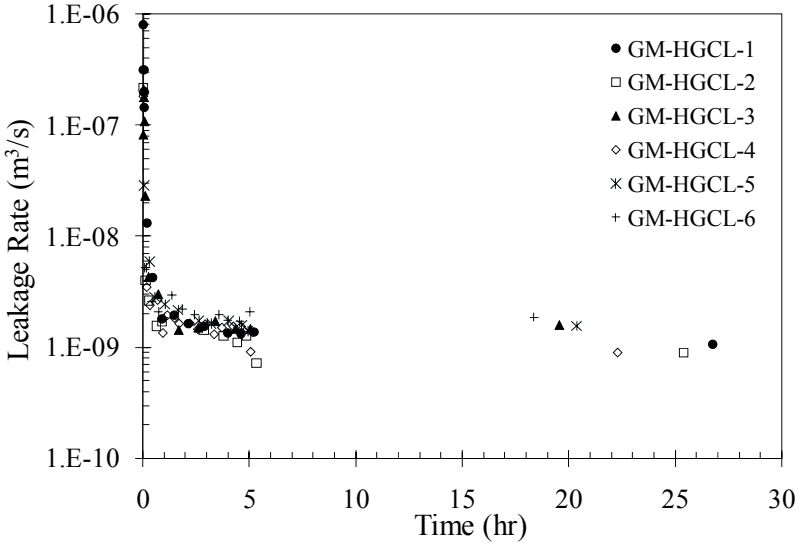

Figure 6.4: Leakage rates with time for GM-HGCL test series

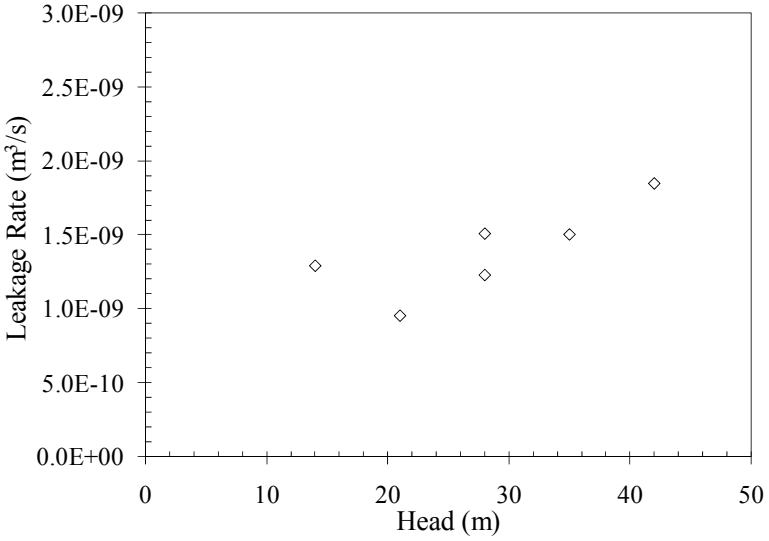

Figure 6.5: Leakage rates with head for hydrated GCL tests

6.2.1.3 Upper and Lower Bournds

Darcy's law may be used to provide upper and lower bounds of the flow through a GCL due to a defect in a geomembrane. The upper bound of the flow can be estimated as:

$$Q = kiA \tag{6.1}$$

where Q is the leakage rate, k is the hydraulic conductivity of the soil, i is the hydraulic gradient, and A is the cross-sectional area of the permeameter cell. The hydraulic conductivity that was used to calculate the flow rates was the equivalent hydraulic conductivity of the GCL-sand system, based on each component's thickness and hydraulic conductivity. The hydraulic gradient is the change in total head loss across the GCL and sand layer divided by the length of the entire lining system. Flow rates that were calculated using the total cross-sectional area of the permeameter are representative of the flow rate through an unlined system. The upper bound of the flow is shown in Figure 6.6, along with the data from the GM-GCL test series. Lower bound flow rates were also calculated using only the area of the defect. The lower bound flow rates were significantly smaller than the measured leakage rates. The measured flow rates were less than the upper bound flow rates calculated using the total area of the permeameter.

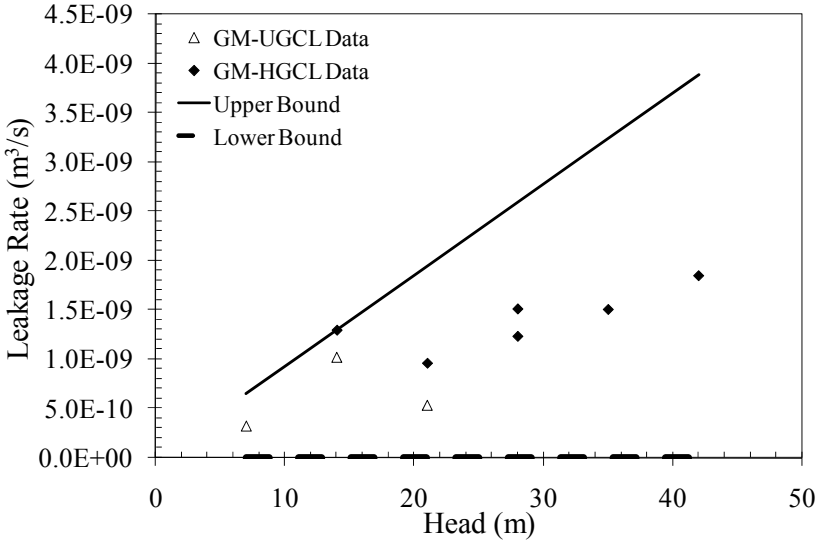

Figure 6.6: Comparison of Darcy flow and leakage rates from GM-UGCL & GM-HGCL tests)

6.2.2 Evaluation of the Effect of Hydration of the GCL

The measured leakage rates for the GM-UGCL and GM-HGCL test series are compared in Figure 6.7. For a given hydraulic head, the ultimate leakage rates from the GM-UGCL test series appear to be smaller than the leakage rates for the GM-HGCL test series (see tests with hydraulic heads of 14 and 21 m). The leakage rate for test GM-UGCL-1, which was subjected to a head of 7 m, was less than the leakage rates of the remaining tests.

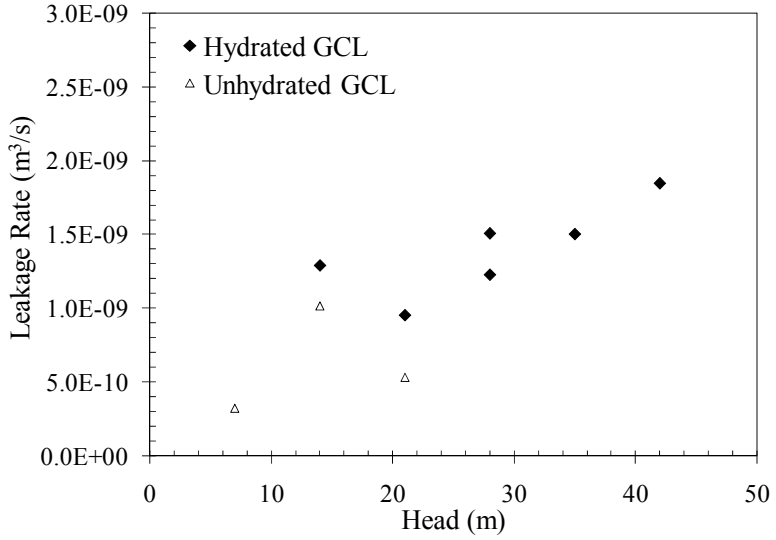

Figure 6.7: Comparison of leakage rates for tests involving unhydrated and hydrated GCLs

However, the difference between the leakage rates for systems with unhydrated GCLs and systems with hydrated GCLs is not significant. A GCL that is initially unhydrated begins to hydrate as water infiltrates through a defect in the overlying geomembrane. The final leakage rates for the initially unhydrated GCL are similar to those for the tests with a pre-hydrated GCL. Consequently, it appears that there is no benefit to pre-hydrating a GCL in the field, at least for the case of water leakage.

6.2.3 Evaluation of the Quality of Contact between a Geomembrane and GCL

Additional tests were conducted to evaluate the effect that contact quality on the leakage rates through GM-GCL composite liners. The properties of the soil layers, properties of the GCLs, interface quality and the leakage rates for these additional tests are listed in Tables 6.3 and 6.4. Also included in Tables 6.3 and 6.4 are the leakage rates that would correspond to a frequency of one geomembrane defect per acre.

As listed in Table 6.3, Test GM-UGCL-1P was conducted using the same hydraulic head as GM-UGCL-1 but the quality of the contact between the geomembrane and the GCL was "poor." The "poor" contact was achieved by slightly reducing the thickness of the underlying sand layer, decreasing the support layer beneath the GCL. The leakage rate of the test with "good" contact was three orders of magnitude smaller than that of the test with "poor" contact. A test was also conducted on a liner system that consisted of an unhydrated GCL placed directly over the sand layer (i.e., without a geomembrane). The leakage rate obtained for the UGCL-Only test can be reported as the flow rate per unit area (i.e., $L^3/T/L^2$ or lphd). The leakage rate of UGCL-Only in lphd (112,000 lphd) is significantly higher than the leakage rates through a defect in a geomembrane liner (assuming one defect per acre of geomembrane liner), even if the interface contact is poor in quality.

Table 6.3: Test details and leakage rates for tests with different interface contact quality for the GM-UGCL test series.

Test #	Head Above Liner (m)	Monterey #30 Sand		Bentofix GCL		Contact Quality	Leakage Rate per Defect (m^3/s)	Leakage Rate ($m^3/s/m^2$)*	Leakage Rate (lphd)*
		Unit Weight (kN/m^3)	Porosity, n	Final Water Content, w (%)	Final Thickness (mm)				
GM-UGCL-1	7	15.9	0.39	99.5	10.1	Good	3.3×10^{-10}	8.2×10^{-14}	0.071
GM-UGCL-1P	7	15.7	0.40	109.8	-	Poor	3.9×10^{-7}	9.6×10^{-11}	83.3
GM-UGCL-2	14	15.8	0.39	104.3	-	Good	1.0×10^{-9}	2.5×10^{-13}	0.213
UGCL-Only	14	15.8	0.39	94.9	-	-	-	1.3×10^{-7}	112,000

*Assuming 1 defect per acre

The effect of the quality of the interface contact between the geomembrane and GCL was also investigated for the tests involving hydrated GCLs. The leakage rates for these tests are listed in Table 6.4. The leakage rate for the test with a "poor" contact (GM-HGCL-P) was an order of magnitude higher than the test with "good" contact quality (GM-HGCL-1). As with the unhydrated GCL tests, a test was conducted without a geomembrane placed over the hydrated GCL. The leakage rate obtained for the HGCL-

Only test can be considered as the flow rate per unit area (i.e., $L^3/T/L^2$ or lphd). The leakage rate of HGCL-Only in lphd (1,120,000 lphd) is significantly higher than the leakage rates through a defect in a geomembrane liner (assuming one defect per acre of geomembrane liner), even if the interface contact is poor in quality.

Table 6.4: Comparing effect of geomembrane for the GM-HGCL test series

Test #	Head Above Liner (m)	Monterey #30 Sand		Bentofix GCL		Contact Quality	Leakage Rate per Defect (m^3/s)	Leakage Rate ($m^3/s/m^2$)*	Leakage Rate (lphd)*
		Unit Weight (kN/m^3)	Porosity, n	Final Water Content, w (%)	Final Thickness (mm)				
GM-HGCL-1	14	15.9	0.39	103.0	8.0	Good	1.3×10^{-9}	3.2×10^{-13}	0.278
GM-HGCL-P	7	15.9	0.39	94.7	6.9	Poor	2.0×10^{-8}	4.9×10^{-12}	4.27
HGCL-Only	14	15.6	0.40	115.4	7.0	-	-	1.3×10^{-6}	1,120,000

*Assuming 1 defect per acre

Tests involving geomembranes in intimate contact with the underlying GCL had lower leakage rates than the tests without geomembranes, considering a frequency of one defect per acre of geomembrane. Even for tests in which the geomembrane was not in good contact with the GCL, the leakage rate was significantly reduced when a geomembrane was placed over the GCL. However, the magnitude of the decrease is dependent on the quality of contact at the interface between the geomembrane and the GCL.

6.2.4 Transmissivity of the Interface

The analytical model developed by Touze-Foltz et al. (1999) [Equation (2.24)] was used to back-calculate the transmissivity of the interface between the geomembrane and the GCL. Since the bentonite in the GCL is confined by two geotextiles, the transmissivity of the interface between the geomembrane and the GCL is largely controlled by the transmissivity of the upper geotextile.

An important consideration in this analysis is that, for tests involving GCLs that initially are unhydrated, the initial hydraulic conductivity of the GCL will change during

the test as the bentonite hydrates. Indeed, it is unclear whether the unhydrated GCL will become saturated by the time steady-state flow was reached. It should be noted that the model developed by Touze-Foltz et al (1999) is appropriate for predicting leakage rates considering saturated GCLs. However, as was discussed in Section 6.2.2, there are no significant differences between the final leakage rates for systems with unhydrated GCLs and those for systems with hydrated GCLs.

The transmissivity was back-calculated using the analytical model developed by Touze-Foltz et al. (1999). The transmissivity was varied until the calculated leakage rate was equal to the leakage rate measured in the laboratory. The back-calculated values for the interface transmissivity for tests involving unhydrated GCLs (GM-UGCL) and tests involving hydrated GCLs (GM-HGCL) are shown in Figure 6.8. As shown in Figure 6.8a, the harmonic mean of the transmissivity for the tests involving unhydrated GCLs was 1.8×10^{-10} m^2/s and the transmissivity for GM-HGCL tests was 3.7×10^{-11} m^2/s. The average transmissivity for the hydrated GCL tests was less than an order of magnitude lower than that of the unhydrated GCL tests. Pre-hydration of the GCL appears to affect the interface transmissivity even though the final leakage rates appear to be unaffected by the initial hydration condition. Touze-Foltz and Barroso (2006) developed a simple equation to estimate the transmissivity for a geomembrane-GCL contact [Equation (2.41)]. As shown in Figure 6.8b, the transmissivity calculated using Equation (2.41) was very similar to the average transmissivity back-calculated from the laboratory data.

Based on Figure 6.8, it does not appear that head affects the transmissivity of the interface for both unhydrated and hydrated GCLs. The leakage rate increased linearly as the hydraulic head increased (Figure 6.7) but there were minimal variations in the transmissivity with respect to changes in head above the geomembrane liner. Higher

heads lead to higher leakage rates, but also to a thinner interface gap, which contributes to a lower transmissivity across the interface.

Also, the back-calculated transmissivity for the tests involving unhydrated GCLs was slightly higher than those back-calculated for tests involving hydrated GCLs. The unhydrated GCLs were more prone to bentonite loss than GCLs that were hydrated prior to testing. The higher bentonite loss could contribute to a higher transmissivity. The tests using unhydrated GCLs could also have not been completely hydrated by the end of the test, which would influence the transmissivity.

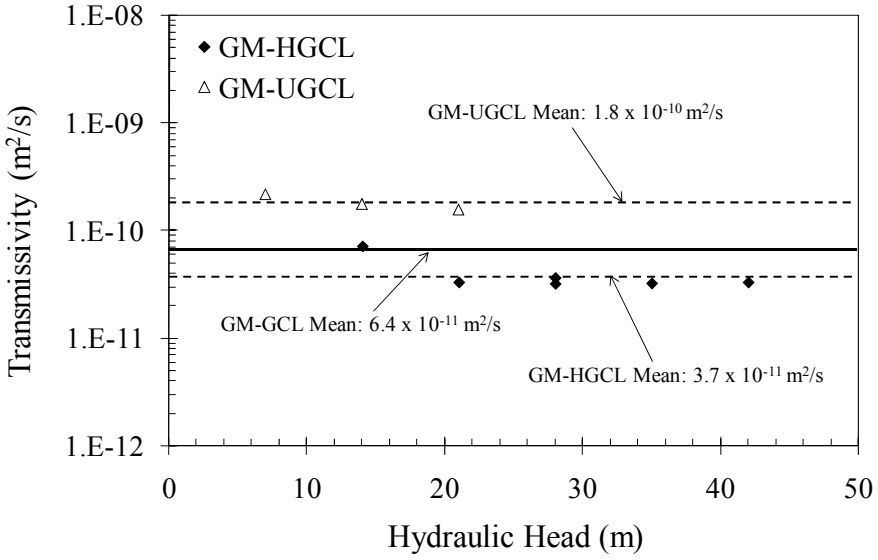

(a)

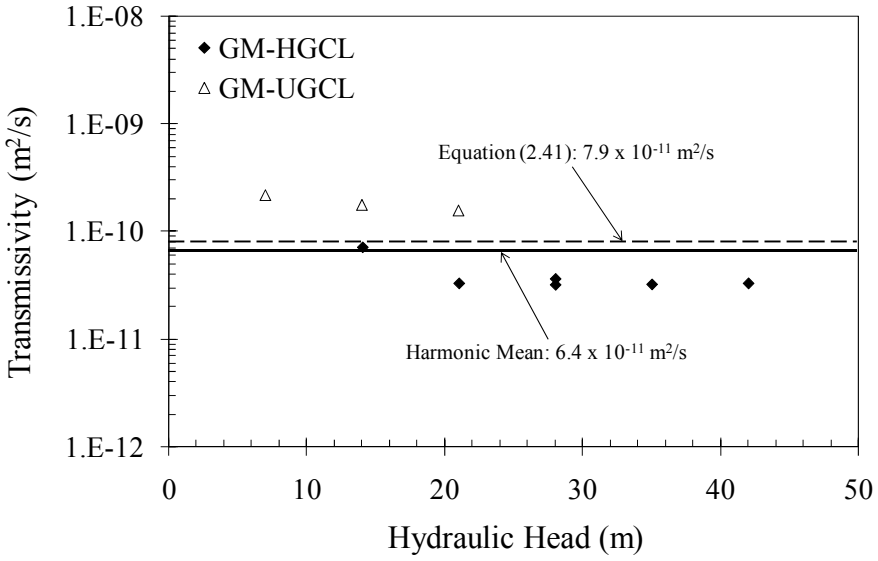

(b)

Figure 6.8: a) Back-calculated transmissivities for tests with GCLs and b) comparison of the average back-calculated transmissivity with transmissivity predicted using Barroso et al. (2006)

The average value for the transmissivities back-calculated in this study was used to predict flow rates using the analytical model developed by Touze-Foltz et al. (1999) [Equation (2.24)]. Flow rates were also calculated using the transmissivity defined using Equation (2.41) that was developed by Touze-Foltz and Barroso (2006). Both sets of calculations were conducted over the range of head corresponding to the experimental testing program and for the same defect size and soil thickness. The predicted flow rates are shown in Figure 6.9 along with the GM-GCL experimental data. As shown in the figure, the measured and predicted leakage rates are very similar, with the transmissivity that was back-calculated for this study providing the best fit.

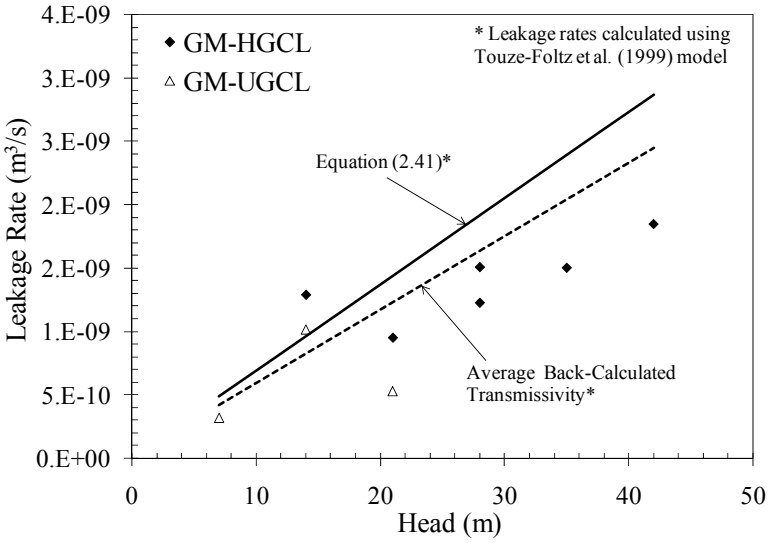

Figure 6.9: Comparison of leakage rates calculated using Touze-Foltz et al. (1999) model for transmissivities obtained from different methods

The average back-calculated transmissivity for tests with GCLs (6.4×10^{-11} m^2/s) was slightly higher than the transmissivity calculated for the GM-CCL tests (3.0×10^{-11} m^2/s). The transmissivity of the interface has been reported to correlate well with the hydraulic conductivity of the soil beneath the geomembrane. It should be noted that

although bentonite has a lower hydraulic conductivity than the CL soil used in the GMC test series, the average transmissivity obtained for tests involving GCLs was higher than that obtained for the GMC test series. This can be attributed to the presence of the nonwoven carrier geotextile in the GCL, which prevents the direct contact of the geomembrane with the bentonite. Even at higher heads, when the geotextile is compressed, the material is expected to still carry water in the planar direction.

6.2.5 Radius of Interface Flow

Using the analytical solution developed by Touze-Foltz et al. (1999) for field conditions [Equation (2.19)], the radius of interface flow was back-calculated by matching the measured flow rates with the calculated flow rates. The radii of interface flow predicted using Equation (2.19) for the GM-HGCL test series are listed in Table 6.5. The predicted radii of interface flow from the GM-UGCL test series are listed in Table 6.6. The measured leakage rates are included for comparison. The tests with the lowest leakage rates also have the smallest predicted radii of interface flow. It should be noted that the estimated radius of interface flow for all tests exceeds 15 cm, although the diameter of the permeameter cell for these tests was 15 cm. That is, the estimated radii of interface flow were beyond the limits of the small permeameter cell. The predicted radius of interface flow for the tests with unhydrated GCLs was smaller than those obtained for the tests with hydrated GCLs. However, the tests using unhydrated GCLs were conducted under lower heads than the tests using hydrated GCLs.

Table 6.5: Radii of interface flow for tests with hydrated GCLs predicted using Touze-Foltz et al. (1999)

Test	Predicted Wetted Radius (m)	Measured Leakage Rate (m^3/s)
GM-HGCL-1	0.33	1.3×10^{-9}
GM-HGCL-2	0.25	9.6×10^{-10}
GM-HGCL-3	0.31	1.4×10^{-9}
GM-HGCL-4	0.26	1.2×10^{-9}
GM-HGCL-5	0.31	1.5×10^{-9}
GM-HGCL-6	0.32	1.9×10^{-9}

Table 6.6: Radii of interface flow for tests with unhydrated GCLs predicted using Touze-Foltz et al. (1999)

Test	Predicted Wetted Radius (m)	Measured Leakage Rate (m^3/s)
GM-UGCL-1	0.19	3.3×10^{-10}
GM-UGCL-2	0.29	1.0×10^{-9}
GM-UGCL-3	0.18	5.3×10^{-10}

6.2.6 Bentonite Loss

During tests involving GCLs, and independent of initial hydration conditions, it was observed that the effluent was cloudy. This indicated that bentonite was being flushed out of the GCL. An example of effluent collected from one of the tests involving GCLs is shown in Figure 6.10. Since bentonite loss could lead to an increase in the flow rate through the system, the concentration of the bentonite in the effluent was measured.

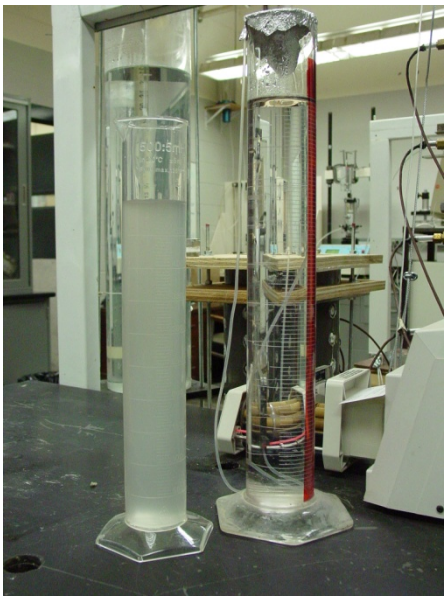

Figure 6.10: Cloudy effluent from test involving GCL

Samples of the effluent were taken over the course of the test and the bentonite concentration was measured for each sample. The average bentonite concentration in the effluent for each time period was plotted for a variety conditions to assess the effects of head, contact quality, initial hydration condition, and presence of a geomembrane on bentonite. It should be noted that bentonite loss was negligible in tests conducted with hydraulic heads above 21 m and very few of the tests involving hydrated GCLs exhibited bentonite loss. In fact, the only two GM-HGCL tests that showed cloudy effluent were the test with "poor" contact quality (GM-HGCL-P) and the test with a hydraulic head of 14 m (GM-HGCL-1).

The bentonite loss was evaluated for two different hydraulic heads (14 and 21 m) using two tests involving unhydrated GCLs. The leakage rates for the two tests, designated GM-UGCL-2 and GM-UGCL-3, are listed in Table 6.1. As shown in Figure 6.11, the concentration of bentonite in the effluent is comparatively high in the early

stages of both tests. However, the bentonite concentration in the effluent decreased rapidly for GM-UGCL-2, becoming negligible after about 180 minutes. The GCL under the higher hydraulic head continued to lose bentonite for a longer period of time. However, the test for a head of 14 m (GM-UGCL-2) had a leakage rate that was twice that of the test with the higher head (see Table 6.1). From the measurements of bentonite concentration, it appears that a higher loss of bentonite from the GCL did not result in a higher leakage rate.

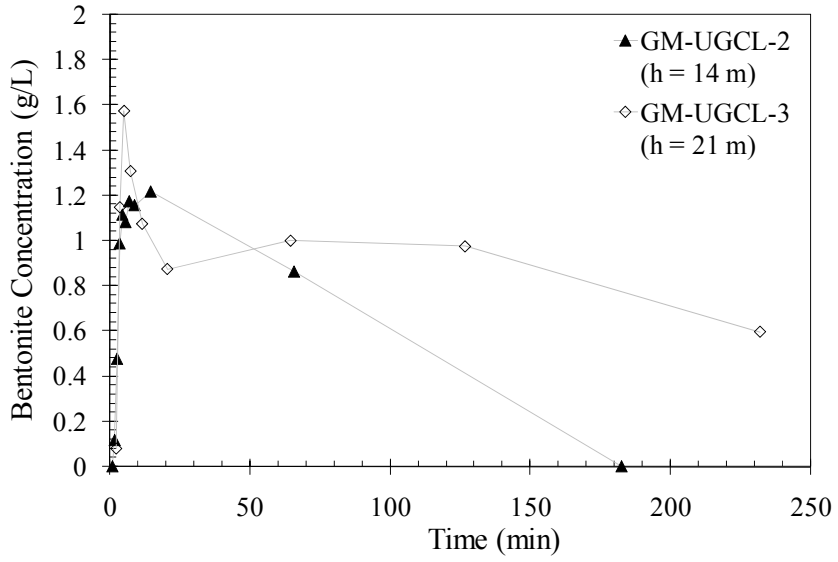

Figure 6.11: Effect of head on bentonite loss for unhydrated GCLs

The bentonite loss was evaluated for tests with and without a geomembrane, or GM-UGCL-2 and UGCL-Only, respectively. As shown in Figure 6.12, the test that included a geomembrane exhibited a larger loss of bentonite in the effluent over a longer period of time than the system without a geomembrane. For Test GM-UGCL-2, the flow through the geomembrane defect should be concentrated over only a small area (i.e., the area of the defect), although the area of flow is likely greater than the area of the defect due to flow across the interface, and the concentrated flow would lead to the higher loss

of fines from the GCL. With the UGCL-only test, the hydraulic head was distributed over the entire surface area of the GCL specimen, so hydration occurred over the entire GCL at the same time. This ultimately resulted in the low concentrations of bentonite observed in the effluent of the test without a geomembrane. Despite having higher concentrations of bentonite in the effluent, the test with the geomembrane had a lower leakage rate than UGCL-only test (see Table 6.3).

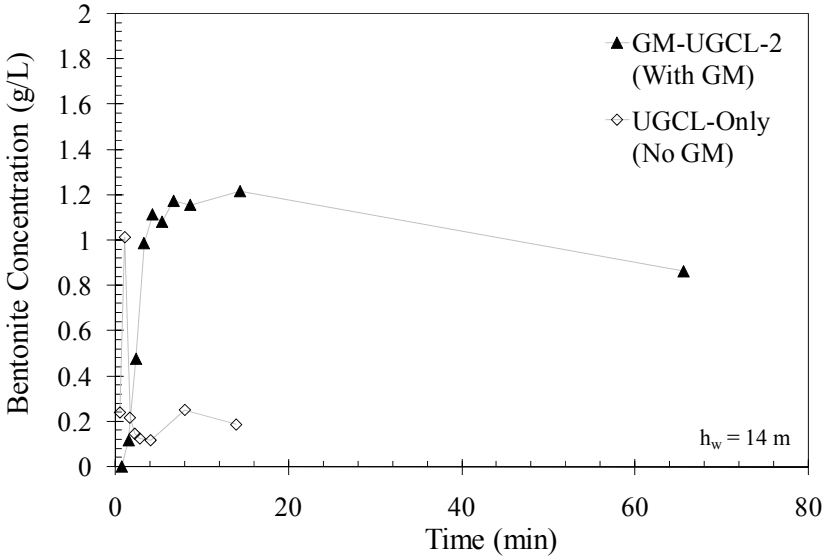

Figure 6.12: Effect of presence of geomembrane on bentonite loss for unhydrated GCLs

Two tests were compared to evaluate the effect of pre-hydration on the loss of bentonite: GM-UGCL-1P and GM-HGCL-P. The final leakage rates and GCL and soil properties for these tests are included in Tables 6.3 and 6.4. A hydrated GCL is expected to lead to less bentonite loss than an unhydrated GCL. As shown in Figure 6.13, the bentonite concentration in the effluent from the unhydrated GCL test was higher after about 10 minutes than the effluent from the test with a hydrated GCL. The loss of bentonite for the unhydrated GCL was higher over a longer period of time, as shown in

Figure 6.13. Consequently, the leakage rate for Test GM-UGCL-1P was one order of magnitude higher than the test with a hydrated GCL (GM-HGCL-P).

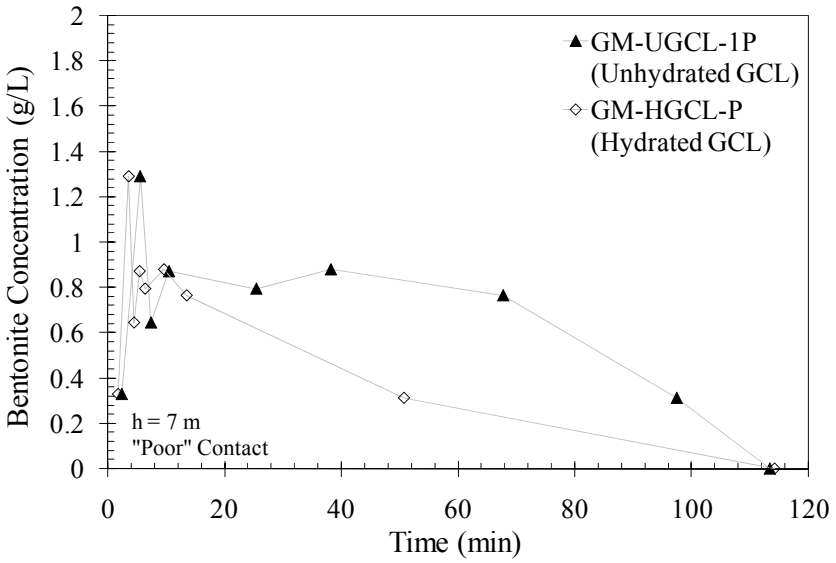

Figure 6.13: Effect of hydration on bentonite loss

The effect of contact quality (between the geomembrane and the GCL) on the loss of bentonite can be evaluated by comparing the results of tests GM-HGCL-1 and GM-HGCL-P. The details for these tests are included in Table 6.4. It could be speculated a "good" contact condition would result in less bentonite loss than a "poor" contact condition because of the smaller area of flow. Alternatively, it could be expected that the concentrated flow at the location of the defect could possibly result in higher bentonite loss for a "good" contact condition.

As shown in Figure 6.14, the concentration of bentonite in the effluent for the "good" quality contact decreases sooner and at a higher rate than the test with a "poor" quality contact. It should be noted that the bentonite loss in the test with the hydrated GCL in intimate contact with the geomembrane was lower than test with "poor" contact, even though the hydraulic head was greater. The test with a "good" contact (GM-HGCL-

1) has a lower leakage rate than the test with a "poor" contact quality (GM-HGCL-P). The lower leakage rate corresponds with the lower amount of bentonite loss for the test with "good" contact.

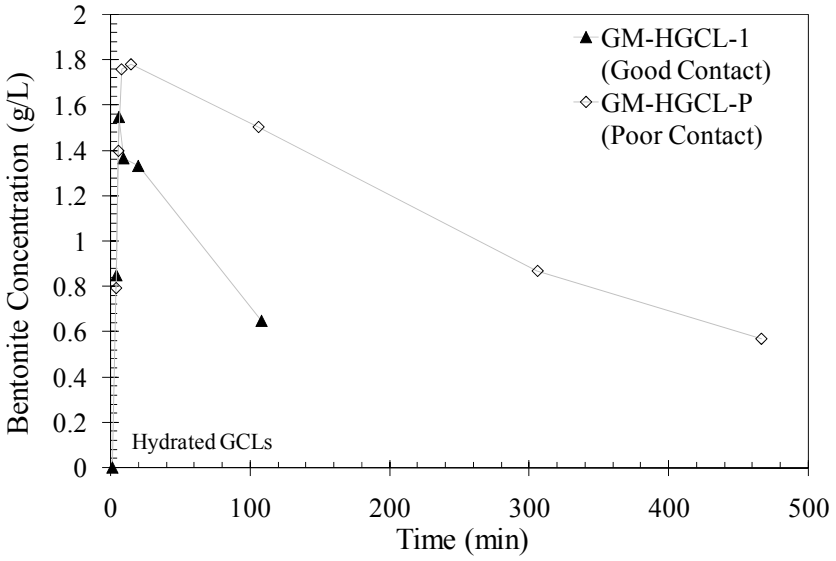

Figure 6.14: Effect of contact quality on bentonite loss

6.3 COMPARISON OF ULTIMATE LEAKAGE RATES AMONG TEST SERIES

Three main test series were conducted as part of the experimental study to evaluate the leakage through defects in geomembrane liners under high hydraulic heads. The three test series were compared against each other to determine the effect of each systems' components (i.e., soil type, presence of GCL).

The ultimate leakage rates for the GM-Only test series and the tests involving GCLs were compared. The y-axis in Figure 6.15 (leakage rate) is on a logarithmic scale since the differences in leakage rates is several orders of magnitude. The equivalent hydraulic conductivity for the combination of a GCL and the sand layer, using the thicknesses of each component and the corresponding hydraulic conductivities, was 2×10^{-9} m/s. The hydraulic conductivity of the sand alone is 4×10^{-5} m/s. The difference

between these values is also about four orders of magnitude. Note that the change in leakage rate over the entire range of hydraulic head was approximately the same for both test series. By including a GCL in geomembrane-sand lining system, the leakage rates are significantly reduced when compared with just the geomembrane alone (i.e., GM-Only).

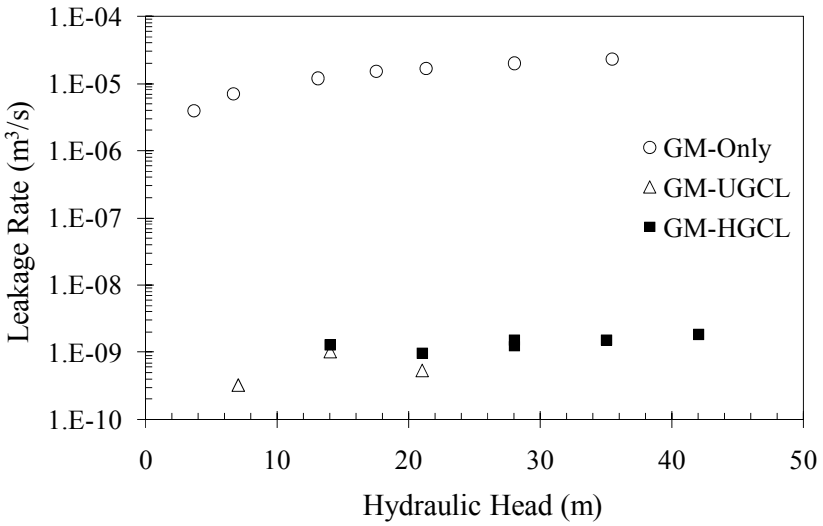

Figure 6.15: Comparing leakage rates from GM-Only, GM-UGCL and GM-HGCL test series

As shown in Figure 6.16, the leakage rates for the GM-CCL, GM-UGCL and GM-HGCL test series are similar over the same range of hydraulic head. The hydraulic conductivity of the RMA Soil Type II is $7x10^{-9}$ m/s. The equivalent hydraulic conductivity of the system with a GCL over a sand layer is $2x10^{-9}$ m/s. However, the geomembrane for the GMC test series was in direct contact with the clay layer whereas, for the tests involving GCLs, a geotextile is between the geomembrane and the bentonite. The combination of the effects system hydraulic conductivity and the interface contact resulted in similar leakage rates for the two systems.

It should be noted that the leakage rates from the GM-CCL test series and from the tests involving GCLs were similar (Figure 6.16) even though the transmissivities are different. However, the hydraulic conductivity of the clay is higher than the equivalent hydraulic conductivity of the GCL-sand system, which could account for the leakage rates from both test series being on the same order of magnitude.

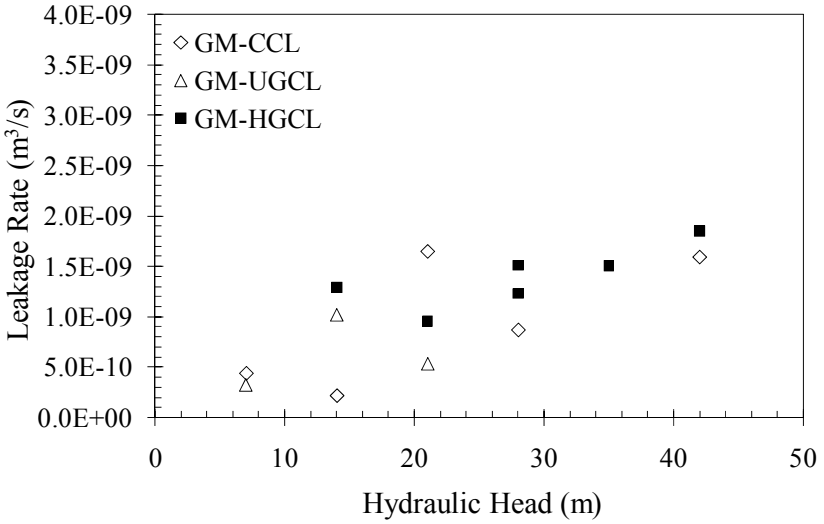

Figure 6.16: Comparing leakage rates from GM-CCL, GM-UGCL and GM-HGCL test series

6.4 SIMPLIFIED EQUATIONS

Several equations are currently available to estimate leakage through defects in a geomembrane liner. As discussed in Section 5.4, Touze-Foltz and Giroud (2003) developed equations for systems with a geomembrane placed over a low-permeability clay layer. Touze-Foltz and Barroso (2006) developed an equation, similar to those developed by Touze-Foltz and Giroud (2003), to estimate flow for systems involving a geomembrane over a GCL. The equation for a geomembrane-GCL contact is discussed in this section.

The existing equation for a geomembrane-GCL composite lining system was not empirical by definition as it was not based on the experimental data. Also, the existing equation was developed for landfills (i.e., low heads). Despite these drawbacks, the methods that were used to develop the existing equation was used in this study as an initial basis for the development of a new simplified equation and new empirical equation, based on the data obtained for high heads in the experimental testing program.

6.4.1 Existing Equations

Equations (2.38) through (2.40) were developed by Touze-Foltz and Giroud (2003) to estimate leakage through a defect in a geomembrane liner that is placed over a low-permeability soil layer. The term "low-permeability" was used to define soil with a hydraulic conductivity between 10^{-10} and 10^{-8} m/s. Since a GCL has a hydraulic conductivity less than $5x10^{-11}$ m/s, Touze-Foltz and Barroso (2006) developed a simplified equation that can be used to estimate leakage through a system with a geomembrane-GCL contact (Equation 2.42). As with the simplified equations developed by Touze-Foltz and Giroud (2003), Equation (2.42) is a simplified version of the analytical equation developed by Touze-Foltz et al. (1999) but for a lower range of hydraulic conductivity. Leakage rates were predicted using Equation (2.42) using the same input parameters (e.g., area of defect, hydraulic conductivity) as were used in the tests for the GM-CCL test series. The hydraulic head used for the calculation of the flow rates ranged from 7 to 42 m.

The flow rates predicted using Equation (2.42) developed by Touze-Foltz and Barroso (2006) are plotted in Figure 6.17 along with the data from permeameter tests involving GCLs. The flow rates predicted using Equation (2.42) are at least one order of magnitude higher than the measured leakage rates for the GM-HGCL and GM-UGCL test series. The difference between the estimated and measured values can be attributed

to the fact that the heads used in the experimental study were outside the range of heads used in the development of Equations (2.42). The equations were developed using hydraulic heads below 3 m, while the hydraulic heads used in the experimental testing program were over 3 m.

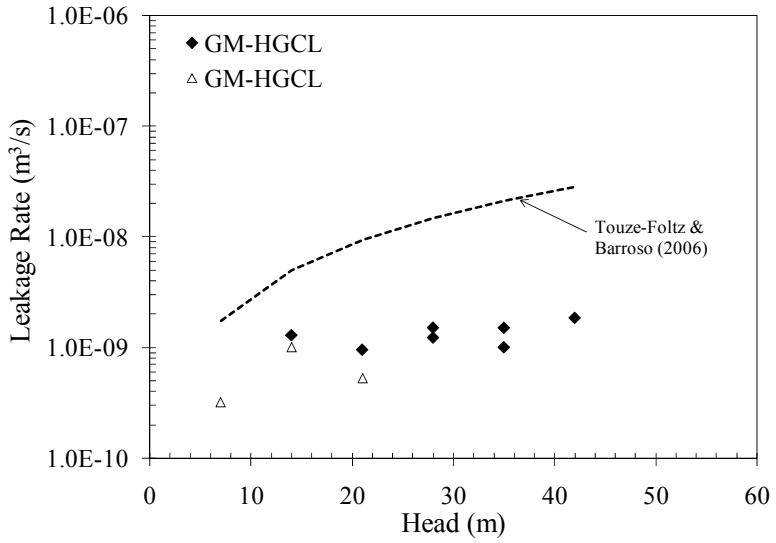

Figure 6.17: Comparison of measured leakage rates and leakage rates predicted using existing simplified equations for GM-GCL data

6.4.2 New Equation for Estimating Leakage for GM-GCL Lining Systems

Since the existing equations were not developed for estimating flow rates under high heads, a new equation was developed to predict flow through a system with a geomembrane overlying a GCL. The new simplified equation was developed using the same methodology as described by Touze-Foltz and Giroud (2003). In order to maintain consistency in the development of new equations, the general form of the equation selected for the GM-GCL lining system was the same as that used for the GM-CCL lining system [Equation (5.10)].

As explained in Section 2.3.5.3, the exponents in Equation (5.10) were obtained using results from a sensitivity analysis for a range of values for each variable in the new equation. The ranges for each of the four parameters that were used to perform the calculations of the analytical model are listed in Table 6.7. One parameter was varied over the range of values listed in Table 6.7 while the rest of the parameters were kept constant to determine the sensitivity of the leakage rate for each variable. For each combination, the flow rates were calculated using the analytical solution presented by Touze-Foltz et al. (1999) [Equation (2.19)]. Linear regression was used to approximate the value of each exponent based on the results of the rigorous calculations using the analytical solution.

A value for the transmissivity of the interface is needed to solve the analytical solution, so the harmonic mean of the back-calculated transmissivity for the GM-GCL test series was utilized (see Section 6.2.4). Like the "empirical" equations developed by Touze-Foltz and Giroud (2003), Equation (5.10) was not developed directly using the experimental data. Instead, the back-calculated transmissivity was based on the experimental results and that transmissivity was used in the development of the new simplified equation.

Table 6.7: Range of values used to develop simplified equation

Variable	**Range (Units)**
Area of Defect, a	0.02 - 1.3 (cm^2)
Hydraulic Head, h_w	7 - 50 (m)
Soil Thickness, H_s	0.3 - 50 (m)
Hydraulic Conductivity, k_s	$3x10^{-10}$ - $2x10^{-7}$ (m/s)

For the experimental testing program, the GCL was placed over a layer of Monterey #30 sand with a hydraulic conductivity of $4x10^{-5}$ m/s. The hydraulic conductivity used in the calculations for the analytical solution [Equation (2.19)] was the harmonic mean of the entire system, taking into account the thickness and hydraulic conductivity of each layer. The system hydraulic conductivity varied due to the weighted average of two components (i.e., GCL and sand layer). The change of soil thickness was actually the sand layer and not the GCL, since the GCL and its hydraulic conductivity are fixed values (Table 6.7). The range of hydraulic conductivity that was used for the analysis is the system hydraulic conductivity (or equivalent hydraulic conductivity) and corresponds to a range in the hydraulic conductivity of the GCL of $1x10^{-11}$ to $5x10^{-11}$ m/s.

The new equation for estimating leakage through defects in geomembrane-GCL composite liners under high heads is:

$$Q = 0.038 H_s^{0.13} h_w^{0.73} a^{0.22} k_s^{0.73} \qquad (6.2)$$

Equation (6.2) must be used with SI units. The leakage rates calculated by Equation (6.2) were compared with the measured leakage rates from the experimental testing program (Figure 6.18). Equation (6.2) provides a better estimate of leakage through a defect in a geomembrane over a GCL under high hydraulic heads than the existing simplified equation developed by Touze-Foltz and Barroso (2006).

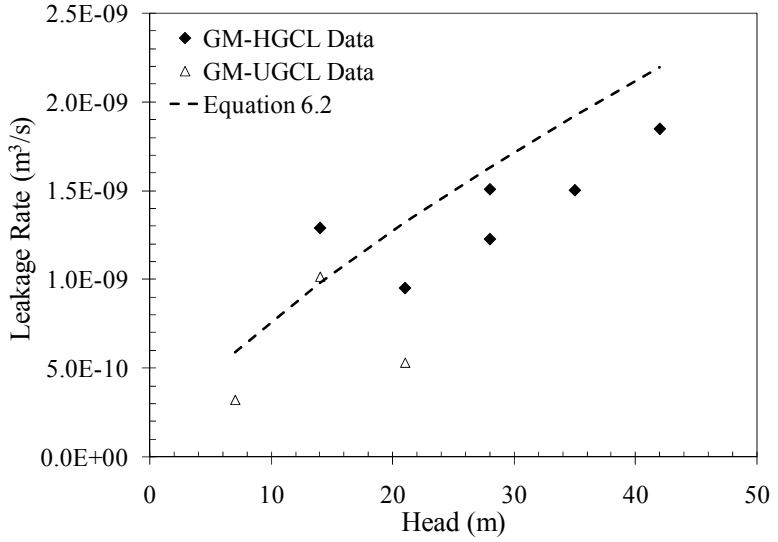

Figure 6.18: Comparison of measured and leakage rates predicted using new simplified equation for tests with GM-GCLs

The simplified equation for the GM-CCL systems [Equation (5.11)] and the new simplified equation for the GM-GCL systems [Equation (6.2)] are compared in Figure 6.19. As discussed in 6.3, the leakage data are similar for the GM-CCL and GM-GCL test series. The new simplified equations for the respective test series are also similar. However, since the range of hydraulic conductivities is slightly different for the GM-GCL equation, the use of only one of these equations for all liner combinations (e.g., geomembrane-clay, geomembrane-GCL) may not be appropriate.

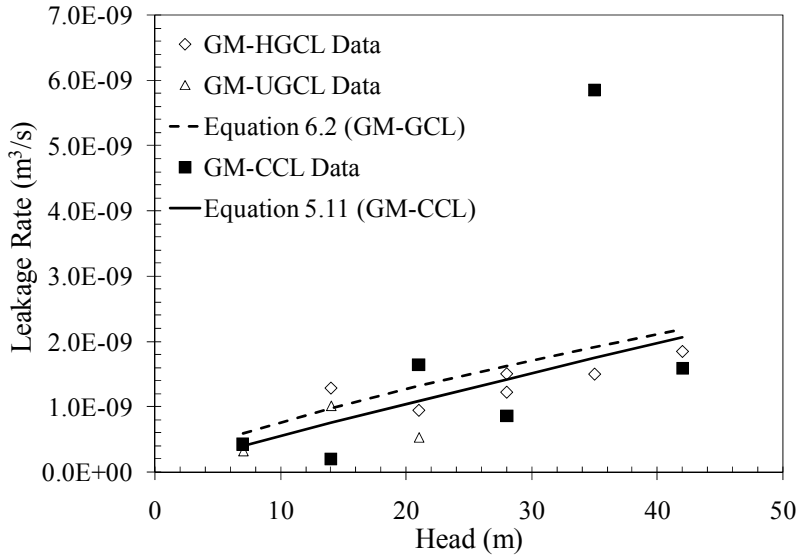

Figure 6.19: Comparison of the experimental results and the new simplified equations for GM-CCL and GM-GCL test series

It should be noted that the analytical model developed by Touze-Foltz et al. (1999) for field conditions can be solved using a spreadsheet that incorporates the use of modified Bessel functions. An example of this spreadsheet is shown in Appendix C. Equation (6.2) was developed in order to assist engineers in design by providing a quick and simple way to estimate the leakage rate through defects in composite liners that include GCLs. However, the analytical model provides a more rigorous method to determine leakage rates.

Chapter 7: Numerical Simulation of Leakage through Defects in Geomembrane Lining Systems

7.1 INTRODUCTION

The numerical modeling component of this study was conducted to provide additional insight into the flow through geomembrane defects under high hydraulic heads. Specifically, numerical analyses were performed to: i) validate and further understand the results obtained in the experimental component, ii) evaluate an analytical model and its assumptions (i.e., one-dimensional flow within soil layer) to determine the effect on the leakage rate through a lining system, iii) incorporate the relationship for predicting leakage (i.e., equations presented in Section 5.5.1) as flux boundary conditions in actual design, and iv) evaluate the effect of leakage through defects on the design of actual dam configurations (e.g., stability, presence of blanket drains).

The finite element method was used to approximate the solution for a boundary-value problem by dividing the domain of the problem in a finite number of subdomains, or elements (Becker et al. 1981). Axisymmetric, two-dimensional and three-dimensional finite element analyses were performed as part of this study. Limit-equilibrium analyses were also conducted as part of this study to determine the impact of leakage on the stability of the downstream face of earth dams.

SoilVision's SVFlux (Thode and Stianson 2006) was used in this study to simulate the tests conducted as part of the experimental component of this study (i.e., GM-Only, GM-CCL, and GM-GCL tests series). SVFlux was also used to simulate the conditions in a dam with a geomembrane lining system located on its upstream face. SVFlux is capable to simulating the pore water pressure distribution in unsaturated and saturated soils due to groundwater movement (Thode and Stianson 2006). The finite-

element calculations are performed using FlexPDE, an equation solver capable of solving one-, two- and three-dimensional problems, as well as axisymmetric problems. For each problem, the mesh is automatically generated and, if necessary, adaptive mesh refinement is automatically performed. FlexPDE performs calculations for both steady-state and transient problems. In particular, the ability of the program to automatically refine the mesh was found to be useful for problems involving flux through defects in a geomembrane liner. The mesh spacing was automatically decreased in the vicinity of the defect. The axisymmetric capabilities of SVFlux were useful in simulating the tests conducted in the permeameter cells and the 3D capabilities were useful in simulating a dam with a geomembrane lining system on the upstream face.

7.2 SIMULATION OF LABORATORY TESTS

As discussed in Chapters 4 through 6, laboratory tests were conducted using permeameter cells with diameters of 6 inches and 13 inches. These tests were performed to determine the leakage rates through a defect in a geomembrane liner when placed over a soil layer. Soils used in the experimental component of this study included a silty clay (RMA Soil Type II) and a uniform medium-fine sand (Monterey #30). The flow rates obtained during the laboratory tests were assumed to be the steady-state leakage rates.

Finite element simulations of the laboratory tests were performed in order to gain additional insight into the results of the experimental component of this study and to extrapolate the findings to a range of parameters beyond those used in the experimental program. Three scenarios were investigated for each test series: a) no geomembrane (soil only), b) geomembrane in perfect contact with the underlying soil layer, and c) geomembrane with an interface gap between the liner and the soil layer. Examples of the FlexPDE code for the simulations of the permeameter tests are included in Appendix B.

7.2.1 Problem Setup

The finite element analysis of the permeameter tests was performed using an axisymmetrical coordinate system. The center of the geomembrane defect was the axis of symmetry. The dimensions of the problem geometry (i.e., dimensions of the small permeameter cell) used in the simulations are shown in Figure 7.1. The width of the regions of soil shown in Figure 7.1a and 7.1b corresponds to the radius of the permeameter cell used in the experimental component of this study. The length of the soil layer also corresponds to that of the permeameter cell used in the laboratory tests. The defect was modeled as a circular defect with a radius of 1 mm, which is only slightly larger than the radius of 0.8 mm used in the permeameter tests. A defect with a radius of 1 mm was used instead of 0.8 mm because 0.001 m (1 mm) is the smallest increment for length allowed in the SVFlux CAD program. The thickness of the GCL is 0.008 m (see Figure 7.1b), which corresponds to the average thickness of the GCLs measured as part of the experimental component of this study.

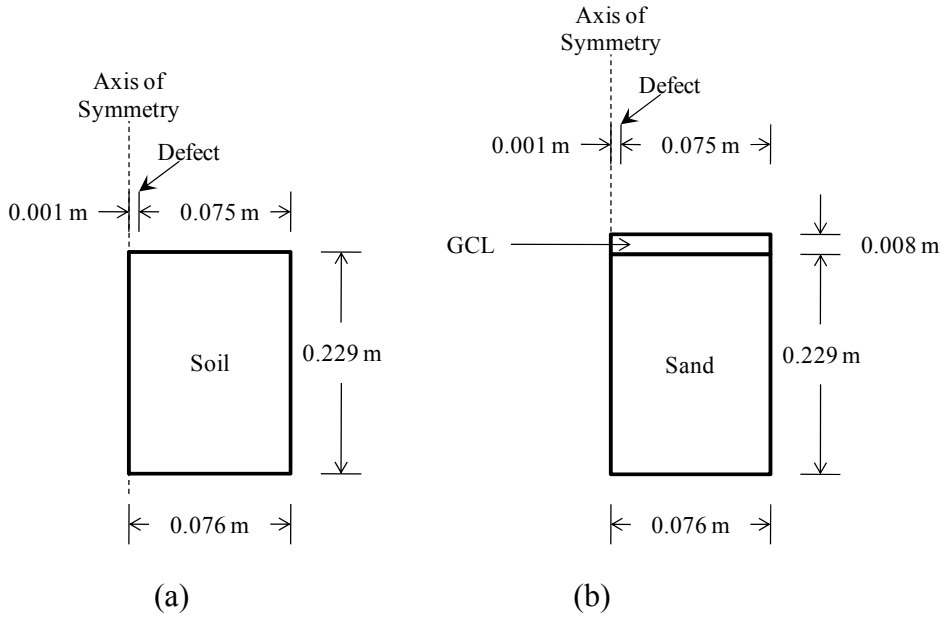

Figure 7.1: Geometry for finite element model: a) geomembrane on soil and b) geomembrane/GCL on soil

7.2.1.1 Material Properties

For transient flow problems, the water retention curve (WRC) for each soil is required in order to solve Richards' equation for unsaturated flow. In SVFlux, the WRC may be characterized using either laboratory data or the available models, such as Brooks and Corey (1964) and van Genuchten (1980). The van Genuchten (1980) model was selected to approximate the WRC for the two soils (RMA Soil Type II silty clay and Monterey #30 sand) and for the GCL used for the finite element analysis. The van Genuchten parameters and the saturated hydraulic conductivity used in the simulations for the soils and the GCL are listed in Table 3.1.

7.2.1.2 Boundary Conditions

The boundary conditions specified for the simulation are shown in Figure 7.2. For systems without a geomembrane shown in Figure 7.2a, the hydraulic head was

specified for the entire top boundary. However, when modeling a system in which a geomembrane is present (Figure 7.2b), the hydraulic head is only imposed within the area of the defect (the center of the defect is the axis of symmetry). The remainder of the top boundary is assigned a no-flow boundary, which simulates the presence of the geomembrane (Figure 7.2b). The lower boundary was designated as a seepage face boundary, which acts as a no-flow boundary until it becomes saturated, at which point flow is allowed to occur across the boundary.

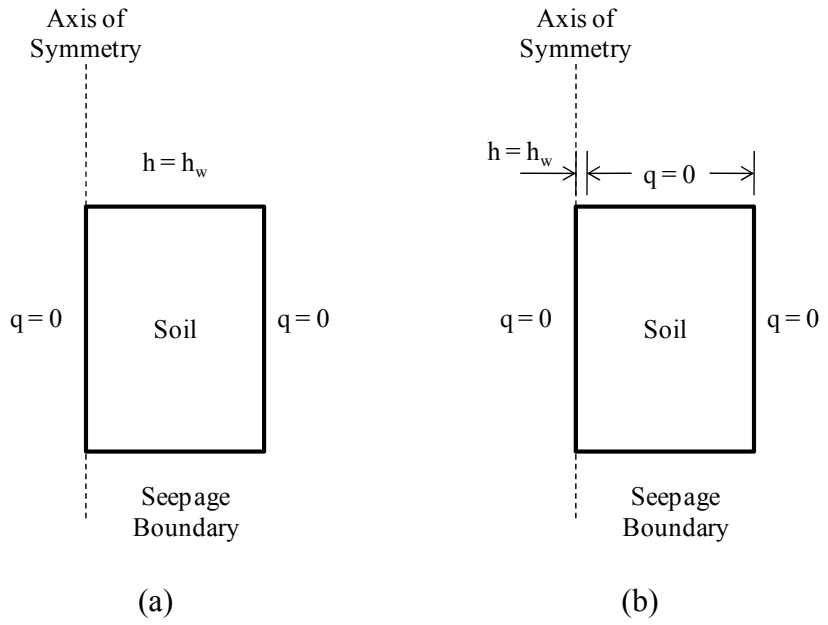

Figure 7.2: Boundary conditions for finite element model for: a) no geomembrane and b) geomembrane with a defect

7.2.1.3 Interface Gap

The interface gap between the geomembrane and the underlying soil layer can be characterized by its transmissivity, which is the product of the thickness of the gap and the hydraulic conductivity of the gap. However, in the finite element model, the transmissivity cannot be directly assigned to the interface. Instead, the gap thickness was

specified in the geometry and hydraulic conductivity of the gap was defined as a material property. It was assumed that the interface gap can be represented by assigning the correct transmissivity, even if the actual thickness and hydraulic conductivity values are different than those used in the simulation.

Appropriate values for the gap thickness and the interface transmissivity are needed to define the hydraulic conductivity of the interface. However, there is limited information available with regards to gap size and/or interface transmissivity. Brown et al. (1987) used an analytical model to back-calculate gap thickness values from their experimental tests for a range of hydraulic conductivity, as was listed in Table 2.3. These values are not direct measurements, so they depend on the accuracy of the correlations developed by Touze-Foltz et al. (1999). However, the values for gap thickness listed in Table 2.3 provide an initial basis for the thickness of the interface gap. Also, the transmissivity is needed in order to characterize the interface between the geomembrane and the soil layer. Values for the interface transmissivity were obtained using Equation (2.25) developed by Touze-Foltz et al. (1999). The average transmissivities for the laboratory tests that were estimated using Equation (2.25) are listed in Table 5.2.

The transmissivity values from Table 5.2 and the thicknesses for the interface gap from Table 2.3 define the actual hydraulic conductivity of the interface for each test series. However, modeling of the interface gap proved to be difficult because the estimated thickness was smaller than the minimum size that could be used in SVFlux. Specifically, the problem geometry in SVFlux is limited to increments of 0.001 m. Brown et al. (1987) estimated that the gap thickness for a soil with a hydraulic conductivity on the order of 10^{-9} m/s would be on the order of 10^{-5} m (see Table 2.3). Consequently, simulations were performed using an exaggerated gap thickness of 0.001 m, which is the minimum value that can be specified in SVFlux. A lower hydraulic

conductivity for the interface "medium" was adopted and thus maintaining a consistent interface transmissivity. The geometry for the finite element model that includes the "exaggerated" interface gap is shown in Figure 7.3.

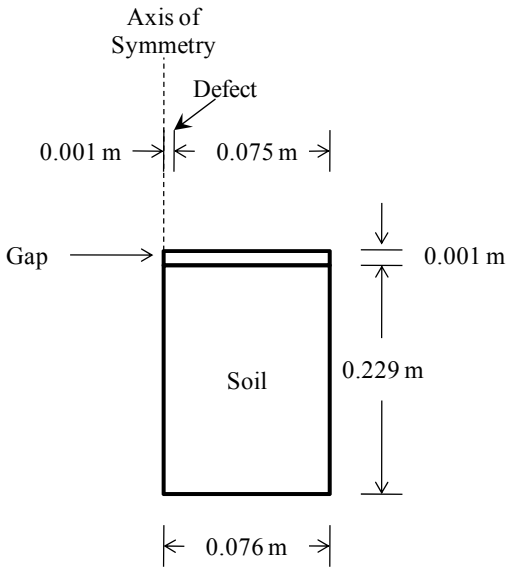

Figure 7.3: Dimensions for permeameter cell simulations involving an interface gap

7.2.2 Results of Finite Element Simulations of Laboratory Tests

In SVFlux, "flux sections" are used to monitor flow into and/or out of a region. Flux sections are used to report the flow rate across a boundary or within a portion of the problem (SoilVision 2006). Using these flux sections, the flow rates were recorded for each system analyzed using finite elements. Also, the head and pore pressures within the soil layer were reported for the simulations.

7.2.2.1 Geomembrane-CCL Tests

Simulations were performed to evaluate the GM-CCL tests, where the geomembrane was placed over a soil layer of RMA Soil Type II. Three scenarios were investigated, each with hydraulic heads ranging from 7 m to 42 m: a) no geomembrane

(soil only), b) geomembrane in perfect contact with an underlying soil layer, and c) geomembrane with an interface gap. The first two scenarios provide the upper and lower bounds, respectively, for the problem. Since the geomembrane is not expected to be in perfect contact with the soil layer, the third scenario accounts for flow across the interface between the geomembrane and the soil layer. The interface was characterized by a hydraulic conductivity obtained considering a gap thickness of 0.001 m and an interface transmissivity of 3.0×10^{-11} m^2/s (average back-calculated transmissivity of GM-CCL test series).

The steady-state leakage rates are shown in Figure 7.4 as a function of the imposed hydraulic head for the numerical simulations, along with the data from the GM-CCL test series. The results from the numerical simulation for the case without a geomembrane (upper bound) are included in Figure 7.4a but are not shown in Figure 7.4b in order to provide more detailed comparison between experimental and numerical results.

The numerical results for leakage rates where the geomembrane is in perfect contact with the underlying soil layer (no interface gap) provide a lower bound for the flow rate. The numerical results obtained for the perfect contact case was not the same as the lower bound results determined using Darcy's Law in Section 5.2.1.3. This is because flow rates calculated in Section 5.2.1.3 using Darcy's Law for only the area of the defect considers one-dimensional flow. On the other hand, axisymmetric flow was allowed in the finite element analysis. The flow rates for the system with perfect contact (e.g., 1.2×10^{-9} m^3/s for a head of 42 m) are significantly higher than those calculated using 1-D Darcy's Law (e.g., 1×10^{-12} m^3/s for a head of 42 m).

The flow rates for the system without a geomembrane, shown in Figure 7.4a, provide an upper bound for the data from the experimental component of this study. The

leakage rates measured in the GM-CCL test series are smaller than the numerically-calculated upper boundary. The results of the simulations involving an interface gap match more closely the experimental results. The transmissivity of the interface was simulated using the average back-calculated transmissivity estimated from the laboratory data using Equation (2.24) developed by Touze-Foltz et al. (1999). The scatter in the predicted transmissivity for the GM-CCL tests, shown in Figure 5.2, could explain the difference between the simulated flow rates for a system with an interface gap and the laboratory tests.

As shown in Figure 7.4b, the lower bound line for simulations with a geomembrane in perfect contact with the soil layer is close to the leakage rates obtained in the laboratory tests. A possible explanation for the proximity of the lower bound line with respect to the experimental data is the fact that there was scatter in the leakage data from the GM-CCL test series. Also, the contact between the geomembrane and soil in the testing program could not be precisely duplicated every time a soil layer was molded and trimmed.

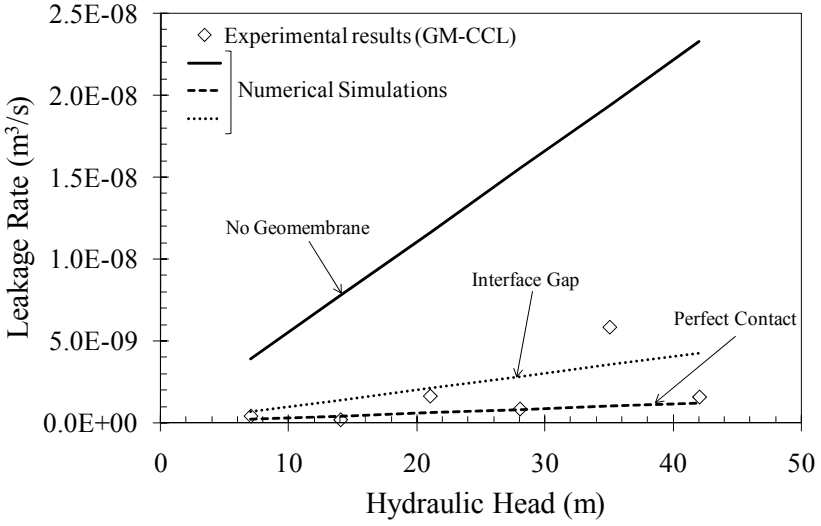

(a)

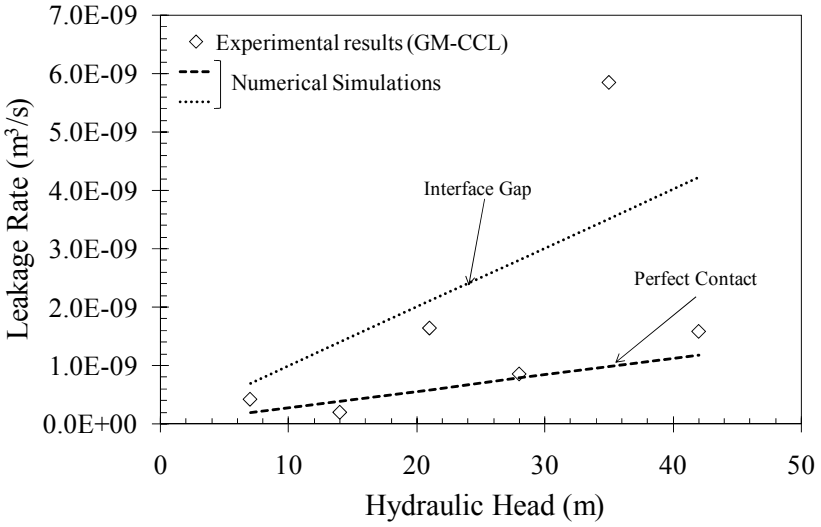

(b)

Figure 7.4: Comparison of the leakage rates from the finite element simulations with GM-CCL test results for: a) no geomembrane, perfect and imperfect interface contact and b) perfect and imperfect interface contact

The simulated flow rates for the soil layer without a geomembrane were compared with the flow rates calculated using Darcy's Law (upper bound from Section 5.2.1). As shown in Figure 7.5, the two sets of calculated flow rates are identical. The flow measured in the permeameter cell tests without a geomembrane is assumed to be 1-D flow through a column of soil. The agreement between the two sets of calculated flow rates verifies this assumption.

As discussed in Section 3.2.2.1, several tests were conducted using only RMA Soil Type II in the small permeameter (i.e., without a geomembrane). The results from these tests were also included in Figure 7.5. As shown in the Figure, the measured leakage rates are virtually identical to the calculated leakage rates.

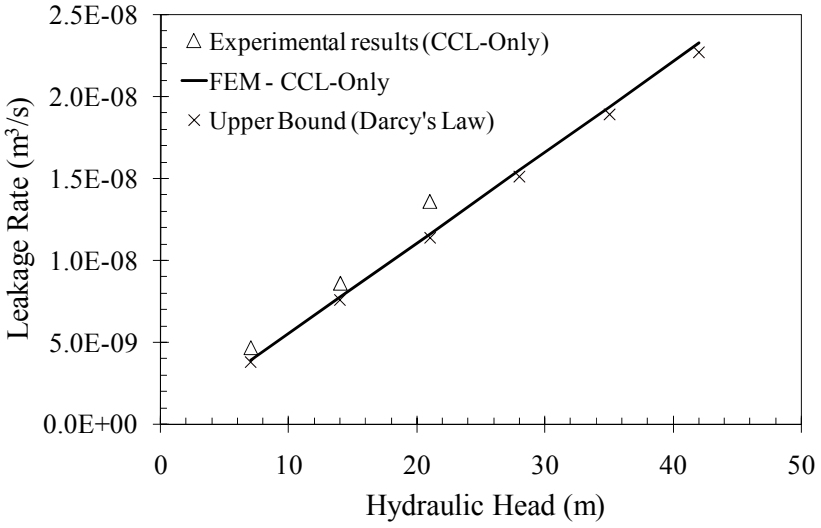

Figure 7.5: Comparison of calculated and measured leakage rates for RMA Soil Type II

7.2.2.2 Geomembrane-GCL Tests

Simulations were performed of the two test series involving GCLs (GM-HGCL and GM-UGCL test series), where the geomembrane was placed over a GCL. The GCL is underlain by a layer of Monterey #30 sand. Three scenarios were investigated, each

for hydraulic heads ranging from 7 m to 42 m: a) no geomembrane (GCL only), b) geomembrane in perfect contact with the GCL, and c) an interface gap between the geomembrane and the GCL. The first two scenarios provide an upper and lower bound, respectively, for the system being simulated involving GCLs.

Harpur et al. (1993) suggested that the transmissivity of the interface between a geomembrane and a GCL consists of flow across the interface between the geomembrane and the upper geotextile of the GCL, flow through the upper geotextile itself, and flow across the interface of the upper geotextile and the bentonite inside the GCL. Even if the geomembrane is in perfect contact with the GCL (i.e., there is no gap, and thus no flow, at the interface of the geomembrane and the upper geotextile), there are still two additional mechanisms that contribute to the transmissivity of the geomembrane-GCL interface. The interface was characterized by a hydraulic conductivity defined using a gap thickness of 0.001 m and an interface transmissivity of 6.4×10^{-11} m^2/s.

The steady-state leakage rates are shown in Figure 7.6 as a function of the imposed hydraulic head for the numerical simulations, along with the data from the GM-UGCL and GM-HGCL test series. The results from simulations of a system with a perfect contact between the geomembrane and the soil layer (lower bound) are included in Figure 7.6a but are not shown in Figure 7.6b in order to provide more detailed comparison between experimental and numerical results. Note that the y-axis in Figure 7.6a is on a logarithmic scale while the y-axis in Figure 7.6b is on a natural scale.

The lower bound leakage rates are approximately two orders of magnitude lower than the experimental data. The lining system simulated with a perfect contact between the GCL and the geomembrane is not an accurate representation of the GM-GCL permeameter tests because the geotextile between the geomembrane and the bentonite in the GCL used in the laboratory tests was not included in the simulation. The geotextile

was accounted for in the simulations that included an interface gap between the geomembrane and the GCL. The simulated flow rates for the lining system that included an interface gap is shown in Figure 7.6b, along with the flow rates for the upper bound case (no geomembrane). The simulated flow rates for an imperfect contact (i.e., an interface gap) provided a close match to the leakage rates measured in the laboratory tests. However, the match between the simulated and measured leakage rates could be improved if the transmissivity of the interface was changed.

The simulated leakage rates for the GCL-only system and the GM-GCL system with an imperfect contact were more similar than the corresponding simulations of the GM-CCL systems (Figure 7.4a) because the presence of the geotextile at the interface allowed more interface flow to occur in systems involving GCLs. The average back-calculated transmissivity for the GM-GCL tests included the effects of in-plane flow within the geotextile at the interface and for the low hydraulic conductivity of the GCL.

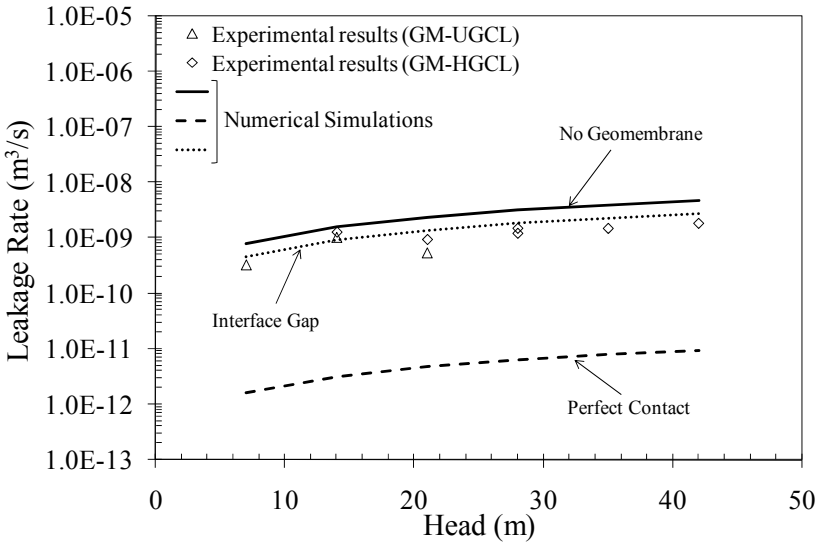

(a)

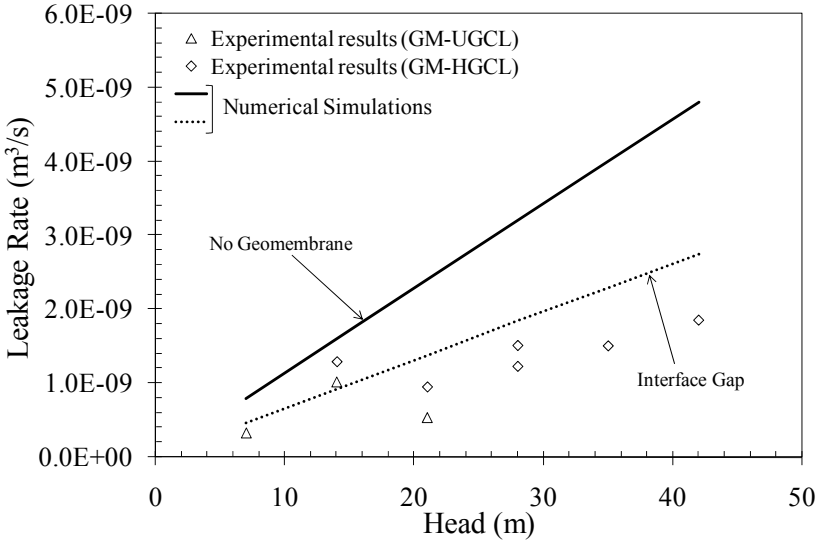

(b)

Figure 7.6: Comparison of the leakage rates from the finite element simulations with GM-GCL test results for: a) no geomembrane, perfect and imperfect interface contact and b) perfect and imperfect interface contact

7.2.3 Discussion of Simulations of the Permeameter Tests

The transmissivity used for the simulations discussed in Section 7.2.2 was the average value estimated using Equation (2.24) developed by Touze-Foltz et al. (1999). The discrepancies between the experimental data and numerical results could be attributed to the method used to estimate the interface gap. The gap thickness used in the finite element analyses was 0.001 mm, which is about two orders of magnitude larger than the gap thickness estimated by Brown et al. (1987). To compensate for the larger gap thickness, the hydraulic conductivity of the interface gap was changed in order to obtain the desired (or selected) value for the transmissivity. Simulations were conducted to evaluate the effect of changing the gap thickness on the leakage rates; the results of these simulations for gap thicknesses of 1, 2 and 5 mm are shown in Figure 7.7. Increasing thickness of the gap, along with the corresponding decrease in hydraulic conductivity to maintain the same transmissivity, results in a decrease in the leakage rates. Regardless, the finite element simulations provide a good estimation of the leakage rates that were measured in the laboratory.

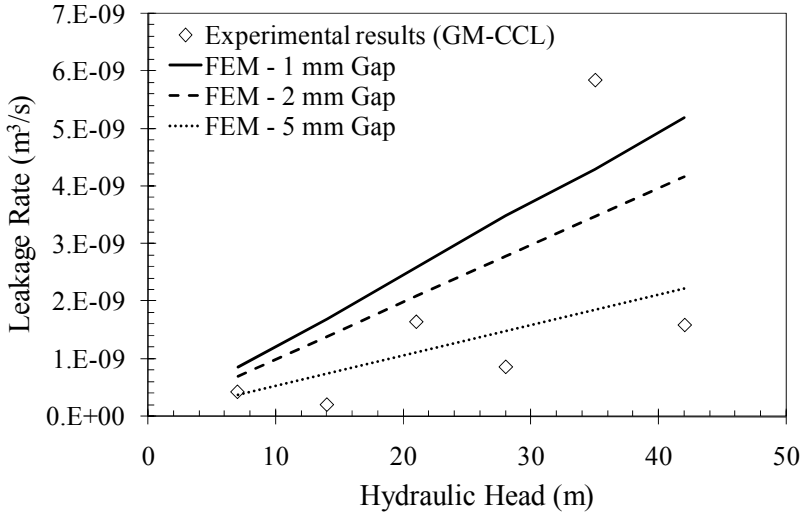

Figure 7.7: Effect of specified gap thicknesses on simulated leakage rates

The leakage rates were calculated for the small permeameter cell with a 2 mm defect in the geomembrane, a 0.23 m thick underlying soil layer with a hydraulic conductivity of 7×10^{-9} m/s, and an excellent contact ($\theta = 3.0 \times 10^{-11}$ m^2/s). However, the hydraulic heads used for the numerical simulations were 50, 75 and 100 m. The results of the simulations were compared with the experimental data. As shown in Figure 7.8, the results of the numerical extrapolation appear to follow the same trend as the experimental data. Also, the numerical results were compared with leakage rates predicted using the new simplified equation [Equation (5.13)] for excellent contact conditions and a small permeameter (C_q = 1, C_{lf} =1). The leakage rates predicted using the simplified equation agreed well with the extrapolated results as well as the experimental data.

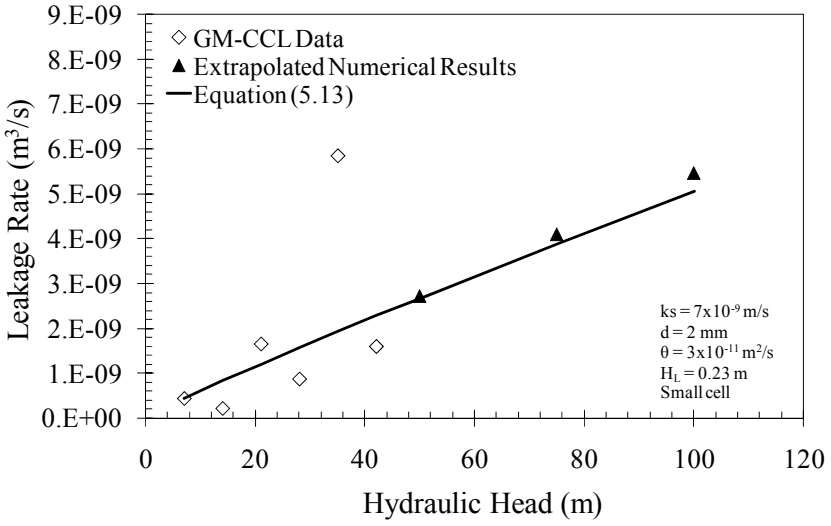

Figure 7.8: Comparison of experimental results with numerically extrapolated and new simplified equation leakage rates for defect size of 2 mm

The leakage rates were calculated for a 0.23 m thick underlying soil layer with a hydraulic conductivity of $7x10^{-9}$ m/s, and an excellent contact ($\theta = 3.0x10^{-11}$ m^2/s). However, the hydraulic heads used for the numerical simulations were 7, 50, 75 and 100 m and a defect diameter of 40 mm. Since the defect was larger, the diameter of the profile was also increased as well. As shown in Figure 7.9, the numerical results were compared with leakage rates predicted using the new simplified equation [Equation (5.13)] for excellent contact conditions and a larger extent in the radial direction (C_q = 1, C_{lf} = 3). The leakage rates calculated using the simplified equation agreed well with the extrapolated results.

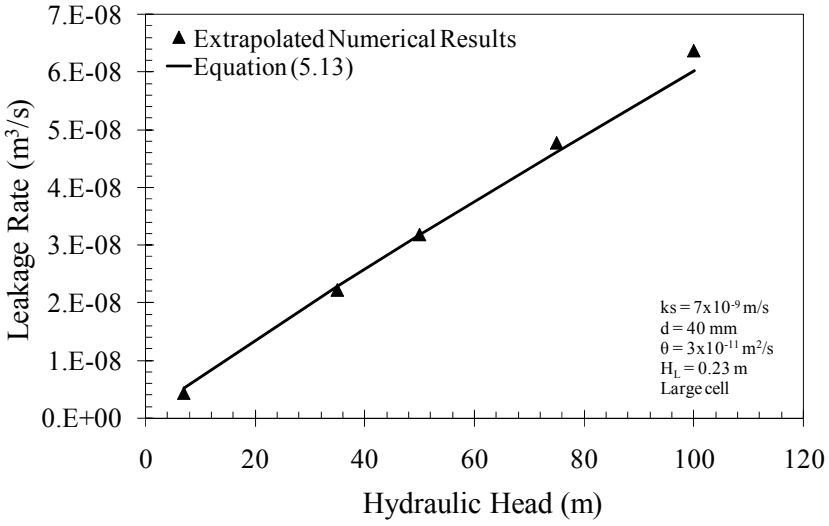

Figure 7.9: Comparison of numerically extrapolated results with the new simplified equation for a larger diameter cell

7.3 UNDERSTANDING MECHANISMS OF FLOW IN THE UNDERLYING SOIL LAYER

The permeameter tests were relatively small, especially when compared to field conditions. The walls of the cells restricted lateral flow and likely altered the leakage rate. The analytical models developed by Touze-Foltz et al. (1999) for laboratory and field conditions were used to analyze the experimental results through the back-calculation of the transmissivity and prediction of the radius of interface flow, respectively. The analytical models were developed under the assumptions that flow is restricted to the "radius of wetted area" and that flow into the soil layer is one-dimensional. In this section, the "radius of interface flow" will be referred to as the "radius of wetted area," since the analytical model is the main focus of the discussion. The new simplified equation for the GM-CCL system [Equation (5.13)] was developed using the average back-calculated transmissivity. As such, the simplified equation in its original form [Equation (5.11)] could only be used to estimate flow in confined systems

and could not account for lateral flow. However, a coefficient was added to the equation to account for lateral flow in the field. The question is: How different is the leakage rate determined using Touze-Foltz et al. (1999) and the leakage rate for 3D (or in this case, axisymmetric) systems that include lateral flow outside the radius of wetted area?

The analytical model developed by Touze-Foltz et al. (1999) for field conditions [Equation (2.19)] was derived using the assumption that flow into the soil underlying a geomembrane liner is one-dimensional (in the vertical direction). Another assumption used to develop the model by Touze-Foltz et al. (1999) was that the flow into the underlying soil layer is confined to the radius of wetted area. Lateral flow, or radial flow in an axisymmetric system, was not taken into consideration and flow outside the radius of wetted area was neglected. An analysis using axisymmetric finite element simulations was conducted to determine the overall effect that the assumptions of the analytical model have on flow through a defect in a geomembrane lining system.

7.3.1 Geometry and Properties of Finite Element Simulations of Analytical Model

Two soil profiles were analyzed using axisymmetry to investigate the effects of the area of flow on the leakage rate through a defect. The first profile (Case I) was used to simulate flow through a defect in a geomembrane liner for a large area of flow (relative to the diameter of the defect), which allowed lateral flow to be evaluated. The second profile (Case II) was used to simulate flow through a defect in a lining system in which the radius of the axisymmetric profile was defined as the radius of wetted area as defined by the model developed by Touze-Foltz et al. (1999) [Equation (2.19)]. Lateral flow outside of the radius of wetted area was not accounted for in Case II.

The soil profile for Case I is shown in Figure 7.1a with the axisymmetric dimensions of the soil layer and the defect. The axis of symmetry is the center of the 2 cm diameter defect. The area being simulated in Case I has diameter of 4 m (radius of 2

m, as shown in Figure 7.10a) and a depth of 1 m. The depth of the soil layer and hydraulic head (a head of 3 m was used in the simulation) selected for the evaluation of the analytical model were consistent with landfill conditions, since Touze-Foltz et al. (1999) developed the model for predicting leakage through landfill liners.

The soil profile for Case II is shown in Figure 7.10b, with the axis of symmetry at the center of the 2 cm diameter defect and a depth of 1 m. Case II was used to simulate the conditions of flow that occur under the assumptions made by Touze-Foltz et al. (1999) for the analytical model. For Case II, the leakage rate and radius of wetted area were determined for the geomembrane lining system using the model developed by Touze-Foltz et al. (1999). A CL soil with a hydraulic conductivity of $8x10^{-9}$ m/s was selected for the analysis. The diameter of the defect defined for the lining system was 2 cm. The soil profile had a thickness of 1 m and the height of water above the geomembrane liner was 3 m. The average back-calculated transmissivity of $3.0x10^{-11}$ m^2/s obtained in the experimental component for RMA Soil Type II and excellent contact (see Section 5.2.4) was used to calculate the flow rate and wetted radius. The predicted flow rate obtained using the analytical model was $3.4x10^{-10}$ m^3/s and the predicted radius of wetted area was 0.106 m. Therefore, the radius of the axisymmetric profile used in Case II was 0.106 m.

The boundary conditions for Case I (i.e., simulation considering a large area of flow and accounting for lateral flow) are also shown in Figure 7.10a. The radius of wetted area as estimated by the analytical model for the defined variables was also used in Case I as part of the upper boundary condition. The upper boundary outside the radius of wetted area was assigned a no-flow boundary condition, which simulated the presence of the geomembrane liner and that the hydraulic head beyond the radius of wetted is zero. Within the radius of wetted area, the upper boundary was assigned a head boundary

condition based on Equation (2.12) developed by Touze-Foltz et al. (1999). Equation (2.12) was used to define the hydraulic head distribution with respect to radius [h(r)] for the upper boundary from the axis of symmetry to the radius of wetted area, which simulated the head distribution at the interface between the geomembrane and the soil layer. A representation of the head distribution used in the simulations for Cases I and II is shown in Figure 7.10. The right boundary and the left boundary (i.e., the axis of symmetry) were both assigned a no-flow boundary condition. The lower boundary was designated as a zero head boundary, which is consistent with a landfill lining system underlain by a drainage layer or leak detection layer. As shown in Figure 7.10b, the boundary conditions for Case II are the same as for Case I but Case II does not have an upper boundary outside of the wetted radius.

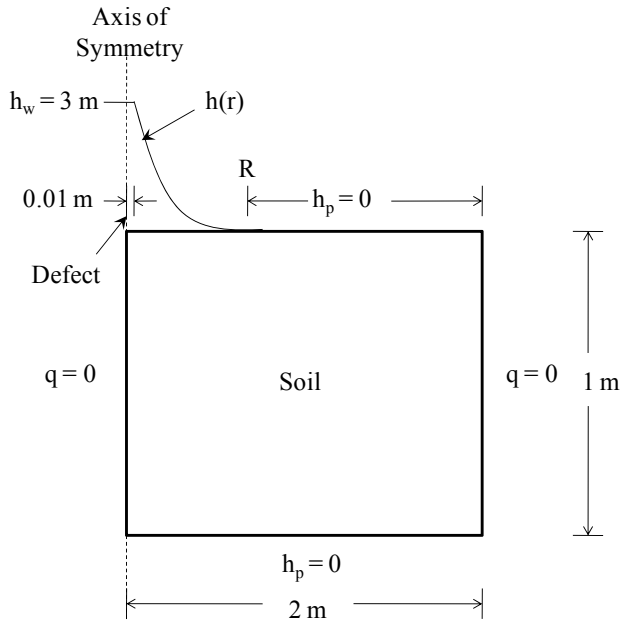

(a)

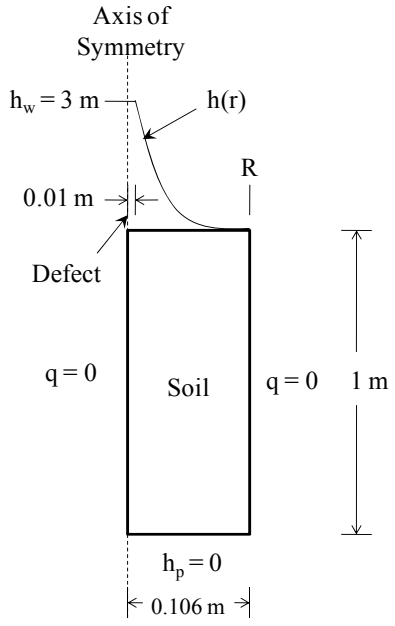

(b)

Figure 7.10: Geometry and boundary conditions for: a) Case I and b) Case II

The pressure head outside the radius of wetted area and the pressure head at the base of the lining system are both assumed to be zero for a geomembrane lining system in a landfill. Based on these, flow is still occurring within the soil layer outside the wetted radius. Although the pressure head outside the radius of wetted area is zero (a boundary condition of the analytical model), the total head at the surface of the soil layer is not equal to zero due to the elevation head. If the datum (z = 0) is defined at the base of the liner system (i.e., 1 m below the surface of the soil layer and geomembrane), the bottom boundary has a total head of zero but the upper boundary would have a total head of 1 m outside the radius of wetted area. The change in total head indicates that flow is occurring through the soil layer even though it is outside the radius of wetted area. This flow is not accounted for by the analytical model for field conditions [Equation (2.19)]. However, the simulations conducted for Cases I and II are expected to provide insight into the effect of including the lateral flow outside the radius of wetted area in the calculation of the leakage rate through a geomembrane defect.

7.3.2 Results of Finite Element Simulations for Analytical Model

The steady-state flow rate and pressure head distribution from the finite element simulations were obtained for each soil profile. For Case I (i.e., profile with a radius of 2 m), the leakage rate through the defect calculated by finite elements was 3.6×10^{-9} m^3/s. The pressure head distribution for the large soil profile that accounts for lateral flow is shown in Figure 7.11. The radius of wetted area predicted by the analytical model developed by Touze-Foltz et al. (1999) was 0.106 m and is indicated by the $h_p = 0$ (contour 'c') in Figure 7.11. The numerically-calculated pressure head at the interface between the geomembrane and the soil layer was consistent with the imposed pressure head boundary condition, as shown in Figure 7.12.

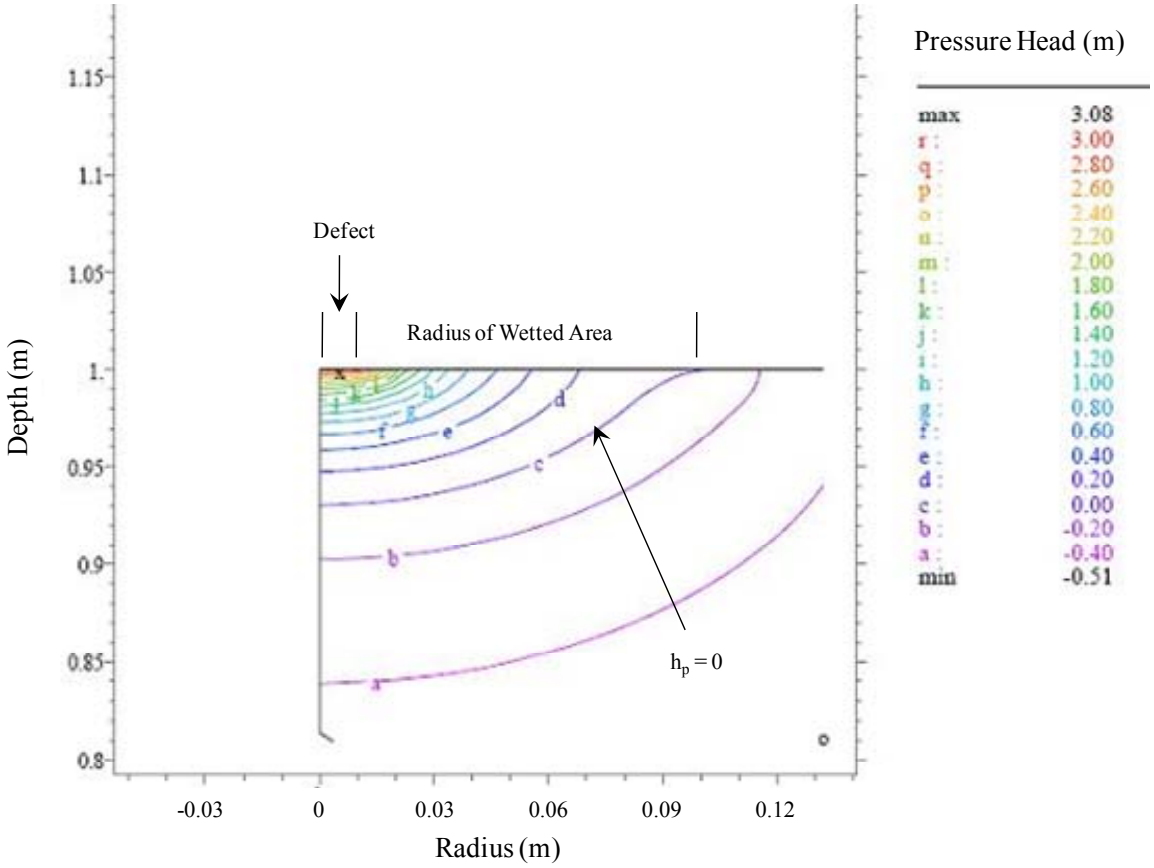

Figure 7.11: Pressure head distribution within the underlying soil layer for Case I (head at interface is defined by the analytical model)

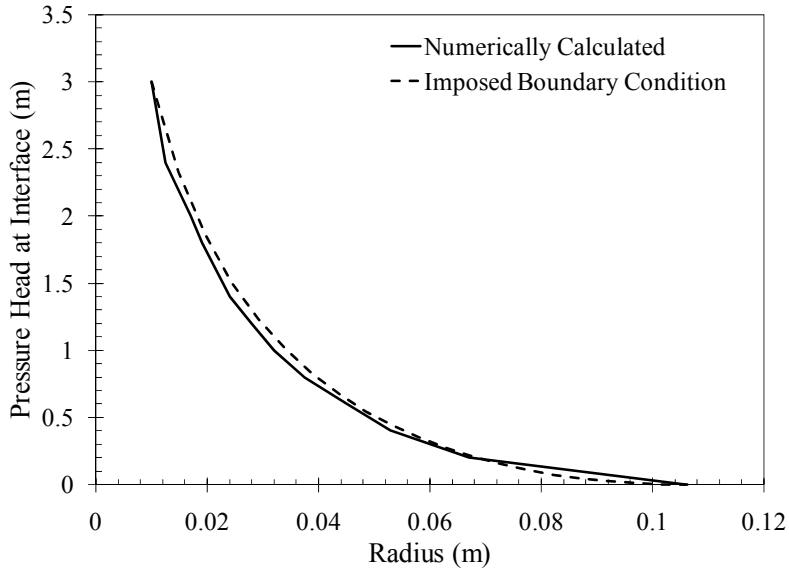

Figure 7.12: Comparison of numerically calculated and the imposed boundary pressure head along the interface gap between the geomembrane and the soil layer

For the soil profile for Case II [i.e., radius of 0.106 m, the radius of wetted area as predicted using the analytical model], the leakage rate through the defect calculated by finite elements was 2.2×10^{-10} m^3/s, which is slightly lower than that predicted by Touze-Foltz et al. (1999) for field conditions (3.4×10^{-10} m^3/s). The pressure head distribution for Case II, which neglects lateral flow, is shown in Figure 7.13. As shown in this figure, a line of zero pressure head is located at the upper right edge of the soil layer, which is the radius of wetted area as defined for by the boundary condition at the interface of the geomembrane and the soil layer. The numerically calculated flow rate for Case II is one order of magnitude lower than for Case I. In Figure 7.13, the area of flow for Case II is restricted by the no-flow boundary at R = 0.106 m whereas the flow for Case I shown in Figure 7.11 is not restricted by a no-flow boundary on the right side, or at least the effect of the no-flow boundary at a radius of 2 m is negligible.

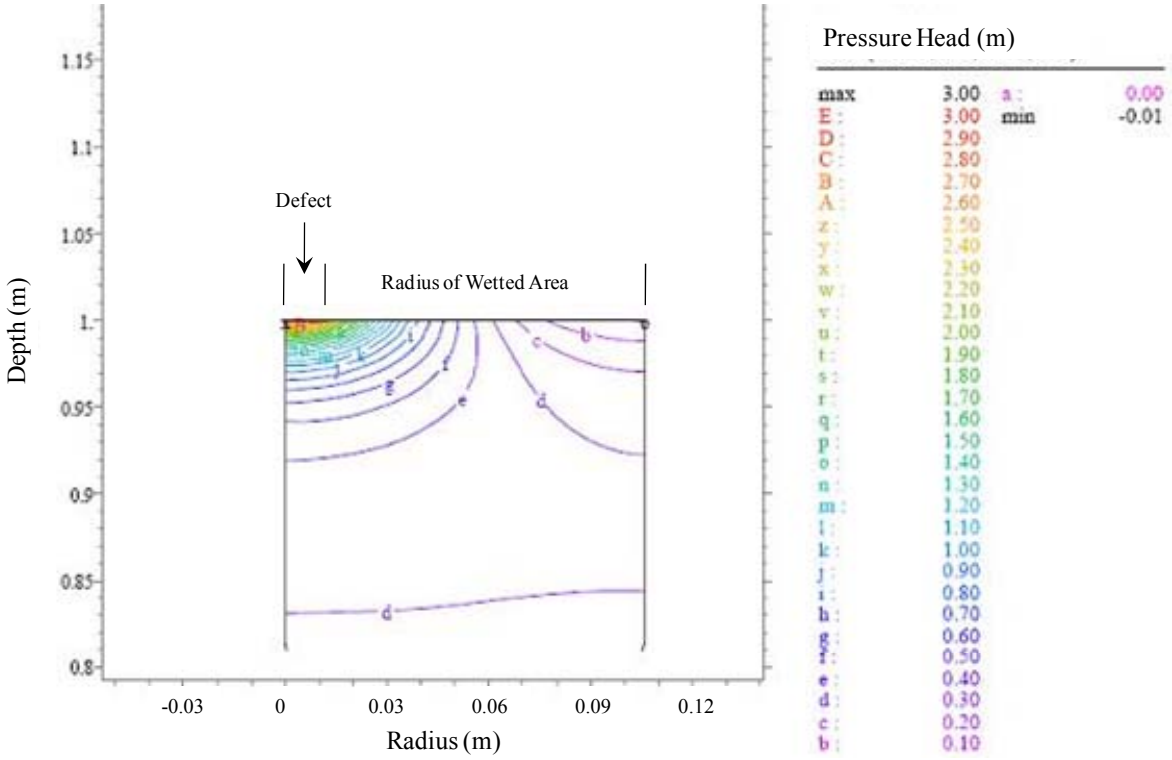

Figure 7.13: Pressure head distribution within the underlying soil layer for Case II (head at interface is defined by the analytical model)

The analytical model developed by Touze-Foltz et al. (1999) does not take into account flow that occurs laterally within a soil layer; only one-dimensional flow is considered through the use of Darcy's law for the vertical direction. Flow due to the negative pressure heads (or suctions) in the soil layer outside the radius of wetted area were also not accounted for in the analytical models. In the finite element model based on the assumption that flow through the lining system is confined within the radius of wetted area, the flow through the soil layer is actually one order of magnitude lower than if flow outside the radius of wetted due to suction gradients was taken in account.

This analysis justifies the use of a coefficient for lateral flow that was incorporated into the new simplified equation for GM-CCL system [Equation (5.13)], as there is a difference between the leakage rates measured in the laboratory and the leakage

rates expected in the field. This analysis also justifies the change in terminology from "radius of wetted area" to the "radius of interface flow," as flow is occurring outside the "radius of wetted area" as defined by Touze-Foltz et al. (1999).

7.4 EVALUATION OF IMPACT OF DEFECTS ON THE DESIGN OF DAMS

The experimental testing program and the subsequent numerical analysis of the permeameter tests discussed in Section 7.2 has provided a basis for the use of finite element methods to evaluate flow through a defect in a geomembrane placed over a soil layer. Validation for the new simplified equation for GM-CCL [Equation (5.13)] for use with field conditions was also presented in the previous sections. Accordingly, finite element simulations were conducted in order to evaluate the impact of leakage through defects in a geomembrane on the design of embankment dams. This analysis will provide insight into the beneficial effect of using geomembranes in the design of a dam. To this effect, conservative assumptions will be made regarding defects in the geomembrane and the resulting pore pressure generation due to leakage through defects on the design of a blanket drain and on the stability of the dam itself.

Finite element simulations were conducted for an earth dam with a geomembrane liner on the upstream face. The configuration of the dam used for this analysis is that of an actual dam being constructed in the central United States as part of a water storage impoundment system. A schematic of the dam used for this analysis is shown in Figure 7.14. The embankment dam has a height of 14 m and upstream and downstream slopes of 1V:3H. The dam was designed to retain 12 m of water in the reservoir. The designers of the dam were contemplating the use of a geomembrane liner on the upstream face in order to minimize costs associated with construction of a sand blanket drain at the downstream side. The primary concern was the effect leakage through defects in the

geomembrane liner could have on the pore pressures and the stability of the dam if the geomembrane was damaged.

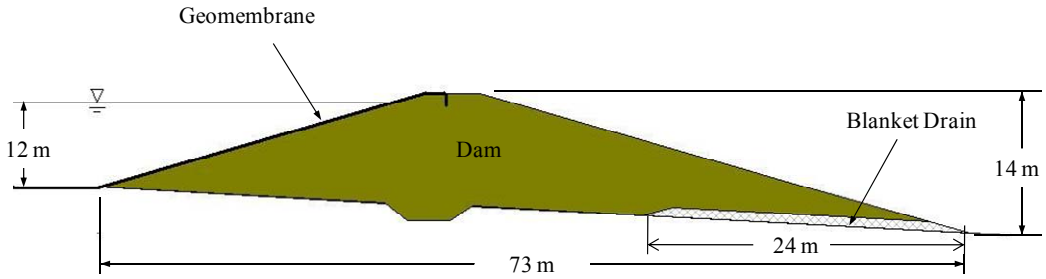

Figure 7.14: Cross-section of embankment dam used in finite element analysis

The phreatic surface, also referred to as the line of seepage, indicates the location of the water table in an earth dam. Drainage blankets placed at the downstream toe are used to control, or eliminate, the exit point of the phreatic surface on the downstream face. The exit point where the phreatic surface intersects the downstream face defines the location below which seepage occurs on the downstream face. The size, frequency and location of defects will affect the location of the phreatic surface within the dam. If the blanket drain is eliminated, it is important to determine what conditions, with regard to defects in a geomembrane liner, would lead to discharge on the downstream face of the dam. The line of zero pore pressure obtained from the seepage analyses was used to indicate the approximate location of the line of seepage within the earth dam. The line of zero pore pressure was used in this analysis to depict the location of the positive and negative pore water pressures.

To assess the geomembrane defect characteristics and conditions that may result in discharge on the downstream face, two-dimensional (2D) finite element analyses were conducted for the homogeneous embankment dam, shown in Figure 7.14, with and

without a blanket drain. Three-dimensional (3D) finite element analyses were performed to evaluate leakage through defects as predicted using the new simplified equation presented in Section 5.4.2.

The stability of the embankment dam under unlined and lined conditions was evaluated using the results of the finite element analyses. As water flows through a defect, there is an increase in the pore pressure in the area surrounding the defect. An increase in the pore pressures in an embankment dam may contribute to instability in the dam. Limit equilibrium analyses were subsequently conducted, using pore pressures obtained from the finite element analysis, to assess the effect leakage through defects in a geomembrane liner on the slope stability of the embankment dam.

Examples of the FlexPDE code used for the simulations of dams using flux and constant head boundary conditions and for dams with and without blanket drains are included in Appendix B.

7.4.1 Geometry and Material Properties for Finite Element Simulations of a Dam

7.4.1.1 Soils

The soil used in the body of the dam was a silty clay, classified as a CL soil using Unified Soil Classification System (USCS), with a saturated hydraulic conductivity of $2x10^{-7}$ m/s. For unsaturated flow, the water characteristic curve was approximated using the van Genuchten parameters listed in Table 7.1.

Table 7.1: van Genuchten parameters used in FE analysis of dam

Parameters	Clay (Dam)	Sand (Drain)
α	0.46	0.10
n	2.64	3.00
Residual VWC, θ_r	0.02	0.13
Saturated VWC, θ_s	0.45	0.38

For the analyses involving a drainage blanket at the downstream toe, a medium grain-sized sand was used to model the drainage material. The soil was classified as an SP soil according to USCS with a saturated hydraulic conductivity of $2x10^{-5}$ m/s.

7.4.1.2 Geomembrane Defects

The defects were simulated by using either an imposed flux boundary condition or a constant head boundary condition. The flux imposed on the boundary at the location of the defect was determined by using the new simplified equation developed during this study [Equation (5.13)]. In the finite element analysis of a dam, an interface gap is difficult to simulate due to the large extent of the dam and the thinness of the gap layer. A defect simulated using a constant head boundary condition would simulate a perfect contact condition, as with the permeameter test simulations in Section 7.3 when an interface gap was not included. In order to account for the interface gap in the numerical simulations of a dam, the new simplified equation [Equation (5.13)] was imposed at the defect locations. Equation (5.13) was developed using the average transmissivity from the experimental tests and includes a factor for less intimate contact conditions.

The defects in the geomembrane liner for the 2D simulations were modeled by imposing a constant head boundary over the defect. The rest of the upstream face of the dam was assigned a no-flow boundary. Since a 2D analysis assumes the dam is infinitely long, the defect corresponds to a strip. This is a worst-case scenario that is not likely to occur in the field. More realistic defect sizes can be simulated using a 3D finite element analysis.

7.4.1.3 Boundary Conditions

Four types of boundary conditions were used in this study: i) no-flow boundary, ii) seepage face boundary, iii) flux boundary, and iv) constant head boundary. The

boundary conditions specified in the analyses of the dam are shown in Figure 7.15. A no-flow boundary condition was used to simulate the geomembrane on the upstream face of the dam. A boundary that is specified as a seepage face will act as a no-flow boundary as long as it remains unsaturated; however, once it becomes saturated, flow will occur across the boundary. For models that did not include a blanket drain, a seepage face boundary condition was specified for the downstream face in order to determine the exit point for the line of seepage. For models that include the blanket drain, the seepage face boundary condition was instituted at the drain and a no-flow boundary was defined for the downstream face. The geomembrane liner was simulated by assigning a no-flow boundary along the upstream face except at the desired location for the defect. The defect itself was simulated by imposing either a constant flux or a constant head boundary condition. A no-flow boundary condition was used for the base of the dam.

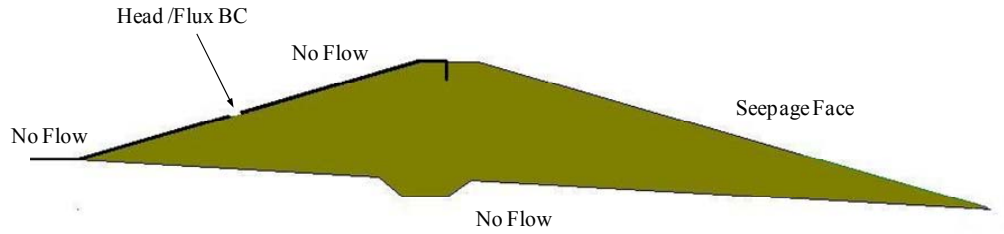

(a)

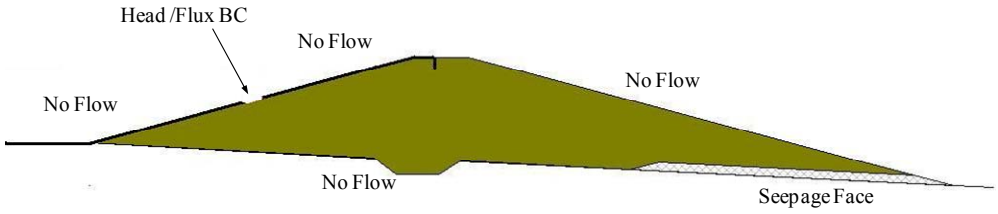

(b)

Figure 7.15: Boundary conditions for embankment dam for: a) no blanket drain and b) with a blanket drain

7.4.2 Analysis of Downstream Discharge Face and Need for Blanket Drain in a Dam

To assess the geomembrane defect characteristics and conditions that may result in discharge on the downstream face, two-dimensional (2D) finite element analyses were conducted for the homogeneous embankment dam, shown in Figure 7.14, with and without a sand blanket drain at the downstream toe. Also, stability analyses were conducted to determine the effect of the pore pressures due to leakage through defects on the slope stability of the downstream side of the dam.

7.4.2.1 Evaluation of Effect of Blanket Drain using Finite Element Simulations

The analyses included evaluation of an embankment with and without a blanket drain for two conditions, which were: a) an unlined dam, and b) a geomembrane-lined dam with a defect located at mid-slope (see Figure 7.16 for location of defect). The defects used for the 2D analyses are large, representing the worse-case scenario, and were simulated using a constant head boundary condition of 12 m. It should be noted that the geomembrane is in perfect contact with the soil and that an interface gap was not included in the analysis.

The lines of zero pressures (approximating the lines of seepage) for the analyses conducted without a blanket drain are shown in Figure 7.16. The line of zero pressure for the unlined dam had the highest elevation within the dam than the line of zero pore pressure for the lined dam, indicating that positive pore water pressures were present in a larger portion of the unlined dam than the lined dam. The approximated line of seepage for the lined dam had an exit point on the downstream face that was slightly lower than that for the unlined dam, indicating that seepage face was smaller if a geomembrane was present. The approximate steady-state line of seepage for a lined dam with a defect is lower in elevation than for an unlined dam, but the potential energy in the water (i.e., height of water in the reservoir drives flow through the defect) is higher than the elevation of the defect. Therefore, the elevation of the estimated line of seepage for flow through a defect is higher than the elevation of the defect itself.

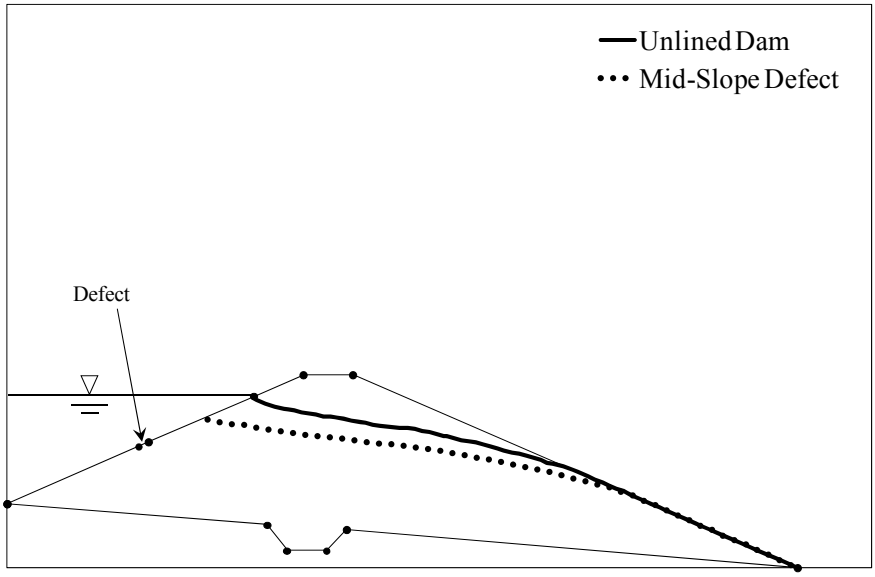

Figure 7.16: Lines of zero pressure for 2D earth dam without a blanket drain

The blanket drain at the toe of the downstream slope of the dam is 24 m long, as shown in Figure 7.17. The lines of seepage for the analyses conducted with the sand blanket drain at the downstream toe are shown in Figure 7.17. The line of zero pressure for the unlined dam has the highest elevation within the dam than the line of zero pressure for the lined dam. The presence of a blanket drain results in an elimination of a discharge face on the downstream slope. The simulation for a mid-slope defect resulted in a line of seepage with an elevation at the upstream face higher than the location of the defect. The energy potential in the water flowing through the defect in the geomembrane causes the approximate line of seepage to stabilize at an elevation above the location of the defect, but below the height of water being retained by the dam (12 m).

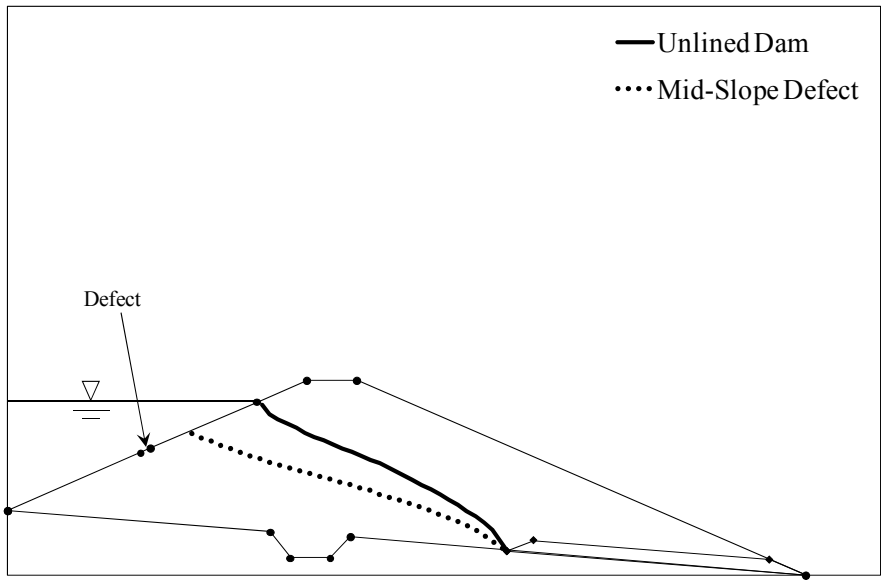

Figure 7.17: Lines of zero pressure for 2D earth dam with a blanket drain

7.4.2.2 Analyses to Determine Effect of Leakage on Stability of Dam

Using the lines of zero pressure from the 2D finite element simulations for unlined and lined dams with and without blanket drains, stability analyses were conducted to determine the effect of leakage through a defect on the stability of the downstream slope and the need for a blanket drain. The slope stability computations were performed using UTEXAS4 (Wright 2007), which uses limit equilibrium methods to determine the factor of safety for a slope. For this analysis using UTEXAS4, Spencer's procedure was selected for the stability analyses of a circular failure surfaces that passed through the crest of the dam. A floating grid search was used to find the most critical failure surface for the downstream slope of the dam. The U.S. Army Corps of Engineers (1970) recommends for dams and levees a factor of safety of 1.5.

The geometry of the slope and the soil strength parameters are required to perform the limit equilibrium analyses. The shear strength parameters for the dam and

the drain are listed in Table 7.2. The silty clay was assumed to have no cohesion. The dam configuration used in the stability analysis is shown in Figure 7.18 and is the same as that used for the finite element analysis. The dimensions of the earth dam are shown in Figure 7.14. The embankment dam has a downstream slope of 1V:3H. The pore pressures obtained from the 2D flow analyses for unlined and lined dams with and without a blanket drain were used to interpolate pore pressures in UTEXAS4. Negative pore pressures were not considered in the analyses; the use of negative pore pressures would yield unconservative results.

Table 7.2: Shear strength parameters for soil used in the embankment dam

Soil	Cohesion Intercept, c (kPa)	Friction Angle, φ' (°)
Silty Clay (Dam)	0	29.5
Sand (Toe Drain)	0	36

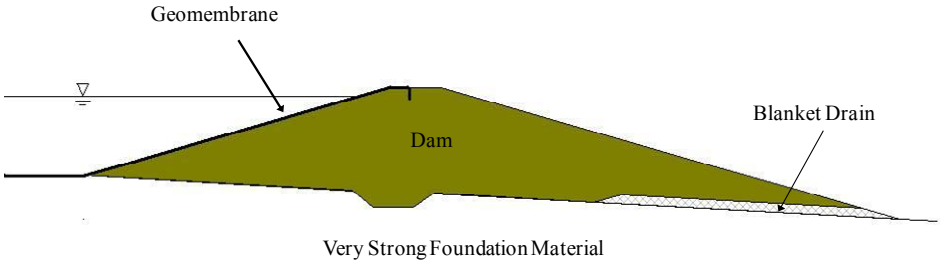

Figure 7.18: Schematic of dam used for slope stability analyses

The embankment dam without a blanket drain and without a geomembrane liner has a factor of safety of 1.62. The factor of safety for the unlined embankment dam shown in Figure 7.18 is above the value recommended by the U.S. Army Corps of

Engineers of 1.5. The factor of safety is expected to change with changes in the pore pressures due to the presence of a geomembrane liner and leakage through defects in the liner. The factor of safety of the downstream slope was defined using UTEXAS4 for an unlined and lined dam with and without a blanket drain and the corresponding steady-state pore pressures obtained from the finite element analyses. The factors of safety for each of these cases presented in Section 7.4.2.1 are listed in Table 7.3.

Table 7.3: Factors of safety for embankment dams with blanket drains (2D analysis)

Geomembrane Status	**Factor of Safety**	
	No Drain	**Blanket Drain**
Unlined	1.62	1.85
Mid-Slope Defect	1.65	1.85

The critical failure surfaces for the embankment dams without a blanket drain are shown in Figure 7.19, along with the line of zero pressure for the unlined dam, for two cases: i) unlined and ii) lined with one mid-slope defect. The failure surfaces for both cases are shallow and are located on the downstream slope below the exit point of the approximate line of seepage (i.e., line of zero pressure). There was a slight improvement in the stability of the downstream face for the lined dam when compared to an unlined dam. This was expected as the line of zero pressure for the lined dam was slightly lower than for the unlined dam.

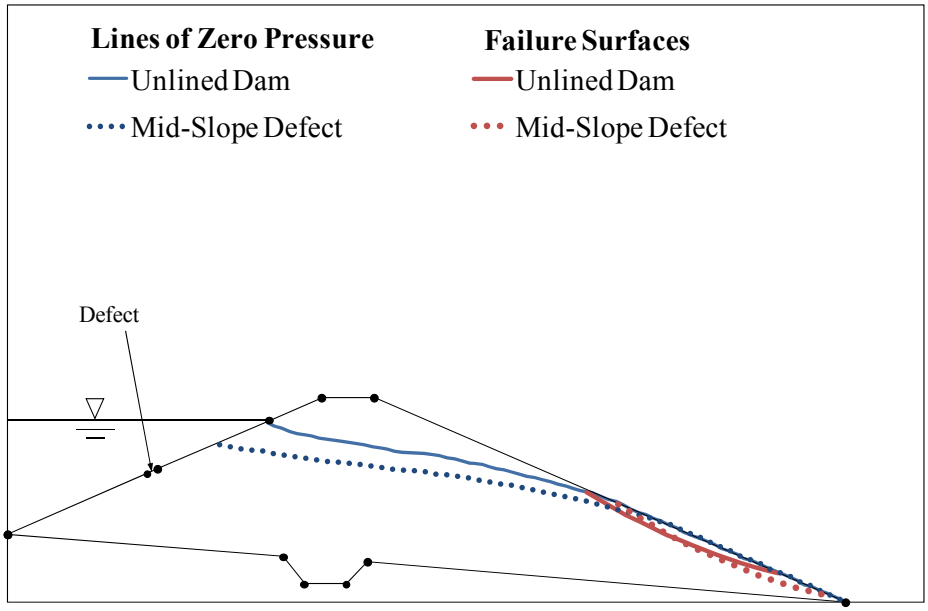

Figure 7.19: Critical failure surfaces for unlined and lined embankment dam without blanket drain using pore pressures obtained from 2D finite element analyses

The factors of safety for the embankment dams with a blanket drain were not affected by the presence of a geomembrane liner on the upstream face as the values were the same (i.e., FS = 1.85) for both the unlined case and the case with a lined with a mid-slope defect. The critical failure surfaces for these two cases are shown in Figure 7.20, along with the lines of zero pressure. As shown in Figure 7.20, the critical failure surfaces for the two cases analyzed did not intersect the area of positive pore water pressures in the dams. Note that the critical failure surfaces for the cases without a blanket drain were shallower than for the dam with a blanket drain; however, the pore pressures acting on the failure surface were greater for the cases without a blanket dam. The presence of the blanket drain resulted in a line of zero pressure far from the downstream slope. The blanket drain also increases the strength of the downstream toe and the failure surface does not intersect the drain. The presence of the blanket drain, as

well as the location of the line of zero pressures, could account for the higher factor of safety when compared to the stability of the dams without a blanket drain.

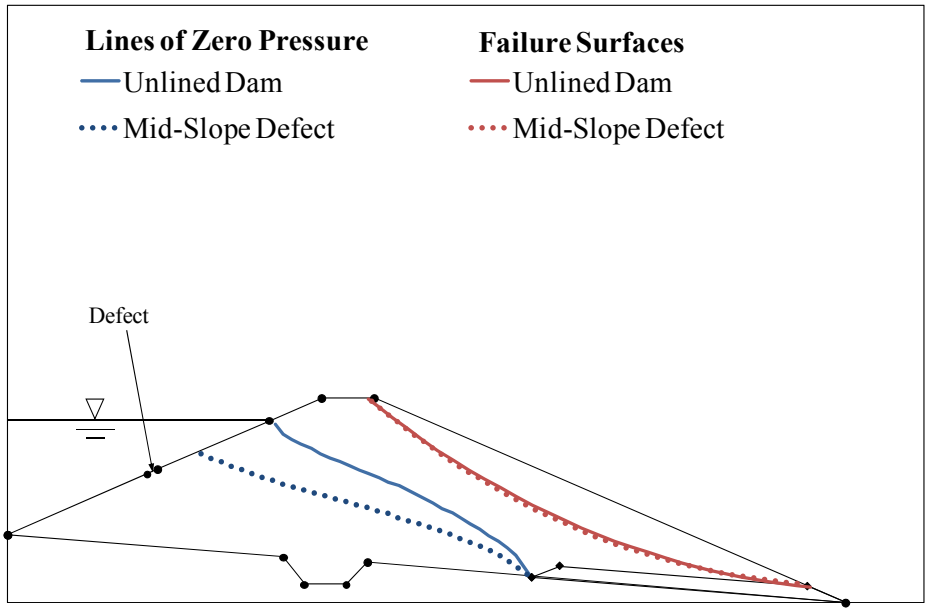

Figure 7.20: Critical failure surfaces for unlined and lined embankment dam with a blanket drain using pore pressures obtained from 2D finite element analyses

Since the finite element simulations were performed using two-dimensional analyses, the factors of safety are for the worst case scenario. The factors of safety are expected to be less for a three-dimensional analysis (and more realistically sized defects) than those reported in this section.

7.4.3 Three-Dimensional Analyses of Leakage through Defects

The 2D finite element simulations are considered to be worst-case scenarios since the defect is analyzed as an infinitely long tear (strip) in the geomembrane. The 3D finite element analyses were performed to evaluate leakage through defects using more realistically sized defects (finite diameters). The 3D simulations were also used to

evaluate the leakage through defects as predicted using the new simplified equation [Equation (5.13)].

For the 3D model, the embankment dam shown in Figure 7.14 was given a length of 150 m. The CL soil used in the 2D analyses for the embankment dam was also used in the 3D analyses. Nosko and Touze-Foltz (2000) found the majority of the defects in the side-slope of landfills to have diameters between 0.8 cm to 3.6 cm; however, the largest defects found during the study conducted by Nosko and Touze-Foltz (2000) were over 10 cm in diameter. Circular defects with diameters of less than 4 cm were numerically unstable. For this study, circular defects with diameters of 20 cm were used to evaluate the leakage through a geomembrane liner. A defect with a diameter of 20 cm represents the larger end of the spectrum for defect diameters that could be expected in the field if CQA was not performed.

The defects were simulated using either a flux boundary condition [e.g., a value calculated using Equation (5.13) for a head of 12 m] or a constant head boundary condition of 12 m. The flux boundary condition allows an imperfect contact to be taken into account while the constant head boundary condition assumes a perfect contact between the geomembrane and the underlying soil. The results for both types of boundary conditions are compared. A transient analysis was used for the simulations and the model was conducted for a 10-year period.

7.4.3.1 Constant Head Boundary Condition

3D simulations were conducted to evaluate the leakage through a defect in a geomembrane liner on the upstream face of the dam when the defect is simulated by a constant head boundary condition of 12 m and a perfect interface contact between the geomembrane and the underlying soil layer. The total head contours for the dam after 10 years are shown in Figure 7.21 and the location of the defect is marked by an ‘x’. The

head at the location of the defect is the same as the imposed constant head boundary condition used to simulate the defect. The contours represent the equipotential lines of a flownet. The pore pressure distribution in the dam is shown in Figure 7.22. Note that the line of zero pressure (contour 'y') is not visible in Figure 7.22, even at the base of the dam. Only the area around the defect is saturated, exhibiting positive pore pressures. The numerically-calculated flow rate through the defect was 0.09 m^3/d, or 1.0×10^{-6} m^3/s. This leakage rate is lower than the flux of 3.4×10^{-6} m^3/s expected to occur when accounting for imperfect contact between the geomembrane and the underlying clay layer.

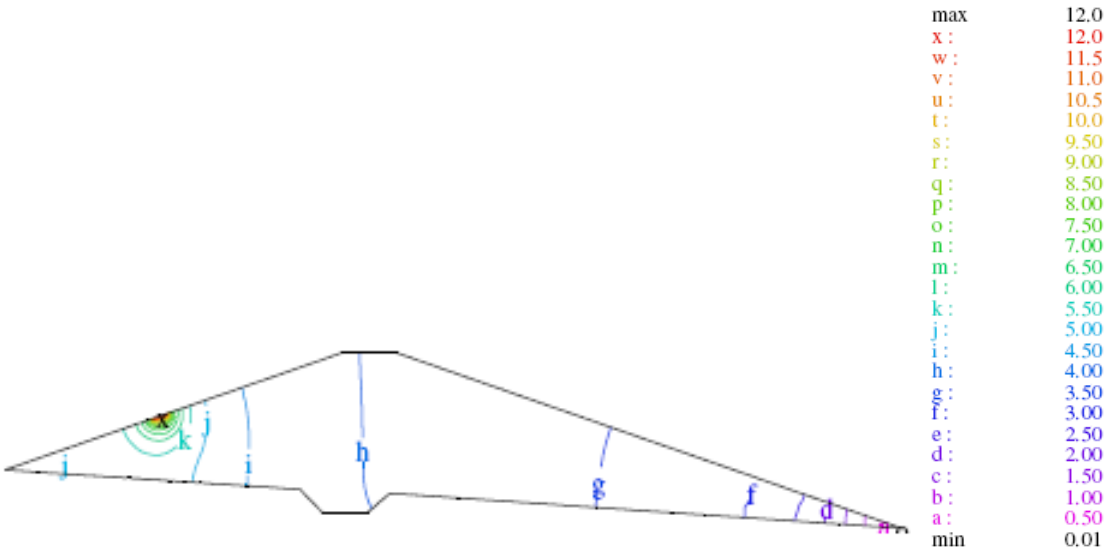

Figure 7.21: Hydraulic heads from 3D analysis of dam with constant head boundary condition at the defect

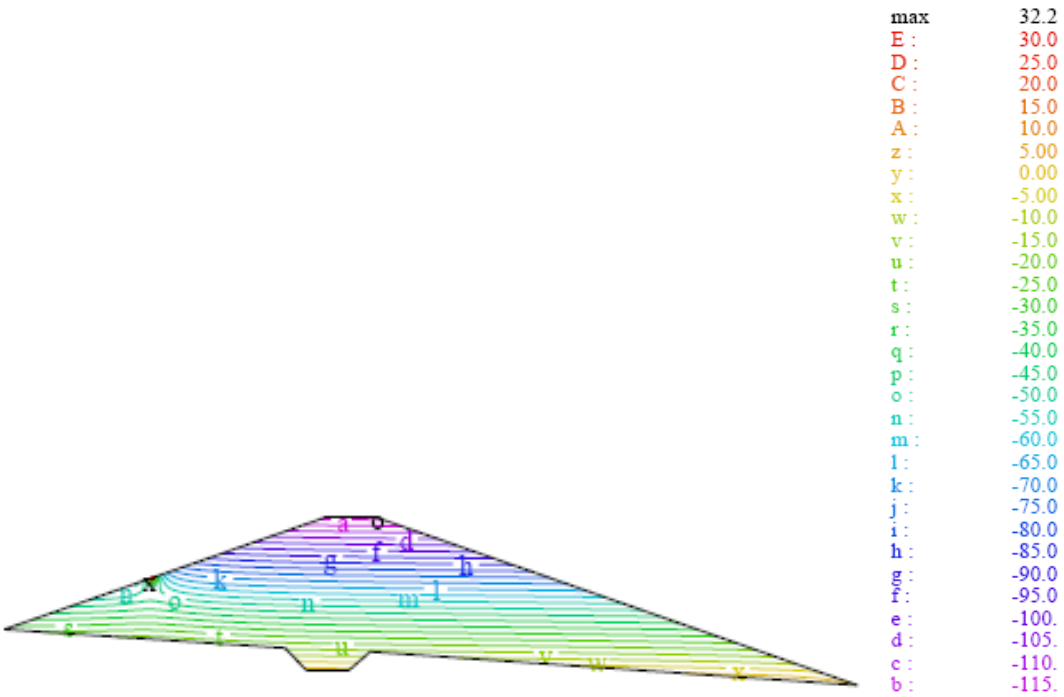

Figure 7.22: Pore pressure within embankment dam for a defect simulated using a constant head boundary condition of 12 m

A simulation was also conducted for the same lined embankment dam but, instead of one defect at midpoint of the dam, three defects with 0.2 m diameters were placed equally spaced along the upstream face of the dam at the midpoint of the dam (Y=75). The defects were simulated using constant head boundary conditions of 12 m. The locations of the defects can be seen in Figure 7.23, which shows the total head distribution for steady-state conditions. The pore pressure distribution within the dam is shown in Figure 7.24. The line of zero pressure (contour 'k' in Figure 7.24 is the line of zero pressure) is at the base of the dam and is at a significantly lower elevation within than the lines of zero pressure shown in Figure 7.16. The numerically-calculated flow rate through each one of the defects was 0.077 m^3/d, or 8.9×10^{-7} m^3/s.

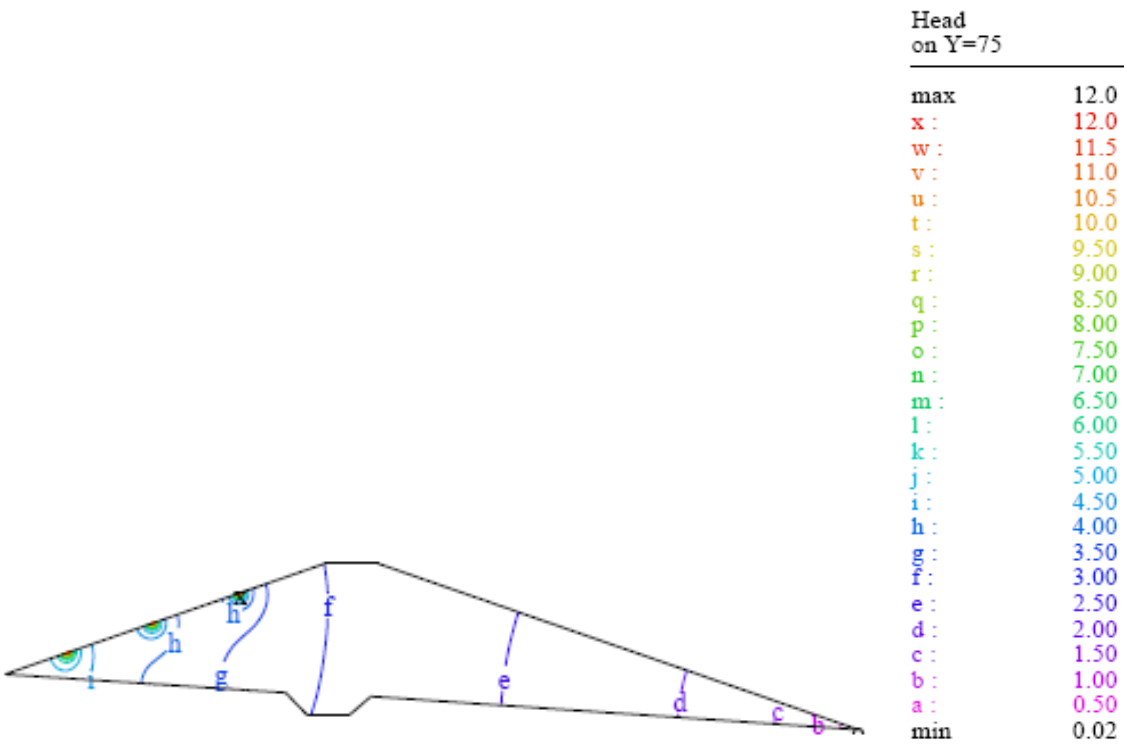

Figure 7.23: Total head distribution within embankment dam for three defects with a constant head boundary condition of 12 m

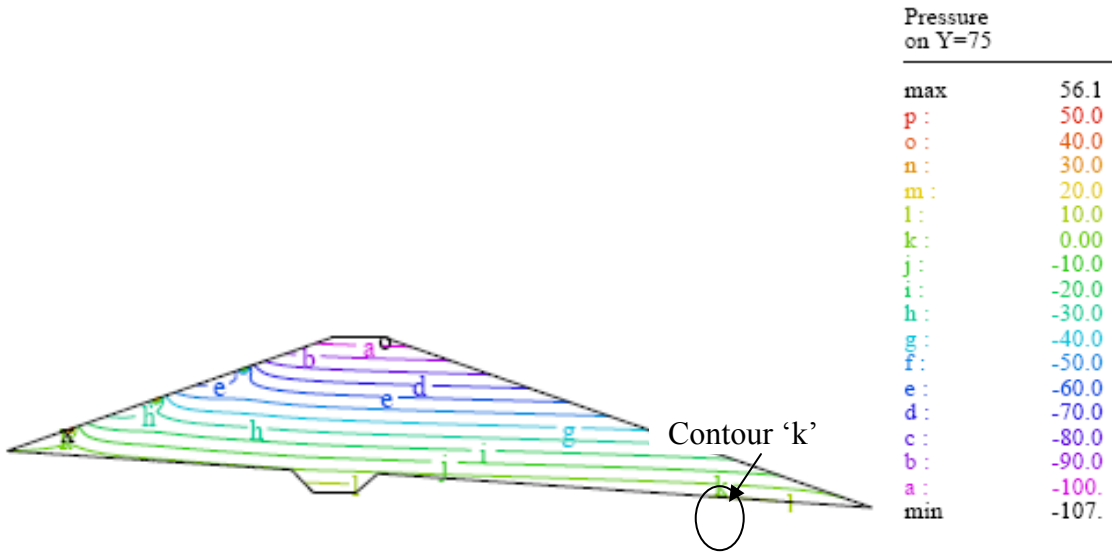

Figure 7.24: Pore pressure distribution within embankment dam for three defects with a constant head boundary condition of 12 m

7.4.3.2 Flux Boundary Condition

One of the objectives of the experimental study was to develop an empirical equation that estimates the leakage rate through a defect in a geomembrane. The new GM-CCL simplified equation [Equation (5.13)] was developed using the same methodology as Touze-Foltz and Giroud (2003), but two coefficients were added to take into account contact quality for high heads and the three-dimensional lateral flow that will occur in the field outside the radius of interface flow. Simulations were conducted to evaluate the leakage through a geomembrane liner with an imperfect contact between the liner and the soil. The evaluation was accomplished by imposing a flux boundary condition at the location of the defect. The flux used as the boundary condition was calculated using Equation (5.13).

The defect was modeled using a normal flux boundary condition with units of [$L^3/T/L^2$]. The GM-CCL simplified equation [Equation (5.13)] was used to calculate flow rates using the hydraulic conductivity of the soil ($2x10^{-7}$ m/s), the area of the defect (for a diameter of 0.2 m), hydraulic gradient, and the hydraulic head imposed on the geomembrane liner (12 m). The hydraulic gradient was determined using the localized gradient near the defect for the constant head boundary condition. A hydraulic gradient of 2.78 was used to calculate the flow rates using Equation (5.13). The flow rate predicted using the GM-CCL simplified equation was $3.4x10^{-6}$ m^3/s, using a C_q = 68.7 and a C_{lf} = 3 in Equation (5.13). This flow rate is higher than that numerically calculated under a constant head boundary condition. This is expected because the constant head boundary condition corresponds to a perfect contact condition, while the new simplified equation takes into account the presence of an interface gap and a less intimate contact condition.

The hydraulic heads obtained from the 3D analysis on leakage through one defect on the upstream face simulated using flux boundary conditions are shown in Figure 7.25. For a flux boundary condition obtained using the GM-CCL new equation [Equation (5.13)], the head at the defect was 35 m which was almost three times higher than the head used to calculate flow.

max	35.0
r :	34.0
q :	32.0
p :	30.0
o :	28.0
n :	26.0
m :	24.0
l :	22.0
k :	20.0
j :	18.0
i :	16.0
h :	14.0
g :	12.0
f :	10.0
e :	8.00
d :	6.00
c :	4.00
b :	2.00
a :	0.00
min	-0.69

Figure 7.25: Total hydraulic heads within the homogeneous dam for a flux boundary condition for one defect

The pore pressures within the dam generated by flow through the defect under a flux boundary condition of 3.8×10^{-6} m^3/s are shown in Figure 7.26. Considering pore pressures, the system simulated using the GM-CCL empirical equation [Equation (5.13)] as a flux boundary condition had positive pore pressures that were located only around the defect. The line of zero pressure (contour 'e') is not visible in the body of the dam, indicating that not enough water infiltrates through the defect to develop a phreatic surface such as those shown in Figure 7.16. This was also true for the constant head boundary condition, as shown in Figure 7.22.

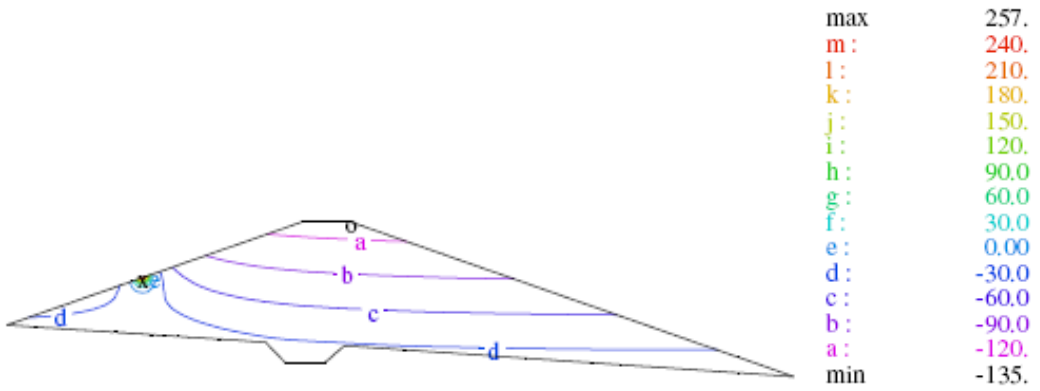

Figure 7.26: Pore pressure distribution in the dam due to leakage from a flux boundary condition for one defect

A simulation was also conducted for the same lined embankment dam but, instead of one defect at midpoint of the dam, three defects with 0.2 m diameters were placed equally spaced along the upstream face of the dam at the midpoint of the dam (Y=75). The defects were simulated using flux boundary conditions calculated using the new simplified equation. The imposed flux was 3.4×10^{-6} m^3/s, using a C_q = 68.7 (obtained from a head of 12 m) and a C_{lf} = 3 in Equation (5.13) The numerically-calculated flow rate for a constant head boundary condition was 0.55 m^3/d, or 8.9×10^{-7} m^3/s. The flux boundary condition takes into account a less intimate contact than the system with a constant head boundary condition. Therefore, the leakage rate into the system is higher for the system using a flux boundary condition based on Equation (5.13). To obtain an equivalent leakage rate for perfect contact conditions, the constant head imposed on the defects would have to be 53 m.

The hydraulic heads obtained from the 3D analysis on leakage through three defects on the upstream face simulated using flux boundary conditions are shown in Figure 7.27. For the flux boundary condition obtained using the GM-CCL new equation

[Equation (5.13)], the head at the defect was 34 m which was almost three times higher than the head used to calculate flow.

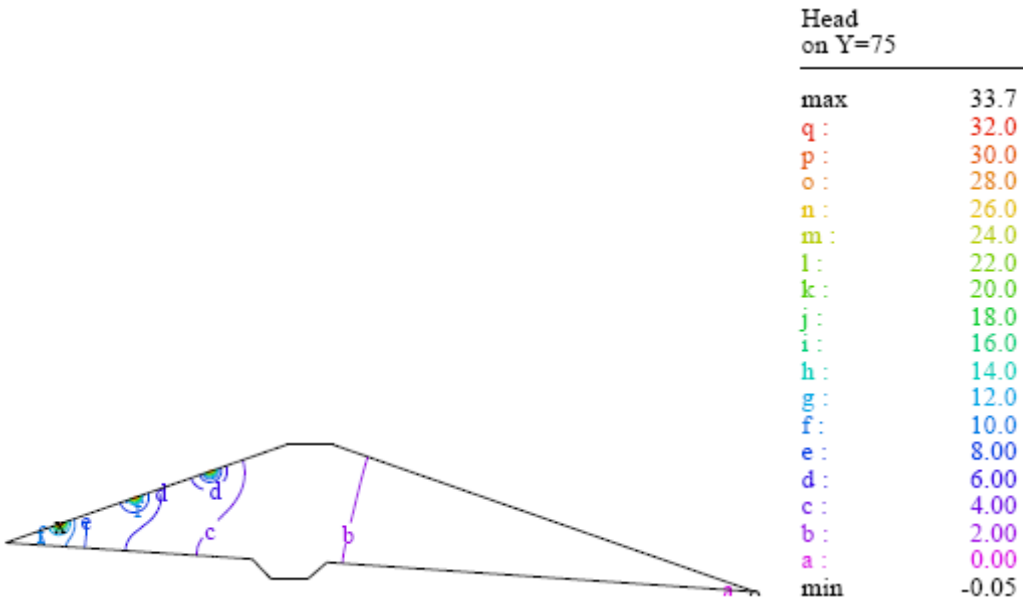

Figure 7.27: Total hydraulic heads within the homogeneous dam for a flux boundary condition for three defects

The pore pressures within the dam generated by flow through three defects defined by a flux boundary condition are shown in Figure 7.28. Considering pore pressures, the system simulated using the GM-CCL empirical equation [Equation (5.13)] as a flux boundary condition had positive pore pressures that were located only around the defect. The line of zero pressure (contour 'f') located near the upstream side at the base of the dam. The line of zero pressure is still considerably lower in elevation than those shown in Figure 7.16.

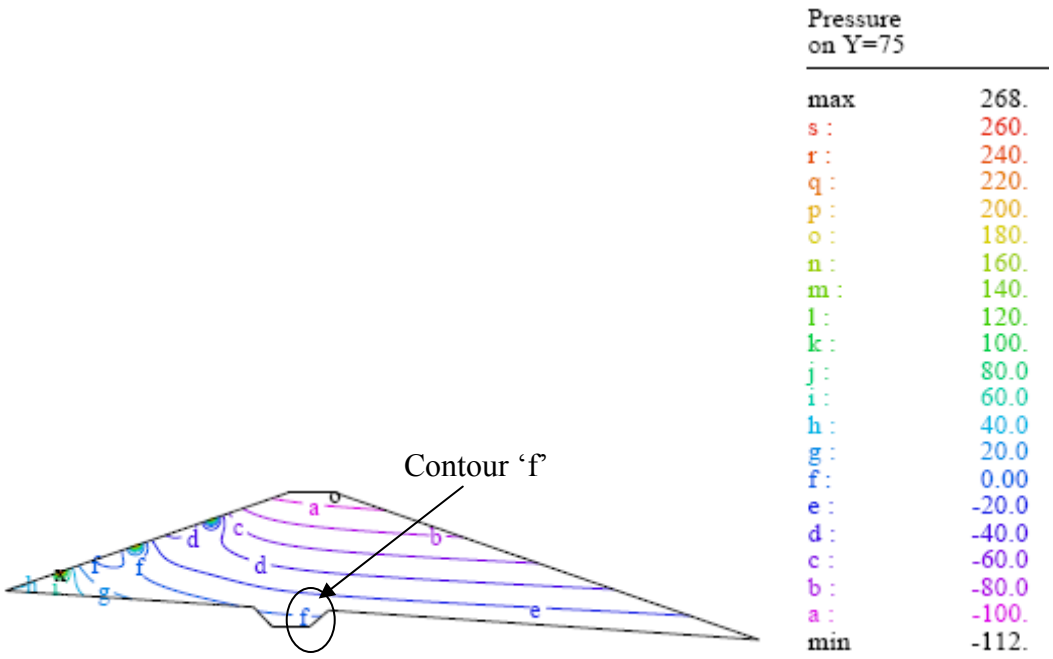

Figure 7.28: Pore pressure distribution in the dam due to leakage from a flux boundary condition for three defects

A parametric study was performed to determine the equivalent defect size between a constant and a flux boundary condition. For a hydraulic gradient of 2.78 (result from a finite element simulation for a constant head of 12 m), hydraulic conductivity of $2x10^{-7}$ m/s and a head of 12 m, the defect diameter was changed to determine the difference between using a constant head boundary condition and flux boundary condition. The results of parametric study include the numerically calculated flux for the constant head boundary condition and the flux boundary condition calculated using Equation (5.13) and are listed in Table 7.4. Only the defect diameter was changed; all other variables were held constant. For a constant head boundary of 12 m and a defect diameter of 0.15 cm, the numerically reported flux at the location of the defect was 0.04 m^3/d. To obtain a flow rate of 0.04 m^3/d using Equation (5.13), the diameter of the defect would need to be 0.005 m. In other words, to obtain the same flow rate, the defect

needs to be much larger in size for perfect interface contact (as simulated by the constant head boundary condition) than if an interface gap and poor contact are considered (as simulated by the new simplified equation).

Table 7.4: Equivalent defect sizes for two types of boundary conditions for 3D embankment dam

Boundary Condition	Defect Diameter (m)	Flux (m^3/d)
Contstant Head (12 m)	0.15	0.04
Flux (new simplified equation [Equation 5.13])	0.005	0.04

7.4.3.3 Analysis of the Pore Pressures

Additional 3D simulations were conducted to evaluate the pore pressures within the dam. The size of the defects was increased since smaller (and more realistic) defect sizes did not seem to provide enough water into the dam to develop a noticeable line of zero pore pressure (i.e., approximate line of seepage); the pore pressures in the dam were negative even under steady-state conditions (see Figure 7.22). The 3D simulations performed to evaluate the pore pressures involved circular defects with a diameter of 1 m. This size of a defect was significantly larger than the defects observed by Nosko and Touze-Foltz (2000). For the case involving only one defect, the defect was located midway up the slope on the upstream face of the dam at the midpoint of the width of the dam (i.e., at 75 m of 150 m width of the dam). For the simulation involving three defects, the defects were located midway up the slope on the upstream face of the dam with at equal spacing between the defects (i.e., defects were located at 37.5, 75 and 112.5 m along the 150 m width of the dam). The frequency of defects was determined by taking the area of the upstream face of the dam and dividing by the number of defects

used for the simulation. The frequency of defects per area for the simulation involving one defect corresponds to approximately one defect per 4000 m^2, while the frequency for the simulation that includes three defects corresponds to approximately one defect per 1600 m^2. Giroud and Bonaparte (1989) recommends the use of one defect per 4000 m^2 when evaluating leakage, while Nosko and Touze-Foltz (2000) found that defects occur once every 800 m^2 prior to CQA.

The defect(s) were simulated using a flux boundary condition using a leakage rate of 3.9×10^{-6} m^3/s as predicted by Equation (5.13). A blanket drain was not included in this evaluation of the pore pressures because the leakage through the defects was assumed to be significantly less than in the 2D analyses. Also, the blanket drain minimized the effect of the pore pressures. The effect of the presence of the geomembrane with its defects was an integral part of the evaluation presented herein.

The results of the 3D simulations of the earth dam without a blanket drain are shown in Figures 7.32. The line of zero pressure for the unlined dam was higher in elevation than either of the two simulations involving a lined dam. The approximate lines of seepage shown in Figure 7.29 for the 3D models were significantly affected by the presence of the geomembrane. At steady-state, the lines of zero pressure were well below those found in the 2D flow analyses. The amount of water flowing through the finite, albeit relatively large, defects in the 3D analyses is less than that in the 2D analyses for defects with infinite length.

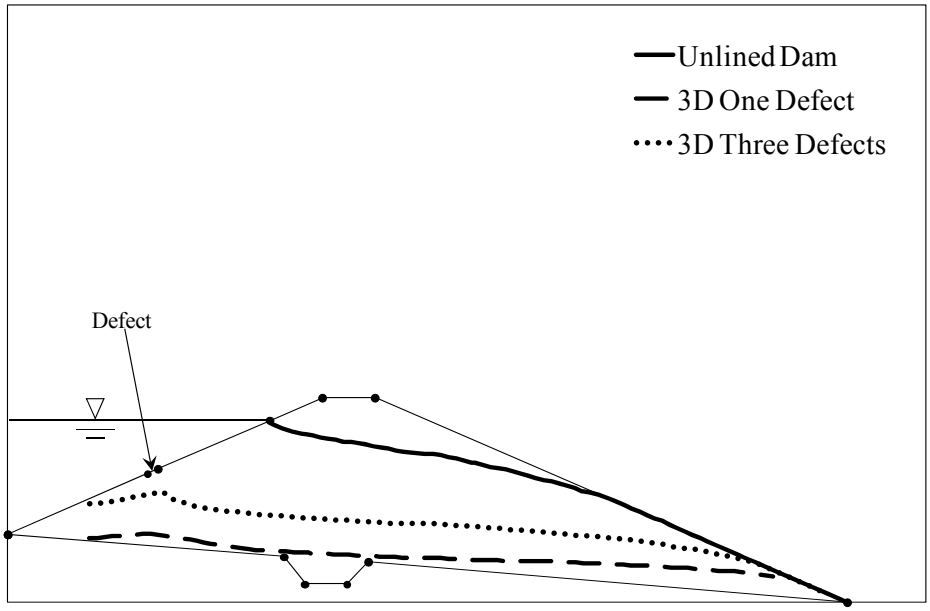

Figure 7.29: Lines of zero pressure for 3D dam without blanket drain and a flux boundary condition at the defect

Stability Analysis

Stability analyses were conducted to determine the effect of leakage through a defect on the downstream slope using the pore pressures obtained from the 3D finite element simulations shown in Figure 7.29. Since the dam has three dimensions, a projection in the X-Z direction at Y=75 m was taken to determine the pore pressures. The dam is 150 m so the projection was taken at the middle of the dam, through the center of a defect. Two-dimensional slope stability computations were performed using UTEXAS4 (Wright 2007), which uses limit equilibrium methods to determine the factor of safety for a slope. For this analysis using UTEXAS4, Spencer's procedure was selected for the stability analyses of a circular failure surfaces that passed through the crest of the dam. A floating grid search was used to find the most critical failure surface for the downstream slope of the dam. The slope stability for the downstream slope was

determined for the same geometry and shear strength parameters presented in Section 7.4.2.2.

The factors of safety for an unlined dam, a lined dam with one defect and a lined dam with three defects are listed in Table 7.5. As with the 2D analysis, the factor of safety for the embankment dam without a geomembrane liner is the lowest value (FS = 1.62). The presence of the geomembrane leads to an increase in the factor of safety, regardless of the number of large defects. The critical failure surfaces as well as the lines of zero pressure for the unlined dam, a lined dam with one defect and a lined dam with three defects are shown in Figure 7.30. The failure surfaces for the lined dams are shallow, similar to that of the unlined dam, but are located above the exit point on the downstream face of the dam. However, independent of the frequency of the defects, the factors of safety evaluated using the pore pressures from the 3D seepage analyses of lined dams are the highest for all cases investigated in this study, with exception of the dams that incorporate a blanket drain.

Table 7.5: Factors of safety for stability analysis considering 3D flow analyses

Geomembrane Status	**Factor of Safety**
Unlined	1.62
One Defect	1.72
Three Defects	1.72

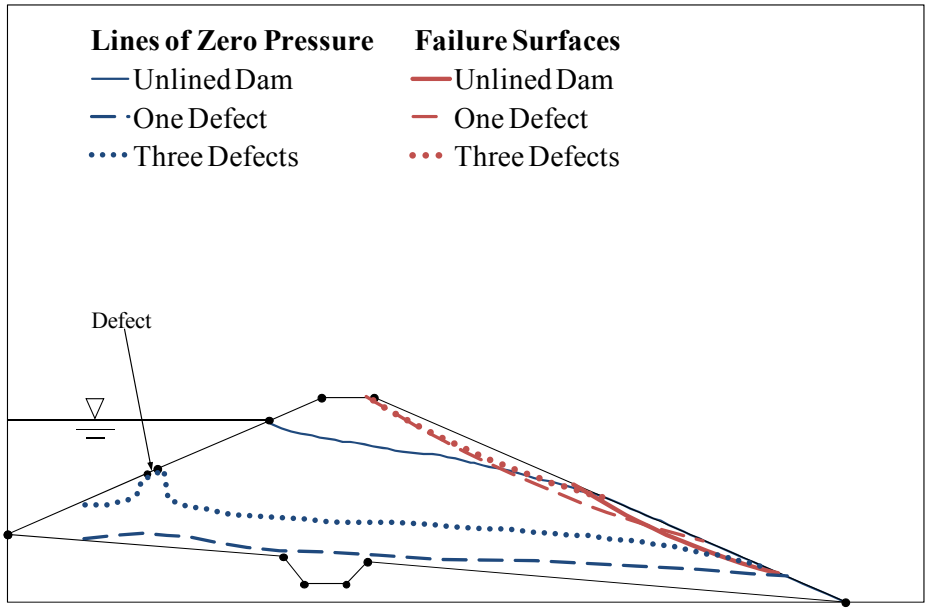

Figure 7.30: Critical failure surfaces for unlined and lined embankment dams based on pore pressures obtained from 3D seepage analyses

In the simulations, placing a geomembrane liner on the upstream face of the dam generally increases the factor of safety on the downstream face, although the magnitude of the increase is dependent on the size and frequency of defects in the geomembrane liner. According to the stability analysis, the downstream slope is sufficiently stable even if the dam is unlined and does not have a blanket drain. The factor of safety can be increased if a geomembrane is placed on the upstream face of the dam. Also, by installing a blanket drain, the factor of safety for the downstream slope is increased.

The analysis presented herein provided insight into the beneficial effect of using geomembranes on the design of a dam. Geomembrane liners significantly reduce the amount of water infiltrating the dam and may eliminate the need for a blanket drain, even if multiple large defects are present. Because seepage at the downstream toe of the dam will still occur even if the dam is sufficiently stable, measures should be taken to protect

the lower portion of the downstream slope. Leakage through defects could still cause piping and internal erosion so the design of the dam with a geomembrane liner should take this into consideration.

Beyond the two- and three-dimensional analyses of dams, the numerical simulations provided valuable insight into the laboratory tests conducted as part of the experimental component of this study. Once properly calibrated, the numerical model is capable of extrapolating results outside the range of parameters used in the laboratory. The analytical model was also evaluated using finite elements and was determined to underestimate the leakage rate expected through a defect due to the limitations of the model. However, the analytical models may still provide value to design as the equations are quicker to set up and use when compared to a three-dimensional finite element simulation. Overall, numerical methods are useful design tools that can assist an engineer in identifying the important parameters to be considered during the design process.

7.5 CASE HISTORY: PALMDALE RESERVOIR

A practical example of the use of geomembrane liners in embankment dams involves a group of holding ponds for a water treatment plant. The holding ponds were retained by 7 linear miles of embankments. The homogeneous embankments and holding reservoirs were lined with geomembranes and were left uncovered. The primary concern regarding the use of geomembrane liners in the holding ponds and embankments was that, if there were large defects in the liner, the water being retained would seep through the embankments and require blanket drains to be installed at the toes of the embankments. SVFlux was used to evaluate the effectiveness of the geomembrane liner at minimizing flow through this series of embankments. Simulations were conducted for two cases: i) unlined and ii) lined with a large defect at the midpoint of the upstream face.

Only one section of the embankments was analyzed; however, differences in the native soil and embankment soil were not expected.

7.5.1 Embankment Geometry and Material Properties

The geometry of the embankment simulated in this study, shown in Figure 7.31, was a typical cross-section for the site. Although not all of the 7 miles of embankment had the exact same cross-section, using a typical cross-section can provide a close approximation of the rest of the embankment sections. Also, the analysis of a typical cross-section can give an indication of any problems that may be caused by the leakage through a defect in the geomembrane liner. The dimensions for cross-section of the reservoir analyzed for this study are shown in Figure 7.31. The three-dimensional model was given a length (direction into the page in Figure 7.27) of 381 m, which was a quarter of the length of one of the embankments in the series of reservoirs.

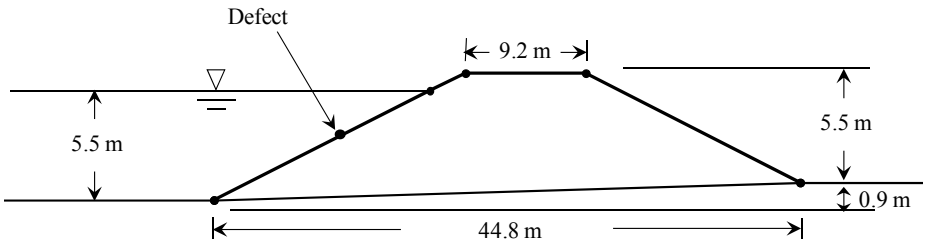

Figure 7.31: Geometry for the reservoir embankment

7.5.1.2 Soils

The actual hydraulic conductivity values of the soils at the site and of the soils used to construct the embankment were not available. However, conservative estimates of the hydraulic conductivities and the expected anisotropy at the site were assumed. Van Genuchten (1980) parameters were also selected in order to approximate the hydraulic characteristics for the unsaturated soil; these values are listed in Table 7.4.

Table 7.6: Material properties for reservoir embankment

Material Properties	Native Soil	Embankment Soil
k_v (m/s)	1.4×10^{-6}	5×10^{-6}
k_h/k_v (Anisotropy)	10	10
van Genuchten Parameters		
α (kPa^{-1})	0.08	0.55
n	1.23	1.4
m	0.19	0.29
θ_r	0.0032	0.03
θ_s	0.38	0.46

7.5.1.3 Defects

For the lined embankment case, the defect was simulated as a circular hole with a diameter of 1 m. The size of a defect was significantly larger than the defects observed by Nosko and Touze-Foltz (2000). However, like with the previously discussed simulations in Section 7.4.3, these are conservative analyses that were undertaken to evaluate the changes in pore pressures due to leakage through a defect in a geomembrane liner.

The defect was simulated by using an imposed flux boundary condition. In particular, the defect was modeled using a normal flux boundary condition with units of $[L^3/T/L^2]$. The GM-CCL simplified equation [Equation (5.13)] was used to calculate

flow rates using the hydraulic conductivity of the embankment soil ($5x10^{-6}$ m/s), the area of the defect (for a diameter of 1 m), hydraulic gradient, and the hydraulic head imposed on the geomembrane liner (5.5 m). The hydraulic gradient was determined using the localized gradient near the defect for the constant head boundary condition. A hydraulic gradient of 2.17 was used to calculate the flow rates using Equation (5.13). The flow rate predicted using the GM-CCL simplified equation was $1.1x10^{-5}$ m^3/s, using a C_q = 85.6 and a C_{lf} = 3 in Equation (5.13).

7.5.1.4 Boundary Conditions

The defect was assigned a flux boundary condition to simulate the flow through the hole. A no-flow boundary was specified for the rest of the surface around the defect for the face of the embankment and the bottom of the reservoir. A seepage face boundary condition was specified for the bottom boundary and the downstream side of the embankment (opposite of the reservoir). A boundary that is specified as a seepage face will act as a no-flow boundary as long as it remains unsaturated; however, once it becomes saturated, flow will occur across the boundary. The initial condition for the system was obtained from placing a water table at 1 m below the surface of the native soil.

7.5.2 Analysis of Pore Pressures within Embankment

3D finite element simulations were conducted to obtain pore pressures due to leakage through a defect. The results of the simulations are shown in Figures 7.32 for the embankment and reservoir section illustrated in Figure 7.31. The line of zero pressure for the unlined dam was higher in elevation than the simulation involving a lined dam. The line of zero pressure for the unlined dam exits at the downstream toe and the water table is at the surface of the downstream side of the embankment. For the lined embankment,

even with a large defect present, there was not enough water flowing into the system to affect the water table beneath the embankment (i.e., the pore pressures remain unchanged). The approximate lines of seepage shown in Figure 7.32 indicated that the pore pressures were significantly affected by the presence of the geomembrane for this case.

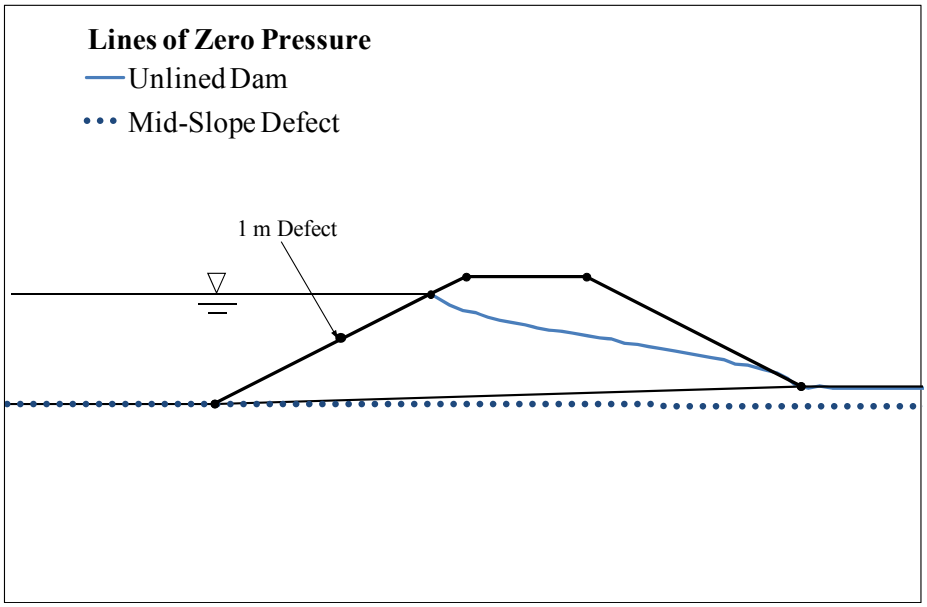

Figure 7.32: Lines of zero pressure for unlined and lined Palmdale embankment section

7.5.3 Stability Analysis

Stability analyses were conducted to determine the effect of leakage through a defect on the downstream slope using the pore pressures obtained from the 3D finite element simulations shown in Figure 7.32. Since the dam has three dimensions, a projection in the X-Z direction at Y=190.5 m was taken to determine the pore pressures. The dam is 381 m so the projection was taken at the middle of the dam, through the center of a defect. Two-dimensional slope stability computations were performed using

UTEXAS4 (Wright 2007), which uses limit equilibrium methods to determine the factor of safety for a slope. For this analysis using UTEXAS4, Spencer's procedure was selected for the stability analyses of a circular failure surfaces that passed through the crest of the dam. A floating grid search was used to find the most critical failure surface for the downstream slope of the dam. The slope stability for the downstream slope was determined for the same geometry as shown in Figure 7.31. The shear strength parameters for both the native soil and the embankment were assumed to be the same as the silty clay in Table 7.2.

The factors of safety for an unlined dam and a lined dam with one defect at mid-slope are listed in Table 7.7. The factor of safety for the embankment dam without a geomembrane liner is the lowest value (FS = 1.68). The presence of the geomembrane leads to a slight increase in the factor of safety. The critical failure surfaces as well as the lines of zero pressure for the unlined dam, a lined dam with one defect and a lined dam with three defects are shown in Figure 7.30. The failure surfaces for both cases are shallow. The failure surface for the unlined case is located on the downstream slope below the exit point of the approximate line of seepage (i.e., line of zero pressure). The improvement in the factor of safety for the lined case over the unlined case would be more pronounced if negative pore pressures were being considered in the analysis, as the entire failure surface is above the line of zero pressure. A factor of safety of 1.99 was obtained when negative pore pressures are considered. However, this was a conservative analysis and negative pore pressures were not taken into consideration when determining the stability of the downstream slope.

Table 7.7: Factors of safety for Palmdale embankment stability analyses

Geomembrane Status	Factor of Safety
Unlined	1.68
One Defect	1.70

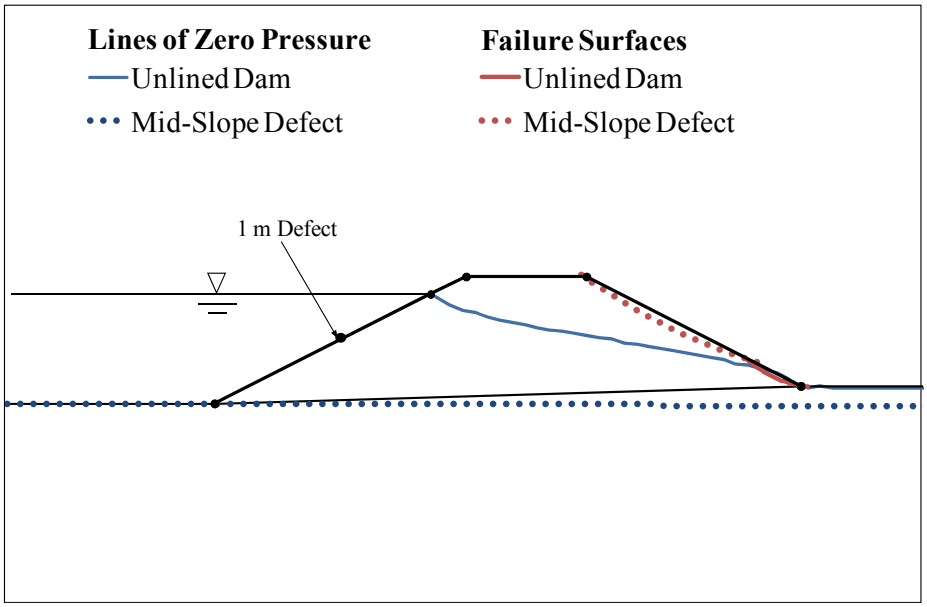

Figure 7.33: Critical failure surfaces for unlined and lined Palmdale embankment section based on pore pressures obtained from 3D seepage analyses

Chapter 8: Conclusions

8.1 Summary of Research Components

The primary goals of this study are to quantify the leakage through defects in geomembrane lining systems for dams and to evaluate the implications of the variables governing the design. Experimental, analytical and numerical analyses were conducted as part of this investigation. Ultimately, the laboratory tests and subsequent analyses were used to develop a set of tools (i.e., empirical models, design recommendations, etc.) that are expected to assist engineers in the design of geomembrane lining systems for dams. This study is expected to contribute towards a better understanding of how geomembranes will perform as dam liners and promote the use of geomembranes in dams.

The specific objectives of this study were reached by conducting the following research components:

- An experimental testing program, which allowed:
    - Compilation of a database of experimental results that quantified the leakage rates through geomembrane defects for high hydraulic heads;
    - Determination of the impact of contact quality between the geomembrane liner and the underlying soil layer;
    - Quantification of the radius of interface flow using visualization techniques;
- An analytical evaluation of the experimental data, which allowed:
    - Characterization of the interface transmissivity between the geomembrane and underlying material using analytical methods based on the experimental data;

- Comparison of the measured radius of interface flow against values obtained using analytical methods;
- Comparison of flow rates calculated using existing equations, developed for low hydraulic heads, against the leakage rates obtained from the experimental testing program to determine their validity for systems with high hydraulic heads;
- Development of new simplified and empirical equations using data from the experimental program to estimate leakage through defects in geomembrane liners under high hydraulic heads.

- Numerical analyses conducted using finite elements, which allowed:
  - Evaluation of the characteristics of the flow behind a geomembrane defect under high hydraulic heads and its implications in the dam performance;
  - Evaluation of the leakage predicted by the analytical model developed by Touze-Foltz et al. (1999) using finite element analysis;
  - Simulation of the permeameter tests for comparison against the leakage rates obtained experimentally;
  - Determination of the effect of the size and frequency of the defects in geomembrane liners on dams on leakage rate using finite element analysis;
  - Evaluation of the impact of leakage through geomembrane defects on the stability of dams using limit equilibrium analysis;
  - Evaluation of the effect of geomembrane liners and their possible defects on the configuration of dams (e.g., need for a blanket drain).

8.2 CONCLUSIONS FROM THE EXPERIMENTAL AND ANALYTICAL COMPONENTS

- The presence of a geomembrane, even with defects, reduces significantly the amount of leakage that occurs through a soil layer, regardless of the hydraulic conductivity of

the soil. However, contact quality between the geomembrane and the soil affects the magnitude of the reduction in the leakage rate.

- The quality of the contact between the geomembrane and the underlying soil layer affects the leakage rate. However, the impact of contact quality on leakage rates decreases with increasing head.
- Leakage rates increased with increasing hydraulic heads for all systems that were tested. The leakage rates for tests conducted by placing a geomembrane over a uniform sand layer increased non-linearly for increasing hydraulic heads. The leakage rates for geomembrane lining systems involving clay layers or GCLS increased linearly for increasing heads.
- The density of the soil layer beneath the geomembrane affects the leakage rate. Soil layers with low density yielded higher leakage rates than soil layers with higher densities, even under low heads.
- Hydration of GCLs prior to application of a high hydraulic head does not have a significant effect on the final leakage rate, unless the interface contact quality is poor.
- While the effect of hydraulic heads less than 21 m on bentonite loss from unhydrated GCL, when placed under a geomembrane with a defect, was evaluated, the results were inconclusive. Bentonite loss was not observed or was negligible for hydraulic heads greater than 21 m.
- A system with a geomembrane liner placed over an unhydrated GCL experienced a higher loss of bentonite than the same system without a geomembrane. However, the leakage rate for the system with a geomembrane was lower than for the system without a geomembrane.

- Contact quality affects the loss of bentonite from a hydrated GCL. "Poor" contact quality results in a higher bentonite loss and a higher leakage rate, even for low heads.
- Leakage rates calculated using Darcy's Law provide upper and lower bounds to the experimental leakage data.
- The back-calculated transmissivity was found to be independent of head for systems involving GCLs, even though leakage increased with head.
- Based on experimental results, flow into the soil layer is not confined to the radius of wetted area. Lateral flow within the soil layer occurs outside the radius of wetted area. A change in terminology from the "radius of wetted area" to the "radius of interface flow" was proposed.
- "Poor" contact quality between the geomembrane and the soil layer resulted in infiltration into the soil layer that was similar to 1D infiltration into a soil layer without a geomembrane liner. The presence of a geomembrane decreases the infiltration rate as long as there is intimate contact between the liner and the surface of the soil.
- Bernoulli's equation for free flow through an orifice, when used with a properly calibrated flow coefficient C, is suitable for predicting leakage through a defect over a highly permeable material.
- Existing equations that are simplified versions of the analytical model developed by Touze-Foltz et al. (1999) for field conditions greatly overestimate leakage through a defect in a geomembrane liner, as these equations were developed for calculating flow through landfill liners.
- New equations could be developed using the experimental data to estimate leakage through a defect in a geomembrane. The equation for laboratory conditions (i.e.,

excellent contact) provides a better fit to the experimental data than existing equations.

8.3 CONCLUSIONS FROM THE NUMERICAL ANALYSIS

- The flow rates measured experimentally for a layer of clay without a geomembrane agreed well with the flow rates calculated using Darcy's Law (area of flow is the area of the permeameter cell) and the flow rates numerically calculated using finite elements.
- The leakage rates obtained from simulations that included an interface gap agreed well with the leakage rates measured in the laboratory tests.
- Using finite element analyses, it was found that the flow rate estimated by the analytical model developed by Touze-Foltz et al. (1999) for field conditions is an order of magnitude less than if three-dimensional flow within the soil layer was considered.
- For the worst-case scenario, the factor of safety against stability is higher when a geomembrane liner is present than when the dam is unlined.
- Three-dimensional simulation of dams with defects in the geomembrane liner provides a more realistic approximation of the leakage through the defect than the worst-case scenario simulations. The leakage rates, and subsequently the pore pressures, are lower when a geomembrane is present than when the dam is unlined.
- For a dam with a geomembrane lining system, defects simulated using a flux boundary condition in the geomembrane liner yielded higher leakage rates than defects simulated using a constant head boundary condition. A constant head boundary condition assumes a perfect contact condition whereas a flux boundary condition based on the new equation takes into account the interface gap. Use of a flux boundary condition provides an engineer with a conservative design.

- A blanket drain increases the factor of safety of the downstream slope of a dam by minimizing the pore pressures in the dam. Also, simulations indicate that the use of a geomembrane liner increases the stability of the downstream slope by minimizing the pore pressures in the body of the dam and keeping a discharge face from forming on the downstream slope. A geomembrane may also eliminate the need for a blanket drain at the downstream toe, which could decrease the cost of construction.

8.4 RECOMMENDATIONS FOR FUTURE RESEARCH

Recommendations for future research include conducting experimental tests on geomembranes over geotextile over soil, preferably using large scale testing equipment. Previous studies, one using low heads (Brown et al. 1987) and one using high heads (Fukuoka 1986), have indicated that placing a geotextile beneath the geomembrane actually results in a lower leakage rate through a defect. The use of a geotextile may be an alternative to using a composite liner system to minimize seepage through a dam. Placing a geotextile behind the geomembrane would also protect the liner, particularly when the soil surface is not smooth (e.g., the soil contains gravel). Also recommended is to conduct further tests to investigate the effect of high pressures acting on the interface transmissivity and contact between the geomembrane and the underlying soil layer. The transmissivity should be evaluated for the low head range and compared with the back-calculated values to discover the cause or validity of the low leakage rates obtained in this study.

The dams analyzed in this study using finite elements involve simple configurations (homogeneous dams). Additional simulations should be performed for more complex and realistic dams. These analyses could provide additional insight on the effectiveness of geomembranes at reducing seepage through dams. The analyses should include different frequencies of defects and a variety of defect sizes. Also, the

simulations should be conducted to investigate the use of geomembranes near or within the core of a dam.

To fully understand the flow through defects in geomembrane liners under high heads, actual seepage data from the field is needed. Laboratory tests and finite element simulations are based on assumptions that affect the measured leakage rates. A full-scale embankment dam with a defect in a geomembrane liner could provide further insight into leakage under high hydraulic heads, especially concerning flow for non-horizontal surfaces (i.e., sloped facing of a dam). The embankment should be heavily instrumented in order to obtain invaluable seepage data behind the geomembrane and within the dam itself. Leakage rates and changes in pore water pressures obtained from the experimental, analytical and numerical components of this study could be validated using the field monitoring data.

Appendix A

The results from each test of the experimental testing program are included in this Appendix. The cumulative volume for both inflow and outflow were recorded over the duration of each test. The flow rates for water flowing in and out of the permeameter cell were determined using the cumulative volume data. The final leakage rate for the each test was reported as the final value of the flow rate into the cell and also as the average value over the last four or five inflow data points. The unit weight, porosity, initial and final water contents, and initial and final degree of saturation were measured and recorded for each test sample. TDR probes were used to record volumetric water contents in several tests and the data from the probes were recorded over the duration of each test. The information regarding the geomembrane and the imposed defect were listed for each test. The transmissivity and the radius of interface flow were back-calculated for each test using the analytical models developed by Touze-Foltz et al. (1999). The flow rates for each test were estimated using equations that were developed as part of this study. All of this information is included in this Appendix.

TEST GMC-L1 (h=0.53 m)
Test conducted: September 1, 2004

Test Details

Hydraulic Head:	0.75 psi (0.53 m)	Geomembrane:	LLDPE (GSE UltraFlex)
Cell Diameter:	6 in. (15 cm)	GM Thickness:	40 mil (1 mm)
Interface Contact:	Poor	Defect Shape:	Circular
		Defect Size:	1/16 in. (1.6 mm)

Comments:
3 TDR probes placed at elevations of 5, 10, and 15 cm

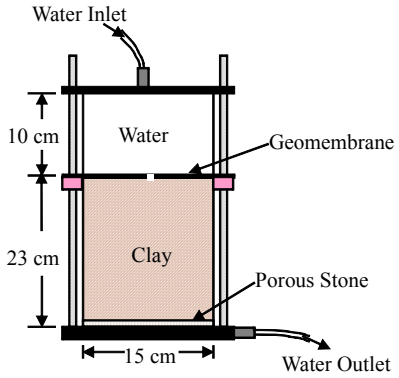

Soil Properties Summary

Soil Type & Classification:	RMA Type II (CL)
Relative Compaction (%)	66
Dry Unit Weight, γ_d (kN/m^3)	12.9
Porosity, n	0.52
Initial Gravimetric Water Content, w_i%	7.3
Initial Degree of Saturation, S_{Ri}%	18.6
Final Gravimetric Water Content, w_f%	29.4
Final Degree of Saturation, S_{Rf}%	74.7

Flow Rate Summary

End Value	1.17E-07	m^3/s
Avg Leakage Rate (3 pts)	1.10E-07	m^3/s

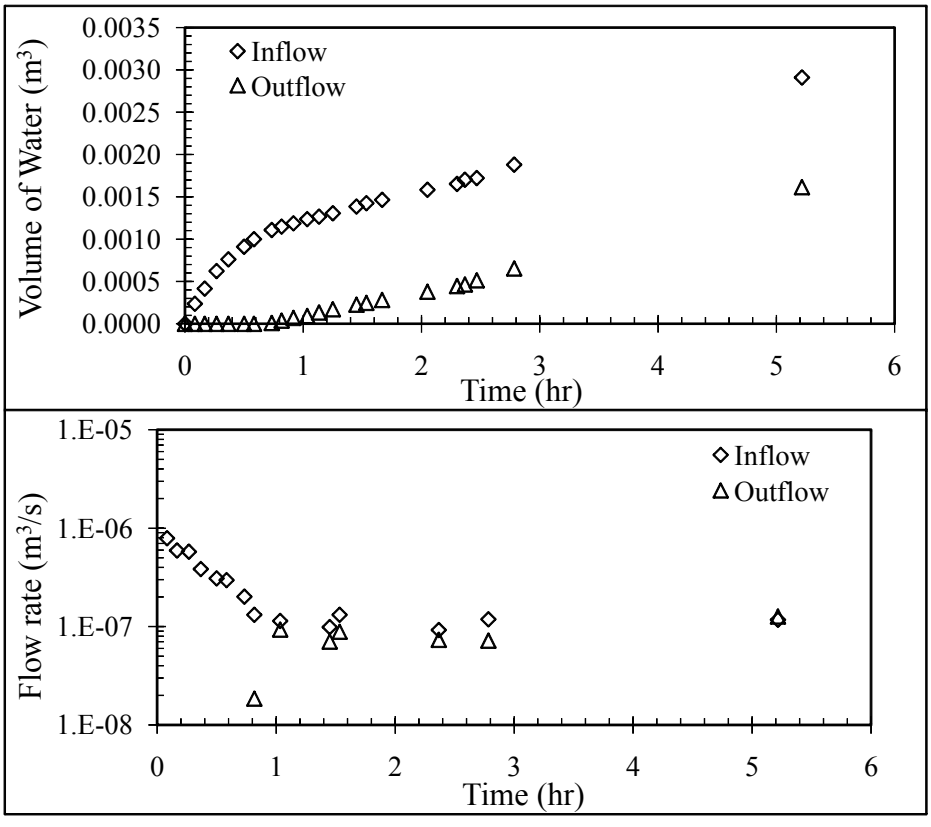

TEST GMC-L1 (h=0.53 m) - Continued

Analytical Models:

Touze-Foltz et al. (1999)	Flow Rate, Q	1.09E-07	m^3/s
	Transmissivity, θ	5.80E-07	m^2/s
	Radius of Wetted Area	0.283	m

Simplified Equations:

Touze-Foltz and Giroud (2003)	Flow Rate, Q_{Poor}	2.34E-06	m^3/s
	Flow Rate, Q_{Good}	4.28E-07	m^3/s
	Flow Rate, $Q_{Excellent}$	1.96E-07	m^3/s

TDR Data

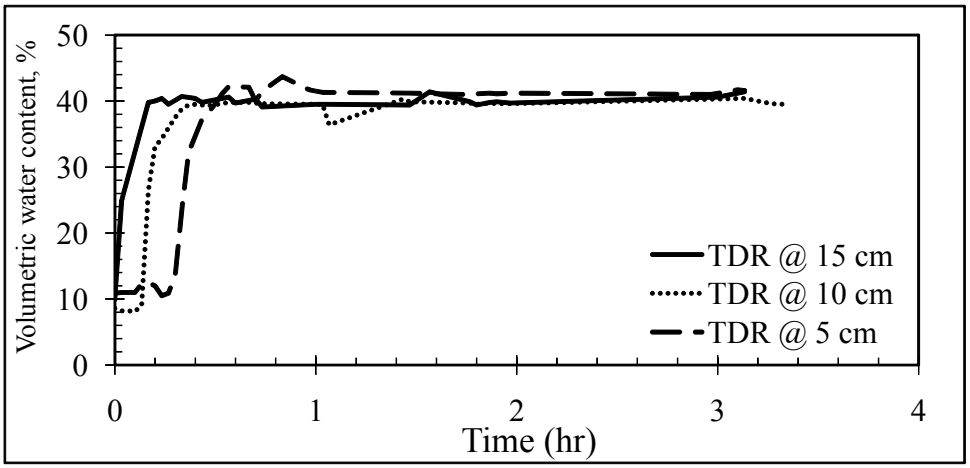

TEST GMC-L2 (h=0.53 m)
Test conducted: September 8-15, 2004

Test Details

Hydraulic Head:	0.75 psi (0.53 m)	Geomembrane:	LLDPE (GSE UltraFlex)
Cell Diameter:	6 in. (15 cm)	GM Thickness:	40 mil (1 mm)
Interface Contact:	Good	Defect Shape:	Circular
		Defect Size:	1/16 in. (1.6 mm)

Comments:
3 TDR probes placed at elevations of 5, 10, and 15 cm

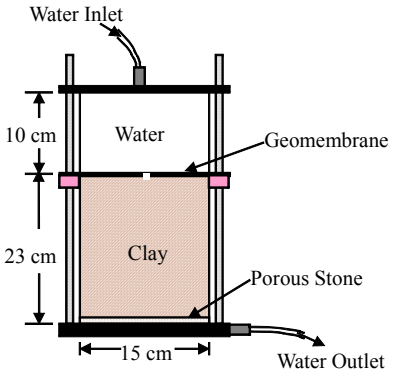

Soil Properties Summary

Soil Type & Classification:	RMA Type II (CL)
Relative Compaction (%)	70
Dry Unit Weight, γ_d (kN/m^3)	13.7
Porosity, n	0.48
Initial Gravimetric Water Content, w_i%	7.6
Initial Degree of Saturation, S_{Ri}%	21.9
Final Gravimetric Water Content, w_f%	29.2
Final Degree of Saturation, S_{Rf}%	84.4

Flow Rate Summary

End Value	1.09E-09	m^3/s
Avg Leakage Rate (5 pts)	1.19E-09	m^3/s

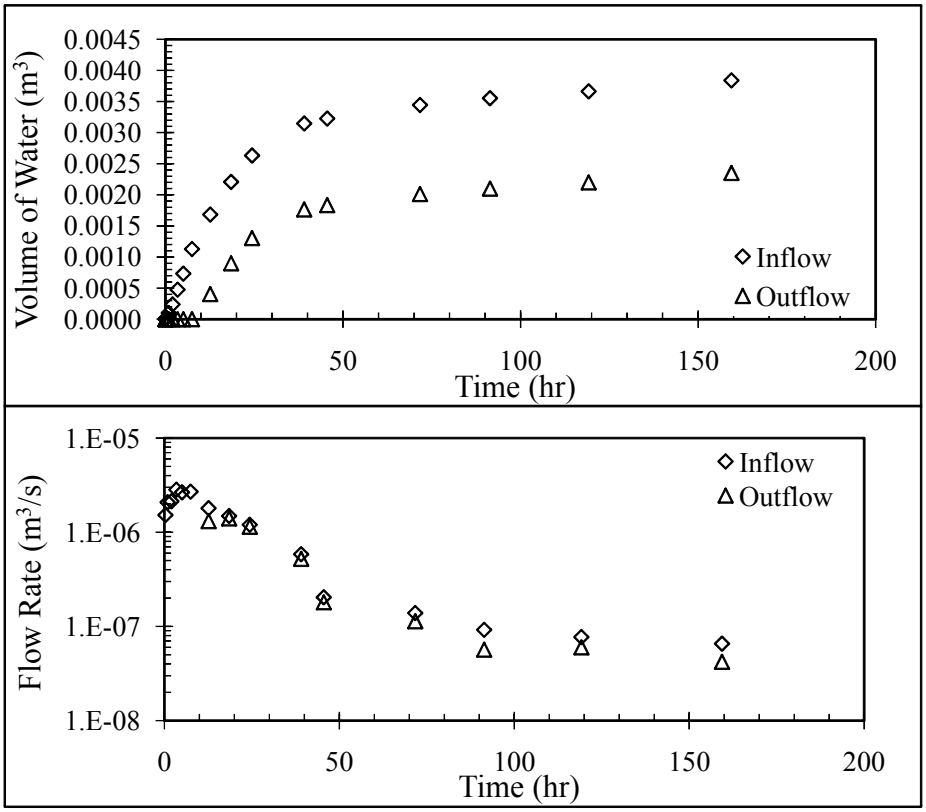

TEST GMC-L2 (h=0.53 m) - Continued

Analytical Models:

Touze-Foltz et al. (1999)	Flow Rate, Q	1.19E-09	m^3/s
	Transmissivity, θ	8.40E-10	m^2/s
	Radius of Wetted Area	0.029	m

Simplified Equations:

Touze-Foltz and Giroud (2003)	Flow Rate, Q_{Poor}	3.44E-06	m^3/s
	Flow Rate, Q_{Good}	6.28E-07	m^3/s
	Flow Rate, $Q_{Excellent}$	2.87E-07	m^3/s

TDR Data

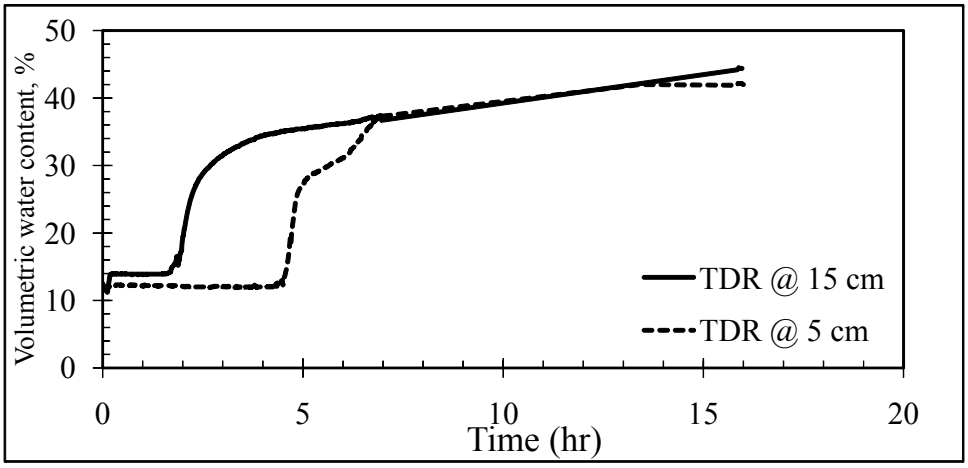

TEST GMC-1 (h=7 m)
Test conducted: November 17-30, 2004

Test Details

Hydraulic Head:	10 psi (7 m)	Geomembrane:	LLDPE (GSE UltraFlex)
Cell Diameter:	6 in. (15 cm)	GM Thickness:	40 mil (1 mm)
Interface Contact:	Good	Defect Shape:	Circular
		Defect Size:	1/16 in. (1.6 mm)

Comments:
3 TDR probes placed at elevations of 5, 10, and 15 cm

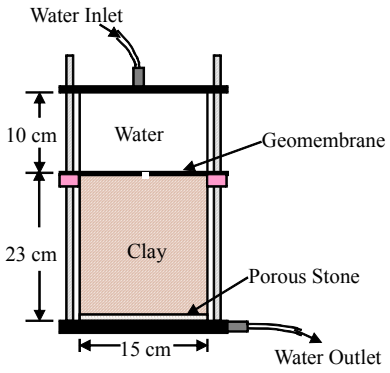

Soil Properties Summary

Soil Type & Classification:	RMA Type II (CL)
Relative Compaction (%)	86
Dry Unit Weight, γ_d (kN/m^3)	16.8
Porosity, n	0.37
Initial Gravimetric Water Content, w_i%	11.5
Initial Degree of Saturation, S_{Ri}%	53.3
Final Gravimetric Water Content, w_f%	17.0
Final Degree of Saturation, S_{Rf}%	78.8

Flow Rate Summary

End Value	4.39E-10	m^3/s
Avg Leakage Rate (5 pts)	4.35E-10	m^3/s

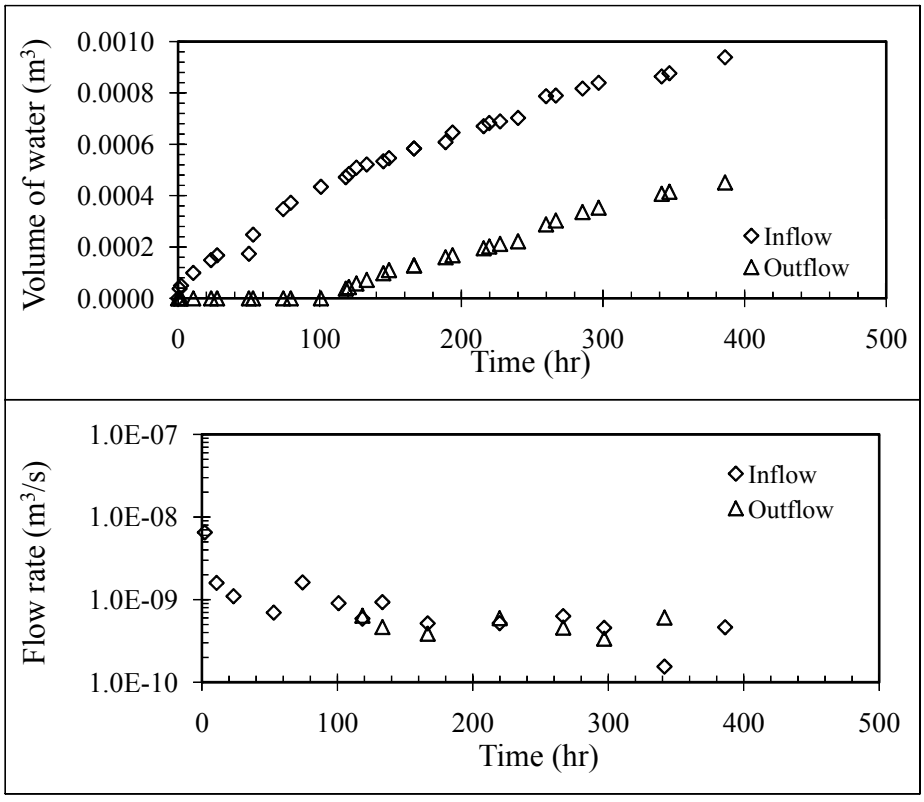

TEST GMC-1 (h=7 m) - Continued

Analytical Models:

Touze-Foltz et al. (1999)	Flow Rate, Q	4.35E-10	m^3/s
	Transmissivity, θ	3.76E-11	m^2/s
	Radius of Wetted Area	0.092	m

Simplified Equations:

Touze-Foltz and Giroud (2003)	Flow Rate, Q_{Poor}	6.02E-06	m^3/s
	Flow Rate, Q_{Good}	1.10E-06	m^3/s
	Flow Rate, $Q_{Excellent}$	5.02E-07	m^3/s
Equation (5.11)	Flow Rate, Q	4.05E-10	m^3/s

TDR Data

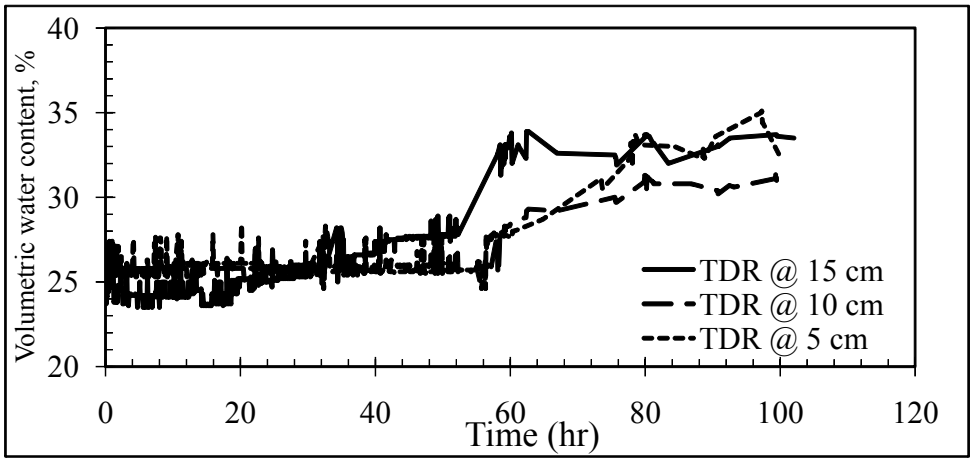

TEST GMC-2 (h=14 m)
Test conducted: April 23, 2007

Test Details

Hydraulic Head:	20 psi (14 m)	Geomembrane:	LLDPE (GSE UltraFlex)
Cell Diameter:	6 in. (15 cm)	GM Thickness:	40 mil (1 mm)
Interface Contact:	Good	Defect Shape:	Circular
		Defect Size:	1/16 in. (1.6 mm)

Soil Properties Summary

Soil Type & Classification:	RMA Type II (CL)
Relative Compaction (%)	87
Dry Unit Weight, γ_d (kN/m^3)	17.0
Porosity, n	0.36
Initial Gravimetric Water Content, w_i%	12.1
Initial Degree of Saturation, S_{Ri}%	58.2
Final Gravimetric Water Content, w_f%	16.5
Final Degree of Saturation, S_{Rf}%	79.2

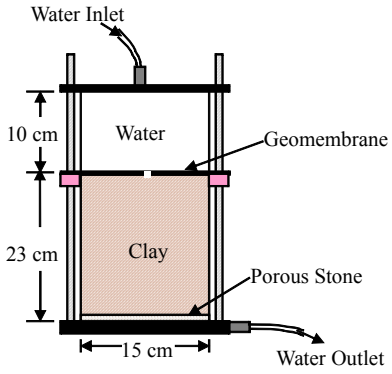

Flow Rate Summary

End Value	1.68E-10	m^3/s
Avg Leakage Rate (3 pts)	2.13E-10	m^3/s

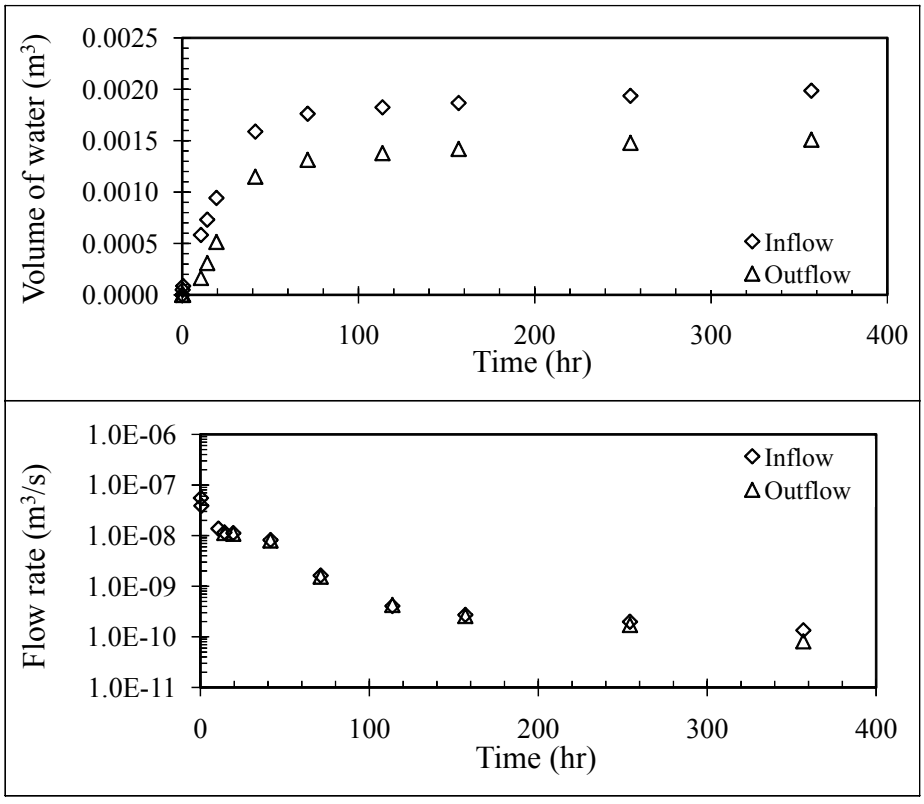

SUMMARY - TEST GMC-2 (h=14 m) - Continued

Analytical Models:

Touze-Foltz et al. (1999)	Flow Rate, Q	2.01E-10	m^3/s
	Transmissivity, θ	6.75E-12	m^2/s
	Radius of Wetted Area	0.036	m

Simplified Equations:

Touze-Foltz and Giroud (2003)	Flow Rate, Q_{Poor}	1.86E-05	m^3/s
	Flow Rate, Q_{Good}	3.40E-06	m^3/s
	Flow Rate, $Q_{Excellent}$	1.56E-06	m^3/s
Equation (5.11)	Flow Rate, Q	7.59E-10	m^3/s

TEST GMC-3 (h=21 m)
Test conducted: June 29, 2006

Test Details

Hydraulic Head:	30 psi (21 m)	Geomembrane:	LLDPE (GSE UltraFlex)
Cell Diameter:	6 in. (15 cm)	GM Thickness:	40 mil (1 mm)
Interface Contact:	Good	Defect Shape:	Circular
		Defect Size:	1/16 in. (1.6 mm)

Soil Properties Summary

Soil Type & Classification:	RMA Type II (CL)
Relative Compaction (%)	88
Dry Unit Weight, γ_d (kN/m^3)	17.1
Porosity, n	0.36
Initial Gravimetric Water Content, w_i%	11.1
Initial Degree of Saturation, S_{Ri}%	54.6
Final Gravimetric Water Content, w_f%	17.0
Final Degree of Saturation, S_{Rf}%	83.8

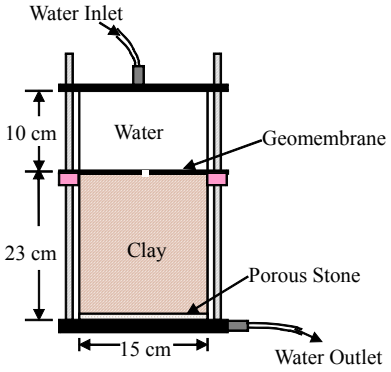

Flow Rate Summary

End Value	1.66E-09	m^3/s
Avg Leakage Rate (4 pts)	1.65E-09	m^3/s

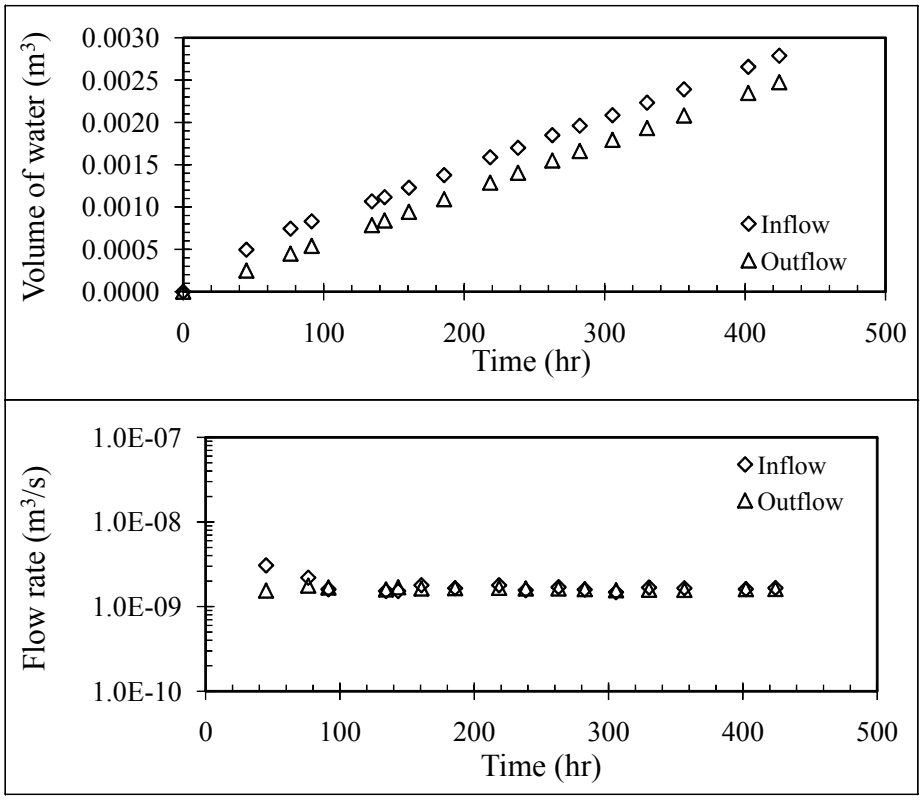

TEST GMC-3 (h=21 m) - Continued

Analytical Models:

Touze-Foltz et al. (1999)	Flow Rate, Q	1.65E-09	m^3/s
	Transmissivity, θ	5.33E-11	m^2/s
	Radius of Wetted Area	0.102	m

Simplified Equations:

Touze-Foltz and Giroud (2003)	Flow Rate, Q_{Poor}	3.70E-05	m^3/s
	Flow Rate, Q_{Good}	6.75E-06	m^3/s
	Flow Rate, $Q_{Excellent}$	3.09E-06	m^3/s
Equation (5.11)	Flow Rate, Q	1.10E-09	m^3/s

TEST GMC-4 (h=28 m)
Test conducted: July 21, 2006

Test Details

Hydraulic Head:	40 psi (28 m)	Geomembrane:	LLDPE (GSE UltraFlex)
Cell Diameter:	6 in. (15 cm)	GM Thickness:	40 mil (1 mm)
Interface Contact:	Good	Defect Shape:	Circular
		Defect Size:	1/16 in. (1.6 mm)

Soil Properties Summary

Soil Type & Classification:	RMA Type II (CL)
Relative Compaction (%)	89
Dry Unit Weight, γ_d (kN/m^3)	17.3
Porosity, n	0.35
Initial Gravimetric Water Content, w_i%	12.8
Initial Degree of Saturation, S_{Ri}%	64.6
Final Gravimetric Water Content, w_f%	-
Final Degree of Saturation, S_{Rf}%	-

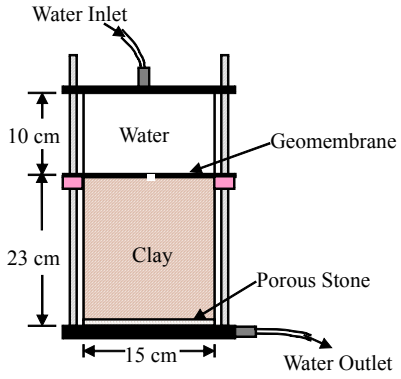

Flow Rate Summary

End Value	2.01E-10	m^3/s
Avg Leakage Rate (4 pts)	8.68E-10	m^3/s

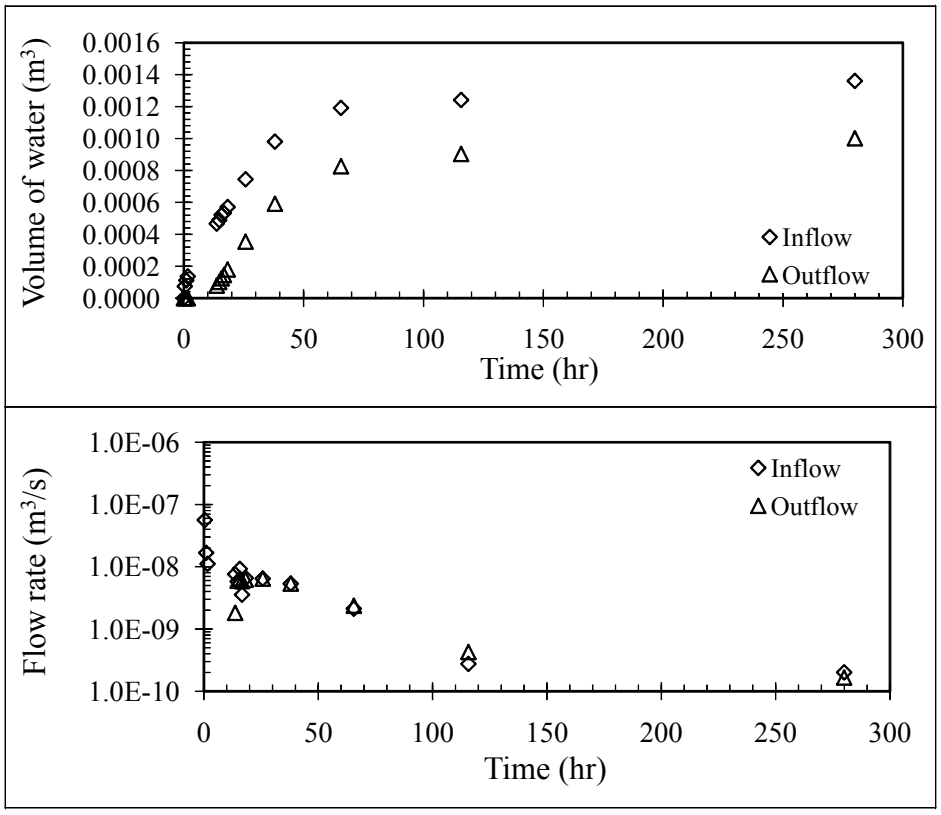

TEST GMC-4 (h=28 m) - Continued

Analytical Models:

Touze-Foltz et al. (1999)	Flow Rate, Q	8.68E-10	m^3/s
	Transmissivity, θ	1.71E-11	m^2/s
	Radius of Wetted Area	0.226	m

Simplified Equations:

Touze-Foltz and Giroud (2003)	Flow Rate, Q_{Poor}	6.09E-05	m^3/s
	Flow Rate, Q_{Good}	1.11E-05	m^3/s
	Flow Rate, $Q_{Excellent}$	5.08E-06	m^3/s
Equation (5.11)	Flow Rate, Q	1.43E-09	m^3/s

TEST GMC-5 (h=35 m)
Test conducted: November 10-15, 2004

Test Details

Hydraulic Head:	50 psi (35 m)	Geomembrane:	LLDPE (GSE UltraFlex)
Cell Diameter:	6 in. (15 cm)	GM Thickness:	40 mil (1 mm)
Interface Contact:	Good	Defect Shape:	Circular
		Defect Size:	1/16 in. (1.6 mm)

Comments:
3 TDR probes placed at elevations of 5, 10, and 15 cm

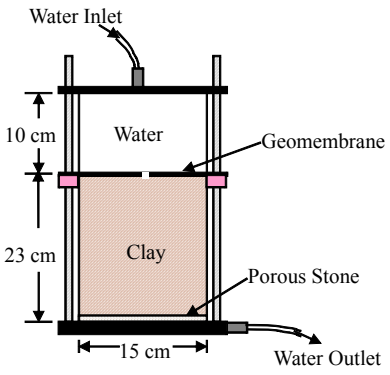

Soil Properties Summary

Soil Type & Classification:	RMA Type II (CL)
Relative Compaction (%)	90
Dry Unit Weight, γ_d (kN/m^3)	17.5
Porosity, n	0.34
Initial Gravimetric Water Content, w_i%	9.8
Initial Degree of Saturation, S_{Ri}%	51.0
Final Gravimetric Water Content, w_f%	15.7
Final Degree of Saturation, S_{Rf}%	81.5

Flow Rate Summary

End Value	5.87E-09	m^3/s
Avg Leakage Rate (5 pts)	5.85E-09	m^3/s

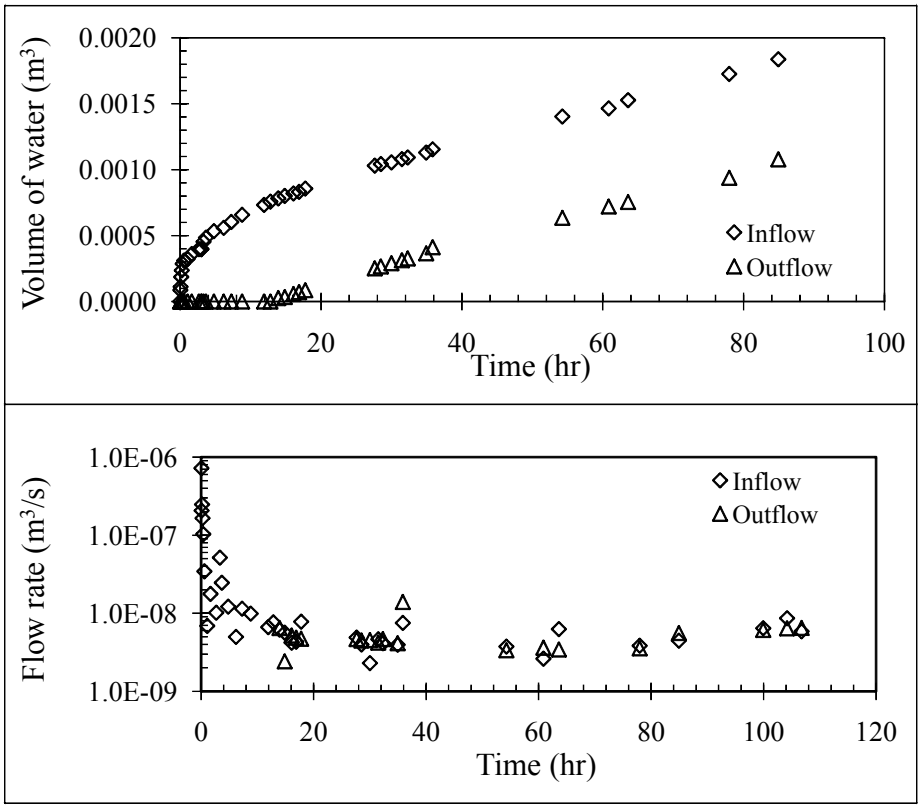

TEST GMC-5 (h=35 m) - Continued

Analytical Models:

Touze-Foltz et al. (1999)	Flow Rate, Q	5.96E-09	m^3/s
	Transmissivity, θ	1.52E-10	m^2/s
	Radius of Wetted Area	0.174	m

Simplified Equations:

Touze-Foltz and Giroud (2003)	Flow Rate, Q_{Poor}	9.17E-05	m^3/s
	Flow Rate, Q_{Good}	1.68E-05	m^3/s
	Flow Rate, $Q_{Excellent}$	7.66E-06	m^3/s
Equation (5.11)	Flow Rate, Q	1.75E-09	m^3/s

TDR Data

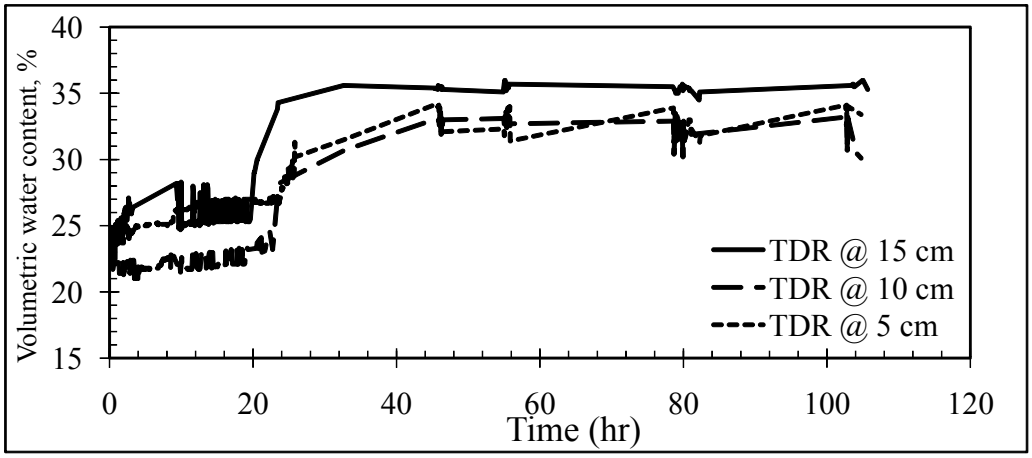

TEST GMC-5P (h=35 m)
Test conducted: January 8-12, 2005

Test Details

Hydraulic Head:	50 psi (35 m)	Geomembrane:	LLDPE (GSE UltraFlex)
Cell Diameter:	6 in. (15 cm)	GM Thickness:	40 mil (1 mm)
Interface Contact:	Poor	Defect Shape:	Circular
		Defect Size:	1/16 in. (1.6 mm)

Comments:
3 TDR probes placed at elevations of 5, 10, and 15 cm

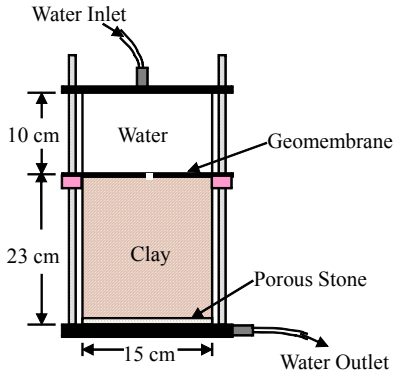

Soil Properties Summary

Soil Type & Classification:	RMA Type II (CL)
Relative Compaction (%)	82
Dry Unit Weight, γ_d (kN/m^3)	16.0
Porosity, n	0.40
Initial Gravimetric Water Content, w_i%	10.7
Initial Degree of Saturation, S_{Ri}%	44.1
Final Gravimetric Water Content, w_f%	16.2
Final Degree of Saturation, S_{Rf}%	66.8

Flow Rate Summary

End Value	2.26E-09	m^3/s
Avg Leakage Rate (4 pts)	2.46E-09	m^3/s

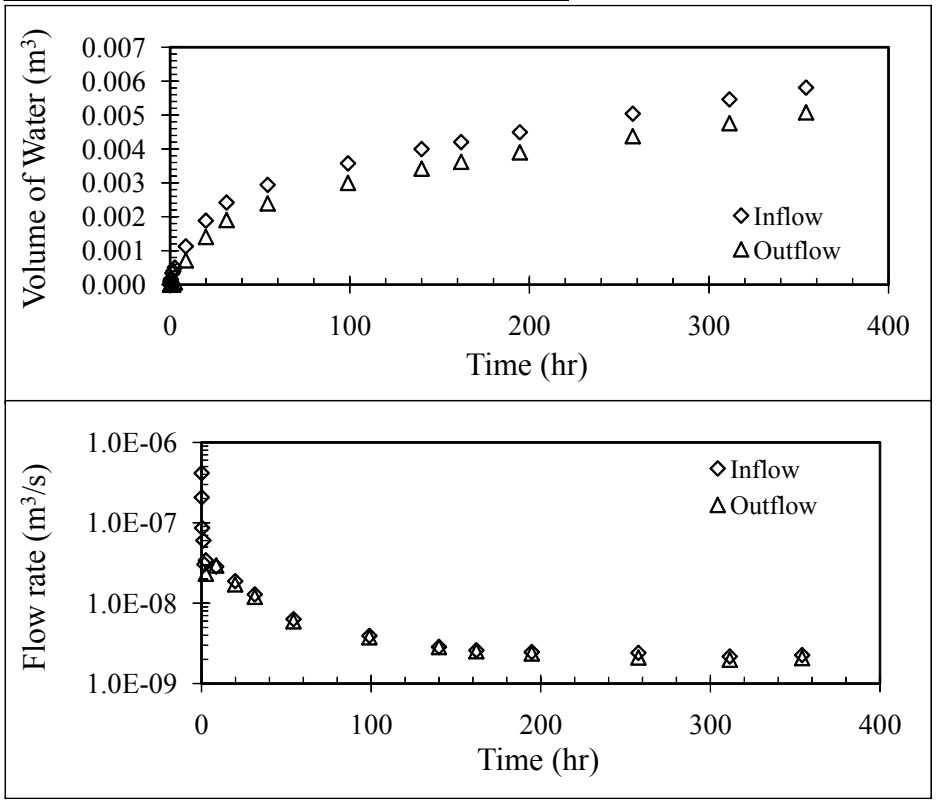

TEST GMC-5P (h=35 m) - Continued

Analytical Models:

Touze-Foltz et al. (1999)	Flow Rate, Q	2.46E-08	m^3/s
	Transmissivity, θ	8.42E-10	m^2/s
	Radius of Wetted Area	0.106	m

Simplified Equations:

Touze-Foltz and Giroud (2003)	Flow Rate, Q_{Poor}	1.10E-03	m^3/s
	Flow Rate, Q_{Good}	2.01E-04	m^3/s
	Flow Rate, $Q_{Excellent}$	9.21E-05	m^3/s

TDR Data

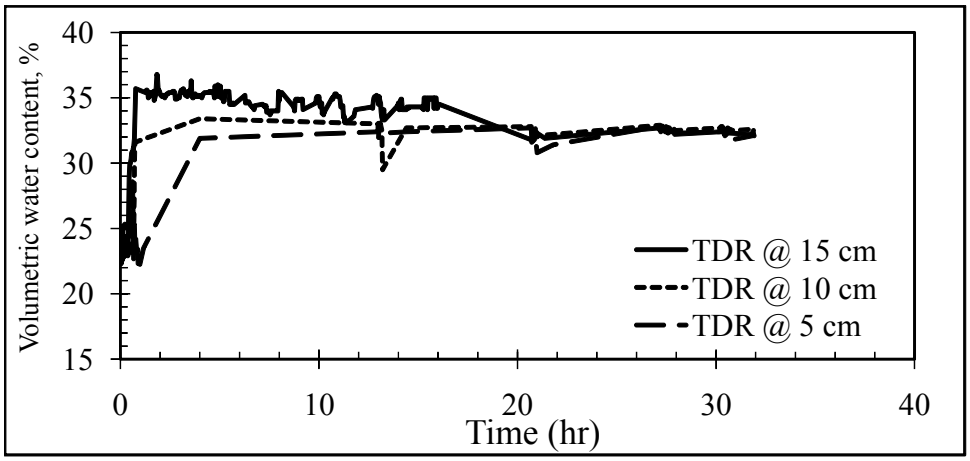

SUMMARY - TEST GMC-6 (h=42 m)
Test conducted: November 15, 2006

Test Details

Hydraulic Head:	60 psi (42 m)	Geomembrane:	LLDPE (GSE UltraFlex)
Cell Diameter:	6 in. (15 cm)	GM Thickness:	40 mil (1 mm)
Interface Contact:	Good	Defect Shape:	Circular
		Defect Size:	1/16 in. (1.6 mm)

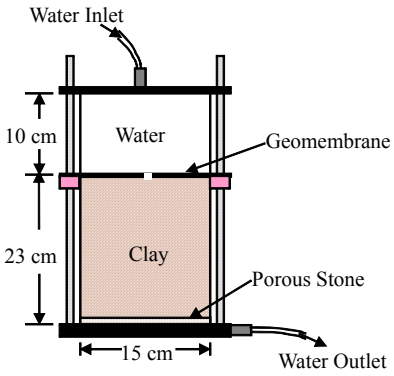

Soil Properties Summary

Soil Type & Classification:	RMA Type II (CL)
Relative Compaction (%)	87
Dry Unit Weight, γ_d (kN/m^3)	17.1
Porosity, n	0.36
Initial Gravimetric Water Content, w_i%	13.7
Initial Degree of Saturation, S_{Ri}%	66.6
Final Gravimetric Water Content, w_f%	-
Final Degree of Saturation, S_{Rf}%	-

Flow Rate Summary

End Value	1.33E-09	m^3/s
Avg Leakage Rate (4 pts)	1.59E-09	m^3/s

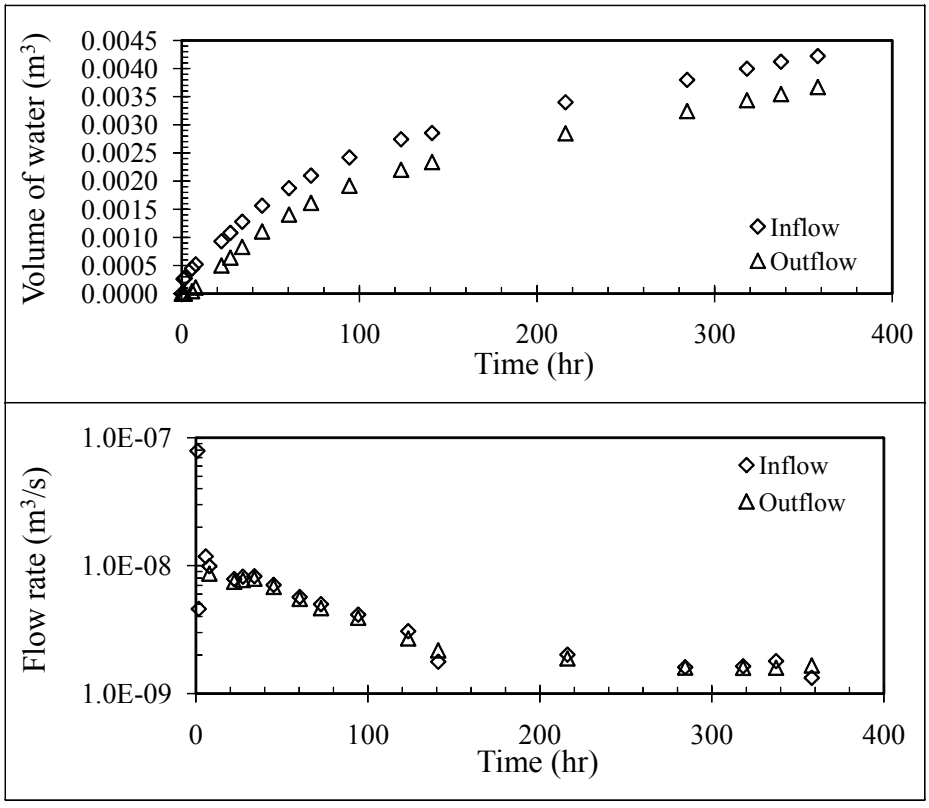

TEST GMC-6 (h=42 m) - Continued

Analytical Models:

Touze-Foltz et al. (1999)	Flow Rate, Q	1.59E-09	m^3/s
	Transmissivity, θ	1.95E-11	m^2/s
	Radius of Wetted Area	0.080	m

Simplified Equations:

Touze-Foltz and Giroud (2003)	Flow Rate, Q_{Poor}	1.24E-04	m^3/s
	Flow Rate, Q_{Good}	2.27E-05	m^3/s
	Flow Rate, $Q_{Excellent}$	1.04E-05	m^3/s
Equation (5.11)	Flow Rate, Q	2.06E-09	m^3/s

TEST GMC-LC1 (h=0.3 m)
Test conducted: May 2007

Test Details

Hydraulic Head:	0.43 psi (0.3 m)	Geomembrane:	LLDPE (GSE UltraFlex)
Cell Diameter:	13 in. (33 cm)	GM Thickness:	40 mil (1 mm)
Interface Contact:	Good	Defect Shape:	Circular
		Defect Size:	1/16 in. (1.6 mm)

Soil Properties Summary

Soil Type & Classification:	RMA Type II (CL)
Relative Compaction (%)	72
Dry Unit Weight, γ_d (kN/m^3)	14.0
Porosity, n	0.47
Initial Gravimetric Water Content, w_i%	11.9
Initial Degree of Saturation, S_{Ri}%	36.0
Final Gravimetric Water Content, w_f%	-
Final Degree of Saturation, S_{Rf}%	-

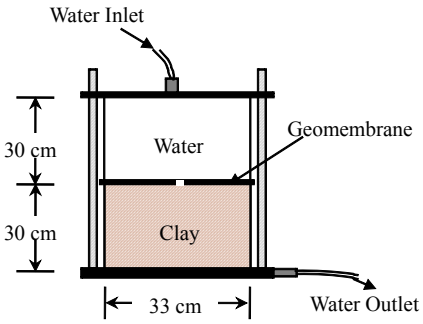

Flow Rate Summary

End Value	3.26E-07	m^3/s
Avg Leakage Rate (4 pts)	3.61E-07	m^3/s

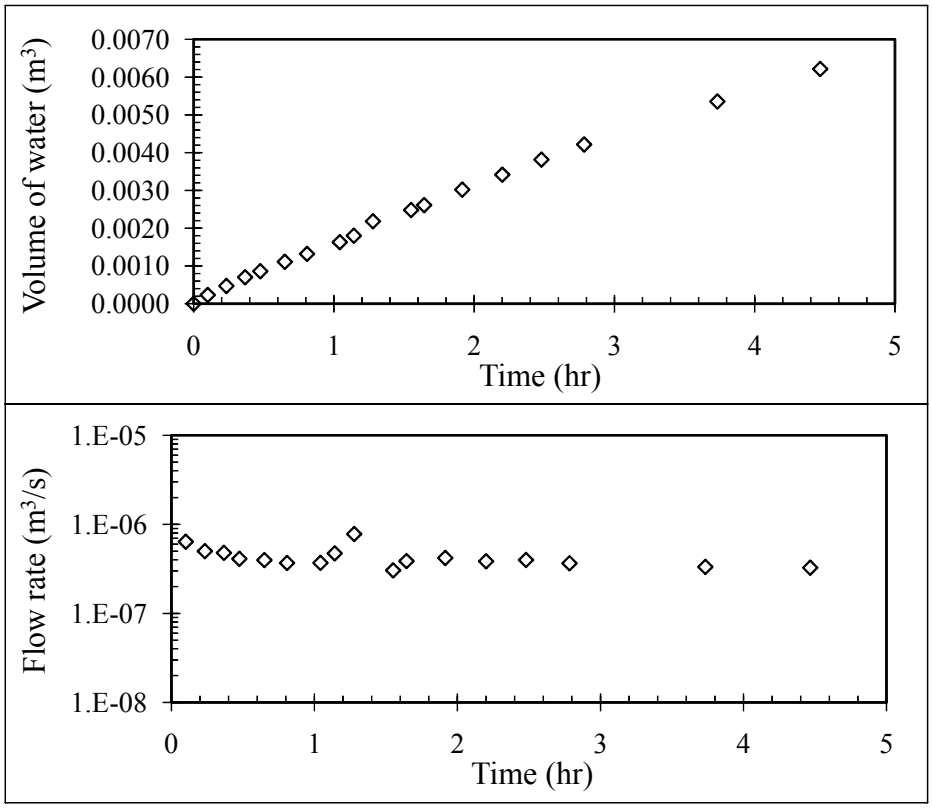

TEST GMC-LC2 (h=7 m)
Test conducted: December 15, 2007

Test Details

Hydraulic Head:	10 psi (7 m)	Geomembrane:	LLDPE (GSE UltraFlex)
Cell Diameter:	13 in. (33 cm)	GM Thickness:	40 mil (1 mm)
Interface Contact:	Good	Defect Shape:	Circular
		Defect Size:	1/16 in. (1.6 mm)

Soil Properties Summary

Soil Type & Classification:	RMA Type II (CL)
Relative Compaction (%)	85
Dry Unit Weight, γ_d (kN/m^3)	16.5
Porosity, n	0.38
Initial Gravimetric Water Content, w_i%	7.0
Initial Degree of Saturation, S_{Ri}%	31.1
Final Gravimetric Water Content, w_f%	19.2
Final Degree of Saturation, S_{Rf}%	85.1

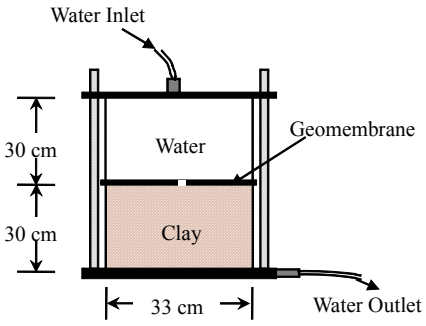

Flow Rate Summary

End Value	8.87E-11	m^3/s
Avg Leakage Rate (4 pts)	9.53E-11	m^3/s

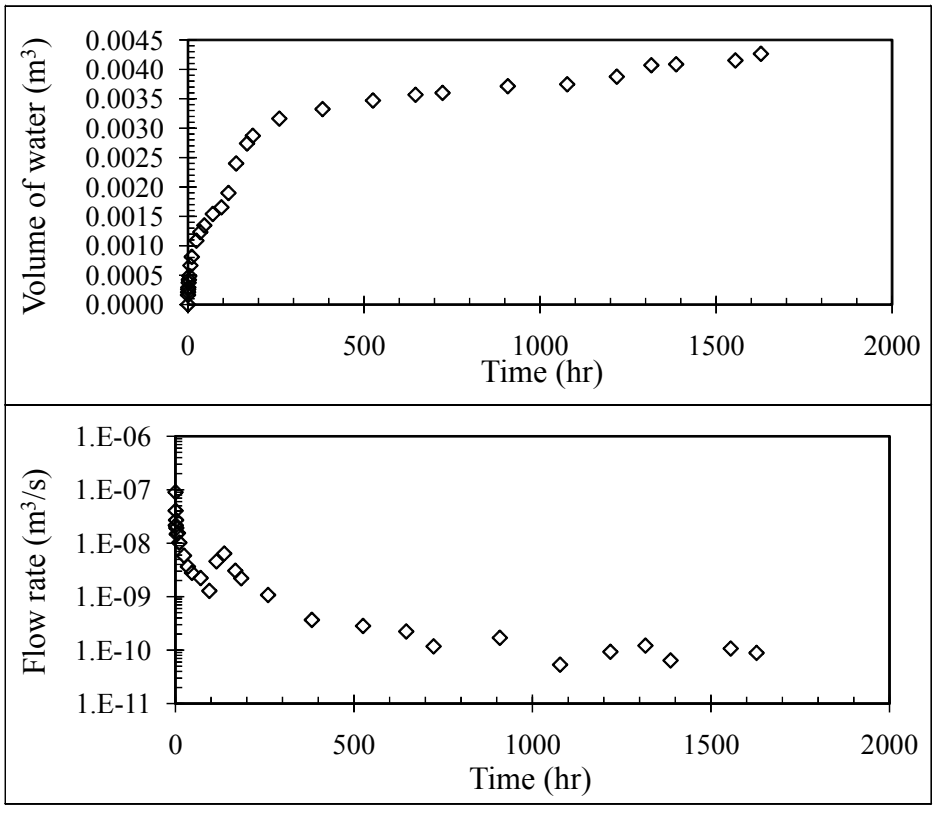

TEST GMC-LC2 (h=7 m) - Continued

Analytical Models:

Touze-Foltz et al. (1999)	Flow Rate, Q	9.52E-11	m^3/s
	Transmissivity, θ	6.32E-12	m^2/s
	Radius of Wetted Area	0.045	m

Simplified Equations:

Touze-Foltz and Giroud (2003)	Flow Rate, Q_{Poor}	5.21E-06	m^3/s
	Flow Rate, Q_{Good}	9.52E-07	m^3/s
	Flow Rate, $Q_{Excellent}$	4.35E-07	m^3/s

TEST GMS-1 (h=3.5 m)
Test conducted: March 16, 2005

Test Details

Hydraulic Head:	5 psi (3.5 m)	Geomembrane:	LLDPE (GSE UltraFlex)
Cell Diameter:	6 in. (15 cm)	GM Thickness:	40 mil (1 mm)
Interface Contact:	Good	Defect Shape:	Circular
		Defect Size:	1/16 in. (1.6 mm)

Soil Properties Summary

Soil Type & Classification:	Monterey #30 Sand (SP)
Unit Weight, γ (kN/m^3)	16.1
Porosity, n	0.38

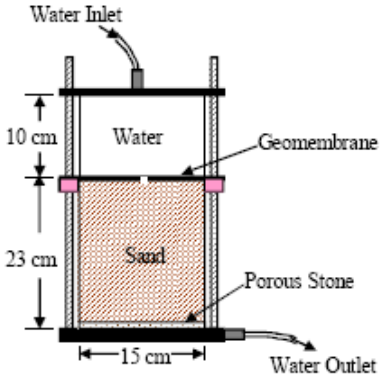

Flow Rate Summary

End Value	3.72E-06	m^3/s
Avg Leakage Rate (3 pts)	3.99E-06	m^3/s

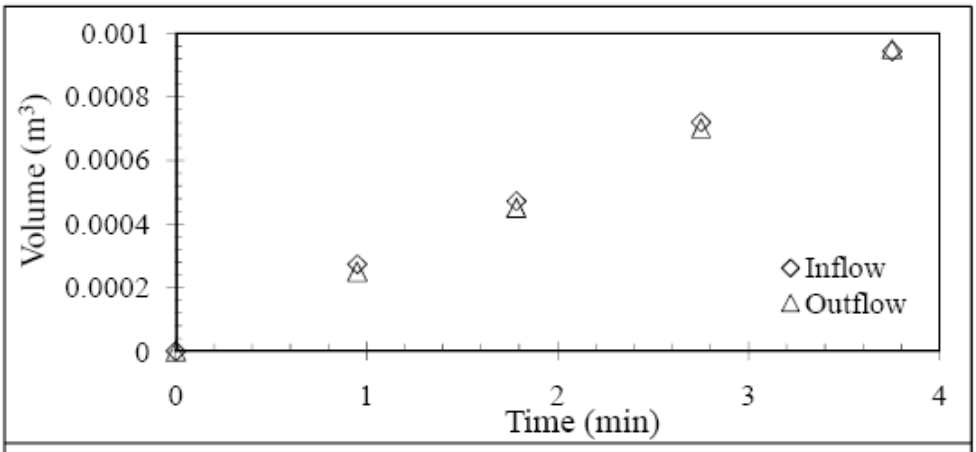

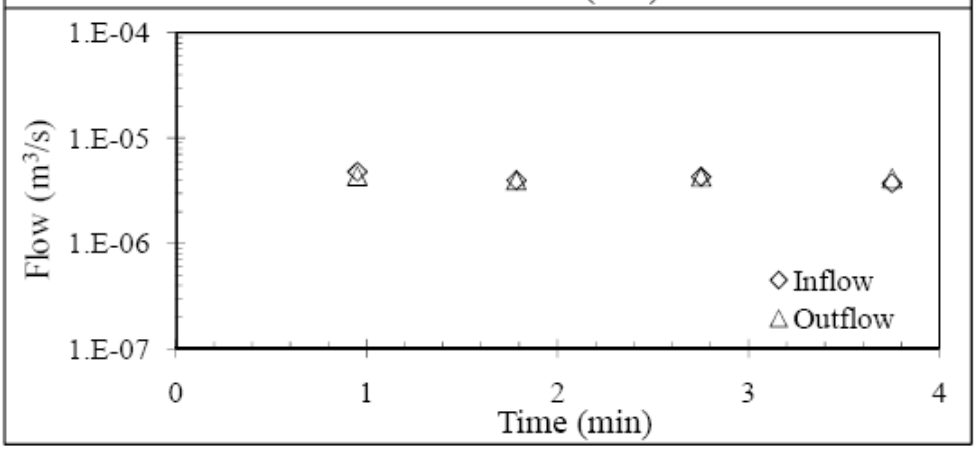

TEST GMS-2 (h=7 m)
Test conducted: March 16, 2005

Test Details

Hydraulic Head:	10 psi (7 m)	Geomembrane:	LLDPE (GSE UltraFlex)
Cell Diameter:	6 in. (15 cm)	GM Thickness:	40 mil (1 mm)
Interface Contact:	Good	Defect Shape:	Circular
		Defect Size:	1/16 in. (1.6 mm)

Soil Properties Summary

Soil Type & Classification:	Monterey #30 Sand (SP)
Unit Weight, γ (kN/m^3)	16.1
Porosity, n	0.38

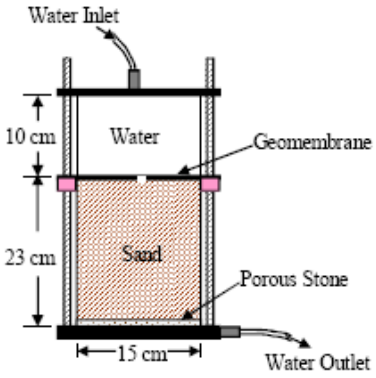

Flow Rate Summary

End Value	6.57E-06	m^3/s
Avg Leakage Rate (4 pts)	7.08E-06	m^3/s

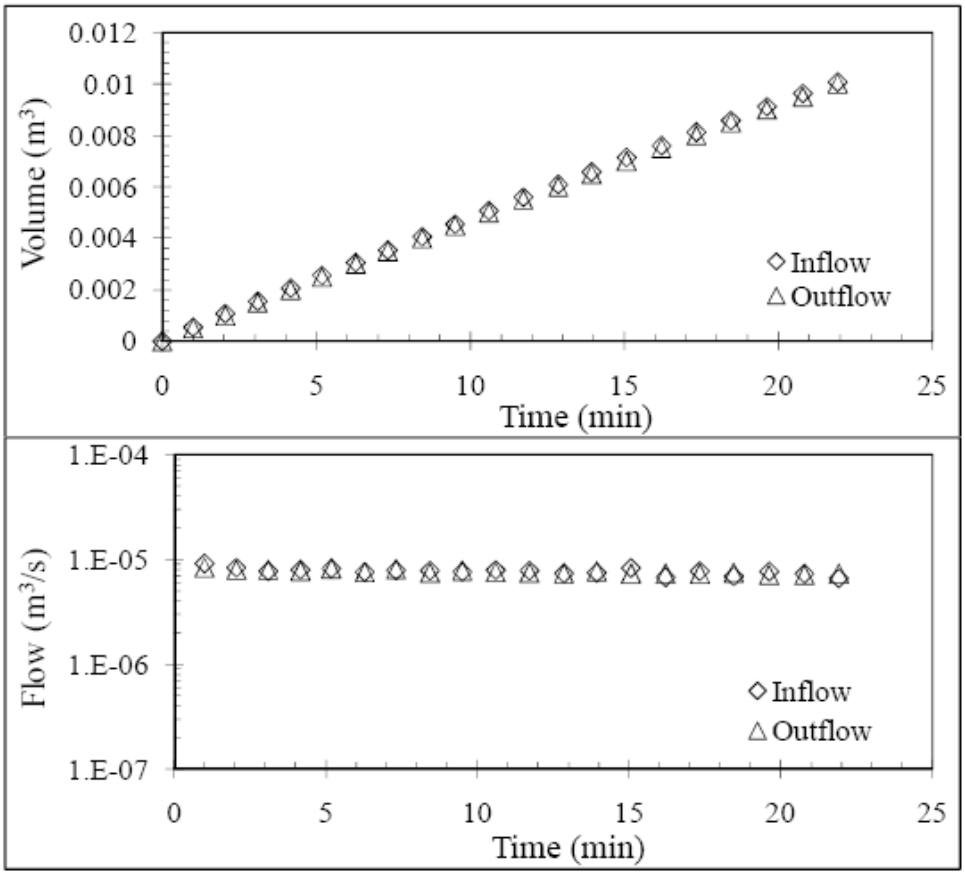

TEST GMS-3 (h=14 m)
Test conducted: March 16, 2005

Test Details

Hydraulic Head:	20 psi (14 m)	Geomembrane:	LLDPE (GSE UltraFlex)
Cell Diameter:	6 in. (15 cm)	GM Thickness:	40 mil (1 mm)
Interface Contact:	Good	Defect Shape:	Circular
		Defect Size:	1/16 in. (1.6 mm)

Soil Properties Summary

Soil Type & Classification:	Monterey #30 Sand (SP)
Unit Weight, γ (kN/m^3)	16.1
Porosity, n	0.38

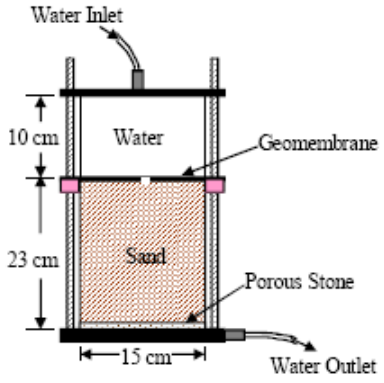

Flow Rate Summary

End Value	1.18E-05	m^3/s
Avg Leakage Rate (3 pts)	1.20E-05	m^3/s

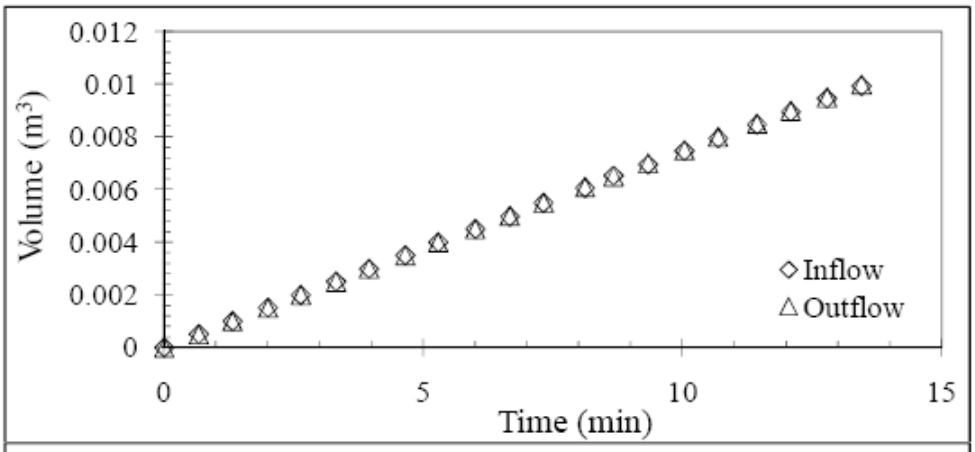

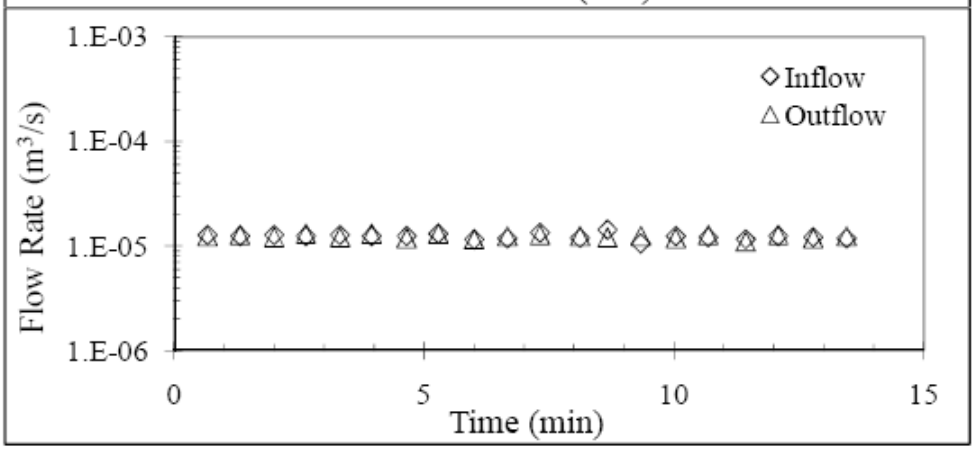

TEST GMS-4 (h=17.5 m)
Test conducted: March 16, 2005

Test Details

Hydraulic Head:	25 psi (17.5 m)	Geomembrane:	LLDPE (GSE UltraFlex)
Cell Diameter:	6 in. (15 cm)	GM Thickness:	40 mil (1 mm)
Interface Contact:	Good	Defect Shape:	Circular
		Defect Size:	1/16 in. (1.6 mm)

Soil Properties Summary

Soil Type & Classification:	Monterey #30 Sand (SP)
Unit Weight, γ (kN/m^3)	16.1
Porosity, n	0.38

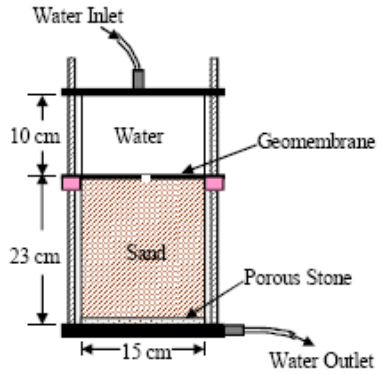

Flow Rate Summary

End Value	1.56E-05	m^3/s
Avg Leakage Rate (4 pts)	1.52E-05	m^3/s

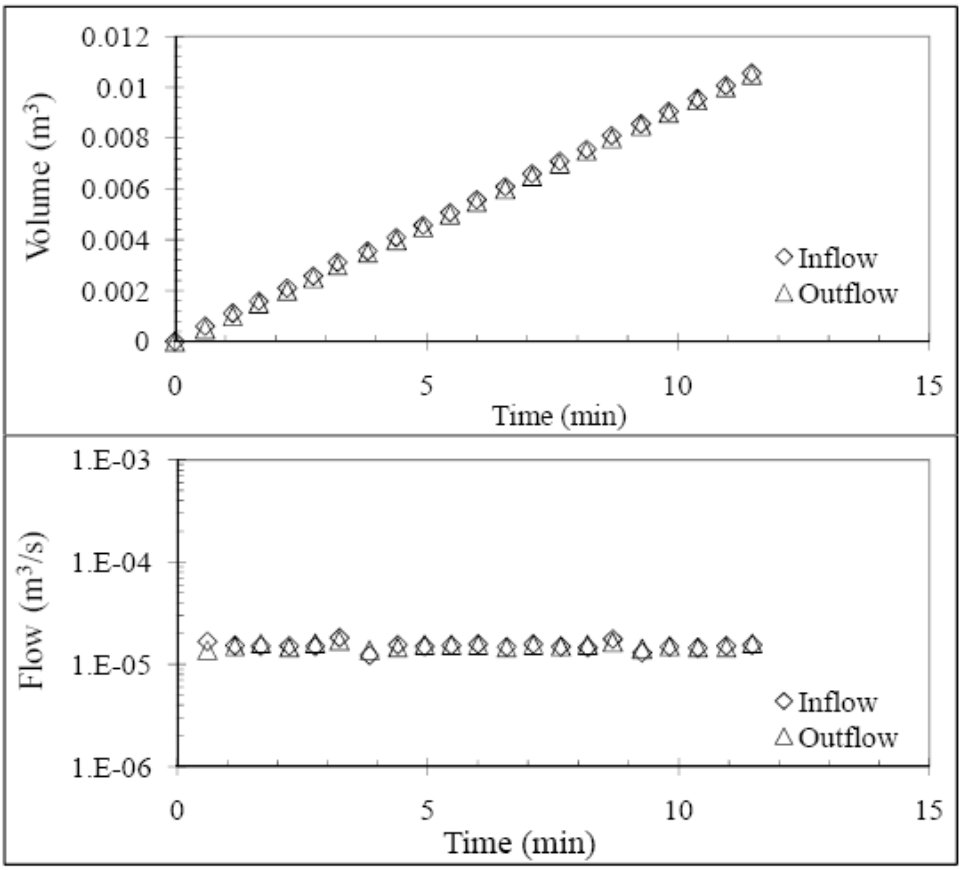

TEST GMS-5 (h=21 m)
Test conducted: March 16, 2005

Test Details

Hydraulic Head:	30 psi (21 m)	Geomembrane:	LLDPE (GSE UltraFlex)
Cell Diameter:	6 in. (15 cm)	GM Thickness:	40 mil (1 mm)
Interface Contact:	Good	Defect Shape:	Circular
		Defect Size:	1/16 in. (1.6 mm)

Soil Properties Summary

Soil Type & Classification:	Monterey #30 Sand (SP)
Unit Weight, γ (kN/m^3)	16.1
Porosity, n	0.38

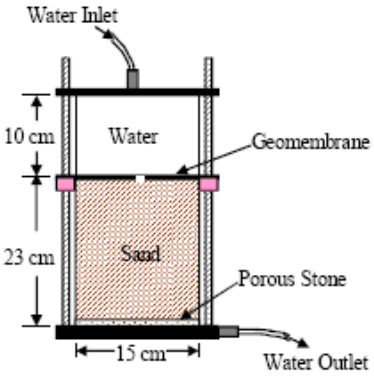

Flow Rate Summary

End Value	1.66E-05	m^3/s
Avg Leakage Rate (5 pts)	1.67E-05	m^3/s

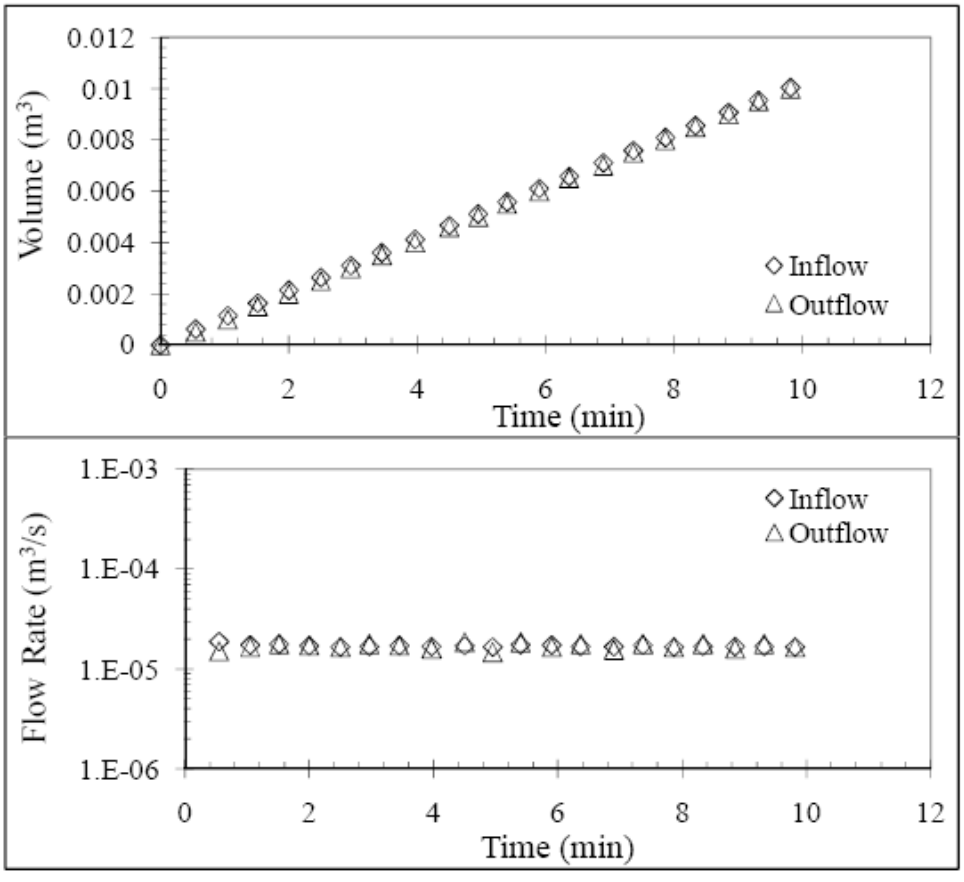

TEST GMS-6 (h=28 m)
Test conducted: March 16, 2005

Test Details

Hydraulic Head:	40 psi (28 m)	Geomembrane:	LLDPE (GSE UltraFlex)
Cell Diameter:	6 in. (15 cm)	GM Thickness:	40 mil (1 mm)
Interface Contact:	Good	Defect Shape:	Circular
		Defect Size:	1/16 in. (1.6 mm)

Soil Properties Summary

Soil Type & Classification:	Monterey #30 Sand (SP)
Unit Weight, γ (kN/m^3)	16.1
Porosity, n	0.38

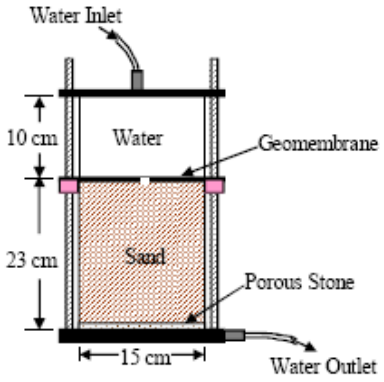

Flow Rate Summary

End Value	2.02E-05	m^3/s
Avg Leakage Rate (5 pts)	2.02E-05	m^3/s

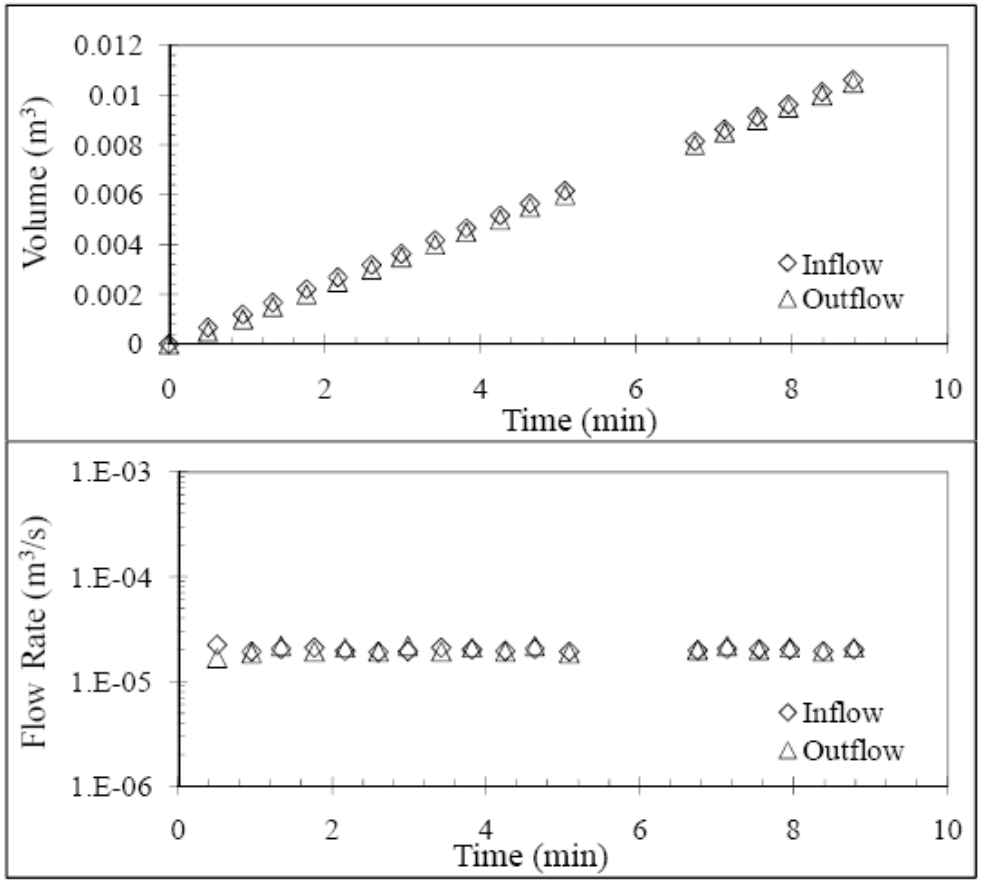

TEST GMS-7 (h=35 m)
Test conducted: March 16, 2005

Test Details

Hydraulic Head:	50 psi (35 m)	Geomembrane:	LLDPE (GSE UltraFlex)
Cell Diameter:	6 in. (15 cm)	GM Thickness:	40 mil (1 mm)
Interface Contact:	Good	Defect Shape:	Circular
		Defect Size:	1/16 in. (1.6 mm)

Soil Properties Summary

Soil Type & Classification:	Monterey #30 Sand (SP)
Unit Weight, γ (kN/m^3)	16.1
Porosity, n	0.38

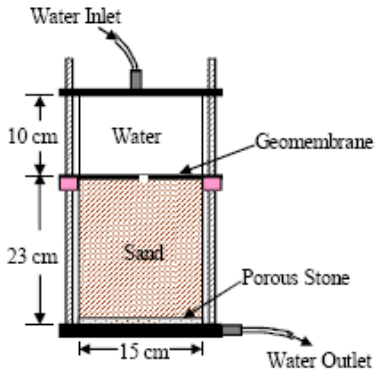

Flow Rate Summary

End Value	2.19E-05	m^3/s
Avg Leakage Rate (5 pts)	2.30E-05	m^3/s

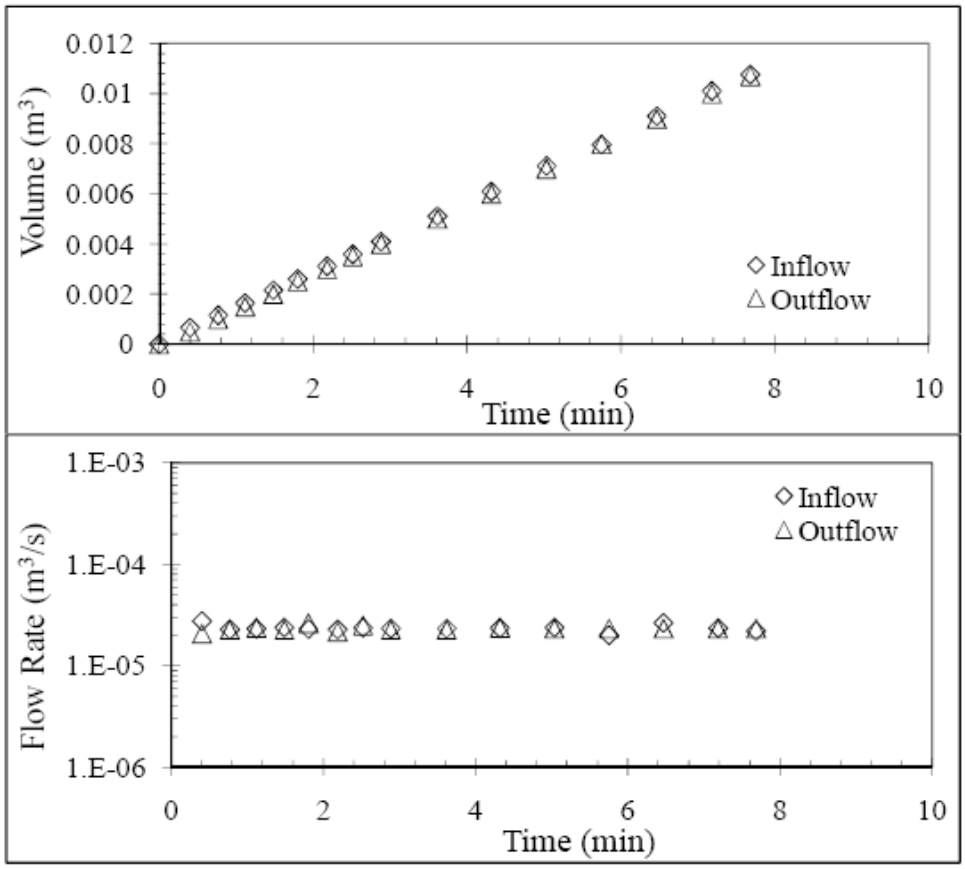

TEST HGCL-1 (h=14 m)
Test conducted: July 28, 2005

Test Details

Hydraulic Head:	20 psi (14 m)	Geomembrane:	LLDPE (GSE UltraFlex)
Cell Diameter:	6 in. (15 cm)	GM Thickness:	40 mil (1 mm)
Interface Contact:	Good	Defect Shape:	Circular
		Defect Size:	1/16 in. (1.6 mm)

GCL Type: Bentofix NWL
Initial Condition: Hydrated under 20 kPa confining pressure

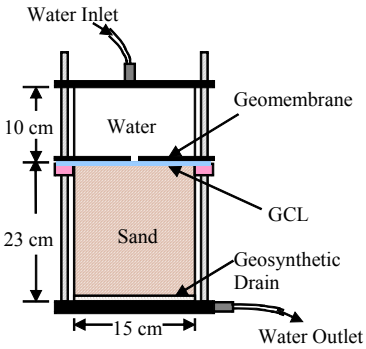

Soil Properties Summary

Soil Type & Classification:	Monterey #30 Sand (SP)
Unit Weight, γ (kN/m^3)	15.9
Porosity, n	0.39
GCL Final Water Content (%)	103.0
GCL Thickness (mm)	6.4

*Sand was saturated before test began.

Flow Rate Summary

End Value	1.08E-09	m^3/s
Avg Leakage Rate (3 pts)	1.29E-09	m^3/s

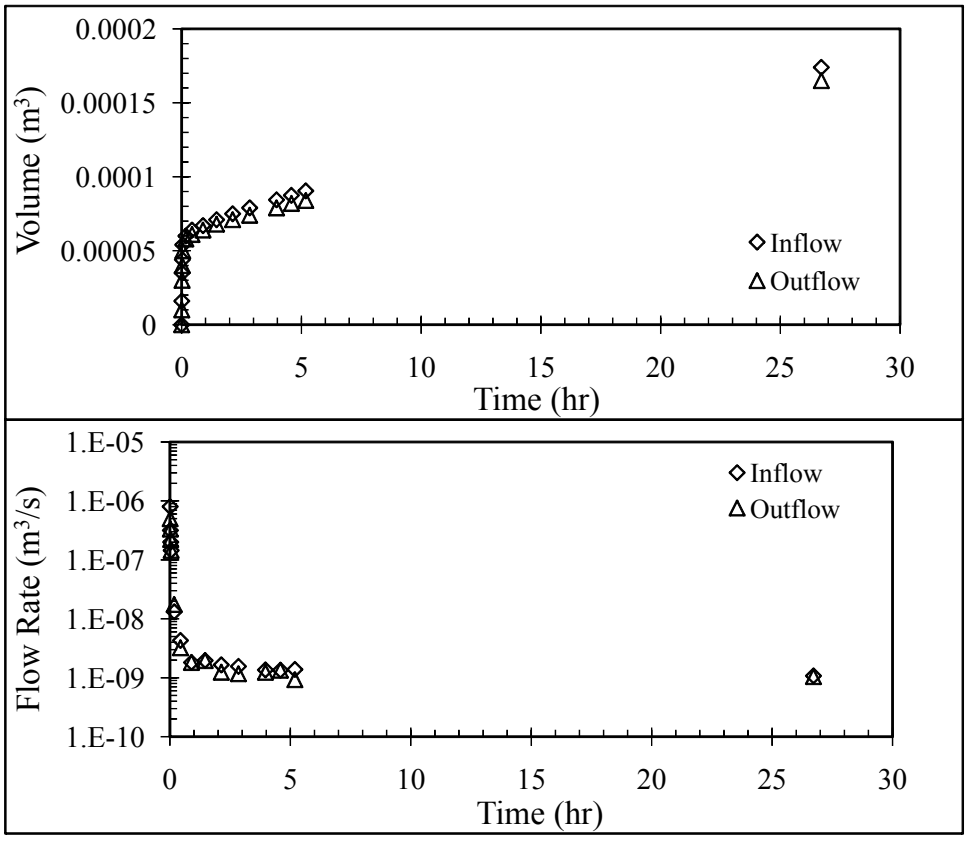

TEST HGCL-1 (h=14 m) - Continued

Analytical Models:

Touze-Foltz et al. (1999)	Flow Rate, Q	1.29E-09	m^3/s
	Transmissivity, θ	7.10E-11	m^2/s
	Radius of Wetted Area	0.325	m

Simplified Equations:

Touze-Foltz and Barroso (2006)	Flow Rate, Q_{GCL}	5.67E-09	m^3/s
Equation (6.2)	Flow Rate, Q	1.33E-09	m^3/s

TEST HGCL-2 (h=21 m)
Test conducted: July 29, 2005

Test Details

Hydraulic Head:	30 psi (21 m)	Geomembrane:	LLDPE (GSE UltraFlex)
Cell Diameter:	6 in. (15 cm)	GM Thickness:	40 mil (1 mm)
Interface Contact:	Good	Defect Shape:	Circular
		Defect Size:	1/16 in. (1.6 mm)

GCL Type: Bentofix NWL
Initial Condition: Hydrated under 20 kPa confining pressure

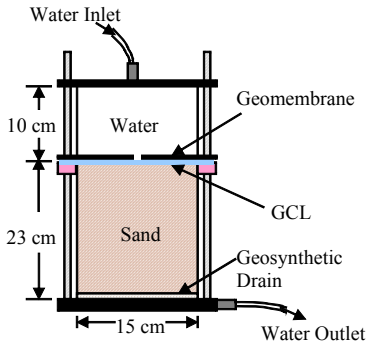

Soil Properties Summary

Soil Type & Classification:	Monterey #30 Sand (SP)
Unit Weight, γ (kN/m^3)	16.0
Porosity, n	0.38
GCL Final Water Content (%)	112.0
GCL Thickness (mm)	8.1

*Sand was saturated before test began.

Flow Rate Summary

End Value	8.87E-10	m^3/s
Avg Leakage Rate (3 pts)	9.55E-10	m^3/s

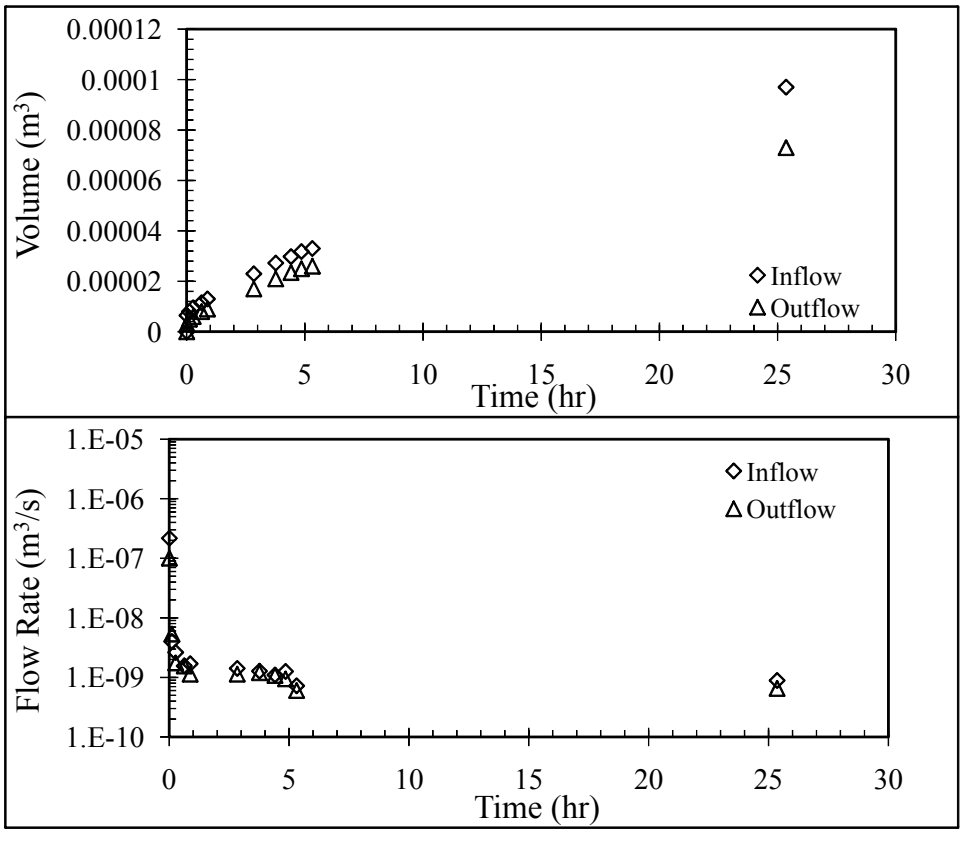

TEST HGCL-2 (h=21 m) - Continued

Analytical Models:

Touze-Foltz et al. (1999)	Flow Rate, Q	9.55E-10	m^3/s
	Transmissivity, θ	3.27E-11	m^2/s
	Radius of Wetted Area	0.249	m

Simplified Equations:

Touze-Foltz and Barroso (2006)	Flow Rate, Q_{GCL}	1.07E-08	m^3/s
Equation (6.2)	Flow Rate, Q	1.79E-09	m^3/s

TEST HGCL-3 (h=28 m)
Test conducted: July 17, 2005

Test Details

Hydraulic Head:	40 psi (28 m)	Geomembrane:	LLDPE (GSE UltraFlex)
Cell Diameter:	6 in. (15 cm)	GM Thickness:	40 mil (1 mm)
Interface Contact:	Good	Defect Shape:	Circular
		Defect Size:	1/16 in. (1.6 mm)

GCL Type: Bentofix NWL
Initial Condition: Hydrated under 2 kPa confining pressure

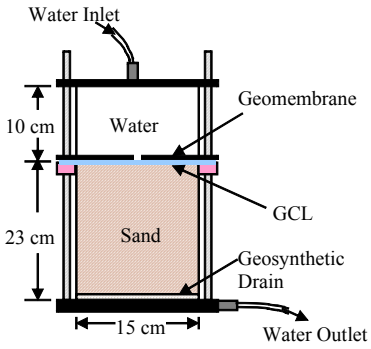

Soil Properties Summary

Soil Type & Classification:	Monterey #30 Sand (SP)
Unit Weight, γ (kN/m^3)	15.9
Porosity, n	0.39
GCL Final Water Content (%)	126.2
GCL Thickness (mm)	10.0

*Sand was saturated before test began.

Flow Rate Summary

End Value	1.59E-09	m^3/s
Avg Leakage Rate (3 pts)	1.51E-09	m^3/s

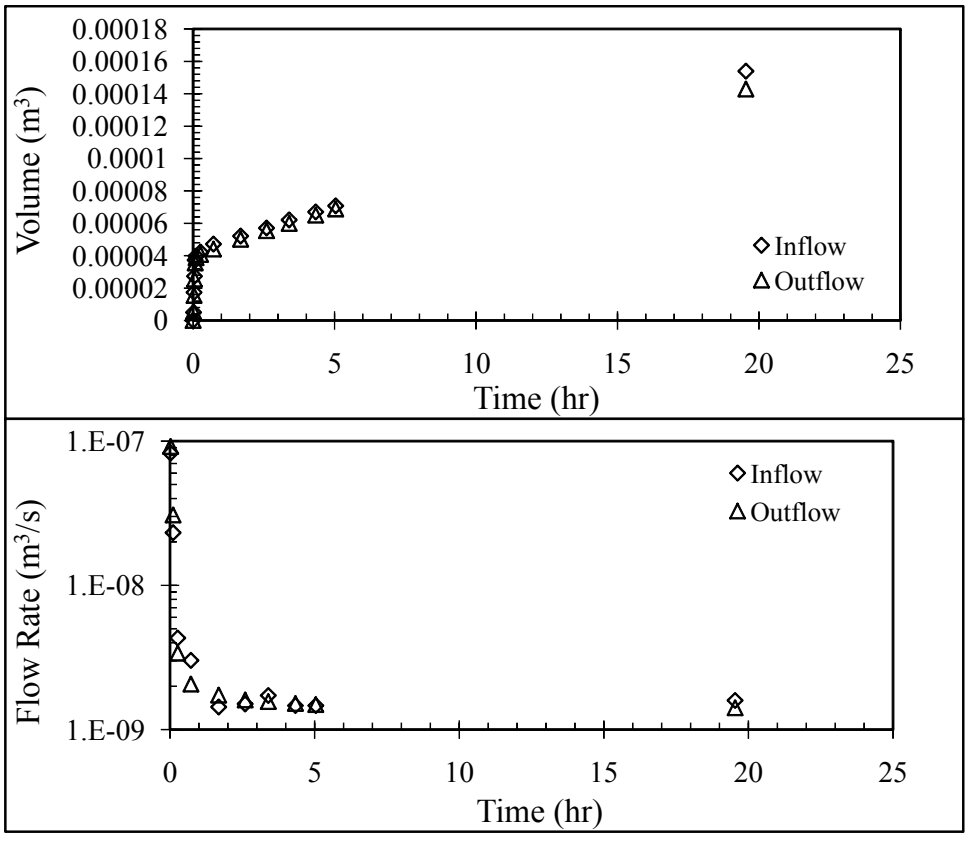

TEST HGCL-3 (h=28 m) - Continued

Analytical Models:

Touze-Foltz et al. (1999)	Flow Rate, Q	1.51E-09	m^3/s
	Transmissivity, θ	3.60E-11	m^2/s
	Radius of Wetted Area	0.307	m

Simplified Equations:

Touze-Foltz and Barroso (2006)	Flow Rate, Q_{GCL}	1.48E-08	m^3/s
Equation (6.2)	Flow Rate, Q	1.91E-09	m^3/s

TEST HGCL-4 (h=28 m)
Test conducted: July 30, 2005

Test Details

Hydraulic Head:	40 psi (28 m)	Geomembrane:	LLDPE (GSE UltraFlex)
Cell Diameter:	6 in. (15 cm)	GM Thickness:	40 mil (1 mm)
Interface Contact:	Good	Defect Shape:	Circular
		Defect Size:	1/16 in. (1.6 mm)

GCL Type: Bentofix NWL
Initial Condition: Hydrated under 20 kPa confining pressure

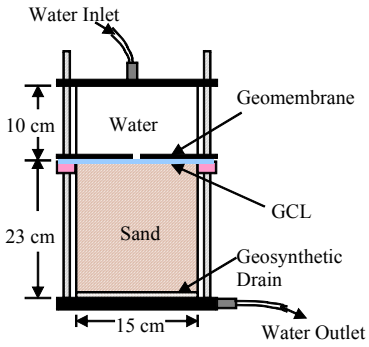

Soil Properties Summary

Soil Type & Classification:	Monterey #30 Sand (SP)
Unit Weight, γ (kN/m^3)	16.0
Porosity, n	0.38
GCL Final Water Content (%)	112.0
GCL Thickness (mm)	8.1

*Sand was saturated before test began.

Flow Rate Summary

End Value	9.02E-10	m^3/s
Avg Leakage Rate (3 pts)	1.23E-09	m^3/s

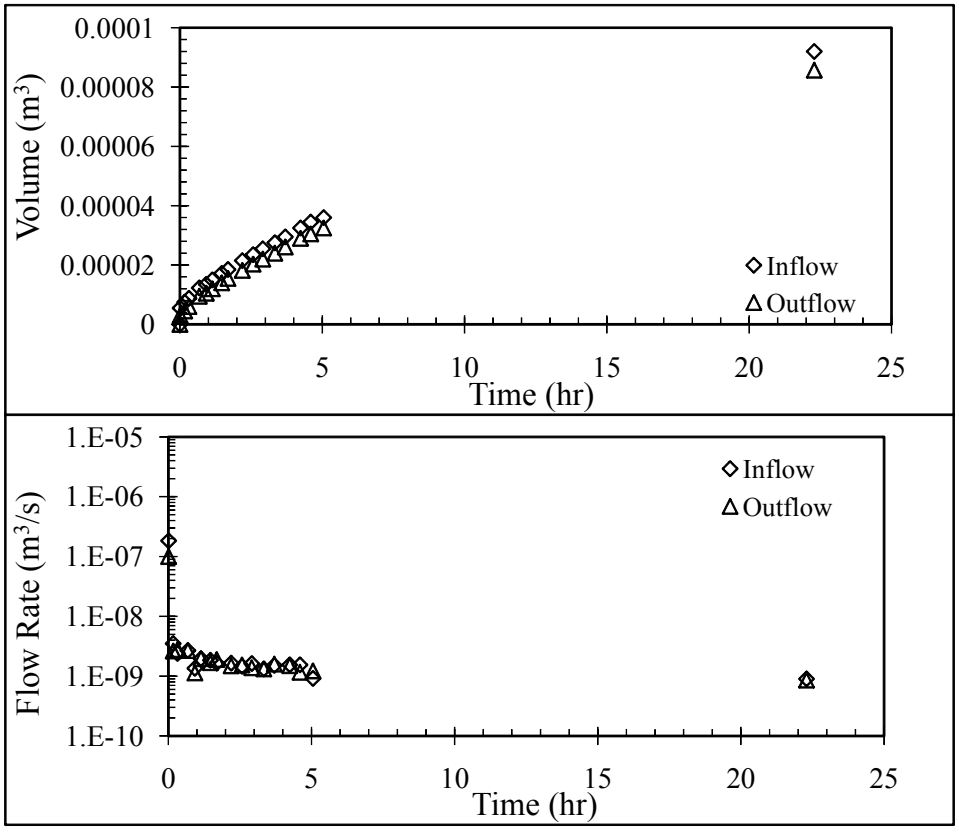

TEST HGCL-4 (h=28 m) - Continued

Analytical Models:

Touze-Foltz et al. (1999)	Flow Rate, Q	1.23E-09	m^3/s
	Transmissivity, θ	3.17E-11	m^2/s
	Radius of Wetted Area	0.263	m

Simplified Equations:

Touze-Foltz and Barroso (2006)	Flow Rate, Q_{GCL}	1.68E-08	m^3/s
Equation (6.2)	Flow Rate, Q	2.20E-09	m^3/s

TEST HGCL-5 (h=35 m)
Test conducted: July 18, 2005

Test Details

Hydraulic Head:	40 psi (28 m)	Geomembrane:	LLDPE (GSE UltraFlex)
Cell Diameter:	6 in. (15 cm)	GM Thickness:	40 mil (1 mm)
Interface Contact:	Good	Defect Shape:	Circular
		Defect Size:	1/16 in. (1.6 mm)

GCL Type: Bentofix NWL
Initial Condition: Hydrated under 2 kPa confining pressure

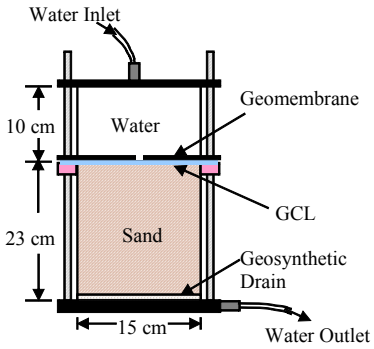

Soil Properties Summary

Soil Type & Classification:	Monterey #30 Sand (SP)
Unit Weight, γ (kN/m^3)	15.9
Porosity, n	0.39
GCL Final Water Content (%)	126.2
GCL Thickness (mm)	10.0

*Sand was saturated before test began.

Flow Rate Summary

End Value	1.55E-09	m^3/s
Avg Leakage Rate (3 pts)	1.51E-09	m^3/s

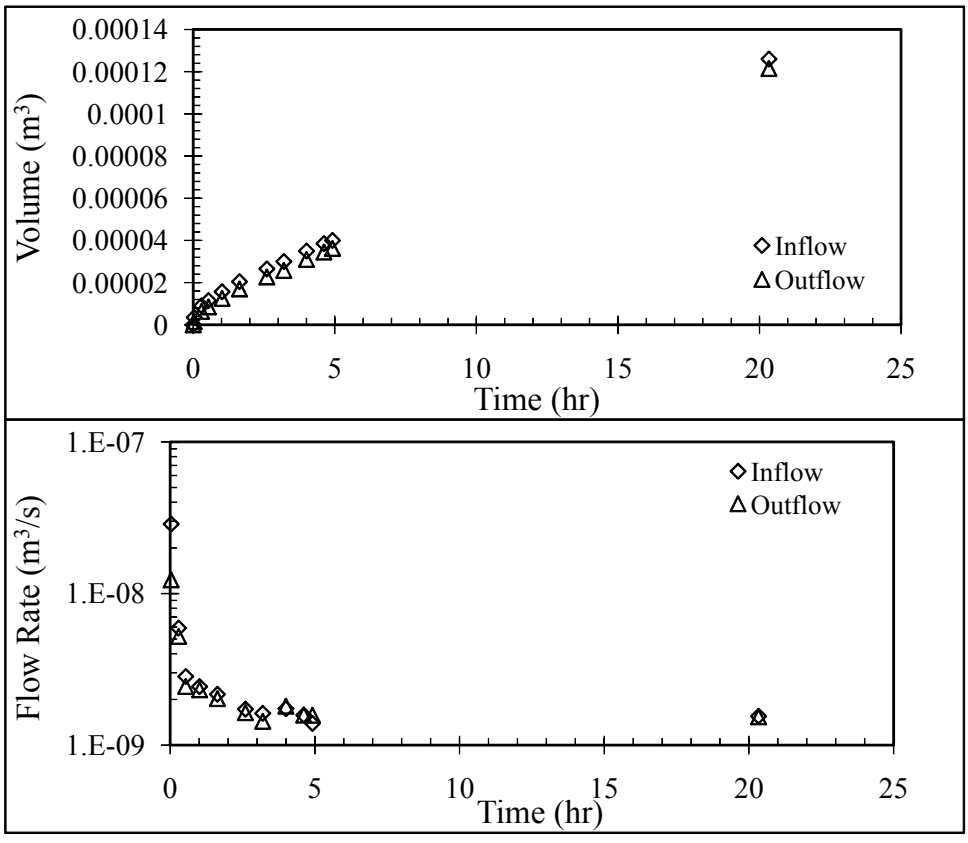

TEST HGCL-5 (h=35 m) - Continued

Analytical Models:

Touze-Foltz et al. (1999)	Flow Rate, Q	1.51E-09	m^3/s
	Transmissivity, θ	3.20E-11	m^2/s
	Radius of Wetted Area	0.305	m

Simplified Equations:

Touze-Foltz and Barroso (2006)	Flow Rate, Q_{GCL}	2.11E-08	m^3/s
Equation (6.2)	Flow Rate, Q	2.24E-09	m^3/s

TEST HGCL-6 (h=42 m)
Test conducted: July 19, 2005

Test Details

Hydraulic Head:	40 psi (28 m)	Geomembrane:	LLDPE (GSE UltraFlex)
Cell Diameter:	6 in. (15 cm)	GM Thickness:	40 mil (1 mm)
Interface Contact:	Good	Defect Shape:	Circular
		Defect Size:	1/16 in. (1.6 mm)

GCL Type: Bentofix NWL
Initial Condition: Hydrated under 2 kPa confining pressure

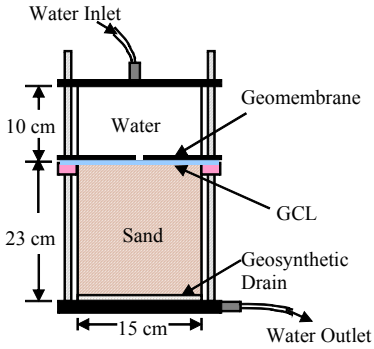

Soil Properties Summary

Soil Type & Classification:	Monterey #30 Sand (SP)
Unit Weight, γ (kN/m^3)	15.9
Porosity, n	0.39
GCL Final Water Content (%)	126.2
GCL Thickness (mm)	10.0

*Sand was saturated before test began.

Flow Rate Summary

End Value	1.86E-09	m^3/s
Avg Leakage Rate (3 pts)	1.85E-09	m^3/s

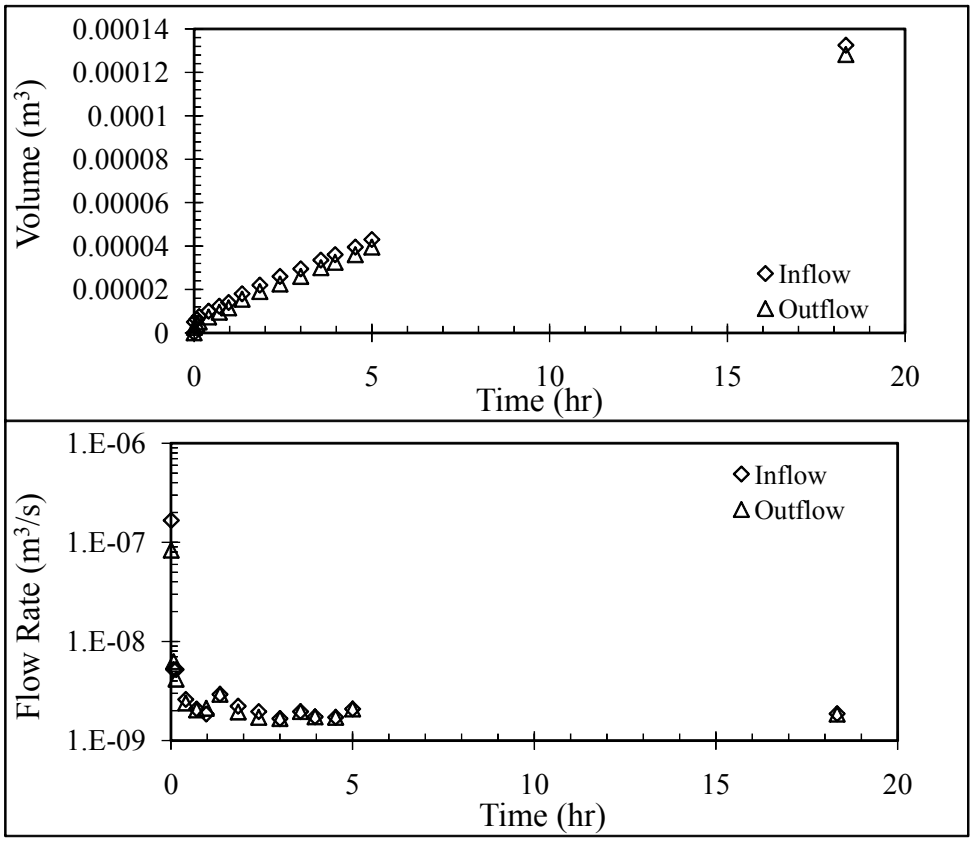

TEST HGCL-6 (h=42 m) - Continued

Analytical Models:

Touze-Foltz et al. (1999)	Flow Rate, Q	1.85E-09	m^3/s
	Transmissivity, θ	3.27E-11	m^2/s
	Radius of Wetted Area	0.321	m

Simplified Equations:

Touze-Foltz and Barroso (2006)	Flow Rate, Q_{GCL}	2.83E-08	m^3/s
Equation (6.2)	Flow Rate, Q	2.56E-09	m^3/s

TEST UGCL-1 (h=7 m)
Test conducted: January 25, 2006

Test Details

Hydraulic Head: 10 psi (7 m)
Cell Diameter: 6 in. (15 cm)
Interface Contact: Good

Geomembrane: LLDPE (GSE UltraFlex)
GM Thickness: 40 mil (1 mm)
Defect Shape: Circular
Defect Size: 1/16 in. (1.6 mm)

GCL Type: Bentofix NWL
Initial Condition: Unhydrated

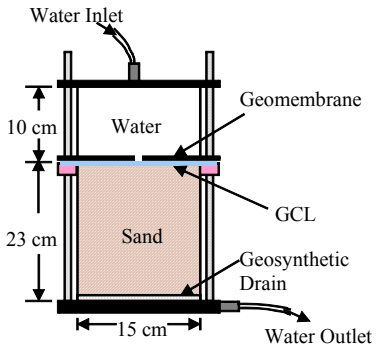

Soil Properties Summary

Soil Type & Classification:	Monterey #30 Sand (SP)
Unit Weight, γ (kN/m^3)	15.9
Porosity, n	0.39
GCL Final Water Content (%)	99.5
GCL Final Thickness (mm)	10.1

*Sand was saturated before test began.

Flow Rate Summary

End Value	3.18E-10	m^3/s
Avg Leakage Rate (4 pts)	3.25E-10	m^3/s

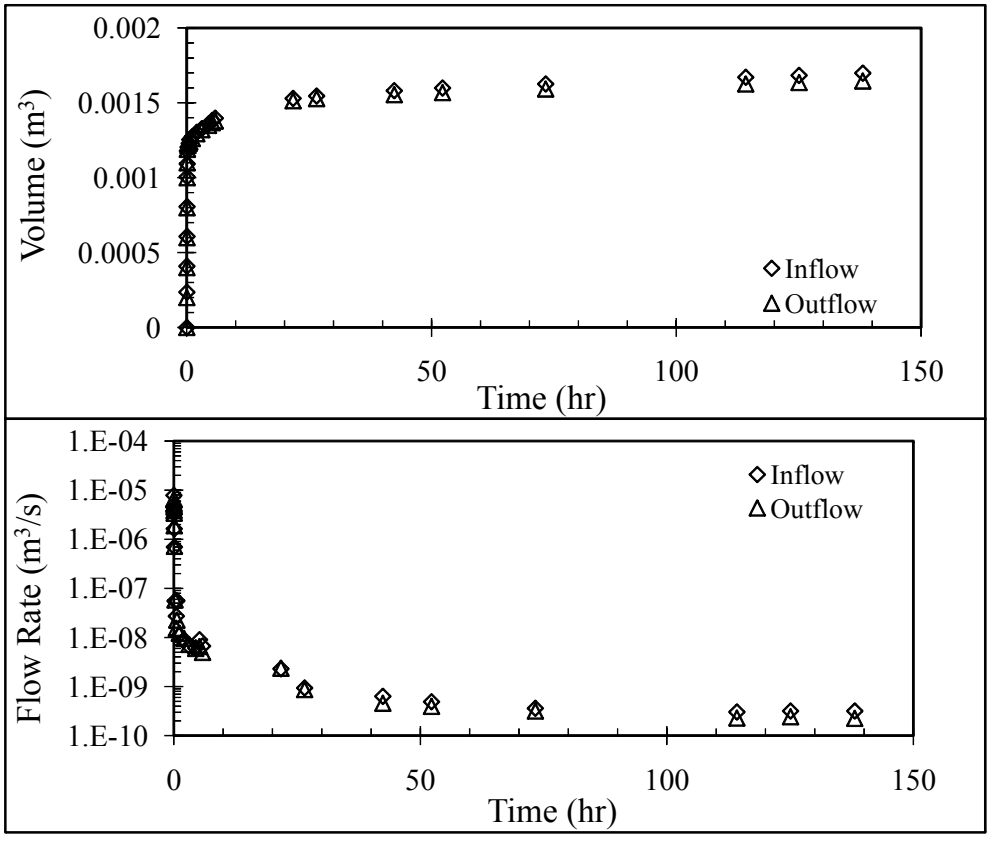

TEST UGCL-1 (h=7 m) - Continued

Analytical Models:

Touze-Foltz et al. (1999)	Flow Rate, Q	3.25E-10	m^3/s
	Transmissivity, θ	2.19E-10	m^2/s
	Radius of Wetted Area	0.321	m

Simplified Equations:

Touze-Foltz and Barroso (2006)	Flow Rate, Q_{GCL}	2.33E-09	m^3/s
Equation (6.2)	Flow Rate, Q	9.70E-10	m^3/s

TEST UGCL-2 (h=14 m)
Test conducted: February 1, 2006

Test Details

Hydraulic Head:	20 psi (14 m)	Geomembrane:	LLDPE (GSE UltraFlex)
Cell Diameter:	6 in. (15 cm)	GM Thickness:	40 mil (1 mm)
Interface Contact:	Good	Defect Shape:	Circular
		Defect Size:	1/16 in. (1.6 mm)
GCL Type:	Bentofix NWL		
Initial Condition:	Unhydrated		

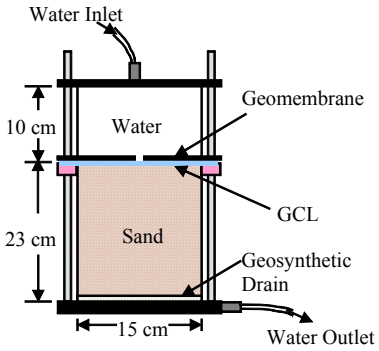

Soil Properties Summary

Soil Type & Classification:	Monterey #30 Sand (SP)
Unit Weight, γ (kN/m^3)	15.8
Porosity, n	0.39
GCL Final Water Content (%)	104.3
GCL Final Thickness (mm)	0.0

*Sand was saturated before test began.

Flow Rate Summary

End Value	9.44E-10	m^3/s
Avg Leakage Rate (3 pts)	1.02E-09	m^3/s

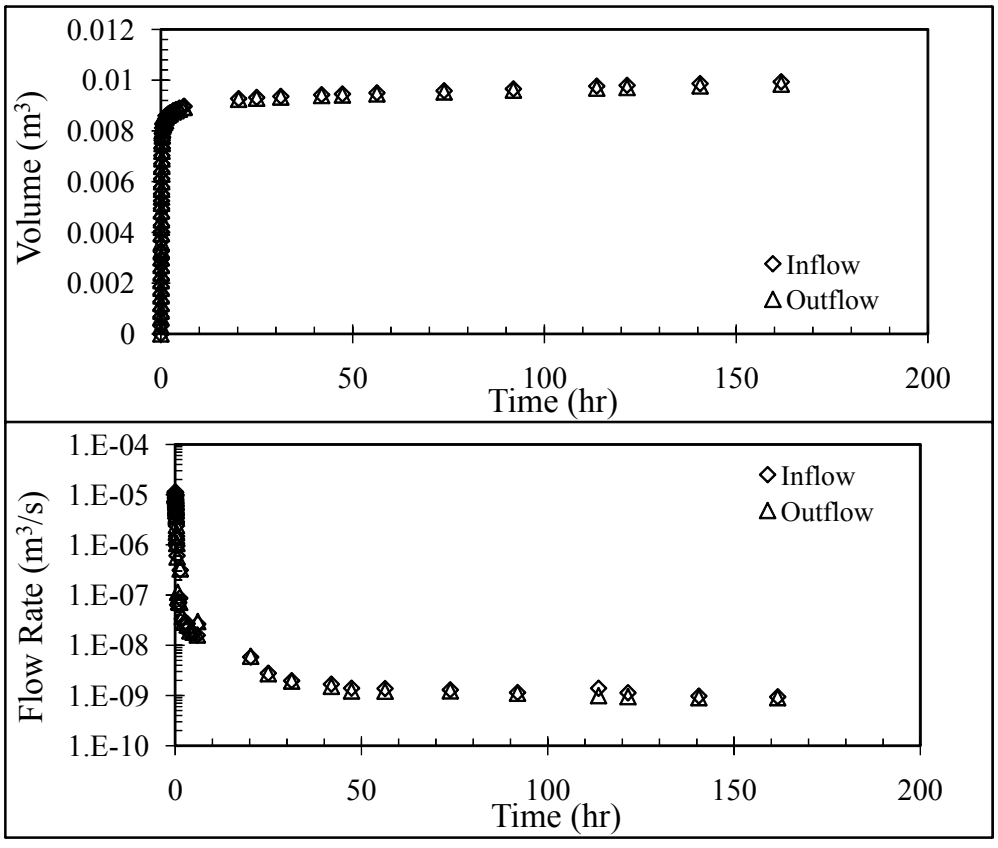

TEST UGCL-2 (h=14 m) - Continued

Analytical Models:

Touze-Foltz et al. (1999)	Flow Rate, Q	1.02E-09	m^3/s
	Transmissivity, θ	1.78E-10	m^2/s
	Radius of Wetted Area	0.321	m

Simplified Equations:

Touze-Foltz and Barroso (2006)	Flow Rate, Q_{GCL}	6.65E-09	m^3/s
Equation (6.2)	Flow Rate, Q	1.59E-09	m^3/s

TEST UGCL-3 (h=21 m)
Test conducted: February 14, 2006

Test Details

Hydraulic Head:	30 psi (21m)	Geomembrane:	LLDPE (GSE UltraFlex)
Cell Diameter:	6 in. (15 cm)	GM Thickness:	40 mil (1 mm)
Interface Contact:	Good	Defect Shape:	Circular
		Defect Size:	1/16 in. (1.6 mm)
GCL Type:	Bentofix NWL		
Initial Condition:	Unhydrated		

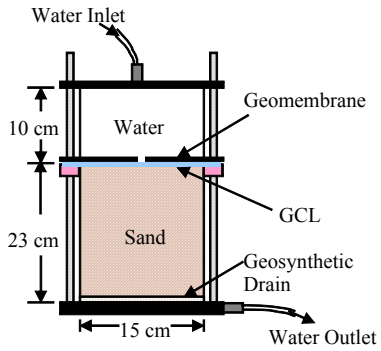

Soil Properties Summary

Soil Type & Classification:	Monterey #30 Sand (SP)
Unit Weight, γ (kN/m^3)	15.7
Porosity, n	0.40
GCL Final Water Content (%)	-
GCL Final Thickness (mm)	-

*Sand was saturated before test began.

Flow Rate Summary

End Value	4.60E-10	m^3/s
Avg Leakage Rate (4 pts)	5.34E-10	m^3/s

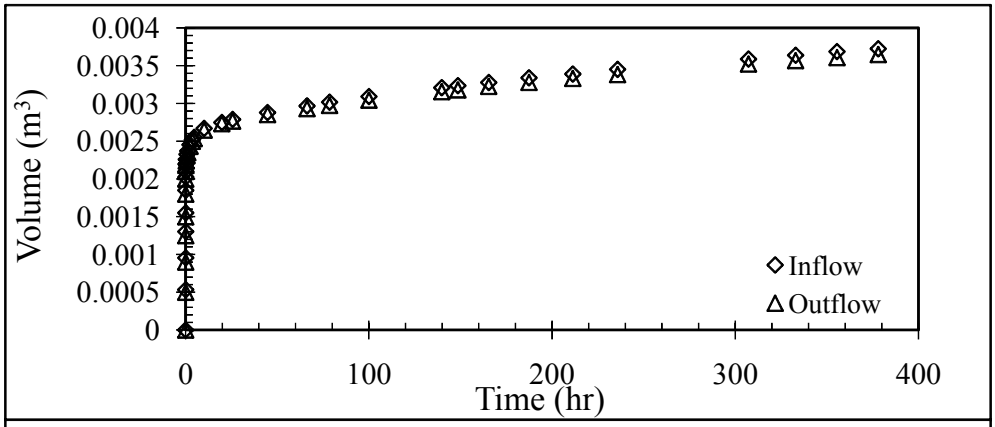

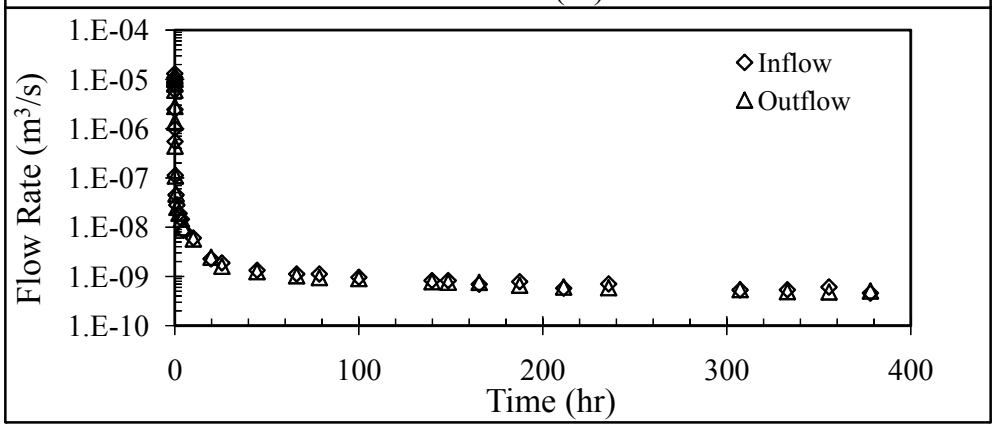

TEST UGCL-3 (h=21 m) - Continued

Analytical Models:

Touze-Foltz et al. (1999)	Flow Rate, Q	5.34E-10	m^3/s
	Transmissivity, θ	1.58E-10	m^2/s
	Radius of Wetted Area	0.321	m

Simplified Equations:

Touze-Foltz and Barroso (2006)	Flow Rate, Q_{GCL}	1.25E-08	m^3/s
Equation (6.2)	Flow Rate, Q	2.13E-09	m^3/s

SUMMARY - NoGM-Clay1 (h=7 m)

Test conducted: October 12, 2007

Test Details

Hydraulic Head:	10 psi (7 m)	Geomembrane:	LLDPE (GSE UltraFlex)
Cell Diameter:	6 in. (15 cm)	GM Thickness:	40 mil (1 mm)
Interface Contact:	Good	Defect Shape:	Circular
		Defect Size:	1/16 in. (1.6 mm)

*** Porous stone was replaced by 10 oz/yd^2 NW Geotextile*

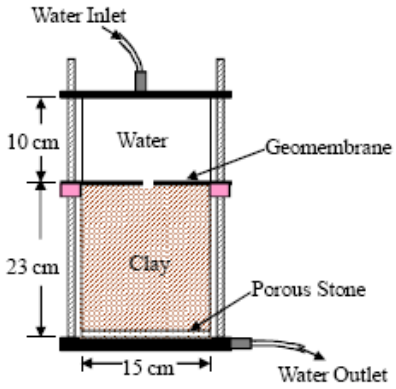

Soil Properties Summary

Soil Type & Classification:	RMA Type II (CL)
Unit Weight, γ (kN/m^3)	19.2
Porosity, n	0.36
Initial Gravimetric Water Content, w_i%	12.3
Initial Degree of Saturation, S_{Ri}%	60.2
Final Gravimetric Water Content, w_f%	19.2
Final Degree of Saturation, S_{Rf}%	94.0

Flow Rate Summary

End Value	4.33E-09	m^3/s
Avg Leakage Rate (4 pts)	4.65E-09	m^3/s

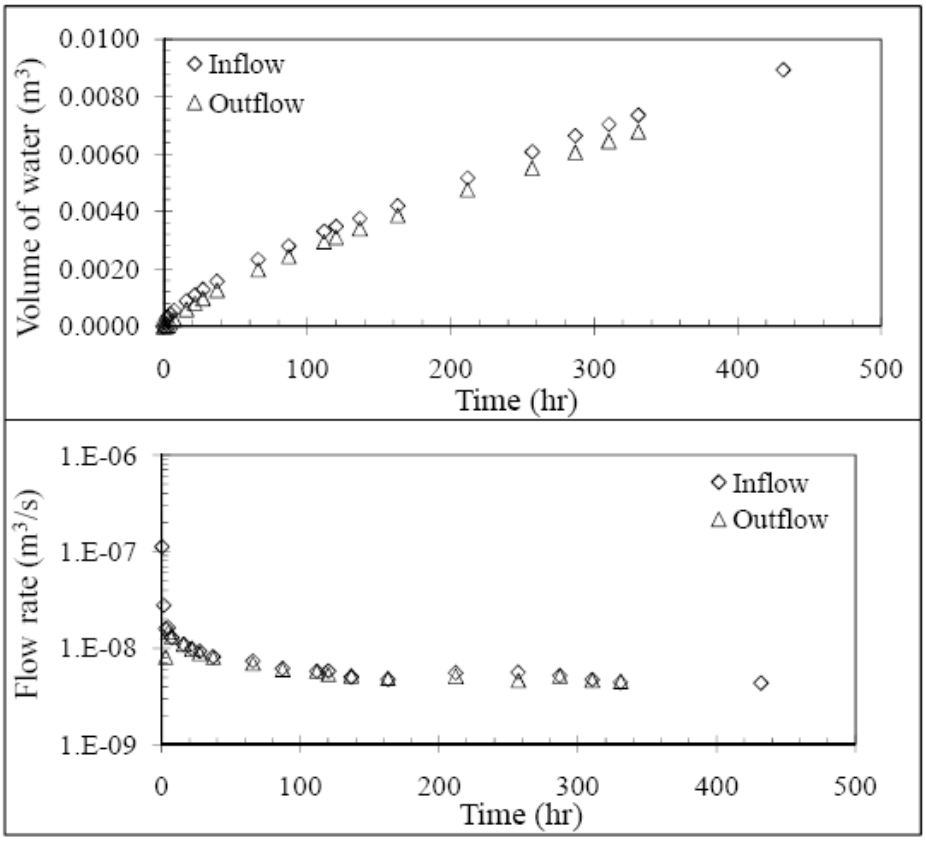

SUMMARY - NoGM-Clay2 (h=14 m)

Test conducted: October 31, 2007

Test Details

Hydraulic Head:	20 psi (14 m)	Geomembrane:	LLDPE (GSE UltraFlex)
Cell Diameter:	6 in. (15 cm)	GM Thickness:	40 mil (1 mm)
Interface Contact:	Good	Defect Shape:	Circular
		Defect Size:	1/16 in. (1.6 mm)

*** Porous stone was replaced by 10 oz/yd^2 NW Geotextile*

Soil Properties Summary

Soil Type & Classification:	RMA Type II (CL)
Unit Weight, γ (kN/m^3)	19.2
Porosity, n	0.36
Initial Gravimetric Water Content, w_i%	12.3
Initial Degree of Saturation, S_{R_i}%	60.2
Final Gravimetric Water Content, w_f%	19.2
Final Degree of Saturation, S_{R_f}%	94.0

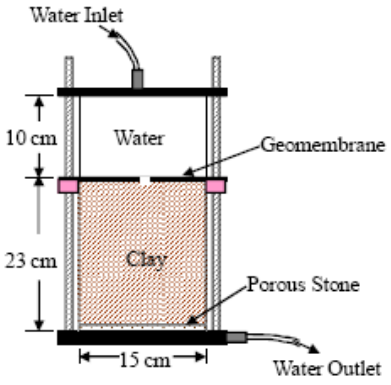

Flow Rate Summary

End Value	8.37E-09	m^3/s
Avg Leakage Rate (4 pts)	8.59E-09	m^3/s

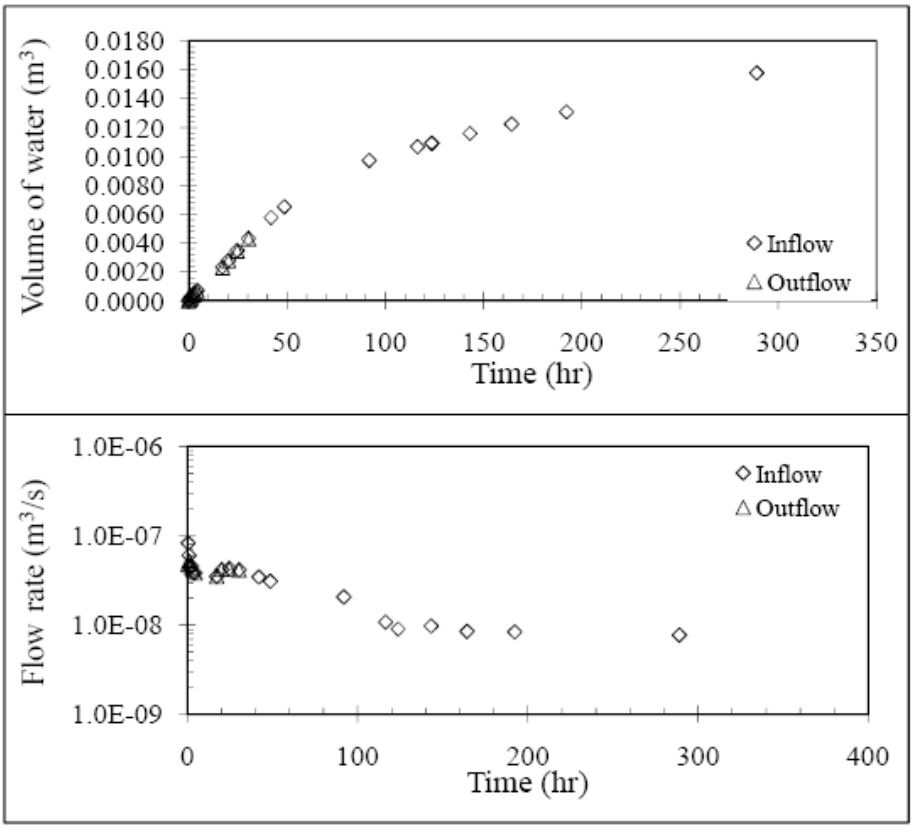

SUMMARY - NoGM-Clay3 (h=21 m)

Test conducted: November 14, 2007

Test Details

Hydraulic Head:	30 psi (21 m)	Geomembrane:	LLDPE (GSE UltraFlex)
Cell Diameter:	6 in. (15 cm)	GM Thickness:	40 mil (1 mm)
Interface Contact:	Good	Defect Shape:	Circular
		Defect Size:	1/16 in. (1.6 mm)

*** Porous stone was replaced by 10 oz/yd^2 NW Geotextile*

Soil Properties Summary

Soil Type & Classification:	RMA Type II (CL)
Unit Weight, γ (kN/m^3)	19.2
Porosity, n	0.36
Initial Gravimetric Water Content, w_i%	12.3
Initial Degree of Saturation, S_{R_i}%	60.2
Final Gravimetric Water Content, w_f%	19.2
Final Degree of Saturation, S_{R_f}%	94.0

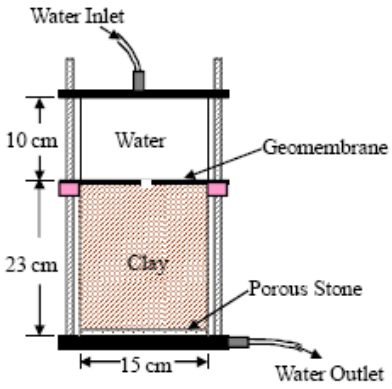

Flow Rate Summary

End Value	1.36E-08	m^3/s
Avg Leakage Rate (4 pts)	1.36E-08	m^3/s

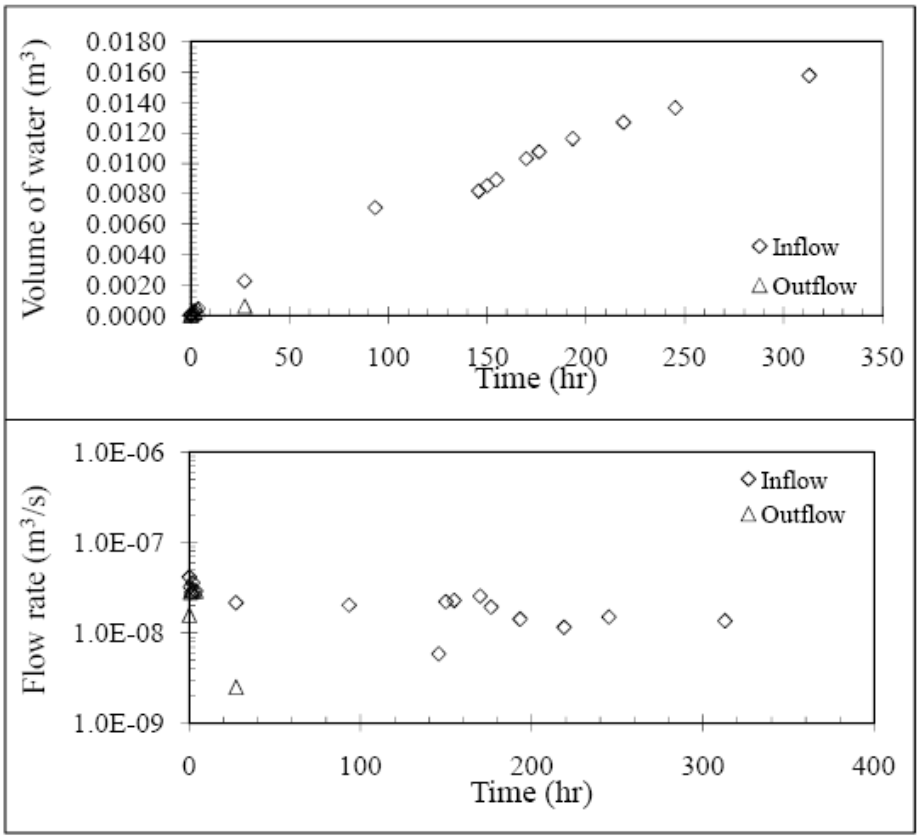

TEST NoGM-Sand1 (h=7 m)

Test conducted: March 16, 2008

Test Details

Hydraulic Head:	10 psi (7 m)	Geomembrane:	LLDPE (GSE UltraFlex)
Cell Diameter:	6 in. (15 cm)	GM Thickness:	40 mil (1 mm)
Interface Contact:	Good	Defect Shape:	Circular
		Defect Size:	1/16 in. (1.6 mm)

Soil Properties Summary

Soil Type & Classification:	Monterey #30 Sand (SP)
Unit Weight, γ (kN/m^3)	16.7
Porosity, n	0.36

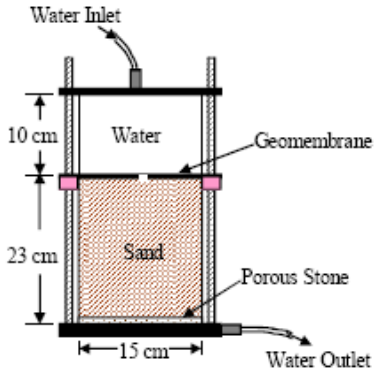

Flow Rate Summary

End Value	2.15E-05	m^3/s
Avg Leakage Rate (4 pts)	2.22E-05	m^3/s

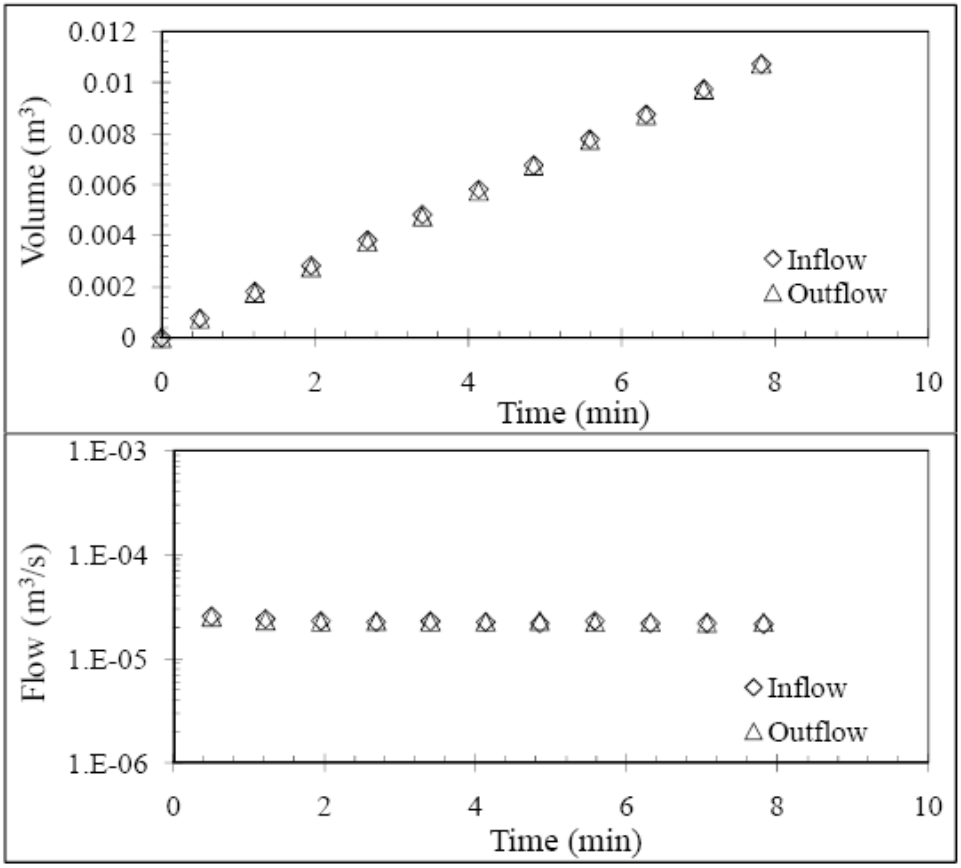

TEST NoGM-Sand2 (h=14 m)

Test conducted: March 16, 2008

Test Details

Hydraulic Head:	20 psi (14 m)	Geomembrane:	LLDPE (GSE UltraFlex)
Cell Diameter:	6 in. (15 cm)	GM Thickness:	40 mil (1 mm)
Interface Contact:	Good	Defect Shape:	Circular
		Defect Size:	1/16 in. (1.6 mm)

Soil Properties Summary

Soil Type & Classification:	Monterey #30 Sand (SP)
Unit Weight, γ (kN/m^3)	16.7
Porosity, n	0.36

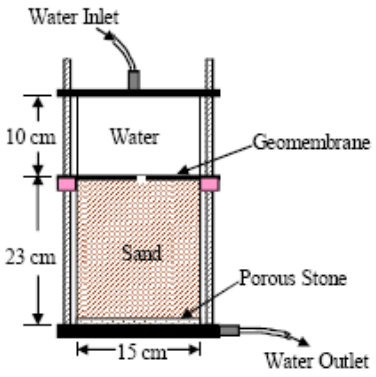

Flow Rate Summary

End Value	3.04E-05	m^3/s
Avg Leakage Rate (3 pts)	3.22E-05	m^3/s

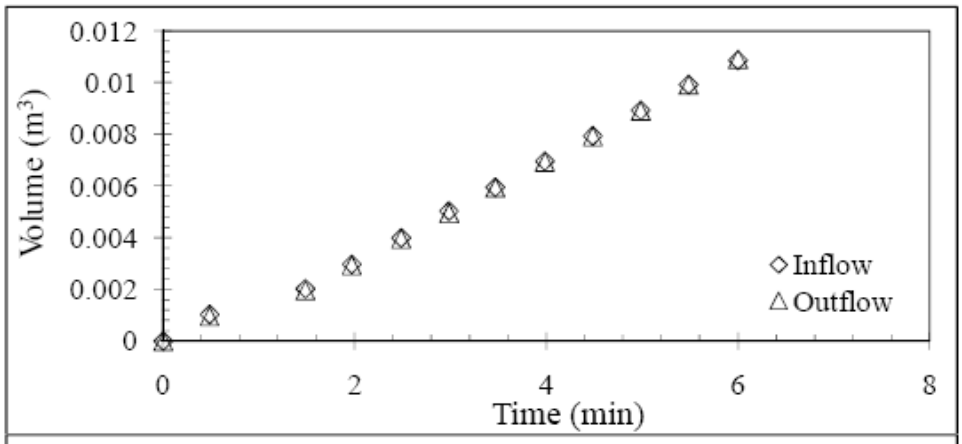

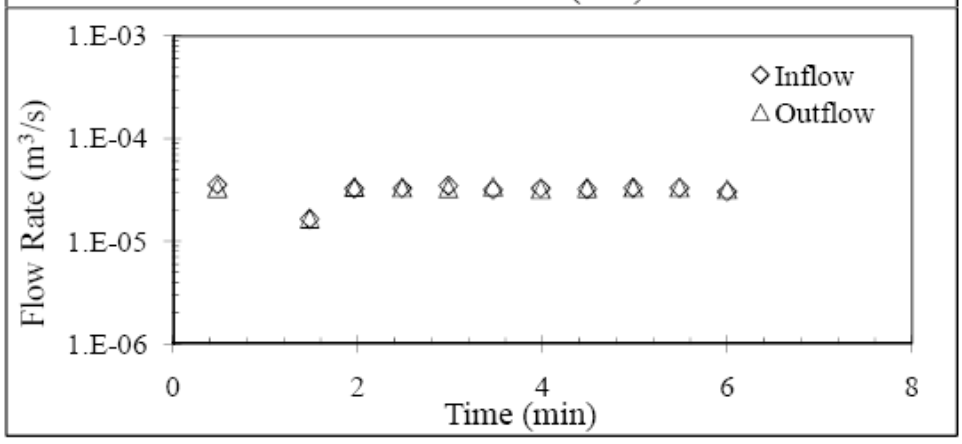

Appendix B

The FlexPDE codes for the two-dimensional, three-dimensional and axisymmetric simulations are included in this Appendix. All codes are for simulations that include a geomembrane (simulated as a no-flow boundary) with a defect, which was simulated using either a constant head or a flux boundary condition. The first two sets of code in this section are for the permeameter test simulations with and without an interface gap. The next two codes are for the two-dimensional simulations of a dam with a blanket drain using steady-state and transient solutions. The next code is for the three-dimensional transient analysis of a dam with a flux boundary condition at the location of the defect. The final FlexPDE code included in this Appendix is the code for the simulation of one of the Palmdale embankments and reservoir.

TITLE"
{ProjectID: CTWeber, ProblemID: RMAGM, Description: Axisymmetric, Steady State, Metric}

```
COORDINATES
 ycylinder

SELECT
 ORDER=3
 STAGES=1
 HISTORY_LIMIT=100000

VARIABLES
 h(THRESHOLD=0.001)

DEFINITIONS
{General definitions}
 uww=9.807 {kN/m^3}, pw=1000 {kg/m^3}, g=9.81 {m/s^2}
 Sat,e,n,vac   {Volume-Mass}

 Roffset=r+(0), Zoffset=z+(0)

{Initial Head}
 h0=-2

 hdiff=h-h0

 u0 = uww*(h0-z)
 u=uww*(h-z) {kPa}, hp=h-z {kPa}
 udiff = u-u0

{Sink/Source}
 S  {m^3/s}
 S_156733_S=0

 {Gradients}
 kr, kz
 Gradr= -dr(h)*kr
 Gradz= -dz(h)*kr

{Hydraulic Conductivity Ratios}
 S_156733_kz_ratio=1

{Hydraulic Conductivity}
 S_156733_Kr=7E-09

{SWCC and Storage Functions}
 vwc, vwc_min=0.0001
 m2w

 {SWCC - van Genuchten}
 avg156733 = 0.08, nvg156733 = 1.229, mvg156733 = 0.186, trvg156733 = 0.01019
 suc156733 = if u>=-0.01 then 0.01 else (if u>=-999999 then -u else 999999)
 Sr156733 = trvg156733+(1-trvg156733)*(1/(1+(suc156733*avg156733)^nvg156733)^mvg156733)
```

```
  dS156733 = -(1 - trvg156733) / ((1 + (avg156733 * suc156733) ^ nvg156733) ^ mvg156733) *
mvg156733 * (avg156733 * suc156733) ^ nvg156733 * nvg156733 / (suc156733 * (1 + (avg156733 *
suc156733) ^ nvg156733))
  S_156733_swcc = 0.38*Sr156733
  S_156733_vwc = if S_156733_swcc > vwc_min then S_156733_swcc else vwc_min
  S_156733_m2w = SWAGE(u+0.01,-(0.38*dS156733),0.0000001,0.02)

{Volume-Mass}
  S_156733_e=0.6129032
  S_156733_Sat=S_156733_vwc*(1+S_156733_e)/S_156733_e
  S_156733_Sa=1-S_156733_Sat
  S_156733_n=S_156733_e/(1+S_156733_e)
  S_156733_vac=S_156733_n-S_156733_vwc

{Water Volume}
  Vw = Vol_Integral(dr(r)^2*dz(z)*vwc)  {m^3}

{Review Boundary Properties}
  BIG=1
  ReviewStatement = if h > z then -BIG * (h-z) else 0

{Flux Sections}
  NFluxR = GradR*normal(1,0)*sign(normal(1,0))
  NFluxZ = GradZ*normal(0,1)*sign(normal(0,1))

  R_Flux_1 = sintegral(NFluxR,"Flux_1")
  Z_Flux_1 = sintegral(NFluxZ,"Flux_1")
  NormalFlux_1 = sintegral(-(normal(GradR, GradZ)),"Flux_1")

  R_Flux_2 = sintegral(NFluxR,"Flux_2")
  Z_Flux_2 = sintegral(NFluxZ,"Flux_2")
  NormalFlux_2 = sintegral(-(normal(GradR, GradZ)),"Flux_2")

INITIAL VALUES
  h=h0

EQUATIONS
  dr(kr*dr(h)) + kr/r*dr(h) + dz(kz*dz(h)) + S = 0

BOUNDARIES
{Regions}
Region 1    'Sample'
  Kr = LUMP(S_156733_Kr)
  Kz = Kr*S_156733_Kz_ratio
  vwc= S_156733_vwc
  m2w= LUMP(S_156733_m2w)
  Sat = S_156733_Sat
  e = S_156733_e
  n = S_156733_n
  vac = S_156733_vac
  S = S_156733_S

start 'BN_Sample_816645781' (0,0)
   natural(h)= ReviewStatement
```

```
  Line to (0.076,0)
   natural(h)=0
  Line to (0.076,0.229)
   natural(h)=0
  Line to (0.001,0.229)
   value(h)=14
  Line to (0,0.229)
   natural(h)=0
  Line to (0,0)

{Flux Sections}
  Feature "Flux_1" Start (0,0.228) Line to (0.0762,0.228)
  Feature "Flux_2" Start (0,0) Line to (0.076,0)

{Review Boundary Paths}
feature start "Review Boundary 1: Sample,Shape 816645781,Point 0" (0,0) Line to (0.076,0)

MONITORS
  Contour(u) as "Pressure"zoom(-0.065,-0.117,0.196,0.469)
  Contour(h) as "Head"zoom(-0.055,-0.104,0.188,0.439)
  Contour(Sat) as "sr"zoom(-0.03,-0.069,0.14,0.369)

{ Flux Section Reports and Histories}
  Summary as "FS: Flux 1"
            report"Flux Section Report: Flux 1"
            report"  From (0,0.228) to (0.0762,0.228)"
            report" "
            report"  Components (signs follow global coordinate system)"
            report" "
            report(R_Flux_1) as "  R Component of Flow in (m^3/s) "
            report(Z_Flux_1) as "  Z Component of Flow in (m^3/s) "
            report" "
            report"  Normal"
            report"   1. On External Region Boundary: Positive Flow is into Region"
            report"   2. On Internal Region Boundary - Region Given: Positive Flow is into Given Region"
            report"   3. On Internal Region Boundary - Region Not Given: Positive Flow is into First
Applicable Region"
            report"   4. Internal: Left Hand Rule"
            report" "
            report(NormalFlux_1) as "  Normal Flow in (m^3/s) "
  Summary as "FS: Flux 2"
            report"Flux Section Report: Flux 2"
            report"  From (0,0) to (0.076,0)"
            report" "
            report"  Components (signs follow global coordinate system)"
            report" "
            report(R_Flux_2) as "  R Component of Flow in (m^3/s) "
            report(Z_Flux_2) as "  Z Component of Flow in (m^3/s) "
            report" "
            report"  Normal"
            report"   1. On External Region Boundary: Positive Flow is into Region"
            report"   2. On Internal Region Boundary - Region Given: Positive Flow is into Given Region"
            report"   3. On Internal Region Boundary - Region Not Given: Positive Flow is into First
Applicable Region"
```

```
        report"   4. Internal: Left Hand Rule"
        report" "
        report(NormalFlux_2) as "  Normal Flow in (m^3/s) "

PLOTS
 Summary as "Problem Properties"
  report "ProjectID: CTWeber"
  report "Project Name: Dam Lining Systems"
  report "ProblemID: RMAGM"
  report "System: Axisymmetric     Type: Steady State"
  report "Problem Created: 11/1/2007 3:32:59 PM by SVFlux 5.76.000"
  report " "
  report "Stages: 1"
  report " "
  report "Description:  "

 Contour(u) as "Pressure"zoom(-0.065,-0.117,0.196,0.469)
 Contour(h) as "Head"zoom(-0.055,-0.104,0.188,0.439)
 Contour(Sat) as "sr"zoom(-0.03,-0.069,0.14,0.369)

{ Flux Section Reports and Histories}
 Summary as "FS: Flux 1"
        report"Flux Section Report: Flux 1"
        report"  From (0,0.228) to (0.0762,0.228)"
        report" "
        report"  Components (signs follow global coordinate system)"
        report" "
        report(R_Flux_1) as "  R Component of Flow in (m^3/s) "
        report(Z_Flux_1) as "  Z Component of Flow in (m^3/s) "
        report" "
        report"  Normal"
        report"   1. On External Region Boundary: Positive Flow is into Region"
        report"   2. On Internal Region Boundary - Region Given: Positive Flow is into Given Region"
        report"   3. On Internal Region Boundary - Region Not Given: Positive Flow is into First
Applicable Region"
        report"   4. Internal: Left Hand Rule"
        report" "
        report(NormalFlux_1) as "  Normal Flow in (m^3/s) "
 Summary as "FS: Flux 2"
        report"Flux Section Report: Flux 2"
        report"  From (0,0) to (0.076,0)"
        report" "
        report"  Components (signs follow global coordinate system)"
        report" "
        report(R_Flux_2) as "  R Component of Flow in (m^3/s) "
        report(Z_Flux_2) as "  Z Component of Flow in (m^3/s) "
        report" "
        report"  Normal"
        report"   1. On External Region Boundary: Positive Flow is into Region"
        report"   2. On Internal Region Boundary - Region Given: Positive Flow is into Given Region"
        report"   3. On Internal Region Boundary - Region Not Given: Positive Flow is into First
Applicable Region"
        report"   4. Internal: Left Hand Rule"
        report" "
```

```
        report(NormalFlux_2) as "  Normal Flow in (m^3/s) "

{Review Boundary Plots}
  Elevation(u) on "Review Boundary 1: Sample,Shape 816645781,Point 0"as"Review Boundary Exit Point
- PWP"

{Output Files}
  Transfer(h)print file "HeadTransfer.trn"

END
```

TITLE"
{ProjectID: CTWeber, ProblemID: RMAGMGap, Description: Axisymmetric, Steady State, Metric}

```
COORDINATES
 ycylinder

SELECT
 STAGES=1
 INITGRIDLIMIT=1
 HISTORY_LIMIT=100000

VARIABLES
 h(THRESHOLD=0.001)

DEFINITIONS
{General definitions}
 uww=9.807 {kN/m^3}, pw=1000 {kg/m^3}, g=9.81 {m/s^2}

 Roffset=r+(0), Zoffset=z+(0)

{Initial Head}
 h0=-2

 hdiff=h-h0

 u0 = uww*(h0-z)
 u=uww*(h-z) {kPa}, hp=h-z {kPa}
 udiff = u-u0

{Sink/Source}
 S  {m^3/s}
 S_302688_S=0
 S_552948_S=0

 {Gradients}
 kr, kz
 Gradr= -dr(h)*kr
 Gradz= -dz(h)*kr

{Hydraulic Conductivity Ratios}
 S_302688_kz_ratio=1
 S_552948_kz_ratio=1

{Hydraulic Conductivity}
 S_302688_Kr=7E-09
 S_552948_Kr=3E-08

{Water Volume}
 Vw = Vol_Integral(dr(r)^2*dz(z))  {m^3}

{Review Boundary Properties}
 BIG=1
 ReviewStatement = if h > z then -BIG * (h-z) else 0
```

```
{Flux Sections}
  NFluxR = GradR*normal(1,0)*sign(normal(1,0))
  NFluxZ = GradZ*normal(0,1)*sign(normal(0,1))

  R_Flux_1 = sintegral(NFluxR,"Flux_1")
  Z_Flux_1 = sintegral(NFluxZ,"Flux_1")
  NormalFlux_1 = sintegral(-(normal(GradR, GradZ)),"Flux_1")

  R_Flux_2 = sintegral(NFluxR,"Flux_2")
  Z_Flux_2 = sintegral(NFluxZ,"Flux_2")
  NormalFlux_2 = sintegral(-(normal(GradR, GradZ)),"Flux_2")

INITIAL VALUES
  h=h0

EQUATIONS
  dr(kr*dr(h)) + kr/r*dr(h) + dz(kz*dz(h)) + S = 0

BOUNDARIES
{Regions}
Region 1    'Sample'
  Kr = LUMP(S_302688_Kr)
  Kz = Kr*S_302688_Kz_ratio
  S = S_302688_S

start 'BN_Sample_816645781' (0,0)
    natural(h)= ReviewStatement
  Line to (0.076,0)
    natural(h)=0
  Line to (0.076,0.229)
    nobc(h)
  Line to (0.001,0.229)
    nobc(h)
  Line to (0,0.229)
    natural(h)=0
  Line to (0,0)

Region 2    'Gap'
  Kr = LUMP(S_552948_Kr)
  Kz = Kr*S_552948_Kz_ratio
  S = S_552948_S

start 'BN_Gap_645732455' (0,0.229)
    nobc(h)
  Line to (0.076,0.229)
    natural(h)=0
  Line to (0.076,0.23)
    natural(h)=0
  Line to (0.001,0.23)
    natural(h)= 1.4e-4
  Line to (0,0.23)
    natural(h)=0
  Line to (0,0.229)
```

```
{Flux Sections}
 Feature "Flux_1" Start (0,0.228) Line to (0.0762,0.228)
 Feature "Flux_2" Start (0,0) Line to (0.076,0)

{Review Boundary Paths}
feature start "Review Boundary 1: Sample,Shape 816645781,Point 0" (0,0) Line to (0.076,0)

MONITORS
 Contour(u) as "Pressure"zoom(-0.065,-0.117,0.196,0.469)
 Contour(h) as "Head"zoom(-0.055,-0.104,0.188,0.439)
 Contour(h) on "Gap" as "h"

{ Flux Section Reports and Histories}
 Summary as "FS: Flux 1"
          report"Flux Section Report: Flux 1"
          report"  From (0,0.228) to (0.0762,0.228)"
          report" "
          report"  Components (signs follow global coordinate system)"
          report" "
          report(R_Flux_1) as "  R Component of Flow in (m^3/s) "
          report(Z_Flux_1) as "  Z Component of Flow in (m^3/s) "
          report" "
          report"  Normal"
          report"   1. On External Region Boundary: Positive Flow is into Region"
          report"   2. On Internal Region Boundary - Region Given: Positive Flow is into Given Region"
          report"     3. On Internal Region Boundary - Region Not Given: Positive Flow is into First
Applicable Region"
          report"   4. Internal: Left Hand Rule"
          report" "
          report(NormalFlux_1) as "  Normal Flow in (m^3/s) "
 Summary as "FS: Flux 2"
          report"Flux Section Report: Flux 2"
          report"  From (0,0) to (0.076,0)"
          report" "
          report"  Components (signs follow global coordinate system)"
          report" "
          report(R_Flux_2) as "  R Component of Flow in (m^3/s) "
          report(Z_Flux_2) as "  Z Component of Flow in (m^3/s) "
          report" "
          report"  Normal"
          report"   1. On External Region Boundary: Positive Flow is into Region"
          report"   2. On Internal Region Boundary - Region Given: Positive Flow is into Given Region"
          report"     3. On Internal Region Boundary - Region Not Given: Positive Flow is into First
Applicable Region"
          report"   4. Internal: Left Hand Rule"
          report" "
          report(NormalFlux_2) as "  Normal Flow in (m^3/s) "

PLOTS
 Summary as "Problem Properties"
   report "ProjectID: CTWeber"
   report "Project Name: Dam Lining Systems"
   report "ProblemID: RMAGMGap"
   report "System: Axisymmetric     Type: Steady State"
```

```
   report "Problem Created: 11/6/2007 2:21:59 PM by SVFlux 5.76.000"
   report " "
   report "Stages: 1"
   report " "
   report "Description:  "

  Contour(u) as "Pressure"zoom(-0.065,-0.117,0.196,0.469)
  Contour(h) as "Head"zoom(-0.055,-0.104,0.188,0.439)
  Contour(h) on "Gap" as "h"

{ Flux Section Reports and Histories}
  Summary as "FS: Flux 1"
          report"Flux Section Report: Flux 1"
          report"  From (0,0.228) to (0.0762,0.228)"
          report" "
          report"  Components (signs follow global coordinate system)"
          report" "
          report(R_Flux_1) as "  R Component of Flow in (m^3/s) "
          report(Z_Flux_1) as "  Z Component of Flow in (m^3/s) "
          report" "
          report"  Normal"
          report"   1. On External Region Boundary: Positive Flow is into Region"
          report"   2. On Internal Region Boundary - Region Given: Positive Flow is into Given Region"
          report"     3. On Internal Region Boundary - Region Not Given: Positive Flow is into First
Applicable Region"
          report"   4. Internal: Left Hand Rule"
          report" "
          report(NormalFlux_1) as "  Normal Flow in (m^3/s) "
  Summary as "FS: Flux 2"
          report"Flux Section Report: Flux 2"
          report"  From (0,0) to (0.076,0)"
          report" "
          report"  Components (signs follow global coordinate system)"
          report" "
          report(R_Flux_2) as "  R Component of Flow in (m^3/s) "
          report(Z_Flux_2) as "  Z Component of Flow in (m^3/s) "
          report" "
          report"  Normal"
          report"   1. On External Region Boundary: Positive Flow is into Region"
          report"   2. On Internal Region Boundary - Region Given: Positive Flow is into Given Region"
          report"     3. On Internal Region Boundary - Region Not Given: Positive Flow is into First
Applicable Region"
          report"   4. Internal: Left Hand Rule"
          report" "
          report(NormalFlux_2) as "  Normal Flow in (m^3/s) "

{Review Boundary Plots}
  Elevation(u) on "Review Boundary 1: Sample,Shape 816645781,Point 0"as"Review Boundary Exit Point
- PWP"

{Output Files}
  Transfer(h)print file "HeadTransfer.trn"
END
```

TITLE"
{ProjectID: CTWeber, ProblemID: GMDrain, Description: 2D, Steady State, Metric}

```
SELECT
  CHANGELIM=2
  ITERATE=500
  STAGES=1
  HISTORY_LIMIT=100000

VARIABLES
  h(THRESHOLD=0.001)

DEFINITIONS
{General definitions}
  uww=9.807 {kN/m^3}, pw=1000 {kg/m^3}, g=9.81 {m/s^2}
  Sat,e,n,vac   {Volume-Mass}

  Xoffset=x+(0), Yoffset=y+(0)

{Initial Head}
  h0     {specified by region}
  hdiff=h-h0

  u0 = uww*(h0-y)
  u=uww*(h-y) {kPa}, hp=h-y {kPa}
  udiff = u-u0

{Sink/Source}
  S  {m^3/day}
  S_488357_S=0
  S_788964_S=0

  {Gradients}
  kx, ky
  Gradx= -dx(h)*kx
  Grady= -dy(h)*ky

{Hydraulic Conductivity Ratios}
  S_488357_ky_ratio=1
  S_788964_ky_ratio=1

{Hydraulic Conductivity}
  S_488357_Kx=0.01728

  S_788964_Kx=0.0888

{SWCC and Storage Functions}
  vwc, vwc_min=0.0001
  m2w

  {SWCC - van Genuchten}
  avg488357 = 0.4577466, nvg488357 = 2.636361, mvg488357 = 0.1120724, trvg488357 = 0.05
  suc488357 = if u>=-0.01 then 0.01 else (if u>=-999999 then -u else 999999)
  Sr488357 = trvg488357+(1-trvg488357)*(1/(1+(suc488357*avg488357)^nvg488357)^mvg488357)
```

```
  dS488357 = -(1 - trvg488357) / ((1 + (avg488357 * suc488357) ^ nvg488357) ^ mvg488357) *
mvg488357 * (avg488357 * suc488357) ^ nvg488357 * nvg488357 / (suc488357 * (1 + (avg488357 *
suc488357) ^ nvg488357))
  S_488357_swcc = 0.449*Sr488357
  S_488357_vwc = if S_488357_swcc > vwc_min then S_488357_swcc else vwc_min
  S_488357_m2w = SWAGE(u+0.1,-(0.449*dS488357),0.0000001,0.02)

  {SWCC - van Genuchten}
  avg788964 = 0.58, nvg788964 = 4.7, mvg788964 = 0.787, trvg788964 = 0.03
  suc788964 = if u>=-0.01 then 0.01 else (if u>=-999999 then -u else 999999)
  Sr788964 = trvg788964+(1-trvg788964)*(1/(1+(suc788964*avg788964)^nvg788964)^mvg788964)
  dS788964 = -(1 - trvg788964) / ((1 + (avg788964 * suc788964) ^ nvg788964) ^ mvg788964) *
mvg788964 * (avg788964 * suc788964) ^ nvg788964 * nvg788964 / (suc788964 * (1 + (avg788964 *
suc788964) ^ nvg788964))
  S_788964_swcc = 0.38*Sr788964
  S_788964_vwc = if S_788964_swcc > vwc_min then S_788964_swcc else vwc_min
  S_788964_m2w = SWAGE(u+0.1,-(0.38*dS788964),0.0000001,0.02)

{Volume-Mass}
  S_488357_e=0.814882
  S_488357_Sat=S_488357_vwc*(1+S_488357_e)/S_488357_e
  S_488357_Sa=1-S_488357_Sat
  S_488357_n=S_488357_e/(1+S_488357_e)
  S_488357_vac=S_488357_n-S_488357_vwc
  S_788964_e=0.6129032
  S_788964_Sat=S_788964_vwc*(1+S_788964_e)/S_788964_e
  S_788964_Sa=1-S_788964_Sat
  S_788964_n=S_788964_e/(1+S_788964_e)
  S_788964_vac=S_788964_n-S_788964_vwc

{Water Volume}
  Vw = Vol_Integral(dx(x)*dy(y)*1*vwc)  {m^3}

{Review Boundary Properties}
  BIG=1
  ReviewStatement = if h > y then -BIG * (h-y) else 0

INITIAL VALUES
  h=h0

EQUATIONS
  div(vector(kx*dx(h),ky*dy(h))) + S = 0

BOUNDARIES
{Regions}
Region 1    'Clay'
  h0=-4.1
  Kx = LUMP(S_488357_Kx)
  Ky = Kx*S_488357_Ky_ratio
  vwc= S_488357_vwc
  m2w= LUMP(S_488357_m2w)
  Sat = S_488357_Sat
  e = S_488357_e
  n = S_488357_n
```

```
  vac = S_488357_vac
  S = S_488357_S

start 'BN_Clay_623192893' (0,4.572)
   natural(h)=0
  Line to (24.079,3.048)
  Line to (25.908,1.219)
  Line to (29.566,1.219)
  Line to (31.394,2.743)
  Line to (45.72,1.715)
   nobc(h)
  Line to (48.158,2.477)
  Line to (69.776,1.125)
   natural(h)=0
  Line to (32.004,13.716)
  Line to (27.432,13.716)
  Line to (13.106,8.931)
   value(h)=12.2
  Line to (12.192,8.626)
   natural(h)=0
  Line to (0,4.572)
  Line to (0,4.572)

Region 2    'Filter'
  h0=0
  Kx = LUMP(S_788964_Kx)
  Ky = Kx*S_788964_Ky_ratio
  vwc= S_788964_vwc
  m2w= LUMP(S_788964_m2w)
  Sat = S_788964_Sat
  e = S_788964_e
  n = S_788964_n
  vac = S_788964_vac
  S = S_788964_S

start 'BN_Filter_409157064' (45.72,1.715)
   natural(h)= ReviewStatement
  Line to (73.152,0)
  Line to (69.776,1.125)
  Line to (48.158,2.477)
  Line to (45.72,1.715)

{Review Boundary Paths}
feature start "Review Boundary 1: Filter,Shape 409157064,Point 0" (45.72,1.715) Line to (73.152,0) Line
to (69.776,1.125) Line to (48.158,2.477) Line to (45.72,1.715)

MONITORS

PLOTS
  Summary as "Problem Properties"
    report "ProjectID: CTWeber"
    report "Project Name: Dam Lining Systems"
    report "ProblemID: GMDrain"
    report "System: 2D     Type: Steady State"
```

```
   report "Problem Created: 3/24/2008 1:08:18 PM by SVFlux 5.76.000"
   report " "
   report "Stages: 1"
   report " "
   report "Description:  "

  Contour(u) as "Pressure"
  Contour(h) as "Head"
  Contour(vwc) as "VWC"

{Review Boundary Plots}
  Elevation(u) on "Review Boundary 1: Filter,Shape 409157064,Point 0"as"Review Boundary Exit Point -
PWP"

{Output Files}
  Table(u) file "PP.tbl" points = (10,10)
  Transfer(h)print file "HeadTransfer.trn"
  Tecplot(Xoffset,Yoffset,u,h,vwc)print file "GMDamNoDrain.dat"

END
```

```
TITLE''
{ProjectID: CTWeber, ProblemID: GMDamDrain, Description: 2D, Transient, Metric}

SELECT
  HISTORY_LIMIT=100000

VARIABLES
  h(THRESHOLD=0.001)

DEFINITIONS
{Time - Units: day}
  StartTime = 0, Timeinc = 1, EndTime = 100000

{General definitions}
  uww=9.807 {kN/m^3}, pw=1000 {kg/m^3}, g=9.81 {m/s^2}
  Sat,e,n,vac   {Volume-Mass}

  Xoffset=x+(0), Yoffset=y+(0)

{Initial Head}

transfer("C:\SVS\SVFlux\My_Problems\CTWeber\2D\Transient\GMDamDrainInit\HeadTransfer_2.trn",h
0)
  hdiff=h-h0

  u0 = uww*(h0-y)
  u=uww*(h-y) {kPa}, hp=h-y {kPa}
  udiff = u-u0

{Sink/Source}
  S  {m^3/day}
  S_133482_S=0
  S_567744_S=0
  S_926347_S=0

  {Gradients}
  kx, ky
  Gradx= -dx(h)*kx
  Grady= -dy(h)*ky

{Hydraulic Conductivity Ratios}
  S_133482_ky_ratio=1
  S_567744_ky_ratio=1
  S_926347_ky_ratio=1

{Hydraulic Conductivity}
  S_133482_Kx=8.64

  S_567744_Kx=0.01728

  S_926347_Kx=0.0888

{SWCC and Storage Functions}
  vwc0, vwc, vwc_min=0.0001
```

```
vwcdiff = vwc-vwc0
m2w0, m2w
m2wdiff = m2w-m2w0

{SWCC - Fredlund and Xing}
afx133482 = 7.865795E-02, nfx133482 = 4.913471, mfx133482 = 0.5387965, hrfx133482 = 0.2884268
suc0133482 = if u0>=-0.1 then 0.1 else (if u0>=-999999 then -u0 else 999999)
Sr0133482 = (1-ln(1+suc0133482/hrfx133482)/ln(1+1000000/hrfx133482))*(1/(ln(exp(1)+(suc0133482/afx133482)^nfx133482)^mfx133482))
dS0133482 = -(1/(hrfx133482*(1+(suc0133482)/hrfx133482)*ln(1+1000000/hrfx133482)*ln(exp(1)+((suc0133482)/afx133482)^nfx133482)^mfx133482))-(1-ln(1+(suc0133482)/hrfx133482)/ln(1+1000000/hrfx133482))*(mfx133482*nfx133482*(((suc0133482)^(nfx133482-1))/((afx133482)^nfx133482)))/((exp(1)+((suc0133482)/afx133482)^nfx133482)*((ln(exp(1)+((suc0133482)/afx133482)^nfx133482))^(mfx133482+1)))
S_133482_swcc0 = 0.2*Sr0133482
S_133482_vwc0 = if S_133482_swcc0 > vwc_min then S_133482_swcc0 else vwc_min
S_133482_m2w0 = SWAGE(u+0.1,-(0.2*dS0133482),0.0000001,0.02)
suc133482 = if u>=-0.1 then 0.1 else (if u>=-999999 then -u else 999999)
Sr133482 = (1-ln(1+suc133482/hrfx133482)/ln(1+1000000/hrfx133482))*(1/(ln(exp(1)+(suc133482/afx133482)^nfx133482)^mfx133482))
dS133482 = -(1/(hrfx133482*(1+(suc133482)/hrfx133482)*ln(1+1000000/hrfx133482)*ln(exp(1)+((suc133482)/afx133482)^nfx133482)^mfx133482))-(1-ln(1+(suc133482)/hrfx133482)/ln(1+1000000/hrfx133482))*(mfx133482*nfx133482*(((suc133482)^(nfx133482-1))/((afx133482)^nfx133482)))/((exp(1)+((suc133482)/afx133482)^nfx133482)*((ln(exp(1)+((suc133482)/afx133482)^nfx133482))^(mfx133482+1)))
S_133482_swcc = 0.2*Sr133482
S_133482_vwc = if S_133482_swcc > vwc_min then S_133482_swcc else vwc_min
S_133482_m2w = SWAGE(u+0.1,-(0.2*dS133482),0.0000001,0.02)

{SWCC - van Genuchten}
avg567744 = 0.4577466, nvg567744 = 2.636361, mvg567744 = 0.1120724, trvg567744 = 0.05
suc0567744 = if u0>=-0.01 then 0.01 else (if u0>=-999999 then -u0 else 999999)
Sr0567744 = trvg567744+(1-trvg567744)*(1/(1+(suc0567744*avg567744)^nvg567744)^mvg567744)
dS0567744 = -(1 - trvg567744) / ((1 + (avg567744 * suc0567744) ^ nvg567744) ^ mvg567744) * mvg567744 * (avg567744 * suc0567744) ^ nvg567744 * nvg567744 / (suc0567744 * (1 + (avg567744 * suc0567744) ^ nvg567744))
S_567744_swcc0 = 0.449*Sr0567744
S_567744_vwc0 = if S_567744_swcc0 > vwc_min then S_567744_swcc0 else vwc_min
S_567744_m2w0 = SWAGE(u+0.1,-(0.449*dS0567744),0.0000001,0.02)
suc567744 = if u>=-0.01 then 0.01 else (if u>=-999999 then -u else 999999)
Sr567744 = trvg567744+(1-trvg567744)*(1/(1+(suc567744*avg567744)^nvg567744)^mvg567744)
dS567744 = -(1 - trvg567744) / ((1 + (avg567744 * suc567744) ^ nvg567744) ^ mvg567744) * mvg567744 * (avg567744 * suc567744) ^ nvg567744 * nvg567744 / (suc567744 * (1 + (avg567744 * suc567744) ^ nvg567744))
S_567744_swcc = 0.449*Sr567744
S_567744_vwc = if S_567744_swcc > vwc_min then S_567744_swcc else vwc_min
S_567744_m2w = SWAGE(u+0.1,-(0.449*dS567744),0.0000001,0.02)
```

```
  {SWCC - van Genuchten}
  avg926347 = 0.58, nvg926347 = 4.7, mvg926347 = 0.787, trvg926347 = 0.03
  suc0926347 = if u0>=-0.01 then 0.01 else (if u0>=-999999 then -u0 else 999999)
  Sr0926347 = trvg926347+(1-trvg926347)*(1/(1+(suc0926347*avg926347)^nvg926347)^mvg926347)
  dS0926347 = -(1 - trvg926347) / ((1 + (avg926347 * suc0926347) ^ nvg926347) ^ mvg926347) *
mvg926347 * (avg926347 * suc0926347) ^ nvg926347 * nvg926347 / (suc0926347 * (1 + (avg926347 *
suc0926347) ^ nvg926347))
  S_926347_swcc0 = 0.38*Sr0926347
  S_926347_vwc0 = if S_926347_swcc0 > vwc_min then S_926347_swcc0 else vwc_min
  S_926347_m2w0 = SWAGE(u+0.1,-(0.38*dS0926347),0.0000001,0.02)
  suc926347 = if u>=-0.01 then 0.01 else (if u>=-999999 then -u else 999999)
  Sr926347 = trvg926347+(1-trvg926347)*(1/(1+(suc926347*avg926347)^nvg926347)^mvg926347)
  dS926347 = -(1 - trvg926347) / ((1 + (avg926347 * suc926347) ^ nvg926347) ^ mvg926347) *
mvg926347 * (avg926347 * suc926347) ^ nvg926347 * nvg926347 / (suc926347 * (1 + (avg926347 *
suc926347) ^ nvg926347))
  S_926347_swcc = 0.38*Sr926347
  S_926347_vwc = if S_926347_swcc > vwc_min then S_926347_swcc else vwc_min
  S_926347_m2w = SWAGE(u+0.1,-(0.38*dS926347),0.0000001,0.02)

{Volume-Mass}
  S_133482_e=0.25
  S_133482_Sat=S_133482_vwc*(1+S_133482_e)/S_133482_e
  S_133482_Sa=1-S_133482_Sat
  S_133482_n=S_133482_e/(1+S_133482_e)
  S_133482_vac=S_133482_n-S_133482_vwc
  S_567744_e=0.814882
  S_567744_Sat=S_567744_vwc*(1+S_567744_e)/S_567744_e
  S_567744_Sa=1-S_567744_Sat
  S_567744_n=S_567744_e/(1+S_567744_e)
  S_567744_vac=S_567744_n-S_567744_vwc
  S_926347_e=0.6129032
  S_926347_Sat=S_926347_vwc*(1+S_926347_e)/S_926347_e
  S_926347_Sa=1-S_926347_Sat
  S_926347_n=S_926347_e/(1+S_926347_e)
  S_926347_vac=S_926347_n-S_926347_vwc

{Water Volume}
  Vw0 = Vol_Integral(dx(x)*dy(y)*1*vwc0)  {m^3}
  Vw = Vol_Integral(dx(x)*dy(y)*1*vwc)  {m^3}
  Vwdiff = Vw-Vw0  {m^3}

INITIAL VALUES
  h=h0

EQUATIONS
  div(vector(kx*dx(h),ky*dy(h))) + S = dt(h)*uww*m2w     {H-Based (Conventional) Formulation}

BOUNDARIES
{Regions}
Region 1    'Clay'
  Kx = LUMP(S_567744_Kx)
  Ky = Kx*S_567744_Ky_ratio
  vwc= S_567744_vwc
  m2w= LUMP(S_567744_m2w)
```

```
  vwc0= S_567744_vwc0
  m2w0= S_567744_m2w0
  Sat = S_567744_Sat
  e = S_567744_e
  n = S_567744_n
  vac = S_567744_vac
  S = S_567744_S

start 'BN_Clay_407444212' (0,4.572)
   natural(h)=0
  Line to (24.079,3.048)
  Line to (25.908,1.219)
  Line to (29.566,1.219)
  Line to (31.394,2.743)
  Line to (45.72,1.715)
   nobc(h)
  Line to (48.158,2.477)
  Line to (69.776,1.125)
   natural(h)=0
  Line to (32.004,13.716)
  Line to (27.432,13.716)
  Line to (27.432,12.802)
  Line to (13.106,8.016)
   value(h)=12.192
  Line to (12.192,7.711)
   natural(h)=0
  Line to (9.144,6.706)
  Line to (7.315,6.096)
  Line to (3.048,6.096)
  Line to (0,4.572)
  Line to (0,4.572)

Region 2    'Cover'
  Kx = LUMP(S_926347_Kx)
  Ky = Kx*S_926347_Ky_ratio
  vwc= S_926347_vwc
  m2w= LUMP(S_926347_m2w)
  vwc0= S_926347_vwc0
  m2w0= S_926347_m2w0
  Sat = S_926347_Sat
  e = S_926347_e
  n = S_926347_n
  vac = S_926347_vac
  S = S_926347_S

start 'BN_Cover_407112121' (-1.219,4.686)
   natural(h)=0
  Line to (0,4.572)
   natural(h)=0
  Line to (3.048,6.096)
  Line to (7.315,6.096)
  Line to (9.144,6.706)
   natural(h)=0
  Line to (6.401,6.706)
```

```
   natural(h)=0
  Line to (3.048,6.706)
  Line to (-1.219,4.686)

Region 3    'Upper cover'
  Kx = LUMP(S_133482_Kx)
  Ky = Kx*S_133482_Ky_ratio
  vwc= S_133482_vwc
  m2w= LUMP(S_133482_m2w)
  vwc0= S_133482_vwc0
  m2w0= S_133482_m2w0
  Sat = S_133482_Sat
  e = S_133482_e
  n = S_133482_n
  vac = S_133482_vac
  S = S_133482_S

start 'BN_Upper cover_403758790' (6.401,6.706)
   natural(h)=0
  Line to (9.144,6.706)
  Line to (12.192,7.711)
   value(h)=12.192
  Line to (13.106,8.016)
   natural(h)=0
  Line to (27.432,12.802)
  Line to (27.432,13.716)
   natural(h)=0
  Line to (6.401,6.706)

Region 4    'Filter'
  Kx = LUMP(S_926347_Kx)
  Ky = Kx*S_926347_Ky_ratio
  vwc= S_926347_vwc
  m2w= LUMP(S_926347_m2w)
  vwc0= S_926347_vwc0
  m2w0= S_926347_m2w0
  Sat = S_926347_Sat
  e = S_926347_e
  n = S_926347_n
  vac = S_926347_vac
  S = S_926347_S

start 'BN_Filter_131084812' (45.72,1.715)
   value(h)=-0.063*X+(4.573)
  Line to (73.152,0)
   natural(h)=0
  Line to (69.776,1.125)
   natural(h)=0
  Line to (48.158,2.477)
  Line to (45.72,1.715)

TIME
   From StartTime To EndTime By TimeInc
   HALT 1E-18
```

```
MONITORS

PLOTS
  For T=StartTime  Summary as "Problem Properties"
    report "ProjectID: CTWeber"
    report "Project Name: Dam Lining Systems"
    report "ProblemID: GMDamDrain"
    report "System: 2D     Type: Transient"
    report "Problem Created: 6/29/2007 1:27:09 PM by SVFlux 5.76.000"
    report " "
    report "Time (day): Start - 0 Increment - 1 End - 100000 "
    report " "
    report "Description:  "

 For CYCLE = 2  Contour(u) as "Pressure"
  Contour(h) as "Head"
  Contour(vwc) as "VWC"

{Output Files}
  For T=0 By 100000 To 100000  Table(u) file "PP.tbl" points = (10,10)
 For CYCLE = 2  Tecplot(Xoffset,Yoffset,u,h,vwc)print file "GMDamNoDrain.dat"

END
```

TITLE"
{ProjectID: CTWeber, ProblemID: FluxDefectTransient, Description: 3D, Transient, Metric}

```
COORDINATES
 Cartesian3

SELECT
 CHANGELIM=0.5
 ITERATE=1000
 NBCMEASURE
 CURVEGRID=Off
 ALIGN_MESH
 HISTORY_LIMIT=100000

VARIABLES
 h(THRESHOLD=0.001)

DEFINITIONS
{Time - Units: day}
 StartTime = 0, Timeinc = 0.001, EndTime = 3650

{General definitions}
 uww=9.807 {kN/m^3}, pw=1000 {kg/m^3}, g=9.81 {m/s^2}
 Sat,e,n,vac   {Volume-Mass}

 Xoffset=x+(0), Yoffset=y+(0)

{Initial Head}
 h0=-.7

 hdiff=h-h0

 u0 = uww*(h0-z)
 u=uww*(h-z) {kPa}, hp=h-z {kPa}
 udiff = u-u0

{Sink/Source}
 S  {m^3/day}
 S_613578_S=0

 {Gradients}
 kx, ky, kz
 Gradx= -dx(h)*kx
 Grady= -dy(h)*ky
 Gradz= -dz(h)*kz

{Hydraulic Conductivity Ratios}
 S_613578_ky_ratio=1
 S_613578_kz_ratio=1

{Hydraulic Conductivity}
 S_613578_Kx=0.0006048

{SWCC and Storage Functions}
```

```
  vwc0, vwc, vwc_min=0.0001
  vwcdiff = vwc-vwc0
  m2w0, m2w
  m2wdiff = m2w-m2w0

  {SWCC - van Genuchten}
  avg613578 = 0.08, nvg613578 = 1.229, mvg613578 = 0.186, trvg613578 = 0.01019
  suc0613578 = if u0>=-0.01 then 0.01 else (if u0>=-999999 then -u0 else 999999)
  Sr0613578 = trvg613578+(1-trvg613578)*(1/(1+(suc0613578*avg613578)^nvg613578)^mvg613578)
  dS0613578 = -(1 - trvg613578) / ((1 + (avg613578 * suc0613578) ^ nvg613578) ^ mvg613578) *
mvg613578 * (avg613578 * suc0613578) ^ nvg613578 * nvg613578 / (suc0613578 * (1 + (avg613578 *
suc0613578) ^ nvg613578))
  S_613578_swcc0 = 0.38*Sr0613578
  S_613578_vwc0 = if S_613578_swcc0 > vwc_min then S_613578_swcc0 else vwc_min
  S_613578_m2w0 = SWAGE(u+0.01,-(0.38*dS0613578),0.0000001,0.02)
  suc613578 = if u>=-0.01 then 0.01 else (if u>=-999999 then -u else 999999)
  Sr613578 = trvg613578+(1-trvg613578)*(1/(1+(suc613578*avg613578)^nvg613578)^mvg613578)
  dS613578 = -(1 - trvg613578) / ((1 + (avg613578 * suc613578) ^ nvg613578) ^ mvg613578) *
mvg613578 * (avg613578 * suc613578) ^ nvg613578 * nvg613578 / (suc613578 * (1 + (avg613578 *
suc613578) ^ nvg613578))
  S_613578_swcc = 0.38*Sr613578
  S_613578_vwc = if S_613578_swcc > vwc_min then S_613578_swcc else vwc_min
  S_613578_m2w = SWAGE(u+0.01,-(0.38*dS613578),0.0000001,0.02)

{Volume-Mass}
  S_613578_e=0.6129032
  S_613578_Sat=S_613578_vwc*(1+S_613578_e)/S_613578_e
  S_613578_Sa=1-S_613578_Sat
  S_613578_n=S_613578_e/(1+S_613578_e)
  S_613578_vac=S_613578_n-S_613578_vwc

{Water Volume}
  Vw0 = Vol_Integral(dx(x)*dy(y)*dz(z)*vwc0)  {m^3}
  Vw = Vol_Integral(dx(x)*dy(y)*dz(z)*vwc)  {m^3}
  Vwdiff = Vw-Vw0  {m^3}

{Review Boundary Properties}
  Big=10000
  ReviewStatement = if h > z then -BIG * (h-z)^2 else 0

{ Surface Flux Sections}
  NFluxX = GradX*normal(1,0,0)*sign(normal(1,0,0))
  NFluxY = GradY*normal(0,1,0)*sign(normal(0,1,0))
  NFluxZ = GradZ*normal(0,0,1)*sign(normal(0,0,1))

  XSurfaceFlux_Surface_2_Region_2 = sintegral(NFluxX,"Surface 2","Defect1")
  TotalXSurfaceFlux_Surface_2_Region_2 = tintegral(XSurfaceFlux_Surface_2_Region_2)
  YSurfaceFlux_Surface_2_Region_2 = sintegral(NFluxY,"Surface 2","Defect1")
  TotalYSurfaceFlux_Surface_2_Region_2 = tintegral(YSurfaceFlux_Surface_2_Region_2)
  ZSurfaceFlux_Surface_2_Region_2 = sintegral(NFluxZ,"Surface 2","Defect1")
  TotalZSurfaceFlux_Surface_2_Region_2 = tintegral(ZSurfaceFlux_Surface_2_Region_2)
  NormalSurfaceFlux_Surface_2_Region_2 = sintegral(-(normal(GradX, GradY, GradZ)),"Surface
2","Defect1")
  TotalNormalSurfaceFlux_Surface_2_Region_2 = tintegral(NormalSurfaceFlux_Surface_2_Region_2)
```

```
{Surfaces}
  SurfaceData_1 = table("CTWeber_FluxDefectTransient_Surface_1.tbl")
  SurfaceData_2 = table("CTWeber_FluxDefectTransient_Surface_2.tbl")

  Surface_1 = SurfaceData_1
  Surface_2 = SurfaceData_2

INITIAL VALUES
  h=h0

EQUATIONS
  div(vector(kx*dx(h),ky*dy(h),kz*dz(h))) + S = dt(h)*uww*m2w              {H-Based (Conventional)
Formulation}

EXTRUSION
  Surface "Surface 1"  z = Surface_1
    Layer "Layer 1"
  Surface "Surface 2"  z = Surface_2

BOUNDARIES

Region 1          'Upstream'
Layer 1
  Kx = LUMP(S_613578_Kx)
  Ky = Kx*S_613578_Ky_ratio
  Kz = Kx*S_613578_Kz_ratio
  vwc= S_613578_vwc
  m2w= LUMP(S_613578_m2w)
  vwc0= S_613578_vwc0
  m2w0= S_613578_m2w0
  Sat = S_613578_Sat
  e = S_613578_e
  n = S_613578_n
  vac = S_613578_vac
  S = S_613578_S

  Surface 1 natural(h)=0
  Surface 2 natural(h)=0

start 'BN1' (0,0)
  Layer 1 natural(h)=0
  Line to (27.432,0)
  Layer 1 nobc(h)
  Line to (27.432,150)
  Layer 1 natural(h)=0
  Line to (0,150)
  Line to (0,0)

Region 2          'Defect1'
Layer 1
  Kx = LUMP(S_613578_Kx)
  Ky = Kx*S_613578_Ky_ratio
```

```
  Kz = Kx*S_613578_Kz_ratio
  vwc= S_613578_vwc
  m2w= LUMP(S_613578_m2w)
  vwc0= S_613578_vwc0
  m2w0= S_613578_m2w0
  Sat = S_613578_Sat
  e = S_613578_e
  n = S_613578_n
  vac = S_613578_vac
  S = S_613578_S

  Surface 1 natural(h)=0
  Surface 2 natural(h)= 9.46E-4

start 'BN2' (12.192,74.543)
  Layer 1 nobc(h)
  Line to (13.106,74.543)
  Line to (13.106,75.457)
  Line to (12.192,75.457)
  Line to (12.192,74.543)

Region 3          'Downstream'
Layer 1
  Kx = LUMP(S_613578_Kx)
  Ky = Kx*S_613578_Ky_ratio
  Kz = Kx*S_613578_Kz_ratio
  vwc= S_613578_vwc
  m2w= LUMP(S_613578_m2w)
  vwc0= S_613578_vwc0
  m2w0= S_613578_m2w0
  Sat = S_613578_Sat
  e = S_613578_e
  n = S_613578_n
  vac = S_613578_vac
  S = S_613578_S

  Surface 1 natural(h)=0
  Surface 2 natural(h)= ReviewStatement

start 'BN3' (32.004,0)
  Layer 1 natural(h)=0
  Line to (73.2,0)
  Layer 1 natural(h)= ReviewStatement
  Line to (73.2,150)
  Layer 1 natural(h)=0
  Line to (32.004,150)
  Layer 1 nobc(h)
  Line to (32.004,0)

Region 4          'Center'
Layer 1
  Kx = LUMP(S_613578_Kx)
  Ky = Kx*S_613578_Ky_ratio
  Kz = Kx*S_613578_Kz_ratio
```

```
  vwc= S_613578_vwc
  m2w= LUMP(S_613578_m2w)
  vwc0= S_613578_vwc0
  m2w0= S_613578_m2w0
  Sat = S_613578_Sat
  e = S_613578_e
  n = S_613578_n
  vac = S_613578_vac
  S = S_613578_S

  Surface 1 natural(h)=0
  Surface 2 natural(h)=0

start 'BN4' (27.432,0)
  Layer 1 natural(h)=0
  Line to (29.566,0)
  Line to (31.394,0)
  Line to (32.004,0)
  Layer 1 nobc(h)
  Line to (32.004,150)
  Layer 1 natural(h)=0
  Line to (31.394,150)
  Line to (29.566,150)
  Line to (27.432,150)
  Layer 1 nobc(h)
  Line to (27.432,0)

{Features}
  Feature "Feature_1" Start (27.432,0)
  Line To (27.432,150)
  Feature "Feature_2" Start (32.004,0)
  Line To (32.004,150)
  Feature "Feature_3" Start (24.079,0)
  Line To (24.079,150)
  Feature "Feature_4" Start (25.908,0)
  Line To (25.908,150)
  Feature "Feature_5" Start (29.566,0)
  Line To (29.566,150)
  Feature "Feature_6" Start (31.394,0)
  Line To (31.394,150)


TIME
   From StartTime To EndTime By TimeInc

MONITORS

PLOTS
  For T=StartTime  Summary as "Problem Properties"
    report "ProjectID: CTWeber"
    report "Project Name: Dam Lining Systems"
    report "ProblemID: FluxDefectTransient"
    report "System: 3D     Type: Transient"
    report "Problem Created: 3/14/2008 3:24:32 PM by SVFlux 5.76.000"
```

```
   report " "
   report "Time (day): Start - 0 Increment - 0.001 End - 3650 "
   report " "
   report "Description:  "

 For CYCLE = 2  Contour(u) on Y=75 as "Pressure"
  Contour(h) on Y=75 as "Head"
  Contour(n) on Y=75 as "Porosity"
  Contour(vwc) on Y=75 as "VWC"
  Contour(u) on Y=37.5 as "PP37"
  Contour(u) on Y=56 as "PP56"

{Surface Flux Reports and Histories}
  Summary as"SF: Surface 2 - R: Defect1"
          report"Surface Flux Report: Surface 2 restricted to Defect1"
          report"Components (signs follow global coordinate system)"
          report" "
          report"Instantaneous Flow Rate"
          report(XSurfaceFlux_Surface_2_Region_2) as "X Component of Flow in (m^3/day) "
          report(YSurfaceFlux_Surface_2_Region_2) as "Y Component of Flow in (m^3/day) "
          report(ZSurfaceFlux_Surface_2_Region_2) as "Z Component of Flow in (m^3/day) "
          report " "
          report"Total Flow"
          report(TotalXSurfaceFlux_Surface_2_Region_2) as "Total X Flow in (m^3) "
          report(TotalYSurfaceFlux_Surface_2_Region_2) as "Total Y Flow in (m^3) "
          report(TotalZSurfaceFlux_Surface_2_Region_2) as "Total Z Flow in (m^3) "
          report(TotalNormalSurfaceFlux_Surface_2_Region_2) as "Total Normal Flow in (m^3) "
          report" "
          report"Normal"
          report"   1. On External Surface: Positive Flow is into Problem"
          report"   2. On Internal Surface: Signs follow global coordinate system"
          report" "
          report"Instantaneous Flow Rate"
          report(NormalSurfaceFlux_Surface_2_Region_2) as "Normal Flow in (m^3/day) "
          report " "
          report"Total Flow"
          report(TotalNormalSurfaceFlux_Surface_2_Region_2) as "Total Normal Flow in (m^3) "

{Output Files}
  For T=0  Transfer(h)print file "HeadTransfer.trn"

END
```

TITLE"
{ProblemID: PalmdaleOneTear, Description: 3D, Transient, Metric}

COORDINATES
 Cartesian3

SELECT
 NBCMEASURE
 NONLINEAR
 NONSYMMETRIC
 CURVEGRID=Off
 ALIGN_MESH
 HISTORY_LIMIT=100000

VARIABLES
 h(THRESHOLD=0.001)

DEFINITIONS
{Time - Units: day}
 StartTime = 0, Timeinc = 0.001, EndTime = 730

{General definitions}
 uww=9.807 {kN/m^3}, pw=1000 {kg/m^3}, g=9.81 {m/s^2}
 Sat,e,n,vac {Volume-Mass}

 Xoffset=x+(0), Yoffset=y+(0)

{Initial Head}
 h0=-30

 hdiff=h-h0

 u0 = uww*(h0-z)
 u=uww*(h-z) {kPa}, hp=h-z {kPa}
 udiff = u-u0

{Sink/Source}
 S {m^3/day}
 S_486413_S=0
 S_627511_S=0

 {Gradients}
 kx, ky, kz
 Gradx= -dx(h)*kx
 Grady= -dy(h)*ky
 Gradz= -dz(h)*kz

{Hydraulic Conductivity Ratios}
 S_486413_ky_ratio=1
 S_486413_kz_ratio=0.1
 S_627511_ky_ratio=1
 S_627511_kz_ratio=0.1

{Hydraulic Conductivity}

```
  S_486413_Kx=1.21

  S_627511_Kx=4.32

{SWCC and Storage Functions}
  vwc0, vwc, vwc_min=0.0001
  vwcdiff = vwc-vwc0
  m2w0, m2w
  m2wdiff = m2w-m2w0

  {SWCC - van Genuchten}
  avg486413 = 0.44, nvg486413 = 3.1, mvg486413 = 0.68, trvg486413 = 0.14
  suc0486413 = if u0>=-0.01 then 0.01 else (if u0>=-999999 then -u0 else 999999)
  Sr0486413 = trvg486413+(1-trvg486413)*(1/(1+(suc0486413*avg486413)^nvg486413)^mvg486413)
  dS0486413 = -(1 - trvg486413) / ((1 + (avg486413 * suc0486413) ^ nvg486413) ^ mvg486413) *
mvg486413 * (avg486413 * suc0486413) ^ nvg486413 * nvg486413 / (suc0486413 * (1 + (avg486413 *
suc0486413) ^ nvg486413))
  S_486413_swcc0 = 0.38*Sr0486413
  S_486413_vwc0 = if S_486413_swcc0 > vwc_min then S_486413_swcc0 else vwc_min
  S_486413_m2w0 = SWAGE(u+0.1,-(0.38*dS0486413),0.0000001,0.02)
  suc486413 = if u>=-0.01 then 0.01 else (if u>=-999999 then -u else 999999)
  Sr486413 = trvg486413+(1-trvg486413)*(1/(1+(suc486413*avg486413)^nvg486413)^mvg486413)
  dS486413 = -(1 - trvg486413) / ((1 + (avg486413 * suc486413) ^ nvg486413) ^ mvg486413) *
mvg486413 * (avg486413 * suc486413) ^ nvg486413 * nvg486413 / (suc486413 * (1 + (avg486413 *
suc486413) ^ nvg486413))
  S_486413_swcc = 0.38*Sr486413
  S_486413_vwc = if S_486413_swcc > vwc_min then S_486413_swcc else vwc_min
  S_486413_m2w = SWAGE(u+0.1,-(0.38*dS486413),0.0000001,0.02)

  {SWCC - van Genuchten}
  avg627511 = 0.44, nvg627511 = 3.1, mvg627511 = 0.68, trvg627511 = 0.14
  suc0627511 = if u0>=-0.01 then 0.01 else (if u0>=-999999 then -u0 else 999999)
  Sr0627511 = trvg627511+(1-trvg627511)*(1/(1+(suc0627511*avg627511)^nvg627511)^mvg627511)
  dS0627511 = -(1 - trvg627511) / ((1 + (avg627511 * suc0627511) ^ nvg627511) ^ mvg627511) *
mvg627511 * (avg627511 * suc0627511) ^ nvg627511 * nvg627511 / (suc0627511 * (1 + (avg627511 *
suc0627511) ^ nvg627511))
  S_627511_swcc0 = 0.38*Sr0627511
  S_627511_vwc0 = if S_627511_swcc0 > vwc_min then S_627511_swcc0 else vwc_min
  S_627511_m2w0 = SWAGE(u+0.1,-(0.38*dS0627511),0.0000001,0.02)
  suc627511 = if u>=-0.01 then 0.01 else (if u>=-999999 then -u else 999999)
  Sr627511 = trvg627511+(1-trvg627511)*(1/(1+(suc627511*avg627511)^nvg627511)^mvg627511)
  dS627511 = -(1 - trvg627511) / ((1 + (avg627511 * suc627511) ^ nvg627511) ^ mvg627511) *
mvg627511 * (avg627511 * suc627511) ^ nvg627511 * nvg627511 / (suc627511 * (1 + (avg627511 *
suc627511) ^ nvg627511))
  S_627511_swcc = 0.38*Sr627511
  S_627511_vwc = if S_627511_swcc > vwc_min then S_627511_swcc else vwc_min
  S_627511_m2w = SWAGE(u+0.1,-(0.38*dS627511),0.0000001,0.02)

{Volume-Mass}
  S_486413_e=0.6129032
  S_486413_Sat=S_486413_vwc*(1+S_486413_e)/S_486413_e
  S_486413_Sa=1-S_486413_Sat
  S_486413_n=S_486413_e/(1+S_486413_e)
  S_486413_vac=S_486413_n-S_486413_vwc
```

```
 S_627511_e=0.6129032
 S_627511_Sat=S_627511_vwc*(1+S_627511_e)/S_627511_e
 S_627511_Sa=1-S_627511_Sat
 S_627511_n=S_627511_e/(1+S_627511_e)
 S_627511_vac=S_627511_n-S_627511_vwc

{Water Volume}
 Vw0 = Vol_Integral(dx(x)*dy(y)*dz(z)*vwc0)  {m^3}
 Vw = Vol_Integral(dx(x)*dy(y)*dz(z)*vwc)  {m^3}
 Vwdiff = Vw-Vw0  {m^3}

{Review Boundary Properties}
 Big=10000
 ReviewStatement = if h > z then -BIG * (h-z)^2 else 0

{ Surface Flux Sections}
 NFluxX = GradX*normal(1,0,0)*sign(normal(1,0,0))
 NFluxY = GradY*normal(0,1,0)*sign(normal(0,1,0))
 NFluxZ = GradZ*normal(0,0,1)*sign(normal(0,0,1))

 XSurfaceFlux_Surface_2_Region_7 = sintegral(NFluxX,"Surface 2","Defect2")
 TotalXSurfaceFlux_Surface_2_Region_7 = tintegral(XSurfaceFlux_Surface_2_Region_7)
 YSurfaceFlux_Surface_2_Region_7 = sintegral(NFluxY,"Surface 2","Defect2")
 TotalYSurfaceFlux_Surface_2_Region_7 = tintegral(YSurfaceFlux_Surface_2_Region_7)
 ZSurfaceFlux_Surface_2_Region_7 = sintegral(NFluxZ,"Surface 2","Defect2")
 TotalZSurfaceFlux_Surface_2_Region_7 = tintegral(ZSurfaceFlux_Surface_2_Region_7)
 NormalSurfaceFlux_Surface_2_Region_7 = sintegral(-(normal(GradX, GradY, GradZ)),"Surface
2","Defect2")
 TotalNormalSurfaceFlux_Surface_2_Region_7 = tintegral(NormalSurfaceFlux_Surface_2_Region_7)
 XSurfaceFlux_Surface_3_Region_6 = sintegral(NFluxX,"Surface 3","Defect")
 TotalXSurfaceFlux_Surface_3_Region_6 = tintegral(XSurfaceFlux_Surface_3_Region_6)
 YSurfaceFlux_Surface_3_Region_6 = sintegral(NFluxY,"Surface 3","Defect")
 TotalYSurfaceFlux_Surface_3_Region_6 = tintegral(YSurfaceFlux_Surface_3_Region_6)
 ZSurfaceFlux_Surface_3_Region_6 = sintegral(NFluxZ,"Surface 3","Defect")
 TotalZSurfaceFlux_Surface_3_Region_6 = tintegral(ZSurfaceFlux_Surface_3_Region_6)
 NormalSurfaceFlux_Surface_3_Region_6 = sintegral(-(normal(GradX, GradY, GradZ)),"Surface
3","Defect")
 TotalNormalSurfaceFlux_Surface_3_Region_6 = tintegral(NormalSurfaceFlux_Surface_3_Region_6)


{Surfaces}
 SurfaceData_1 = table("Geomatrix_PalmdaleOneTear_Surface_1.tbl")
 SurfaceData_2 = table("Geomatrix_PalmdaleOneTear_Surface_2.tbl")
 SurfaceData_3 = table("Geomatrix_PalmdaleOneTear_Surface_3.tbl")

 Surface_1 = SurfaceData_1
 Surface_2 = SurfaceData_2
 Surface_3 = SurfaceData_3

INITIAL VALUES
 h=h0

EQUATIONS
 div(vector(kx*dx(h),ky*dy(h),kz*dz(h))) + S = dt(vwc)     {Mixed (Mass Conservative) Formulation}
```

```
EXTRUSION
  Surface "Surface 1"  z = Surface_1
    Layer "Layer 1"
  Surface "Surface 2"  z = Surface_2
    Layer "Layer 2"
  Surface "Surface 3"  z = Surface_3

BOUNDARIES

Region 1          'Reservoir'
Layer 1
  Kx = LUMP(S_486413_Kx)
  Ky = Kx*S_486413_Ky_ratio
  Kz = Kx*S_486413_Kz_ratio
  vwc= S_486413_vwc
  m2w= LUMP(S_486413_m2w)
  vwc0= S_486413_vwc0
  m2w0= S_486413_m2w0
  Sat = S_486413_Sat
  e = S_486413_e
  n = S_486413_n
  vac = S_486413_vac
  S = S_486413_S

Layer 2
  Kx = LUMP(S_627511_Kx)
  Ky = Kx*S_627511_Ky_ratio
  Kz = Kx*S_627511_Kz_ratio
  vwc= S_627511_vwc
  m2w= LUMP(S_627511_m2w)
  vwc0= S_627511_vwc0
  m2w0= S_627511_m2w0
  Sat = S_627511_Sat
  e = S_627511_e
  n = S_627511_n
  vac = S_627511_vac
  S = S_627511_S

  Surface 1 natural(h)= ReviewStatement
  Surface 2 natural(h)=0

start 'BN1' (0,0)
  Layer 1 natural(h)=0
  Layer 2 nobc(h)
  Line to (96,0)
  Layer 1 nobc(h)
  Layer 2 natural(h)=0
  Line to (96,761.005)
  Line to (96,762.005)
  Line to (96,1524)
  Layer 1 natural(h)=0
  Layer 2 nobc(h)
  Line to (0,1524)
```

```
  Line to (0,0)

Region 2          'Upstream Face'
Layer 1
  Kx = LUMP(S_486413_Kx)
  Ky = Kx*S_486413_Ky_ratio
  Kz = Kx*S_486413_Kz_ratio
  vwc= S_486413_vwc
  m2w= LUMP(S_486413_m2w)
  vwc0= S_486413_vwc0
  m2w0= S_486413_m2w0
  Sat = S_486413_Sat
  e = S_486413_e
  n = S_486413_n
  vac = S_486413_vac
  S = S_486413_S

Layer 2
  Kx = LUMP(S_627511_Kx)
  Ky = Kx*S_627511_Ky_ratio
  Kz = Kx*S_627511_Kz_ratio
  vwc= S_627511_vwc
  m2w= LUMP(S_627511_m2w)
  vwc0= S_627511_vwc0
  m2w0= S_627511_m2w0
  Sat = S_627511_Sat
  e = S_627511_e
  n = S_627511_n
  vac = S_627511_vac
  S = S_627511_S

  Surface 1 natural(h)= ReviewStatement
  Surface 3 natural(h)=0

start 'BN2' (96,0)
  Layer 1 natural(h)=0
  Layer 2 natural(h)=0
  Line to (115.2,0)
  Layer 1 nobc(h)
  Layer 2 nobc(h)
  Line to (115.2,761.005)
  Line to (115.2,762.005)
  Line to (115.2,1524)
  Layer 1 natural(h)=0
  Layer 2 natural(h)=0
  Line to (96,1524)
  Layer 1 nobc(h)
  Layer 2 nobc(h)
  Line to (96,762.005)
  Line to (96,761.005)
  Line to (96,0)

Region 3          'Crest'
Layer 1
```

```
  Kx = LUMP(S_486413_Kx)
  Ky = Kx*S_486413_Ky_ratio
  Kz = Kx*S_486413_Kz_ratio
  vwc= S_486413_vwc
  m2w= LUMP(S_486413_m2w)
  vwc0= S_486413_vwc0
  m2w0= S_486413_m2w0
  Sat = S_486413_Sat
  e = S_486413_e
  n = S_486413_n
  vac = S_486413_vac
  S = S_486413_S

 Layer 2
  Kx = LUMP(S_627511_Kx)
  Ky = Kx*S_627511_Ky_ratio
  Kz = Kx*S_627511_Kz_ratio
  vwc= S_627511_vwc
  m2w= LUMP(S_627511_m2w)
  vwc0= S_627511_vwc0
  m2w0= S_627511_m2w0
  Sat = S_627511_Sat
  e = S_627511_e
  n = S_627511_n
  vac = S_627511_vac
  S = S_627511_S

  Surface 1 natural(h)= ReviewStatement
  Surface 3 natural(h)=0

 start 'BN3' (115.2,0)
  Layer 1 natural(h)=0
  Layer 2 natural(h)=0
  Line to (124.4,0)
  Layer 1 nobc(h)
  Layer 2 nobc(h)
  Line to (124.4,1524)
  Layer 1 natural(h)=0
  Layer 2 natural(h)=0
  Line to (115.2,1524)
  Layer 1 nobc(h)
  Layer 2 nobc(h)
  Line to (115.2,762.005)
  Line to (115.2,761.005)
  Line to (115.2,0)

 Region 4          'Downstream Face'
 Layer 1
  Kx = LUMP(S_486413_Kx)
  Ky = Kx*S_486413_Ky_ratio
  Kz = Kx*S_486413_Kz_ratio
  vwc= S_486413_vwc
  m2w= LUMP(S_486413_m2w)
  vwc0= S_486413_vwc0
```

```
  m2w0= S_486413_m2w0
  Sat = S_486413_Sat
  e = S_486413_e
  n = S_486413_n
  vac = S_486413_vac
  S = S_486413_S

Layer 2
  Kx = LUMP(S_627511_Kx)
  Ky = Kx*S_627511_Ky_ratio
  Kz = Kx*S_627511_Kz_ratio
  vwc= S_627511_vwc
  m2w= LUMP(S_627511_m2w)
  vwc0= S_627511_vwc0
  m2w0= S_627511_m2w0
  Sat = S_627511_Sat
  e = S_627511_e
  n = S_627511_n
  vac = S_627511_vac
  S = S_627511_S

  Surface 1 natural(h)= ReviewStatement
  Surface 3 natural(h)= ReviewStatement

start 'BN4' (124.4,0)
  Layer 1 natural(h)=0
  Layer 2 natural(h)=0
  Line to (140.8,0)
  Layer 1 nobc(h)
  Layer 2 natural(h)= ReviewStatement
  Line to (140.8,1524)
  Layer 1 natural(h)=0
  Layer 2 natural(h)=0
  Line to (124.4,1524)
  Layer 1 nobc(h)
  Layer 2 nobc(h)
  Line to (124.4,0)

Region 5          'Downstream'
Layer 1
  Kx = LUMP(S_486413_Kx)
  Ky = Kx*S_486413_Ky_ratio
  Kz = Kx*S_486413_Kz_ratio
  vwc= S_486413_vwc
  m2w= LUMP(S_486413_m2w)
  vwc0= S_486413_vwc0
  m2w0= S_486413_m2w0
  Sat = S_486413_Sat
  e = S_486413_e
  n = S_486413_n
  vac = S_486413_vac
  S = S_486413_S

Layer 2
```

```
  Kx = LUMP(S_627511_Kx)
  Ky = Kx*S_627511_Ky_ratio
  Kz = Kx*S_627511_Kz_ratio
  vwc= S_627511_vwc
  m2w= LUMP(S_627511_m2w)
  vwc0= S_627511_vwc0
  m2w0= S_627511_m2w0
  Sat = S_627511_Sat
  e = S_627511_e
  n = S_627511_n
  vac = S_627511_vac
  S = S_627511_S

  Surface 1 natural(h)= ReviewStatement
  Surface 2 natural(h)= ReviewStatement

start 'BN5' (140.8,0)
  Layer 1 natural(h)=0
  Layer 2 nobc(h)
  Line to (152.2,0)
  Line to (152.2,1524)
  Line to (140.8,1524)
  Layer 1 nobc(h)
  Line to (140.8,0)

Region 6          'Defect'
Layer 1
  Kx = LUMP(S_486413_Kx)
  Ky = Kx*S_486413_Ky_ratio
  Kz = Kx*S_486413_Kz_ratio
  vwc= S_486413_vwc
  m2w= LUMP(S_486413_m2w)
  vwc0= S_486413_vwc0
  m2w0= S_486413_m2w0
  Sat = S_486413_Sat
  e = S_486413_e
  n = S_486413_n
  vac = S_486413_vac
  S = S_486413_S

Layer 2
  Kx = LUMP(S_627511_Kx)
  Ky = Kx*S_627511_Ky_ratio
  Kz = Kx*S_627511_Kz_ratio
  vwc= S_627511_vwc
  m2w= LUMP(S_627511_m2w)
  vwc0= S_627511_vwc0
  m2w0= S_627511_m2w0
  Sat = S_627511_Sat
  e = S_627511_e
  n = S_627511_n
  vac = S_627511_vac
  S = S_627511_S
```

```
  Surface 1 natural(h)= ReviewStatement
  Surface 3 value(h)=5.5

start 'BN6' (96,761.005)
  Layer 1 nobc(h)
  Layer 2 nobc(h)
  Line to (112.5,761.005)
  Line to (112.5,762.005)
  Line to (96,762.005)
  Line to (96,761.005)

Region 7          'Defect2'
Layer 1
  Kx = LUMP(S_486413_Kx)
  Ky = Kx*S_486413_Ky_ratio
  Kz = Kx*S_486413_Kz_ratio
  vwc= S_486413_vwc
  m2w= LUMP(S_486413_m2w)
  vwc0= S_486413_vwc0
  m2w0= S_486413_m2w0
  Sat = S_486413_Sat
  e = S_486413_e
  n = S_486413_n
  vac = S_486413_vac
  S = S_486413_S

Layer 2
  Kx = LUMP(S_627511_Kx)
  Ky = Kx*S_627511_Ky_ratio
  Kz = Kx*S_627511_Kz_ratio
  vwc= S_627511_vwc
  m2w= LUMP(S_627511_m2w)
  vwc0= S_627511_vwc0
  m2w0= S_627511_m2w0
  Sat = S_627511_Sat
  e = S_627511_e
  n = S_627511_n
  vac = S_627511_vac
  S = S_627511_S

  Surface 1 natural(h)= ReviewStatement
  Surface 2 value(h)=5.5

start 'BN7' (0,761.005)
  Layer 1 nobc(h)
  Layer 2 nobc(h)
  Line to (96,761.005)
  Line to (96,762.005)
  Line to (0,762.005)
  Layer 1 natural(h)=0
  Line to (0,761.005)

{Features}
  Feature "Feature_1" Start (140.8,0)
```

```
 Line To (140.8,1524)
 Feature "Feature_2" Start (96,0)
 Line To (96,1524)
 Feature "Feature_3" Start (124.4,0)
 Line To (124.4,1524)
 Feature "Feature_4" Start (115.2,0)
 Line To (115.2,1524)


TIME
  From StartTime To EndTime By TimeInc
  HALT 1E-18

MONITORS

PLOTS
 For T=StartTime  Summary as "Problem Properties"
   report "ProjectID: Geomatrix"
   report "Project Name: Geomatrix Reservoir Project"
   report "ProblemID: PalmdaleOneTear"
   report "System: 3D     Type: Transient"
   report "Problem Created: 3/11/2008 2:50:20 PM by SVFlux 5.76.000"
   report " "
   report "Time (day): Start - 0 Increment - 0.001 End - 730 "
   report " "
   report "Description:  "

 For CYCLE = 2  Contour(h) on Layer 2 on Y=762 as "Head"
 Contour(h) on Y=762 as "Head" fixed range(-10,5.5)
 Contour(u) on Y=381 as "PP"
 Contour(u) on Y=762 as "PP"
 Contour(h) on Y=762 as "Head"
 Contour(vwc) on Y=762 as "VWC"

{Surface Flux Reports and Histories}
 Summary as"SF: Surface 2 - R: Defect2"
          report"Surface Flux Report: Surface 2 restricted to Defect2"
          report"Components (signs follow global coordinate system)"
          report" "
          report"Instantaneous Flow Rate"
          report(XSurfaceFlux_Surface_2_Region_7) as "X Component of Flow in (m^3/day) "
          report(YSurfaceFlux_Surface_2_Region_7) as "Y Component of Flow in (m^3/day) "
          report(ZSurfaceFlux_Surface_2_Region_7) as "Z Component of Flow in (m^3/day) "
          report " "
          report"Total Flow"
          report(TotalXSurfaceFlux_Surface_2_Region_7) as "Total X Flow in (m^3) "
          report(TotalYSurfaceFlux_Surface_2_Region_7) as "Total Y Flow in (m^3) "
          report(TotalZSurfaceFlux_Surface_2_Region_7) as "Total Z Flow in (m^3) "
          report(TotalNormalSurfaceFlux_Surface_2_Region_7) as "Total Normal Flow in (m^3) "
          report" "
          report"Normal"
          report"   1. On External Surface: Positive Flow is into Problem"
          report"   2. On Internal Surface: Signs follow global coordinate system"
          report" "
```

```
        report"Instantaneous Flow Rate"
        report(NormalSurfaceFlux_Surface_2_Region_7) as "Normal Flow in (m^3/day) "
        report " "
        report"Total Flow"
        report(TotalNormalSurfaceFlux_Surface_2_Region_7) as "Total Normal Flow in (m^3) "

 Summary as"SF: Surface 3 - R: Defect"
        report"Surface Flux Report: Surface 3 restricted to Defect"
        report"Components (signs follow global coordinate system)"
        report" "
        report"Instantaneous Flow Rate"
        report(XSurfaceFlux_Surface_3_Region_6) as "X Component of Flow in (m^3/day) "
        report(YSurfaceFlux_Surface_3_Region_6) as "Y Component of Flow in (m^3/day) "
        report(ZSurfaceFlux_Surface_3_Region_6) as "Z Component of Flow in (m^3/day) "
        report " "
        report"Total Flow"
        report(TotalXSurfaceFlux_Surface_3_Region_6) as "Total X Flow in (m^3) "
        report(TotalYSurfaceFlux_Surface_3_Region_6) as "Total Y Flow in (m^3) "
        report(TotalZSurfaceFlux_Surface_3_Region_6) as "Total Z Flow in (m^3) "
        report(TotalNormalSurfaceFlux_Surface_3_Region_6) as "Total Normal Flow in (m^3) "
        report" "
        report"Normal"
        report"   1. On External Surface: Positive Flow is into Problem"
        report"   2. On Internal Surface: Signs follow global coordinate system"
        report" "
        report"Instantaneous Flow Rate"
        report(NormalSurfaceFlux_Surface_3_Region_6) as "Normal Flow in (m^3/day) "
        report " "
        report"Total Flow"
        report(TotalNormalSurfaceFlux_Surface_3_Region_6) as "Total Normal Flow in (m^3) "

{Output Files}
 For CYCLE = 2  Tecplot(Xoffset,Yoffset,u,h,vwc)print file "PalmdaleOneTear.dat"

END
```

Appendix C

The analytical model developed by Touze-Foltz et al. (1999) for field conditions can be solved by using Modified Bessel functions of the zero- and first degrees. Modified Bessel functions are among the many functions available in the Microsoft Excel. The analytical model developed by Touze-Foltz et al. (1999) is discussed in Section 2.3.3.

A spreadsheet (*filename: Touze-Foltz et al 1999 Field.xlsm)* was developed to calculate the leakage through a defect in a geomembrane placed over a soil layer using the analytical model developed by Touze-Foltz et al. (1999). The spreadsheet for calculating the leakage rate through a defect for field conditions is shown in Figure C.1. The column and row headings are included in the figure and the spreadsheet commands are shown as well. To calculate the leakage rate for a given system, the hydraulic head, the hydraulic conductivity of the underlying soil layer, the thickness of the soil layer and the radius of the defect must be entered into the spreadsheet. A value for transmissivity is also needed to solve for the leakage rate. Once these inputs have been entered into the spreadsheet, Excel's Solver function is used to calculate the radius of interface flow by varying the radius (cell H33 in Figure C.1) until the slope of pressure head curve is equal to zero (cell H31 in Figure C.1). Basically, Newton-Raphson iteration is used to find the root of the equation in cell H31. Once the cell H31 is equal to zero, the value in cell H52 is the calculated leakage rate and the value in K25 is the transmissivity.

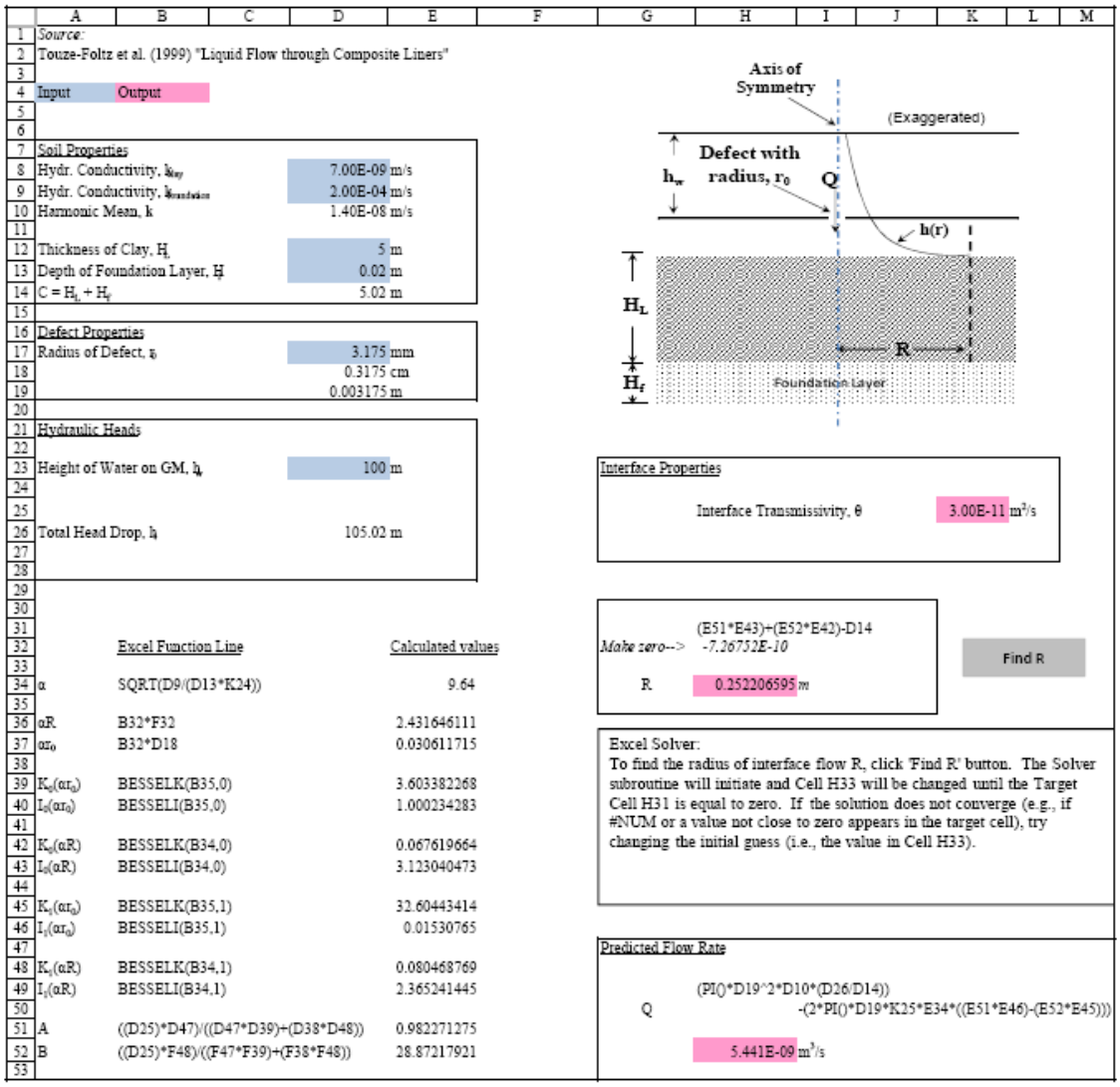

Figure C.1: Sample spreadsheet used to calculate leakage rates using the analytical model developed by Touze-Foltz et al. (1999)

References

ASTM D 4439. Standard Terminology for Geosynthetics. The American Society for Testing and Materials. West Conshohoken, PA.

Barroso, M., Touze-Foltz, N., von Maubeuge, K. and Pierson, P. (2006). "Laboratory investigation of flow rate through composite liners consisting of a geomembrane, a GCL and a soil liner." Geotextiles and Geomembranes, 24(3), pp. 139-155.

Barroso, M. (2005). "Fluid migration through geomembrane seams and through the interface between geomembrane and geosynthetic clay liner." Dissertation, Universities of Grenoble and Coimbra, France and Portugal, 215 pp.

Becker, E.B., Carey, G.F. and Oden, J.T. (1981). Finite Elements: An Introduction. Prentice-Hall, Englewood Cliffs, New Jersey.

Benson, C.H., Tinjum, J.M. and Hussin, C.J. (1995). "Leakage rates from geomembrane liners containing holes." Proc. Geosynthetics '95, pp.745-758.

Bouazza, A. (2002). "Geosynthetic clay liners." Geotextiles and Geomembranes, 20(1), pp. 3-17.

Brooks, R.H., and Corey, A.T. (1964). "Hydraulic properties of porous media." Hydrology Paper 3, Colorado State University.

Brown, K.W., Thomas, C.J., Lytton, R.L., Jayawickrama, P. and Bahrt, S. (1987). "Quantification of leak rates through holes in landfill liners." Rep. No. EPA/600/2-87/062, US EPA, Cincinnati, OH.

California Secretary of State (2006). Proposition No. 1E Results. Statement of Vote: 2006 General Elections, pg. 102.

Cartaud, F., Goblet, P. and Touze-Foltz, N. (2005). "Numerical simulation of the flow in the interface of a composite liner." Geotextiles and Geomembranes, 23(6), pp. 513-533.

Chen, L., and M. H. Young (2006), Green-Ampt infiltration model for sloping surfaces, Water Resour. Res., 42, pg. W07420.

Foose, G.J., Benson, C.H., and Edil, T.B. (2001). "Predicting Leakage through Composite Landfill Liners." J. Geotech. and Geoenvir. Engrg., ASCE, 127(6), 534-539.

Fukuoka, M. (1986). "Large scale permeability test for geomembrane-subgrade system." Proc. 3rd Int. Conf. on Geotextiles, Vienna, Austria, pp. 917-922.

Giroud, J.P (1997). "Equations for calculating the rate of liquid migration through composite liners due to geomembrane defects." Geosynthetics International, 4(3-4), pp. 335-348.

Giroud, J.P. and Bonaparte, R. (1989). "Leakage through liners constructed with geomembranes – Parts I and II." Geotextiles and Geomembranes, 8(1) and 8(2), pp. 27-67 and 71-111.

Giroud, J.P., Khatami, A. and Badu-Tweneboah, K. (1989). "Evaluation of the rate of leakage through composite liners." Geotextiles and Geomembranes, 8(4), pp. 241-271.

Green, W.H. and Ampt, G.A. (1911). Studies on soil physics. J. Agricultural Science, 4(1), 1-24.

GSE (2003). "Bentofix NWL GCL Product Data Sheet." GSE Inc., Houston, TX.

GSE (2004). "GSE UltraFlex Geomembrane Product Data Sheet." GSE Inc., Houston, TX.

Harpur, W.A., Wilson-Fahmy, R.F. and Koerner, R.M. (1993). "Evaluation of the contact between geosynthetic clay liners and geomembranes in terms of transmissivity." Geosynthetic Liner Systems: Innovations, Concerns and Design, Proc. of a Geosynthetic Liner System Seminar, Philadelphia, PA., pp. 143-154.

International Geosynthetics Society (IGS) (2000). Recommended Descriptions of Geosynthetics Functions, Geosynthetics Terminology, Mathematical and Graphical Symbols. International Geosynthetic Society, Fourth Edition.

International Committee on Large Dams (ICOLD) (2007). "Geomembrane Sealing Systems for Dams." ICOLD Bulletin 78, publication pending.

Koerner, R.M. (1998). Designing with Geosynthetics. 4th Edition, Prentice Hall, New Jersey.

Koerner, R.M. and Wilkes, J.A. (2007). "The 2006 ICOLD Bulletin on geomembrane sealing systems for dams." Proc. 27th USSD Conference, United States Society of Dams, March 2007, Philadelphia, PA, pg. 69-78.

Kuhn, J.A. (2007). Personal communication. University of Texas at Austin, Austin, TX.

Lacroix, Yves (1984). "The geomembrane liner at Terzaghi Dam." Proc. Int. Conf. on Geomembranes, Denver, CO, pp. 9-14.

Li, Chunling (2005). "Mechanical response of fiber-reinforced soil." Dissertation, University of Texas at Austin, pp.30-33.

McCartney, J.S. (2007). "Measurement of hydraulic characteristics of unsaturated soils using a centrifuge permeameter." Dissertation, University of Texas at Austin, Texas, USA.

McCray, J. (2004). Class notes: Vadose Zone Hydrology. Spring Semester, 2004.

National Inventory of Dams (NID) (2005). Database, United States Army Corps of Engineers.

Nosko, V. and Touze-Foltz, N. (2000). "Geomembrane liner failure: Modelling of its influence on contaminant transfer." Proc. 2nd European Conf. on Geosynthetics, Vol 2, Bologna, Italy, pp. 557-560.

Schwarzeneggar, A. (2006). "Gov. Schwarzenegger highlights completed levee repairs, presses federal government for reimbursement for work on federal levees." Office of the Governor of California, Press Release, Oct 10, 2006.

Olsta, J. and Carine, D. (2005). "Dam rehabilitation using geosynthetic clay liners." Proc. Dam Safety 2005, Association of State Dam Safety Officials, Orlando, Florida.

Rowe, R.K. (1998). "Geosynthetics and the minimization of contaminant migration through barrier systems beneath solid waste," Keynote Lecture, Proc. 6th Int. Conf. on Geosynthetics, Vol. 1, Atlanta, GA, pp. 27-103.

Sembenelli, P. (1990). "Engineering geosynthetics in design and construction of Jibiya dam." Proc. 4th Int. Conf. on Geotextiles, Geomembranes and Related Products, International Geosynthetics Society, pp. 419-424.

Sembenelli, P. and Rodriguez, E.A. (1996). Geomembranes for earth and rock dams: State of the art report. Proc. Geosynthetics: Applications, Design and Construction: 1st European Geosynthetics Conf., Balkema, Maastricht, The Netherlands: 877-888.

Shan, H-Y. and Daniel, D.E. (1991). "Results of laboratory tests on a geotextile/bentonite liner material." Proc. Geosynthetics '91, Atlanta, GA, pp. 517-535.

Simunek, J., Sejna, M., and van Genuchten, M.Th. (1999). The HYDRUS-2D software package for simulating two-dimensional movement of water, heat, and multiple solutes in variably saturated media. Version 2.0, IGWMC-TPS-53, International Ground Water Modeling Center, Colorado School of Mines, 251pp.

Thode, R. and Stianson, J. (2006). SVFlux User's Manual. SoilVision Systems Ltd., Saskatchewan, Canada.

Tau, T-K., Yan, J., Tang, R-N. and Yang, M. (2002). "Application of geotextile/geomembrane composite in the core wall of a rock-fill dam." Proc. 7th Int. Conf. on Geosynthetics, Nice, France, pp. 991-994.

Terzaghi, K. and Lacroix, Y. (1964). "Mission Dam: An earth and rockfill dam on a highly compressible foundation." Geotechnique, 14(1), pp. 14-50.

Tindall, J.A. and Kunkel, J.R. (1999). Unsaturated Zone Hydrology for Scientists and Engineers. Prentice Hall, New Jersey.

Touze-Foltz, N., Rowe, R.K., and Duquennoi, C. (1999). "Liquid flow through composite liners due to geomembrane defects: Analytical solutions for axi-symmetric and two-dimensional problems." Geosynthetics International, 6(6), pp. 455-479.

Touze-Foltz, N., Rowe, R.K. and Navarro, N. (2001). "Liquid flow through composite liners due to geomembrane defects: Nonuniform hydraulic transmissivity at the liner interface." Geosynthetics International, 8(1), pp. 1-26.

Touze-Foltz, N. and Giroud, J.P. (2003). "Empirical equations for calculating the rate of liquid flow through composite liner due to geomembrane defects." Geosynthetics International, 10(6), pp. 215-233.

Touze-Foltz, N. and Giroud, J.P. (2005). "Empirical equations for calculating the rate of liquid flow through composite liners due to large circular defects in the geomembrane." Geosynthetics International, 12(4), pp. 205-207.

Touze-Foltz, N. and Barroso, M. (2006). "Empirical equations for calculating the rate of liquid flow through GCL-geomembrane composite liners." Geosynthetics International, 13(2), pp. 73-82.

U.S. Army Corps of Engineers (1970). Engineering and Design: Stability of Earth and Rock-Fill Dams. Engineer Manual EM 1110-2-1902, Dept. of the Army, Corps of Engineers, Office of the Chief of Engineers, Washington, D.C.

van Genuchten, M.Th. (1980). "A closed-form equation for predicting the hydraulic conductivity of unsaturated soils." Soil Science Soc. of America Journal, 44, pp. 892-898.

Walton, J., Rahman, M., Casey, D., Picornell, M., and Johnson, F. (1997). "Leakage through flaws in geomembrane liners." J. Geotech. and Geoenvir. Engrg., ASCE, 123(6), pp. 534-539.

World Commission on Dams (2000). Dams and Development: A new framework for decision-making. Earthscan Publications, Ltd., London.

Wright, S.G. (2007). "UTEXAS4: A computer program for slope stability calculations." Shinoak Software, Austin, TX.

Vita

Christine Theresa Weber was born on February 19, 1979 in El Paso, TX to John and Barbara Weber. Christine attended high school at Loretto Academy in El Paso, TX and graduated in May 1997. Christine attended Texas A&M University in College Station, TX for her undergraduate studies. She graduated with a Bachelor of Science Degree in Civil Engineering in December 2001. Christine remained at Texas A&M University to pursue a graduate degree in Civil Engineering with a focus on Geotechnical Engineering. During this time, she was given the opportunity (as a teaching assistant) to teach the undergraduate-level Geotechnical Engineering laboratory for four semesters. Christine received a Master of Engineering Degree in Civil Engineering in May 2003. Driven by a desire to teach and her passion for Geotechnical Engineering, Christine entered the University of Texas at Austin in Fall 2003 to begin work on her PhD. She was awarded the Thrust 2000 Fellowship from the University of Texas' College of Engineering in August 2003. In August 2007, Christine was awarded the Past Presidents' Scholarship from the Society of Women Engineers for outstanding academic achievement in engineering. Christine has published five conference papers.

Permanent address: 810 Hannock Glen Ln.
Spring, TX 77373

This dissertation was typed by the author.